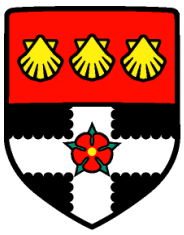

University of Reading

Development of a clinically translatable allogenic umbilical cord-derived mesenchymal stem cell conditioned media.

Andrew James Parnell

September 2025

PhD in Biomedical Sciences (part-time)

School of Biological Sciences

Declaration

I confirm that this is my own work and the use of all material from other sources has been properly and fully acknowledged. – Andrew James Parnell

Acknowledgements

The work conducted here could not have been completed without a number of people. Firstly, I would like to thank Prof. Ketan Patel as my PhD supervisor for facilitating, guiding, and supporting the research. By extension, I would like to acknowledge the past and present members of Prof. Patel's lab who provided help and shared their knowledge with me.

Many thanks also go to Micregen Ltd., who as the industrial partner, finically supported this project. A special mention to Dr Robert Mitchell, as Head of R&D, my colleague and friend who has supported me throughout the project, helping me to develop into the researcher I am today. I would also like to acknowledge my colleagues Dr Ben Mellows and Daniel Feist who also offered support and guidance with their expertise of stem cell conditioned media.

Finally, I would like to acknowledge my family and friends. Especially my wife, Kayleigh Parnell, who has supported me over the last 6 years of study, and who has endured the lows and celebrated the highs every step of the way. With all my love, I dedicate this work to you and our family.

Abstract

Mesenchymal stem cells (MSCs) have featured in the regenerative medical field for decades, with particular focus on their secretomes' paracrine nature for treating disease or regenerating damage. Conditioned medias and subsequent products using the derivates of MSC secretomes have flooded the space over the last two decades, many of which still use crude research laboratory methods for the generation. Although their therapeutic capacity is well documented, the methods for generating them are often far from what would be required for regulatory approval and clinical manufacture. Here, methods of producing clinically relevant umbilical cord-derived MSC conditioned media were explored. In particular, a novel pelleting approach (UCMSC PEL), was evaluated to reveal potent proliferation and migration enhancing and anti-inflammatory properties. Batch-to-batch and donor-to-donor variation was found to be minor. However, the concentration of key components within the secretome and differences in biological outputs compared to an adherent conditioned media (UCMSC ADH), weighed against the UCMSC PEL being a commercially viable product. Thus, UCMSC ADH conditioned media was developed from a research-grade conditioned media to one resembling a clinically compliant, scalable therapeutic candidate with commercial appeal. During the development, the use of bicarbonate buffers or basal medias remained favourable, and scale-up protocols were conceptualised. Finally, mechanisms of action and biological applications of the developed preparation (UCMSC ADH-E) were revealed through in vitro testing to include enhancing proliferation and migration, augmentation of biomolecule activity (metalloproteinases and serine proteases), and potent anti-inflammatory properties against an LPS-induced blood and PBMC assay. Cytokine arrays and gene expression analysis (qPCR) revealed the immunomodulatory nature of UCMSC ADH-E was linked to regulation of NF-κB controlled genes. An in vivo model of muscle regeneration identified anti-fibrotic and anti-haemorrhagic properties, however no acceleration to muscle fibre regeneration was observed, which was later attributed to an anti-differentiation effect from UCMSC ADH-E on myoblast fusion. All in all, this project has identified a clinically relevant UCMSC conditioned media using GMP available material, which is reproducible, scalable, and biologically potent.

Abbreviations

®	- registered trademark
2D	- two dimensional
3D	- three dimensional
AB1190	- human myoblast cell line
ADMSC(s)	- adipose-derived mesenchymal stem cell(s)
AFMSC(s)	- amniotic fluid-derived mesenchymal stem cell(s)
ATCC	- American Tissue Culture Collection
ATMP	- advanced therapy medicinal product
BaV	- *Bitis arietans* venom
BMSC(s)	- bone marrow-derived mesenchymal stem cell(s)
BSA	- bovine serum albumin
CO_2	- carbon dioxide
CTX	- cardiotoxin (*Naja* venom)
DMSO	- dimethyl sulfoxide
DPBS	- Dulbecco's phosphate buffered saline
EBSS	- Earle's balanced salt solution
EC50	- half maximal effective concentration
ECM	- extracellular matrix
ELISA	- enzyme-linked immunosorbent assay

EMA - European Medicines Agency (European Union)

ESCRT - endosomal sorting complex required for transport

EV(s) - extracellular vesicle(s)

FAP(s) - fibro-adipogenic progenitor(s)

FDA - Food and Drug Administration (United States of America)

GLP - good laboratory practice

GMP - good manufacturing practice

GO - Gene Ontology

(d)H_2O - (distilled) water

HBSS - Hank's balanced salt solution

HeLa(s) - human cervical carcinoma cell(s)

HIF - hypoxia-inducible factor

ICH - The International Council for Harmonisation of Technical Requirements for Pharmaceuticals for Human Use

ICTRP - International Clinical Trials Registry Platform

IL- - interleukin-

kDa - kilodalton

LPS - lipopolysaccharide

MEM - Minimum Essential Medium

MHRA - Medicines and Healthcare products Regulatory Agency (United Kingdom)

MP - metalloproteinase

MSC(s) - mesenchymal stem cell(s)

MUO - manufacturing use only

MWCO - molecular weight cut-off

NEC - necrotising enterocolitis

NF-κB - nuclear factor kappa-light-chain-enhancer of activated B cells

NTA - nanoparticle tracking analysis

PBMC - peripheral blood mononucleated cells

PBS - phosphate buffered saline

PDT - population doubling time

PFA - paraformaldehyde

PLA2 - Phospholipase A2

PRP - platelet rich plasma

qPCR - quantitative polymerase chain reaction

RGE - relative gene expression

RCF - relative centrifugal force

RUO - research use only

SEM - standard error of the mean

SP - serine protease

TA - Tibialis Anterior

TLR	- Toll-like receptor
TNFα	- tumour necrosis factor alpha
™	- trademark
UCMSC	- umbilical cord-derived mesenchymal stem cell
UCMSC ADH	- conditioned media generated from adherent UCMSC culture in basal media
UCMSC ADH-E	- developed conditioned media generated from adherent UCMSC culture in EBSS
UCMSC PEL	- conditioned media generated from pelleted UCMSC culture in PBS
v/v	- volume per volume

Contents

Figures

Tables

Chapter 1 - General Introduction

Stem Cells

The term “stem cell” first appeared in scientific literature as early as 1868 in the works of Ernst Haeckel, an eminent German biologist. Although first applied to the field of evolution to describe the ancestral unicellular organism from which all multicellular organisms evolved, he later used the term “stem cell” to describe the fertilised egg in 1877 (Ramalho-Santos and Willenbring, 2007). Despite the acknowledgement of the premise of stem cells in the second half of the 1800s, it was nearly a century later the existence of stem cells, as we recognise them today, was confirmed. In the 1960s, the first genetic evidence for stem cells was produced by studies by Till, McCulloch, Wu, Becker and Siminovitch on haematopoietic stem and progenitor cells (Weissman et al., 2001).

Stem cells are “unspecialised” cells capable of self-renewal and/or differentiating into different cell types (Zakrzewski et al., 2019). It has been described that stem cells have four fates. These being maintenance of a quiescent state, symmetric self-renewal, asymmetric self-renewal (where one of the daughter cells go on to differentiate), and symmetric division without self-renewal (Biehl and Russell, 2009, Molofsky et al., 2004). The term “stem cell” encompasses a wide range of cell types, seeing “embryonic” or “adult” / “somatic” being used to distinguish stem cells by the developmental stage from which they originate. However, with the possibility to turn somatic cells into embryonic-like stem cells, these terms are slowly becoming outdated. Another way to sub divided stem cells would be to sort them by biological properties, these being potency and morphology (Biehl and Russell, 2009).

Potency

Stem cell potency describes the potential of differentiation into different cell types. Stem cells can be described as totipotent, pluripotent, multipotent, oligopotent or unipotent. Totipotent stem cells can differentiate into cells of the whole organisms. Totipotency is the highest differentiation potential and allows cells to become both embryo and extra-embryonic structures (Zakrzewski et al., 2019). The zygote, which is formed when an egg is fertilised by a sperm, is an example of a true totipotent stem cell. Pluripotent stem cells have the next highest differentiation potential. Descending from totipotent

cells which formed blastocysts, pluripotent stem cells can be isolated from embryo or foetal tissue. They have the capability to become any cell in the body, from any of the three germ layers, however, they cannot form extraembryonic structures such as the placenta (Donovan and Gearhart, 2001). In recent years pluripotent stem cells are now being produced from somatic cells, following the identification of four key factors to induce pluripotency. In 2006 Takahashi and Yamanaka identified that through the artificial expression of Oct-4, Sox-2, Klf-4 and c-Myc (termed OSKM), adult fibroblasts were able to be converted to a pluripotent state. These cells were simply termed induced pluripotent stem cells (iPSC) (Takahashi and Yamanaka, 2006).

Multipotent stem cell can differentiate in many cell types, however, have a reduced capacity than that of pluripotent stem cells. Multipotent stem cells can specialise into discrete cells of specific lineages, for example, haematopoietic stem cells can become several types of blood cells. Following differentiation, these stem cells become oligopotent, which although still have the capability to become many different cell types, they are restricted to one cell lineage. On the other hand, some multipotent stem cells have the capability to become cells of unrelated types, suggesting there could be some that are more pluripotent-like than others (Zakrzewski et al., 2019). Lastly, there is unipotency, which is when a cell is capably of self-renewal, but can only differentiate into a single cell type (Zhang et al., 2009).

Morphology

The use of the term “morphology” to describe the type of a stem cell is possibly a misuse of the term, however, stem cells are commonly described using morphological states. Morphologically, stem cells can be classified as epithelial or mesenchymal. Epithelial stem cells are typically found in niches within self-renewing tissues that require a constant supply of new cells to replace those lost through shedding or sloughing into the environment (Cotsarelis, 2006). Epithelial stem cells are present in tissue such as the gut epithelium (Trentesaux et al., 2020), the epidermis of the skin and the hair follicle. A stem cell classified as epithelial has a strong connection to a basal lamina, limiting their

ability to migrate. Typically, an epithelial stem cell's function is to replace a single cell type, within their tissue of origin (Cotsarelis, 2006). On the other hand, mesenchymal stem cells (MSCs) have been identified in numerous tissues and are often multipotent, which has made them appealing to study in the field of stem cell medicine. The classical definition dictates them as adherent in culture and express the cell surface markers, CD73, CD90 and CD105, whilst not expressing CD34, CD45, CD14 or CD11b, CD19 or CD79α and HL-DR (otherwise known as the haematopoietic markers) (Dominici et al., 2006).

Lastly, there are the haematopoietic stem cells. Being the first described stem cells, they were named not by their morphological characteristics, but by the lineage of terminal differentiated progeny. These stem cells are responsible for the production of the numerous blood cell types, undergoing several stages of differentiation through the committed progenitor cells known as common myeloid progenitor (erythrocytes, platelets, mast cells, granulocytes and monocytes lineage) and common lymphocyte progenitor (B-cells, T-cells and NK cells lineage) (Dzierzak and Philipsen, 2013).

The Human Umbilical Cord

The rudimentary umbilical cord forms between the 4th and 8th weeks of gestation in humans. Consequentially, expansion of the amnion envelopes tissue from the body stalk, the omphalomesenteric duct, and the umbilical coelom to form this early structure. Around the end of the 5th week of gestation blood flow is established within the umbilical cord. Within the body stalk there are two umbilical arteries, two umbilical veins and the allantois. As the umbilical cord develops the allantois, arisen from the yolk sac diverticulum, regresses between the 6th and 8th week of gestation. Likewise, the right umbilical vein is obliterated around the 6th week of gestation leaving the single, persisting left vein (Kozadinos et al., 2025). In addition to the body stalk, the umbilical coelom and omphalomesenteric ducts were enveloped. Both structures regress during the cord development, with the omphalomesenteric duct first, between the 7th and 10th weeks of gestation, and the umbilical coelom around the 12th week of gestation. The fully developed umbilical cord normally contains two

umbilical arteries, one umbilical vein, the remnant of the allantois all embedded in Wharton's Jelly and surrounded by a single layer of amnion (Spurway et al., 2012).

First described in 1656 by Thomas Wharton, the Wharton's Jelly is a mucoid connective tissue which surrounds and supports the umbilical vesicles (Davies et al., 2017). This mesenchymal tissue is primarily made up of mucopolysaccharides such as hyaluronic acid and chondroitin sulfuric acid (Bergman et al., 1961). In addition to structure functionalities, Wharton's Jelly has been identified as an abundant source of mesenchymal stem cells (Davies et al., 2017).

Umbilical Cord-derived Mesenchymal Stem Cells

Umbilical cord-derived stem cells can be isolated from either from umbilical cord blood (UCBMSCs) or from the Wharton's Jelly (UCMSCs). UCMSCs have been popular in the scientific community for many years, due to being embryonically derived and above ethical concerns as they can be isolated form the otherwise discarded umbilical cord post-birth. Furthermore, UCMSCs have been shown to possess the ability to differentiate in the three germ layers, to localise in damaged or inflamed tissues, to promote tissue repair and to modulate the host immune system (Nagamura-Inoue and He, 2014).

Isolation of UCMSCs have been successful from various compartments of the umbilical cord, with Wharton's Jelly seemingly the most popular source of MSCs. Wharton's Jelly is reported to be rich in UCMSCs with numbers of cells reaching up to 4,700,000 MSCs/cm of the umbilical cord. Furthermore, these cells are proliferative with a short doubling time (Stefańska et al., 2020). UCMSCs fit the minimum criteria for MSC classification, as laid out by Dominici et al, with the addition of expressing of some pluripotent makers being reported. Human UCMSCs have been shown to express low levels of Oct-4, NANOG, Sox-2, c-Kit as well as Tra-1-60, Tra-1-81 SSEA-1 and SSEA-4 (Batsali et al., 2013).

Moreover, UCMSCs have been differentiated in the multiple cell types. Traditionally, associated to MSCs, osteogenic, chondrogenic and adipogenic lineages have been derived successfully (Batsali et al., 2013, Dong et al., 2020, Stefańska et al., 2020). Additionally to these three mesodermal cell types, UCMSCs have been successfully differentiated into cardiomyocytes (Wang et al., 2004), and skeletal

muscle (Conconi et al., 2006). Outside of the mesoderm, many studies have explored the potential for neurogenic differentiation (ectoderm), with Mitchell et al. being the first study to observe neuronal differentiation following a complex multistep process (Mitchell et al., 2003). Lastly, endodermal cell types have also been produced from UCMSCs, with hepatocyte and pancreatic islet-like cell differentiation being recorded (Stefańska et al., 2020, Batsali et al., 2013). This wide-ranging differentiation potential has been attributed to the extra-embryonic origins of UCMSCs, however, despite this and the expression of pluripotent markers, UCMSCs are not considered pluripotent due to a lack of teratoma formation when implanted in vivo (Fong et al., 2007).

Stem Cells in Medicine

The use of stem cells in regenerative medicine is not a new concept. In 1958, the French oncologist Georges Mathé, was the first to successfully save the lives of six nuclear researchers, following accidental irradiation, with bone marrow grafts. It was not long after, in the early 1960s, the first genetic evidence for stem cells was produced by studies by Till, McCulloch, Wu, Becker and Siminovitch on haematopoietic stem and progenitor cells (Weissman et al., 2001). In 1963, Mathé once again astonished the scientific community by curing a case of leukaemia through bone marrow transplantation, following a growing number of studies into allogenic bone marrow transplantation in various animal species (Mathé et al., 1965). These initial medical marvels opened the doors to floods of scientific research into stem cells and their applications in regenerative medicine, particularly an attention was given to mesenchymal stem cells (MSCs). MSCs sparked interest for their ability to differentiate into numerous cell types, bringing the idea of these cells replacing lost or damaged tissues following differentiation into desired cell type.

Over the years, the science and medical communities have demonstrated that stem cells have a vast therapeutic capability. However, it wasn't until 2005 that the notion of stem cells acting through paracrine signalling as opposed to transdifferentiating and fusing with host was first hypothesised by Gnecchi and colleagues (Liang et al., 2014, Gnecchi et al., 2005, Gnecchi et al., 2006). This study

witnessed the restoration of heart function, following surgical-induced myocardial infarction, in less than 72 hours after administration of MSCs, raising the possibility of an action other than myogenic differentiation. Their hypothesis was later confirmed following injection of cell-free conditioned media from hypoxia-stressed MSC into the same model (Gnecchi et al., 2006). This discovery sparked a paradigm shift in stem cell therapeutic research, with many researchers now exploring the functionality and efficacy of conditioned media and its constituent parts. It is now more widely understood that MSCs produce a variety of regenerative bioactive substances (secretome), which include growth factors, cytokines, chemokines, lipid mediators, and extracellular vesicles (e.g. exosomes and microvesicles), nucleic acids (e.g. miRNA and mRNA) and others (González-González et al., 2020). The term 'conditioned media' is used to refer to the secretome when collected from laboratory cultures, which will usually be a culture media altered (conditioned) by the cells within it. MSC conditioned medias have shown activity across a range of bioprocesses, including, immunomodulation, angiogenesis, antioxidative properties and cell migration, homing/targeting and stimulation (Liang et al., 2014).

Mesenchymal stem cell conditioned media

MSC conditioned media comprise a complex secretome of soluble factors and extracellular vesicles, particularly enriched in pro-regenerative and immunomodulatory signals. In particular, it has been identified that UCMSC conditioned media contains high levels of canonical growth factors and cytokines, including TGF-β1, IL-6, IL-8, G-CSF, MCP-1. MIP-1 and CXCL11, which together support angiogenesis, fibroblast and keratinocyte proliferation, and direct cell migrations while modulating inflammatory cell recruitment (Jothimani et al., 2022).

Beyond soluble proteins, MSC conditioned medias are rich in small extracellular vesicles (EVs) (exosomes and other EVs, typically 50-200 nm) carrying lipids, enzymes, transcription-related proteins, and nucleic acids such as regulatory miRNAs (Cheng et al., 2020). This vesicular cargo reflects the parent cells phenotype and can reprogram target cells, through transferring angiogenic and

cytoprotective miRNAs, for example, miR-210. EV membranes enriched in sphingomyelin, ceramides, cholesterol, and phosphatidylserine also support uptake and can mediate receptor-independent signalling at the target cell surface (Shimizu et al., 2026). It is this vast collection of biomolecules and subcellular particles which gives MSC conditioned media its multifactorial therapeutic activity.

Mesenchymal stem cell conditioned media mechanisms of action and applications

It has been widely evidenced that MSC conditioned media have pro-regenerative properties across multiple tissues. There are many studies which have demonstrated the vast benefits of MSCs on tissue repair, many of which strengthen the understanding that they act through an autocrine or paracrine manner to bring about the beneficial changes rather than their direct engraftment (Maguire, 2013). The majority of studies have identified the presence of growth factors in MSC conditioned media which promote the regeneration of damaged tissues, with particular emphasis on enhancing cellular proliferation (Mellows et al., 2017, Mitchell et al., 2019, O'Connell et al., 2021), improved extracellular matrix structure (Sato et al., 2025), anti-fibrosis (Choi et al., 2024a, Choi et al., 2024b, Shi et al., 2024) and angiogenic effects (Tsujimoto et al., 2024, Arutyunyan et al., 2016) which attribute to proper regeneration (Iismaa et al., 2018).

Namely, one of the most published would be the ability of MSC conditioned medias to accelerate wound healing (Kuncorojakti et al., 2024, Li et al., 2017, Shrestha et al., 2013, Sato et al., 2025). For example, a study by Li et al. showed that conditioned media from UCMSCs promoted the proliferation and migration of dermal fibroblasts. Moreover, it was identified that UCMSC conditioned media prevent the differentiation of fibroblasts and fibrosis, which was attributed to transforming growth factors-β (TGFβ) and the ratio of matrix metalloproteinase (MMP) to tissue inhibitor of metalloproteinase (TIMP). Finally in vivo tests demonstrated accelerated wound healing, re-epithelialisation, and reduced scarring (Li et al., 2017). The use of disease models, such as diabetes where delayed re-epithelisation, chronic inflammation and impaired angiogenesis contribute to poor- or non-healing wounds, have shown that MSC conditioned media promotes wound healing even in a

pathological state (Hendrawan et al., 2021). A study by Shrestha and colleagues, comparing transplanted UCMSCs alongside conditioned media in a diabetic mouse model, demonstrated that the conditioned media outperformed the whole cells on a number of measurements including closure time, capillary density, and granulation. Moreover, UCMSC conditioned media treated wounds were found to have increased expression of wound healing related growth factors (PDGF-β and KGF) compared to the whole cells (Shrestha et al., 2013). Other MSC conditioned medias have also been demonstrated to promote wound healing where normal healing is impaired, such as ADMSC conditioned media promoted the proliferation of keratinocytes, modulated ECM lay down in scar tissue formation and improved vascularisation in a rat model of partial-thickness cutaneous thermal burns (Kuncorojakti et al., 2024).

Beyond skin wound healing, MSC conditioned medias have been shown to improve the regeneration of other tissues. As previously mentioned, the first work confirming the paracrine activity of MSCs was conducted in models of ischemic heart damage (Gnecchi et al., 2005, Gnecchi et al., 2006). Studies have shown MSC conditioned media enhances stimulation of cardiomyocyte proliferation as well as promoting the formation of new vasculature (Zhao et al., 2016, Deszcz, 2023) following myocardial infarction. Another example disease appearing frequently in the literature for applying MSC conditioned media treatment is osteoarthritis (OA) and other joint conditions, where whole cell MSC therapies have even reached clinical trials (Holiuk et al., 2025, Giusti et al., 2025). UCMSCs have been shown to ameliorate cartilage erosion, modulate cartilage ECM turn over and balance inflammatory cell involvement in the synovium (Tong et al., 2020). Furthermore, UCMSC conditioned media has been tested in animal models of OA, where one study by Lubis et al. administered UCMSC conditioned media into an OA sheep model and demonstrated macroscopic improvement of cartilage (Lubis et al., 2022). Furthermore, bone marrow-derived MSC (BMSC) conditioned media was able to modulate the inflammatory response in primary equine synoviocytes, chondrocytes and macrophages by altering the released cytokine profile to one less pro-inflammatory (Linde et al., 2025).

The involvement of immune cells is widely established as the mediators of regeneration (Iismaa et al., 2018), and therefore, it's no surprise that the immunomodulatory effect of MSC conditioned media has been well studied establishing that MSC conditioned media possesses anti-inflammatory properties (Lee et al., 2025b, Tabrizi et al., 2025, Sengun et al., 2025, Payão et al., 2025). This attribute of MSC conditioned media's therapeutic package acts mainly through bioactive molecules which inhibit pro-inflammatory pathways and promotes anti-inflammatory or tolerogenic phenotypes in immune cells (Tokhanbigli et al., 2019, Deng et al., 2014). Some of the bioactive molecules identified in the conditioned media include various growth factors and cytokines, such as TGFβ and IL-10, as well as miRNAs such as let-7b, miR-21, miR-146a and miR-181 (Li et al., 2024). Moreover, MSC conditioned media has been shown to modulate the proliferation, activation and function of immune cells, from both the innate (Lee et al., 2025a) and adaptive (Sengun et al., 2025) immune system. For example, MSC conditioned media has been shown to reduce pro-inflammatory activation of macrophages through the inhibition of MAPK and NF-κB signalling, in turn reducing the expression of pro-inflammatory molecules such as IL-1β, IL-8 and TNFα (Zhang et al., 2024). Furthermore, MSC conditioned medias can promote polarisation towards the M2 "anti-inflammatory" phenotype (Lee et al., 2025a). miR-125a-3p and miR-540-3p, also identified in MSC conditioned media, have been connected to supressing the proliferation and differentiation of T-cells (Fujii et al., 2017, He et al., 2024) and miR-21-5p blocks T-cell homing and activation the degradation of CCR7 (Smigielska-Czepiel et al., 2013).

Throughout the scientific literature there is consistent support for these mechanisms of action and more, with a variety of applications demonstrated across most tissues, including liver (Shi et al., 2024), kidney (Rota et al., 2018) and even the brain (Liu et al., 2020, Tang et al., 2023, Aliaghaei et al., 2016). This multifaceted activity is why the field of MSC conditioned media has attracted such excitement within the research and medical communities.

Generating Condition Media

Generating conditioned media from adherent UCMSC in serum free media is a well published method, used for studying the conditioned media itself (Yang et al., 2014, Li et al., 2017, Kuchroo et al., 2015) as well as isolating EVs (Zhou et al., 2013). Whilst this seems to be a standardised method of generating conditioned media, ways to improve the activity of conditioned media have been explored across MSC types (Ferreira et al., 2018). Gnecchi et al. revealed how hypoxic treatment of MSCs promoted the release of trophic factors including VEGF (angiogenic), bFGF (mitogenic), HGF (mitogenic and cell motility) and IGFs (regulation of physiology, mitogenic, anti-apoptotic, cellular growth). This conditioned media displayed a cytoprotective effect against hypoxia stress in adult rat ventricular cardiomyocytes (Gnecchi et al., 2006). Later, other groups compared conditioned media from normal and hypoxic conditions with many groups concluding that exposing the cells to hypoxia produced a more concentrated (greater amount of proteins and nucleic acids release) MSC conditioned media and thus was superior when tested against non-enhanced conditioned medias (Liang et al., 2014).

In addition to hypoxia, other methods have been used to enhance their biological efficacy. For example, culturing in 3D matrices, the addition of pharmacological agents and inflammatory cytokines, as well as changes to their environment such as temperature, have been used to pre-condition these cells (Ferreira et al., 2018, Mellows et al., 2017, Mitchell et al., 2019). 3D-culture is used to closely mimic the physiological conditions found in the respective stem cell niches. 3D-culture of MSCs as spheroids, has been shown to produce increased levels of molecules associated with cell survival, proliferation and vascularisation (Ferreira et al., 2018), such as angiogenin, FGF-2, angiopoietin 2, VEGF and HGF amongst others (Petrenko et al., 2017). Thus, it has been shown that spheroid culture can enhance these cells' immunomodulatory, angiogenic, anti-fibrotic and anti-apoptotic properties (Ferreira et al., 2018).

There is a considerable amount of experimental data on the topic of pre-conditioning MSCs, particularly involving the use of inflammatory cytokines, growth factors, and hormones. The use of

inflammatory cytokines, such as IL-1β, TNFα and IFNγ, as a pre-conditioning agent unsurprisingly promotes an increased immunomodulator state (Ferreira et al., 2018). A 2020 study be Ragni et al. showed how the addition of IFNγ to the culture media of MSCs prior to collection of conditioned media, altered both the protein and nucleic acid components of the secretome. Through bioinformatic pathway analysis, they showed the conditioned media had an increased link to chemotaxis and motility of inflammatory cells as well as remodelling of the extracellular matrix. They applied their findings to mechanisms associated with osteoarthritis, and along with some in vitro data showed that this IFNγ-enhanced conditioned media have an amplified beneficial effect when compared to conditioned media collected from un-primed MSCs (Ragni et al., 2020). Growth factor preconditioning can also augment the secreted factors of MSCs, with TGFα being linked to increased VEGF, which in turn improved the restoration of cardiac function. Furthermore, there have been cases where a combination of pre-conditioning methods has been used to further enhance conditioned media. Addition of TNFα or hypoxia have been used alongside TGFα to give rise to further improvement of cardiac function (Herrmann et al., 2010).

Pelleted-MSC conditioned media generation protocol

Compared to widely utilised conditioned media collection protocols, this project sets out to investigate a novel method of collecting the secretome from UCMSCs. This method has been previously used by this research group on other multipotent stem cell populations: adipose-derived MSCs (ADMSCs) (Mitchell et al., 2019, Mitchell, 2015) and amniotic fluid-derived MSCs (AFMSCs) (Mellows et al., 2017, Mellows, 2018). This method places the cells in a pellet within a standard laboratory buffer, which was hypothesised to enhance the regenerative potential of the secreted factors produced by the cell through challenging these MSCs with hypoxia and nutrient deprivation (Ferreira et al., 2018), as well as increasing the number of cells per saline volume using a 3D pellet over plastic adherence. The induction of the hypoxic state was confirm within these cell pellets cultured in atmospheric conditions, through upregulation of hypoxia inducible factor-1α (HIF-1α) (Mitchell, 2015).

Mitchell's work on ADMSC conditioned media investigated different timepoints for collecting the conditioned media, identifying a 24-hour period where the highest concentration of proteins, RNA and EVs were secreted. When compared against a conditioned media collected over 48-72 hours, ADMSC conditioned media was found to cause an increase in MSC proliferation and migration as well as protecting against stress-induced senescence in lung fibroblast cells. Moreover, Mitchell's work investigated the therapeutic benefits in muscle disease, initially exploring Duchenne's muscular dystrophy (DMD) using the mdx mouse model. Pelleted conditioned media from both ADMSCs and bone marrow-derived MSCs (BMSC) were shown to increase the reduced migration of mdx muscle satellite cells (Mitchell, 2015). Finally, in a muscle regeneration model, ADMSC conditioned media was found to enhance the skeletal muscle regeneration, as evidenced by larger regenerating myofibers, reduced macrophage infiltration and increased microvasculature (Mitchell et al., 2019).

Mellow's work on AFMSC conditioned media, in a similar fashion, identified a 24-hour protocol collected the highest concentration proteins and RNAs compared to 48- and 72-hours. Again, similarly to Mitchell, Mellows tested 24-hour and 72-hour conditioned media on proliferation, migration, and senescence, demonstrating these conditioned media beneficial activity. In addition, Mellows featured in vitro assays showcasing AFMSCs anti-inflammatory properties, in particular how it modulated through NF-κB activity (Mellows, 2018). Furthermore, use of the in vivo muscle regeneration model established that AFMSC conditioned media enhanced tissue repair through increase regenerating fibre sizes and increased angiogenesis, whereas Mellow's found an increase in macrophage infiltration (Mellows et al., 2017).

Hypoxia preconditioning

Since the early investigations into stem cell conditioned media by Gnecchi (Gnecchi et al., 2006), hypoxia has featured in the scientific literature as a method to enhance conditioned media. In standard static culture systems, MSCs are usually cultured in atmospheric conditions (21% oxygen tension). However, it is known that physiological niches where MSCs reside within the human body

have much lower oxygen tensions (Teixeira et al., 2015), which vary tissue to tissue. For example, in the bone marrow (the BMSC niche) has been reported to vary between 1% and 7% (Harrison et al., 2002), adipose tissue (the ADMSC niche) at 10% and 15% oxygen (Bizzarri et al., 2006) and maternal/foetal tissue such as the umbilical cord between 1.5% and 8% (Genbacev et al., 1997, Balgi-Agarwal et al., 2018). Studies have shown that reducing oxygen levels in MSC culture can enhance the therapeutic properties of MSCs (Teixeira et al., 2015). Research has demonstrated that culturing MSCs in 1% oxygen reduces occurrence of senescence whilst elevating the proliferation rate (Tsai et al., 2011). Furthermore, low oxygen cultures were found to improve angiogenic properties of MSC secretomes with increases in vascular endothelial growth factor (VEGF), beta-fibroblast growth factor (bFGF) and hepatocyte growth factor (HGF) (Liu et al., 2013). Although some groups found that prolonged hypoxic culture practices caused an increase in cell death (Volkmer et al., 2008), it has also been demonstrated the cultures under atmospheric conditions can result in increased oxidative stress, due to the generation of reactive oxygen species (ROS), which could alter the metabolic phenotype of MSCs (Lavrentieva et al., 2010).

HIF-1α, the oxygen sensitive subfactor of HIF-1 transcription factor, plays a central role regulating the cellular response to low oxygen conditions. HIF-1α activation drives the expression of over 60 genes with diverse roles, including cellular proliferation and survival (such as IGF and TGFα), angiogenesis (e.g. VEGF) and metabolism (transferrin and Glut-1) (Ke and Costa, 2006). A study by Teixeria comparing the effect of hypoxia and normoxia (21%) culture conditions on UCMSC secretomes, found that hypoxia increased the amount and diversity of proteins and miRNAs promoting an improved neuroregulatory activity, angiogenesis and anti-inflammatory action (Teixeira et al., 2015). Under normal oxygen conditions, HIF-1α is hydroxylated by prolyl hydroxylase domain proteins (PHDs), complexed with Von Hippel-Lindau protein and channelled for degradation in proteasomes (Lando et al., 2002, Del Peso et al., 2003). During hypoxic periods the hydroxylating function (dependant on molecular oxygen) of PHDs is unable to hydroxylate target signalling molecules such as HIF-1α, nuclear factor kappa-light-chain-enhancer of activated B cells (NF-κB) and protein kinase AKT (Eskandani et

al., 2017). The absence of hydroxylation by PHDs results in HIF-1α level build-up and translocation to the nucleus. In the case of NF-κB, inhibitor of κB kinase (IKK) is regulated by PHD, sequestering NF-κB in normoxia. When oxygen levels drop, nonhydroxylated IKK complexes promote the degradation of inhibitor of NF-κB (IκB), which permits the nuclear translocation of NF-κB and subsequent transcription of hypoxia genes (Cummins et al., 2006).

Further to the release of hypoxia induced proteins, studies have shown that EV biogenesis and release can be influenced by hypoxia, for example promoting HIF-dependent microvesicle shedding by small GTPase RAB22A (Wang et al., 2014). Additionally, the content of EVs has been shown in the literature to alter with hypoxic culture conditions. Small non-coding RNAs (miRNA) which have an important function in post-transcriptional regulation (Bartel, 2004). miR-210 is one miRNA which has been shown to be directly regulated by HIF-1α signalling, and has been reported to increase angiogenesis, reduce fibrosis and apoptosis and promote cardiac regeneration in a myocardial infarction mice model (Huang et al., 2010, Hu et al., 2010). More so, miR-126, miR-130a and miR-210 have been identified as proangiogenic (Guduric-Fuchs et al., 2021, Fish et al., 2008, Fan et al., 2020). Hypoxic-exosomal miR-216a-5p has been reported to positively influence chondrocytes through increased proliferation and migration whilst reducing apoptosis (Rong et al., 2021). Numerous other miRNAs have also been reported to be altered by hypoxic preconditioning of MSCs, including miR-22, miR-26a, miR-125b, miR-21, miR-34a-3p, miR-98-3p, miR-181, miR-17 and miR-14a (Nie et al., 2011, Yang et al., 2022).

Extracellular Vesicles

Extracellular vesicles (EVs), membrane-bound vesicles released from cells, have been demonstrated to be involved in more than the originally believed cell-waste disposal system (Abels and Breakefield, 2016). To date, it has been shown that EVs have a role in intercellular communications, both mediating normal physiological systems (Frühbeis et al., 2012, Frühbeis et al., 2013) as well as pathological progression (Regev-Rudzki et al., 2013, Luga et al., 2012, Marcilla et al., 2012, Barteneva et al., 2013). Although the generic term “EV” is currently used, they are in fact highly

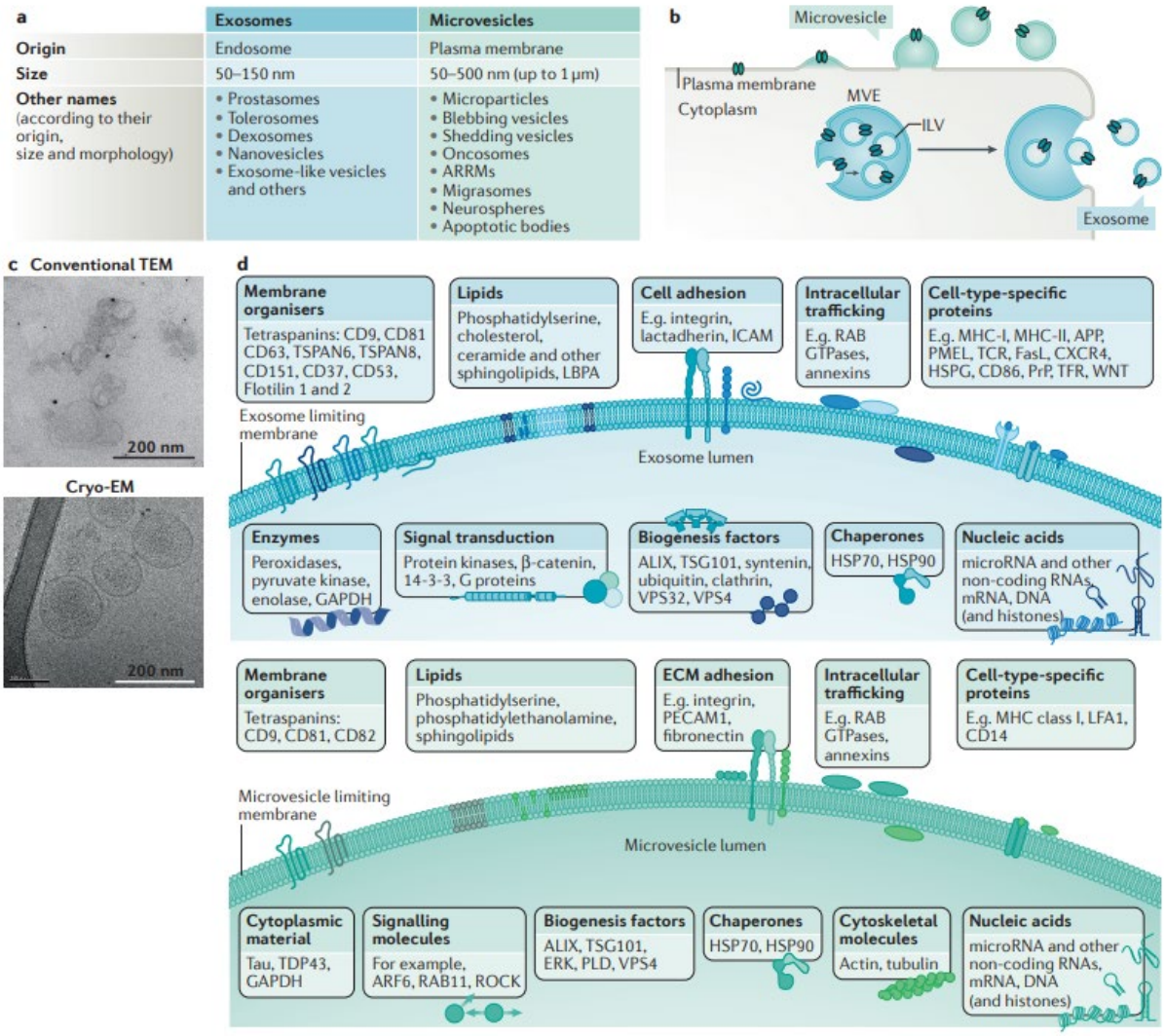

Figure 1.1 Main features of extracellular vesicles from (van Niel et al., 2018)

This graphic depicts the complexity of extracellular vesicles. ***(a)*** *Extracellular vesicles (EVs) are heterogenous in nature are divided into two groups based of size and biogenesis pathway.* ***(b)*** *EVs are formed in one of two ways, either through budding at the cell membrane, releasing microvesicles, or through formation as intraluminal vesicles in the lumen of multivesicular bodies (MVB).* ***(c)*** *Electron microscopy images of EVs during formation.* ***(d)*** *Studies of EVs have revealed numerous components and cargoes, including proteins, lipids and nucleic acids, which vary widely between cell types and conditions leading to EV release. This illustration highlights key molecules identified in exosomes (upper) and microvesicles (lower).*

heterogeneous and are thus further classified into two groups base on their mode of release or size (Figure 1.1a). EVs can be released from "donor-cells" through either outward budding of the plasma membrane resulting in shedding microvesicles (MVs) or ectosomes (Minciacchi et al., 2015), or through inward budding of the endosomal membrane forming multivesicular bodies (MVBs) releasing exosomes upon fusion back with the plasma membrane (Figure 1.1b) (Théry et al., 2002, Denzer et al., 2000). In addition to the differences in biogenesis of EVs, the size of vesicles is used in classification. MVs range from 50 to 1,000 nm in diameter whereas exosomes are smaller with a diameter of 30-150 nm (György et al., 2011). EVs have been revealed to carry a vast range of cargos and have compositions liken to the cell origin, which can affect the fate and function of the EV (Figure 1.1d) (van Niel et al., 2018).

The biogenesis of extracellular vesicles

Exosomes and microvesicles have different modes of biogenesis. Exosomes originate following inward budding of the plasma membrane and subsequent vesiculation of large vesicles, 800-2000 nm in size, termed multivesicular bodies (MVBs) (Mathieu et al., 2021). Fusion of MVBs with the plasma membrane releases the intraluminal vesicles (ILVs) into the extracellular space as exosomes (Arya et al., 2023). In contrast, microvesicles form on the plasma membrane as outward budding vesicles. Despite the distinct origins of exosomes and microvesicles within the cell, both share common intracellular mechanisms and cargo sorting machineries involved in their biogenesis, and for both entities, begin with the sorting of cargo. The physiological or pathological state of the "donor-cell", the stimuli and mechanisms controlling the production and release of EVs often influence the quantity and type of cargoes loaded into the EVs, resulting in cell-type-specific EVs (Minciacchi et al., 2015). First, cargoes are targeted to the site of EV production, either at the membrane of the MVE (for exosomes) or the plasma membrane (for microvesicles). Next, cargoes are enriched in the developing vesicle through a stepwise mechanism of clustering and budding, prior to the fission and vesicle release (Figure 1.2) (van Niel et al., 2018). The machineries involved in EV biogenesis begin to differ from this point onwards.

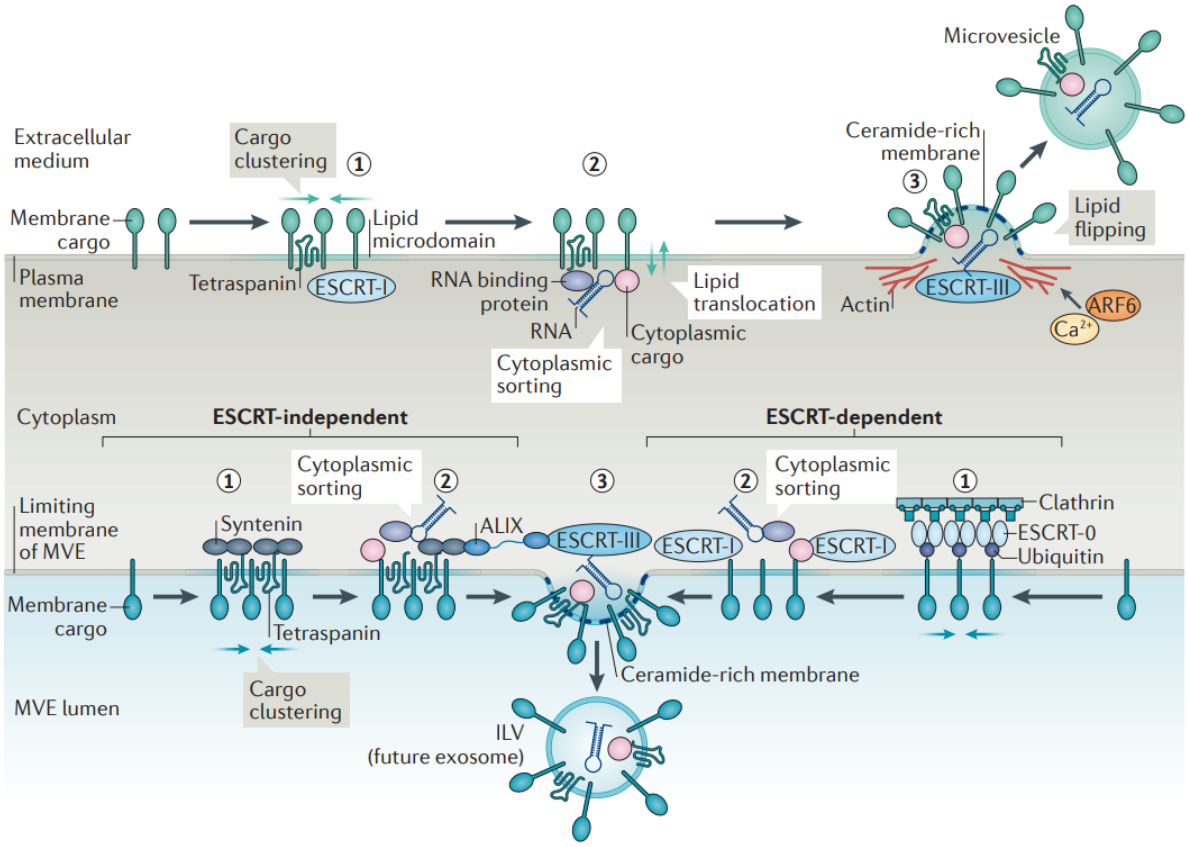

Figure 1.2 Biogenesis of extracellular vesicles, from (van Niel et al., 2018)

This graphic depicts the machinery involved in the biogenesis of microvesicles (upper) and exosomes (lower). Both processes begin with the clustering of ubiquitinated cargoes at on the membrane and the detection of these by molecules such as endosomal sorting complex required for transport (ESCRT). At the cell membrane, for microvesicle release, ESCRT-III, cytoskeletal actin, and ARF-6 are bring about the budding and pinching of the microvesicle. On the membrane of the multivesicular bodies, intraluminal vesicles (ILVs) are form following either ESCRT-dependant or -independent processes.

Exosome biogenesis

Exosome biogenesis initiates at the plasma membrane, where a step-by-step process creates the recognisable architecture of MVBs (vesicle-within-a-vesicle) (Figure 1.3). To begin, endocytosis of the plasma membrane is initiated by multimeric proteins, such as clathrin and caveolae as well as asymmetrical distribution of lipids, such as ceramide and cholesterol (Sharma et al., 2004). Thereafter, the plasma membrane bud undergoes dynamin (Arya et al., 2023) and/or endosomal sorting

complexes required for transport (ESCRT)-dependent fission to produce the new vesicle (Vietri et al., 2020).

The second stage is the formation of ILVs of the MVBs, which begins with the reorganization of the early endosome membrane to become highly enriched in cargoes, such as tetraspanins CD9 and CD63 (Pols and Klumperman, 2009). ILVs formation occurs down the canonical ESCRT-dependant or non-canonical ESCRT-independent pathway (Figure 1.2) (van Niel et al., 2018). The former begins with the recruitment of ESCRTs (Abels and Breakefield, 2016), which there have been four different ESCRTs identified, ESCRT 0, I, II and III (Henne et al., 2011). ESCRT 0 initiates the pathway, binding to both endosomal lipid phosphatidylinositol 3-phosphate (PtdIns3P) and the ubiquitinated-cargo (Raiborg et al., 2001). ESCRT I and II are sequentially recruited to the cytosolic side of the early endosome, binding to ESCRT 0, hepatocyte growth factor-regulated tyrosine kinase substrate (HRS) and ubiquitinate-cargo to initiate the intraluminal membrane budding (Abels and Breakefield, 2016, Shields et al., 2009). Lastly, ESCRT III is recruited through ALG-interacting protein X (ALIX aka, programmed cell death 6 interacting protein) which bridges between the tumour susceptibility gene 101 (TFG101) of ESCRT I and the charges MVB protein 4A (CHMP4A) components of ESCRT III (McCullough et al., 2008). ESCRT III consists of small, highly charged subunits that become active upon binding to ESCRT II, allowing further recruitment and activation of ESCRT III to form a helical polymer (Teo et al., 2004). The ESCRT-dependent pathway can be intersected by synthenin and ESCRT accessory protein, ALIX, which bridges cargo and ESCRT III subunit's vacuolar protein sorting-associated protein 32 (VPS32) (van Niel et al., 2018). In order to complete the ILV formation process, ESCRT III complex requires energy to disassociate from the membrane. This is achieved through the recruitment of deubiquitinating enzyme, which remove the ubiquitin tag from the cargo proteins and AAA-ATPase suppressor-of-potassium-transport-growth-defect-1 protein (SKD1) (Abels and Breakefield, 2016).

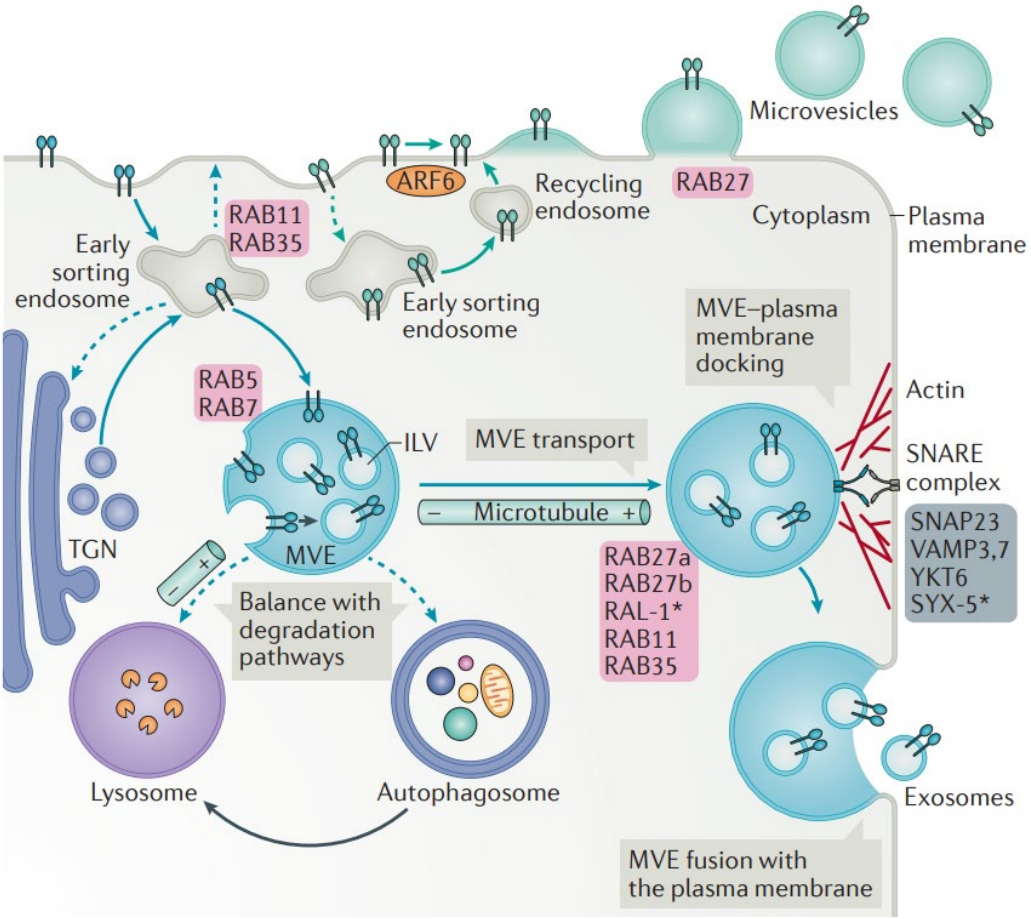

Figure 1.3 Intracellular trafficking routes in the generation of extracellular vesicles, from (van Niel et al., 2018)

This graphic depicts the involvement of multiple intracellular trafficking steps (blue arrows exosomes, green arrows for microvesicles). Cargoes targeted to multivesicular bodies (MVBs) originate for either the plasma membrane brought down in endosomes or added directly from the trans-Golgi network. Endosomes are usual destined for lysosomal destruction, however, major MVBs escape this fate and are moved to the cell membrane, via microtubes under the control of RABs, where they fuse with the plasma membrane via SNARE protein interactions to release their intraluminal vesicles as exosomes.

Microvesicle biogenesis

The biogenesis requires several molecular alterations to the plasma membrane, encompassing changes in lipid and protein compositions, and calcium ion levels (Minciacchi et al., 2015). Ca^{2+}-dependent enzymes including aminophospholipid translocases, scramblases and calpain facilitate rearrangements of the membrane phospholipids along with the restructuring of cytoskeletal actin to bring about budding and formation of microvesicles (Piccin et al., 2007). Externalisation of phosphatidylserine (PS) has been reported to be a main feature of microvesicles (Al-Nedawi et al., 2009), along with lipid raft domains comprised of cholesterol are essential for microvesicle formation (Del Conde et al., 2005). Although distinct from the exosome formation process, the ESCRT system as well as Ras-related GTPase ADP-ribosylation factor 6 (ARF6) are involved in cargo identification and membrane budding (Tricarico et al., 2017) (Figure 1.2).

Extracellular vesicle release

Once formed, microvesicles split from the plasma membrane through the interaction of actin and myosin and ATP-dependant contraction (D'Souza-Schorey and Clancy, 2012) (Figure 1.3). AF6 remodels peripheral actin and mediates the activation of extracellular signal-regulated kinase (ERK) (Pellon-Cardenas et al., 2013) via phospholipase D, which leads to the localisation of myosin light change kinase (MLCK) activity at the site of microvesicle fission (D'Souza-Schorey and Chavrier, 2006). Subsequent phosphorylation of myosin light chain and the activation of the contractile machinery closes the neck of the budding microvesicle and thus completing the “pinching off” and release of the microvesicle (Tricarico et al., 2017). Alternative to ARF-6 mediation, Rho GTPases, such as RhoA, can also phosphorylate myosin light chain via Rho-associated protein kinase (ROCK) signalling (Schlienger et al., 2014).

In contrast, exosome secretion requires additional steps for transport and fusion of MVBs to the cell membrane to release ILVs as exosomes (Figure 1.3). MVBs are predestined to fuse with the lysosome for degradation, however, specific mechanisms can interrupt this fate enabling exosome release (van

Niel et al., 2018). As with any intracellular trafficking, MVB transfer to the plasma membrane involves the association to the cytoskeleton (actin and microtubules), molecular motors (dynein, kinesins and myosins) and small GTPases (Bonifacino and Glick, 2004). This process is initiated by RAB-GTPase RAB7, whose ubiquitylation status determines whether the MVB is destined for lysosomal destruction or secretion, promotes the recruitment of dynein motor proteins. The presence of cholesterol in the endosome membrane is important for recruitment of RAB7 for lysosomal targeting (Möbius et al., 2003), whereas in MVBs cholesterols are enriched in ILVs making this one of the distinguishing factors believed to determine the fate of the MVBs (van Niel et al., 2018). In addition to RAB7, other RABs, such as RAB27a and RAB27b, are essential for exosome secretion. RAB27b is involved in the motility of MVBs towards the cell membrane, after which both isoforms of RAB27 are required for docking at the plasma membrane and promoting fusion (Ostrowski et al., 2010). At the plasma membrane, MVB situated vesicular SNARE (v-SNAREs) proteins interact with complex of SNARE proteins known as target-SNAREs (t-SNAREs) facilitating the coming together of MVB membrane and plasma membrane releasing the ILVs as exosomes into the extracellular space (Hessvik et al., 2023).

Project outline, hypothesis and aims.

This thesis presents the efforts to translate a stem cell conditioned media derived from umbilical cord mesenchymal stem cells to a clinically relevant protocol, using conditioned media content, product efficacy, and commercial appeal as tools to measure and compare conditioned media candidates. It begins with exploring the use of a novel pelleting method described above, which has been theorised to produce an enhanced conditioned media. To determine how this conditioned media preparation performed, a conditioned media from an adherent culture was generated similar to those used in literature. Therefore, the work presented in Chapter 3 address the first hypothesis of this project:

Hypothesis 1: Conditioned media generated using a pelleting method will have more potent therapeutic activity than traditional adherent conditioned media due to elevate cellular stress causing an increase in regenerative secreted factors.

Aims

1. To generate and characterise conditioned media from UCMSCs using the pelleting method.
    a. Collect conditioned media from more than one UCMSC cell line.
    b. Assess the quantity of proteins, nucleic acids and extracellular vesicles compare to an adherent conditioned media protocol generated from the same cell source.
    c. Ascertain the composition of these conditioned media using mass spectrometry and miRNA sequencing analytically methods.
2. To determine the biological activity of UCMSC conditioned medias.
    a. Test the effect on cellular proliferation and migration using established potency assays.
    b. Develop an assay and test for anti-inflammatory properties.

Taking a slightly pivoted direction from the first hypothesis, this project next explored the ways to develop a UCMSC conditioned media from adherent cultures, which would satisfy the requirements of drug regulators, such as MHRA and FDA and include desired manufacturing qualities, such as scalability. Therefore, the work present in Chapter 4 talks to the second hypothesis of this project:

Hypothesis 2: A regulatory compliant UCMSC conditioned media therapeutic candidate can be developed from the adherent-based generation protocol.

Aims

1. To identify appropriate solutions for UCMSC secretome collection.
    a. Test commercially available buffers or culture medias for cell survival, concentration of secretome components collected and their biological activity.
2. To establish a proof-of-concept three-dimensional culture UCMSC conditioned media.
    a. Establish shaker flask cultures of UCMSCs using 3D microcarriers to allow greater scalability.
    b. Collect conditioned media from shaker cultures and test for content concentrations and biological activity.

Further to the requirements laid out by regulators and the clinical manufacturing process, ensuring and understanding the biological activity and potential clinical applications of a developed conditioned media formed the focus of the final results chapter of this thesis. Chapter 5 explores the bioactivity of a clinically relevant adherent conditioned media for its action on inflammations and explores its application on skeletal muscle regeneration following acute injury to address a third hypothesis:

Hypothesis 3: A clinically adapted adherent UCMSC conditioned media has potent biologically activity.

Aims

1. To investigate the biological activity in vitro
    a. Test developed UCMSC conditioned media preparation on in vitro inflammation assay and assessment of inflammatory gene expression.
    b. Test developed UCMSC conditioned media on human myoblasts cell line.

Test developed UCMSC conditioned media in an in vivo mouse model of muscle regeneration.

Chapter 2 - Methodology

Tissue Culture

Unless otherwise stated, all tissue culture was conducted under aseptic conditions in a laminar flow hood, and reagents were prewarmed to 37°C using a water bath. All cell or assay specific details are outline in respective methods.

Thawing cryopreserved cells for culture

Frozen cells were removed from liquid nitrogen storage and thawed rapidly in a 37°C water bath. Cell suspension was transferred to a clean, sterile 15 mL centrifuge tube. 1 mL of culture media was used to rinse the cryovial before adding it to the cell solution. A further 8 mL of culture media was added to the cells slowly to avoid stress. Cell suspension was divided into appropriate culture vessels at a seeding density specific to the individual cell type and experimental design. This was determined either by the recorded cell number on the cryovial or using Trypan Blue (Corning, 25-900-Cl) cell viability count on a haemocytometer. Cells were placed into incubators for 24 hours before the culture media was refreshed, removing the cryopreservation media and non-viable cells.

Passaging adherent cells in culture

Culture media was removed from cells when the desired confluence was reached (typically 60-70% confluency). TrypLE™ Express dissociation enzyme solution (Gibco™, 12604-021) was used to detach cells from the culture surface, typically with an incubation for 3-5 minutes at 37°C at 5% CO_2. Cells were collected into an appropriate centrifuge tube before an equal volume culture media was used to rinse the culture vessel prior to adding to the cells in a 1:1 v/v dilution. Cell suspensions were then centrifuged at 300 RCF for 5 minutes and the resulting supernatant discarded. The cell pellet was re-suspended in culture media, and a sample was taken for cell counting. Trypan Blue staining was used for cell viability assessment, where the sample of cells was diluted 1:1 with Trypan Blue solution (Corning, 25-900-Cl) and counted using a haemocytometer or an automatic cell counter (Thermo Fisher Scientific Inc, Countess 3). Cell numbers were calculated for desired seeding density and

required cells were transferred to a new culture vessel. Culture media was added, and the culture vessel placed within an incubator.

Freezing cells for cryopreservation

Cells were passaged as described above. Following counting, cells for freezing were transferred to a fresh centrifuge tube and centrifuged at 300 RCF for 5 minutes. Supernatant was discarded and the cell pellet was re-suspended in freezing media (10% DMSO, 90% Culture Media) at a concentration of $5x10^5$ – $1x10^7$ cells/mL (however, this could vary between cell types) and transferred to cryovials as 0.5 - 1 mL aliquots. Cryovials were placed with a MrFrosty™ freezing container and frozen overnight at -80°C prior to storage in liquid nitrogen.

Cells and specific culture conditions

Cells were cultured at 37°C with 5% CO_2 and passaged on reaching 60-70% confluency, unless otherwise stated.

Umbilical cord-derived mesenchymal stem cells

Human umbilical cord-derived mesenchymal stem cells (UCMSCs) from a new-born, Caucasian male donor, were sourced from ATCC (PCS-500-010™, Lot: 64310874) under a research-use-only agreement. Cells were cultured in mesenchymal stem cell basal media (ATCC PCS-500-030™) supplemented with mesenchymal stem cell growth kit – low serum (ATCC, PCS-500-040™), and 1% Penicillin-Streptomycin (Gibco™, 15140-122). Unless otherwise stated, UCMSCs were seeded at 5,000 cells/cm^2. This cell will be referred to as "UCMSC ATCC".

A second UCMSC line from a new-born, Caucasian male donor, were sourced from RoosterBio® (RoosterVial™ hUC-10M-XF, C43002UC, Lot: 210255) under a research-use-only agreement. Cells were revived following manufacturer's instructions using Corning® CellBIND surface flasks and RoosterNourish™-MSC-XF media (RoosterBio®, KT-016). Over 2 passages cells were transferred to standard tissue culture plastic and low-serum mesenchymal stem cell media (as above). Unless

otherwise stated, UCSMCs were seeded at 5,000 cells/cm^2. This cell will be referred to as "UCMSC RUO".

A third GMP-grade UCMSC line from a new-born, Caucasian male donor, were sourced from RoosterBio® (RoosterVial™ hUC-20M-CC, C04020UC, [REDACTED]), with rights for use in further manufacture of products. Cells were revived following manufacturer's instructions using Corning® CellBIND surface flasks and GMP-grade ^{prc}RoosterNourish™-MSC-CC media (RoosterBio®, K82304). After the first passage, cells were cryopreserved in vials containing 10 million cells, to create a "translation cell bank". A single vial of this bank was revived onto Corning® CellBIND surface flasks and cultured in non-GMP RoosterNourish™-MSC-XF media (RoosterBio®, KT-016). Cells were expanded for 2 passages and cryopreserved to produce a research cell bank (RCB). All subsequent cultures, unless otherwise specified were cultured from the RCB in RoosterNourish™-MSC-XF media (RoosterBio®, KT-016) with additional 1% Penicillin-Streptomycin (Gibco™, 15140-122). Unless otherwise stated, UCSMCs were seeded at 5,000 cells/cm^2. This cell will be referred to as "UCMSC MUO".

HeLa cells

Human cervical cancer cells, HeLa, were sourced from ATCC (CCL-2-HeLa, Lot: 70016358) and cultured in high glucose, DMEM GlutaMax™ media (Gibco™, 10566-016), supplemented with 10% foetal bovine serum (Gibco™, 10500-064) and 1% Penicillin-Streptomycin (Gibco™, 15140-122). Unless otherwise stated, HeLa cells were seeded at 10,000 cells/cm^2.

AB1190 cells

hTERT-immortalised human myoblasts, AB1190, were generated and provided to Prof. Patel by The Institute of Myology, Paris. AB1190 cells were cultured in Skeletal Muscle Culture Media (PromoCell®, C-23060), supplemented with 1% Penicillin-Streptomycin (Gibco™, 15140-122). Unless otherwise stated, AB1190 cells were seed at 3,000 cells/cm^2 and maintained below 50-60% confluency.

Assessment of Growth and Stem Cell Properties

Population doubling time and viability of umbilical cord mesenchymal stem cells.

UCMSCs were monitored over multiple passages to determine the health of the culture. At each passage, protocol described earlier, total cell number was calculated. Population doubling time (PDT) was calculated using the follow equation:

$$PDT = \frac{Time\ in\ culture\ (hours) \times Log(2)}{Log(End\ cell\ count) - Log(Starting\ cell\ count)}$$

The viability of UCMSCs was measured using Trypan Blue exclusion as described above.

Tri-lineage differentiation of umbilical cord mesenchymal stem cells

Adipogenic differentiation

UCMSCs were seeded into 8-well Nunc® Lab-Tek II® Chamber Slide™ (Thermo Scientific™, 154534) at a density of 10,000 cells/cm^2 in culture media. Following a 48-hour incubation at 37°C at 5% CO_2 for cells to expand to greater than 90% confluence, culture media was replaced with differentiation media (MesenCult™ Adipogenic Differentiation Kit (Human) (STEMCELL TECHNOLOGIES™, 05412) with 1% Penicillin-Streptomycin (Gibco™, 15140-122). Cells were cultured for 25 days in differentiation media at 37°C with 5% CO_2, with media refreshment every 3-4 days.

Differentiation was confirmed with Oil Red O staining for lipid droplets. Briefly, cells were fixed with 2% PFA/PBS for 15 minutes at room temperature following media removal. Cells were washed thrice with PBS before rinsing with 60% isopropanol. Oil Red O (Sigma, O0625) staining solution (6 parts Oil Red O stock solution (2.5 mg/mL in 60% isopropanol) to 4 parts H_2O, filtered) was added for 30 minutes at room temperature. Once the stain was removed, 60% isopropanol was used to rinse the cells twice before allowing them to air dry. Phase contrast images were captured on Axioskop 2 FS plus (Carl Zeiss) microscope at 40x magnification to visualise staining.

Osteogenic differentiation

UCMSCs were seeded into 8-well Nunc® Lab-Tek II® Chamber Slide™ (Thermo Scientific™, 154534) at a density of 10,000 cells/cm^2 in culture media. Following a 48-hour incubation at 37°C at 5% CO_2 for cells to increase numbers to greater than 90% confluence, culture media was replaced with differentiation media (MesenCult™ Osteogenic Differentiation Kit (Human) (STEMCELL TECHNOLOGIES™, 05465) with 1% Penicillin-Streptomycin (Gibco™, 15140-122). Cells were cultured for 15 days in differentiation media at 37°C with 5% CO_2, with media refreshment every 3-4 days. Control cells were cultured in growth media.

Differentiation was confirmed with Alizian Red S staining for the detection of calcium. Briefly, cells were fixed with 2% PFA/PBS for 15 minutes at room temperature following media removal. Cells were washed three times with PBS before Alizian Red S (Sigma, AS533) staining solution (2% in H_2O, pH 4.2, filtered) was added for 30 minutes at room temperature. Once the stain was removed, cells were rinsed three times with water before allowing them to air dry. Phase contrast images were captured on Axioskop 2 FS plus (Carl Zeiss) microscope at 4x magnification to visualise staining.

Chondrogenic differentiation

UCMSCs were pelleted via centrifugation (300 RCF for 10 minutes) as 500,000 cells in 500 µL of differentiation media (MesenCult™ Chondrogenic Differentiation Kit (Human) (STEMCELL TECHNOLOGIES™, 05455) with 1% Penicillin-Streptomycin (Gibco™, 15140-122)), in 15 mL centrifuge tubes. Cell pellets were incubated at 37°C with 5% CO_2 for 21 days. Differentiation media was refreshed every 3-4 days, avoiding disruption of the cell pellet.

Differentiation was confirmed with Alcian Blue staining of acidic polysaccharides. Briefly, pellets were fixed with 2% PFA/PBS for 15 minutes at room temperature following media removal. Pellets were dehydrated using ethanol series (50%, 60%, 70%, 80%, 90%, 95%, 100%, 100% for 30 minutes per solution). Pellets were washed twice in Histo-Clear (National Diagnostics, HS-200) for 1 hour each time. Cleared pellets were placed in Paraplast® tissue embedding wax at 60°C for 2 hours before

replacing wax for an additional overnight incubation. Wax infused cell pellets were embedding into moulds and allowed to set overnight before 5 µM sections were cut using microtome. Sections were dewaxed using Histo-Clear and re-hydrated with the reverse ethanol series prior to staining, ending with three washes in dH_2O. Alcian Blue (Sigma, A3157) staining solution (0.1 mg/mL in 0.1M HCl, filtered) was added for 30 minutes at room temperature. Once the stain was removed, 0.1M HCl was used to rinse the cells thrice before allowing them to air dry. Phase contrast images were captured on Axioskop 2 FS plus (Carl Zeiss) microscope at 40x magnification to visualise staining.

MSC surface marker profile – flow cytometry of umbilical cord mesenchymal stem cells

UCMSCs were dissociated from culture surface as previously described. Following centrifugation, cells were resuspended in PBS (Gibco™, 20012-027) and an equal volume of cold 4% PFA/PBS was added. Cells were fixed for 30 minutes before centrifuging at 300 RCF for 5 minutes. Fixative was removed and cell washed 3x in 0.5% BSA in PBS, centrifuging at 300 RCF for 5 minutes between washes. Non-specific binding was blocked by an incubation of the cells in 0.5% BSA/PBS for 30 minutes at room temperature. Blocking buffer was removed follow centrifugation and cells incubated in desired antibodies (Table 2.1) in the dark for 1 hour at room temperature. Antibodies were pre-incubated in blocking buffer for 1 hour prior to use. Following incubation, cells were washed three times in blocking buffer. Labelled cells were analysed using a Guava EasyCyte™ 8 flow cytometer. Unstained cells were used to set gating criteria and positivity for expression of cell surface marker was determined against iso-type controls.

Table 2.1 Mesenchymal stem cell surface marker antibody panel.

Target Marker	Dilution (in 100 µL)	Manufacture	Product Number	Lot Number
Iso-FITC	3.4 µL	Abcam	ab91356	GR3261772-10
Iso-APC	3.4 µL	Abcam	ab91358	GR3217197-10
CD73-APC	1.7 µL	Abcam	ab155378	GR3261875-1
CD90-FTIC	3.4 µL	Abcam	ab11155	GR227390-12
CD105-FITC	3.4 µL	Abcam	ab11415	GR3249795-12
CD34-FITC	3.4 µL	Abcam	ab78165	GR280302-12
CD45-APC	3.4 µL	Abcam	ab28106	GR3242651-2
CD19-FITC	3.4 µL	Abcam	ab1167	GR3309891-2
CD14-FITC	6.7 µL	Abcam	ab28061	GR3309728-2
HLA-DR-FITC	6.7 µL	Abcam	ab28323	GR3279397-4

Assessment of replicative senescence

UCMSCs which showed an extended population double time (PDT) were seeded at 5,000 cells/cm^2 into a 24-well plate and allowed to adhere overnight at 37°C with 5% CO_2. Culture media was removed, and cells were fixed with 0.2% glutaraldehyde, 2% PFA/PBS solution for 5 minutes. Fixative was removed and cells were washed twice with PBS. 250 µL of senescence staining solution (5 mmol/L sodium phosphate solution pH 6.0, 5 mmol/L potassium ferricyanide, 5 mmol/L potassium ferrocyanide, 125 mmol/L sodium chloride, 50 mmol/L magnesium chloride, 2.5 mg/mL X-gal) was added to each well prior to incubation in the dark at 37°C, in air for 18 hours. Following the incubation, staining solution was removed, and cells were washed twice with PBS and twice with methanol before being air dried. Brightfield images were captured on EVOS Core imaging system (Thermo Fisher Scientific inc) at 20x magnification to visualise staining.

Generation of Conditioned Media

Unless otherwise stated UCMSCs were used at passage 6-8 to produce conditioned media. Variations in conditioned media generation protocols were evaluated here. Briefly, conditioned medias were produced with cells either in adherent culture or a pelleted mass. Following generation, conditioned media was pooled where appropriate and processed through two centrifugation cycles. Firstly, conditioned media was centrifuged at 300 RCF for 10 minutes to remove cells. Next, the supernatant was centrifuged at 2,000 RCF for 20 minutes to remove cellular debris and large vesicles. Conditioned media was then aliquoted and frozen at -80°C.

Adherent conditioned media

UCMSCs were seeded [REDACTED] cells per cm^2 and allowed to adhere in culture media for 24 hours. Culture media was removed, and the cells washed 3x PBS (Gibco™, 20012-027) prior to addition of required generation vehicle. UCMSCs were incubated in generation conditions for the desired time. For example, [REDACTED] cells were seeded into a T225 flask were cultured in [REDACTED] of basal media (ATCC, PCS-500-030™) for 24 hours at 37°C with 5% CO_2. Conditioned supernatant was collected and processed via centrifugation. Referred to as UCMSC ADH.

Pellet conditioned media

Following dissociation from the expansion flasks, UCMSCs were washed 3x in PBS with centrifugation at 300 RCF for 5 minutes. Aliquots of [REDACTED] cells [REDACTED] of PBS ([REDACTED]) were centrifuged at 300 RCF for 5 minutes in 1.5 mL microfuge tubes. Cell pellets were incubated for 24 hours at 21°C. Conditioned supernatant was collected and processed via centrifugation. Referred to as UCMSC PEL.

Post conditioned media viability

Following conditioned media generated, cells are collected through passage for UCMSC ADH or centrifugation for UCMSC PEL conditioned media. Cells were suspended in 200 µL PBS and placed into a round-bottom 96 well plate for a propidium iodide exclusion test. To set up the flow cytometer (BD

Accuri), unstained cells were acquired, where single cells were selected and use to gate for "LIVE" cells in the FL-2 channel. Next, 5 µL of 0.5mg/mL propidium iodide staining solution (Biolegend®, 421301) was added to test wells and incubated for 1 minute prior to data capture. Cells displaying positive staining, outside of the "LIVE" cell gate in the FL-2 channel were recorded as "Dead". The staining and data capture was continued for each test sample.

Characterisation of Conditioned Media

Protein content

Pierce detergent compatible Bradford protein concentration assay

Total protein concentration was calculated using a detergent compatible Bradford assay (Thermo Scientific™, 23246) following the manufacturer's instructions. Briefly, 135 µL conditioned media was added to a well of a clear 96-well plate containing 15 µL 0.5% Triton-X100 solution and incubated for 30 minutes at room temperature. 150 µL of Pierce reagent was added to each well and incubated for a further 10 minutes at room temperature. Absorbance at 595 nm was measured using a spectrophotometer (Molecular Devices iD3) and protein concentration was determined against a series of protein standards ranging from 25 µg/mL to 0 µg/mL produced from bovine serum albumin (BSA) in the matching conditioned media vehicle.

Silver staining

Conditioned media samples were loaded in Laemmli Buffer (3.75 mL 1M Tris-HCl; 1.2 g sodium dodecyl sulphate; 0.93 g dithiothreitol; 6 mg Bromophenol blue; 6 mL glycerol; ultrapure H_2O up to 10 mL. Stored at -20°C in 0.5 mL aliquots) at equal concentrations (v/v) into a pre-cast Novex™ NuPAGE™ 4-12% Bis-Tris SDS PAGE gel (Invitrogen™, NP0321) alongside 1 µL pre-stained protein standard (Invitrogen™, LC5800) in 4 µL Laemmli Buffer. Gel electrophoresis was run at 120V for approximately 2 hours. Once the dye-front reached the bottom of the gel, the current was switched off and the gel processed for silver staining using SilverXpress® silver stain kit (Life Technologies, LC6100). Briefly, the gel was placed into a staining tray (Life Technologies, NI2400) and 200 mL silver stain fixing solution

added for 10 minutes (using ultrapure water to reduce background staining). Following fixation, the gel was sensitised by incubating twice for 30 minutes in 100 mL silver stain sensitising solution. To remove excess sensitising solution, the gel was washed twice for 10 minutes with ultrapure water before being stained for 15 minutes with silver stain staining solution. The gel was washed twice for 5 minutes with ultrapure water before being developed with silver stain developing solution. The time required to develop the gel depended on the concentration of the protein bands and took approximately 1 – 10 minutes. When the bands were sufficiently developed, 5 mL silver stain stopper solution was added to the developing solution/gel and further incubated for a further 10 minutes. Gels were washed thrice for 30 minutes with ultrapure water before being imaged.

Mass spectrometry of proteins

Protein was extracted by adding 5x volume of ice-cold acetone overnight at -20°C. Precipitates were collected following centrifugation for 15 minutes are 12,000 RPM 4°C, and redissolved gel loading buffer. Samples were loaded into a 12% SDS-PAGE gel, and run at 80V for 30 minutes, followed by 120V for 1 hour. Gels were silver stained for visualisation.

In-gel digestion was conducted by slicing gels into 1 mm^3 cubes and transferred to a 1.5 mL microcentrifuge tube. 1 mL of destaining solution (30 mM potassium ferricyanide, 100 mM sodium thiosulfate) and incubated until the colour disappeared. The supernatant was removed and the reactions stop by incubating in 200 µL water for 10 minutes. After discarding the supernatant, 1 mL of ammonium bicarbonate was added for 30 minutes and then removed. 500 µL of acetonitrile was added for 30 minutes before it was removed. Enough 10 mM dithiothreitol was added to cover the gel slice and incubated at 50°C for 1 hour. After removing the dithiothreitol, 500 µL acetonitrile was added for 10 minutes before removal. Next, 50 mM iodoacetamide to just cover the gel slice and incubated for 30 minutes at room temperature in the dark. The iodoacetamide was removed and another 500 µL acetonitrile was added for 10 minutes before removal. Trypsin digestion solution was added just covering the gel slice and incubated on ice for 45 minutes, topping up solution if the volume

weas absorbed by the gel slice prior to incubating overnight at 37°C. The supernatant was recovered and transferred to a fresh 1.5 mL tube. 50 mM ammonium bicarbonate/acetonitrile (1:2 v/v) was added to the gel pieces for 1 hour at 37°C, before the supernatant was transferred and added to the new 1.5 mL tube. 0.1% trifluoroacetic acid was added for 30 minutes before 50 mM ammonium bicarbonate/acetonitrile (1:2 v/v) was added to the gel pieces. All the extracts were combined and lyophilised to near dryness. Extracted peptides were resuspended in 20 µL of 0.1% formic acid ready for analysis.

Nano liquid chromatography (NanoLC) was conducted using Ultimate 3000 UHPLC system (ThermoFisher Scientific, USA), with PepMap C18 100Å, 100 µm x 2 cm, 5 µm trapping columns and PepMap C18, 100Å, 75 µm x 50 cm, 2 µm analytical columns. 1 µL sample was loaded, with mobile phase A (0.1% formic acid in water) at a flow rate of 250 nL/min, changing on a linear gradient to mobile phase B (0.1% formic acid in 80% acetonitrile). The LC linear gradient was collected as follows: 2 to 8% buffer B in 3 minutes, 8 to 20% buffer B in 56 minutes, 20% to 40% buffer B in 37 minutes, and 40% to 90% buffer B in 4 minutes.

For mass spectrometry (MS), the full scan was performed between 300-1,650 m/z at the resolution of 60,000 at 200 m/z. The automatic gain control target was set to $3x10^6$. The MS/MS scan was operated in Top 20 mode using the following settings: resolution 15,000 at 200 m/z; automatic gain control target $1x10^5$; maximum injection time 19ms; normalised collision energy at 28%; isolation window of 1.4 Th; charger state exclusion: unassigned, 1, >6; dynamic exclusion 30 seconds.

Raw MS files were analysed and searched against *Homo sapiens* protein database according to sample species using Maxquant (1.6.2.6). The parameters were set as follows: the protein modifications were carbamidomethylation (C) (fixed), oxidation (M) (variable); the enzyme specificity was set to trypsin; the maximum missed cleaves were set to 2; the precursor ion mass tolerance was set to 10 ppm, and MS/MS tolerance was 0.5 Da.

Nucleic acid content

UV spectroscopy total nucleic acid concentration assay

Equal volumes (100 µL) of conditioned media were loaded into wells of a UV-transparent 96-well plate. Using ID3 Spectramax (Molecular Devices), absorbances of two wavelengths were recorded. Firstly, 260 nm for the nucleic acid content. A series of standards, serially diluted 1:1 from 100 µg/mL to 0 µg/mL, were produced from yeast RNA (Sigma, R6750) in respective conditioned media vehicle and used to calculate total nucleic acid concentration.

Small-RNA sequencing

RNA was extracted from conditioned media samples using Qiagen miRNeasy Serum/Plasma Kit (Qiagen, 217184) following manufacturer's instructions. Briefly, conditioned media samples are lysed in QIAzol Lysis Reagent, prior to separation with chloroform. The upper, aqueous phase containing RNA was extracted, and ethanol was added. The samples were then applied to the RNeasy MiniElute spin column, and through serial centrifugation and washing steps contaminants such as phenols were removed. The retained RNA was then eluted in a small volume of RNase-free water.

Library preparation was completed using QIAseq miRNA Library Kit (Qiagen, 331502) as per manufacturer's instructions. Briefly, extract RNA was sequentially processed for ligation of 3' and 5' adapters. Next, reverse transcription was performed to produce cDNA. Following cDNA cleanup processed with QWN Beads, library samples were amplified using HotStarTaq DNA polymerase, index primers (QMI TF IP1 through IP12) and QMI TF Lib Rev Primer. Following the PCR cycles, miRNA library samples were quality checked using Agilent's Bioanalyzer following manufacturer's instructions and quantified for concentration using Qubit Fluorimeter.

Small RNA sequencing was performed on Illumina platform NovaSeq X Plus using single-end 50 bp reads with the following metrics: ≥50 reads per sample; Q30 ≥ 85%; unique mapping rate ≥90%. BCL files were converted to FASTQ via bclfastq software to yield raw data files for transcriptomic analysis to map reads to the reference genome database.

Extracellular vesicle content

Nanoparticle tracking analysis.

Size distribution profiles and concentration of extracellular vesicles (EVs) were determined using Nanoparticle Tracking Analysis (NTA). Using Nanosight NS500 instrument, EVs were visualised through the light scattering properties of the vesicles using a light microscope. Five consecutive videos, 60 second in duration, were captured of EVs flowing passed a high sensitivity camera at a known flow rate (set at '20'), being automatically introduced by a syringe pump. The NTA software (version 3.2) tracked individual vesicles and using Brownian motion calculated their size and concentration. Samples were diluted in their respective vehicles to give an approximate maximum particle density of $5x10^8$ particles/mL, which for conditioned media this dilution was typically 1:1. Shutter speed and screen gain for each sample were adjusted manually to visualise EVs in the 80-250 nm size range. NTA post capture settings remained constant between samples.

In Vitro Bioactivity of Conditioned Media

Cellular proliferation

HeLa CyQuant® proliferation assay

For testing of conditioned media for effects on cell proliferation, HeLa cells were seeded at low density (500 cells per well) into a black-walled, clear bottom 96-well plate (Corning, 3904). Cells were allowed to adhere in culture media for 6 hours at 37°C at 5% CO2. Once adhered, culture media was aspirated, and cells were washed gently with 150 µL of PBS (Gibco™, 20012-027). Conditioned media was added in reduced serum culture media (2.5% FBS) at a range of concentrations (v/v). The respective conditioned media vehicle was used as the negative control. Cells were incubated for 96 hours at 37°C at 5% CO_2. At the end of the incubation, culture media was aspirated, and cells were washed gently with 150 µL of PBS (Gibco™, 20012-027). Plates were frozen at -80°C, after ensuring all liquid was removed from the wells. Plates remained at -80°C for at least 18 hours, prior to analysing using CyQUANT® cellular proliferation kit (Thermo Scientific™, C7026). Briefly, plates were removed from

the freezer and allowed to warm to room temperature for at least 30 minutes. 200 µL of CyQuant® staining solution (1:20 lysis buffer, 1:400 CyQUANT® GR reagent in ddH_2O) was added to each well and placed immediately into ID3 Spectramax (Molecular Devices) plate reader. Plates were shaken orbitally for 2 minutes, and the florescence was measured at excitation 485 nm, emission 535 nm. Cell number was determined against a series of cell number standards. Briefly, a dilution series of 12,000 cells down to 0 cells, produced from the same cell stock, were seeded into a black-walled, clear bottom 96-well plate. Following the 6-hour incubation for adherence, culture media was aspirated, and cells were washed gently with 150 µL of PBS (Gibco™, 20012-027). Plates were frozen at -80°C, after ensuring all liquid was removed from the wells, and thawed and processed with the test plates.

AB1190 CyQuant® proliferation assay

The AB1190 proliferation assay was conducted in a similar way to the HeLa proliferation assay described above. AB1190 cells were seeded at a low density of 500 cells per well into a black-walled, clear bottom 96-well plate (Corning, 3904). Following a 6-hour incubation at 37% at 5% CO_2 in complete growth media, test media comprising of conditioned media in reduced (25% of normal) skeletal muscle culture media supplement for a 96-day incubation period. At the end of the incubation, test media was removed, and the wells were rinsed once with PBS prior to freezing at -80°C. Similarly to the HeLa proliferation assay, a dilution series of 12,000 cells down to 0 cells, produced from the same cell stock, were seeded into a black-walled, clear bottom 96-well plate. Following the 6-hour incubation for adherence, culture media was aspirated, and cells were washed with PBS. Plates were frozen at -80°C. Plates remained at -80°C for at least 18 hours, prior to analysing using CyQUANT® cellular proliferation kit (Thermo Scientific™, C7026) as described previously.

Cellular migration

HeLa transwell migration assay

For testing of conditioned media for effects on cell migration, HeLa cells were seeded at high density (30,000 cells) into the upper chamber of a transwell insert (8 µm pore PC-membrane, Brand™, 782706

| 8 µm pore PET-membrane, Sarstedt, 83.3932.800) in serum free culture media. Conditioned media was combined 1:1 to reduced serum culture media (5% FBS, yielding a final concentration of 2.5% FBS) and added to the lower chamber of the transwell system. The respective conditioned media vehicle was used as the negative control. Cells were incubated for 24 hours at 37°C at 5% CO_2 to allow cells to migrate through the membrane. At the end of the incubation, culture media was aspirated, and cells on both side of the membrane were fixed with 4% PFA/PBS for 15 minutes. Membranes were washed twice in PBS prior to staining with crystal violet solution (Stock: 20 g/L in 20% methanol, diluted 1:3 in PBS) for 15 minutes. Staining solution was removed, and membranes rinsed thrice in PBS. Using a cotton swab, the upper surface of the membrane was wiped to remove non-migrated cells, repeated until the cotton swab remained clear of stain. Membranes were allowed to air dry before bright field images of were captured of the whole membrane using EVOS Core imaging system (Thermo Fisher Scientific inc) at 4x magnification.

Images were merged using Adobe Photoshop and cropped to a circle with a diameter of 2,500 pixels (the membrane area), and canvas resized uniformly. Cropped images were analysed in Fiji ImageJ. Briefly, images were converted to 8-bit greyscale and the threshold, using the "Yen" method, selected the percentage area of migrated cells.

AB1190 single cell tracking

For testing conditioned media on the migration of myoblasts, a single cell tracking assay was used. Firstly, AB1190 cells are seeded at a density of 2000 cells per well of a 24-well plate and were allowed to attach overnight at 37°C 5% CO_2. The following day, culture media was aspirated and replaced with fresh culture media with 10% v/v conditioned media or vehicle treatment. Timelapse images were immediately capture using Nikon Eclipse Ti-E microscope with NIS Elements software. Movies were generated with bins collected 10 minutes apart for 23 hours. Cell migration (speed) was measured using CellTracker Software (Piccinini et al., 2015).

Inflammation

Whole blood inflammation assay

For testing conditioned media for effects on inflammation, whole human blood was used to assess the response to inflammatory stimulation through the release of TNFα. Ethical review and approval was granted by the School of Biological Sciences' Research Ethics Committee at the University of Reading, reference code: SBS22-23 41.

Blood, from consenting human donors, was collected in sodium heparin coated BD Vacutainer™ (BD, 367876) and used within 2 hours of donation. Heparinised blood was mixed 1:3 with RMPI 1640 media (Gibco™, 11875-093|PAN Biotech UK Ltd, P04-18047) containing 1% gentamycin (Gibco™, 15710-064), and 800 µL of the mixture was added to wells of a 24-well plate. Conditioned media concentrations were added in a total volume of 100 µL to each well and incubated for 1 hour at room temperature, with the respective conditioned media vehicle being used as the negative control. Following the pre-incubation period, 100 µL of *E. coli* LPS (Invitrogen™, 00-4976-93) was added in RPMI media so that LPS had a final concentration of 1 ng/mL, or RPMI media alone as the unstimulated control. Blood cultures were further incubated for 5 hours at 37°C at 5% CO_2. Cultures were collected and centrifuged for 20 minutes at 2000 RCF, following which the supernatants were frozen at -80°C.

Enzyme-linked immunosorbent assay (ELISA)

Levels of TNFα released were measured using ELISA (Human TNF-alpha DuoSet ELISA; R&D Systems, DY210)). Briefly, 96-well plates were coated with capture antibody overnight at room temperature. Plates were washed with wash buffer (0.05% Tween® in PBS pH 7.2-7.4; R&D systems, WA126) thrice prior to blocking with Reagent Diluent (1% BSA in PBS pH 7.2-7.4; R&D systems, DY995) for 1 hour at room temperature. Plates were wash thrice with wash buffer and samples loaded. A TNFα standard series was added (2-fold dilution 1000 pg/mL to 15.6 pg/mL) for calculating sample concentrations. Samples were incubated at room temperature for 2 hours. Again, plates were washed thrice with wash buffer before the detection antibody was added for a 2-hour incubation at room temperature.

Following washing, streptavidin-HRP was added to the plate and incubated for a further 20 minutes at room temperature. Once washed, HRP substrate solution (1:1 mix of H_2O_2 with Tetramethylbenzidine; R&D Systems, DY999) was added for a 20-minute room temperature incubation, which was followed by the addition of a stop solution (2N H_2SO_4; R&D Systems, DY994) and thorough mixing. Absorbance at 450 nm and 540 nm was measured using ID3 Spectramax (Molecular Devices) plate reader. 540 nm readings were subtracted from 450 nm to correct for optical imperfections. Concentrations of TNFα were calculated from each plate's respective standard curve.

Human cytokine/chemokine multiplex array

Samples for multiplex analysis were sent to Eve Technologies Inc (a fee for service provider). Using multiplexing technology, uniquely coloured beads are tagged with capture antibodies for target molecules, similar to an ELISA. Since each bead is distinguishable from the next, multiple targets can be identified from a single sample. In this case, using the "Human Cytokine/Chemokine Panel A 48-plex Discovery Assay® Array" (HD48A), 48 different beads/capture antibodies were added to the sample. Following washing of the beads to remove any unbound sample, biotinylated detection antibodies are added and incubated to allow binding to captured target molecules. Once any unbound detection antibodies are washed away, streptavidin conjugated with phycoerythrin bind to the biotinylated antibodies. The beads were then passed through a Bio-Plex 200 analyser, which operates with a dual laser system. The first laser detects the unique coloured bead (identifying the target molecule) while the second laser detects the level of streptavidin-phycoerythrin bound to the bead. Combined with a standard curve, the concentration of each target molecule can be calculated.

Isolation of PBMCs

Blood, from consenting human donors, was collected in sodium heparin coated BD Vacutainer™ (BD, 367876) and used within 2 hours of donation. Heparinised blood was mixed with an equal volume of RMPI 1640 media (Gibco™, 11875-093 | PAN Biotech UK Ltd, P04-18047) containing 1% gentamycin (Gibco™, 15710-064). A SepMate50 isolation tube (STEMCELL™ Technologies, 85450) was loaded with

room temperature Lymphoprep™ density gradient medium (STEMCELL™ Technologies, 07851) in the bottom chamber. The Blood/RPMI mixture was then loaded on top of the Lymphoprep™ layer carefully to avoid mixing and blood entering the lower chamber. Blood to Lymphoprep™ ratios were kept to manufactures specifications. Tubes were centrifuged at 1200 RCF for 10 minutes at room temperature, with the brake on. Following centrifugation, the upper phase of the supernatant (in the upper chamber of the tube) containing the mononucleated cells and plasma was decanted into a new tube with a swift pouring action. The cell mixture was diluted in RMPI 1640 media containing 1% gentamycin to a final volume equal to four times the original blood volume processed.

For "washed-PBMCs" the above cell mixture was centrifuged at 200 RCF for 10 minutes at room temperature with the brake off. The plasma and platelets were then aspirated off with the supernatant before the pelleted PBMCs were resuspended in RMPI 1640 media containing 10% foetal bovine serum (Gibco™, 10500-064) and 1% gentamycin at a volume equal to the four times original volume of blood processed.

PBMC inflammation assay

To explore effect of conditioned media on inflammation further, peripheral blood mononucleated cells (PBMCs) were isolated and used to assess the response to inflammatory stimulation through the release of TNFα. 800 µL of the PBMC mixture, isolated above, was added to wells of a 24-well plate. Conditioned media concentrations were added in a total volume of 100 µL to each well and incubated for 1 hour at room temperature, with the respective conditioned media vehicle being used as the negative control. Following the pre-incubation period, 100 µL of *E. coli* LPS (Invitrogen™, 00-4976-93) was added in RPMI media yielding a final concentration of 1 ng/mL, or RPMI media alone as the unstimulated control. PBMC cultures were further incubated for 5 hours at 37°C at 5% CO_2. Cultures were collected and centrifuged for 20 minutes at 2000 RCF, following which the supernatants were frozen at -80°C. Culture supernatants were tested for levels level of TNFα released using ELISA (Human TNF-alpha DuoSet ELISA; R&D Systems, DY210)) as described previously.

RNA isolation from PBMCs

Following stimulation and treatment, PBMCs were pelleted with centrifugation at 200 RCF for 10 minutes without a break, and supernatant was removed. PBMC pellets were lysed with RLT buffer, 350 µL per $0.5x10^6$ to $2x10^6$ cells, from Qiagen RNeasy kit (Qiagen, 74104) and frozen at -80°C.

RNA was isolated following the manufacturer's instructions, which included a series of precipitation/elution steps using spin columns to separate the nucleic acids from other cellular material. The final step collects isolated RNA in nuclease-free water, which was then assessed for concentration and purity using a Nanodrop spectrometer. The RNA concentration was determined by the absorbance of the 260 nm wavelength of light, using Beer-Lambert Law. The purity was assessed by comparing the ratios of 280 nm and 230 nm with the 260 nm absorbance. A ratio of A_{260}/A_{280} of 1.8-2.1 is considered a pure RNA sample, with lower values indicating contamination with protein. The ratio of A_{260}/A_{230} was used to assess contamination of molecules such as guanidine thiocyanate, EDTA, detergents like Triton™ X-100 and/or phenols. Pure RNA samples should have a ratio greater than 1.5. Any samples found to be impure were reprocessed through the RNeasy kit and retested on the Nanodrop.

Complementary DNA synthesis

Isolated RNA was used as a template to synthesize complementary DNA (cDNA) for use in quantitative polymerase chain reaction analysis (qPCR). Using RevertAid RT Kit (Thermo Scientific™, K1691) and following manufacturer's instructions, equal concentrations (between 0.1 ng – 5 µg) of RNA was added to a random hexamer primer and nuclease-free water. Next, reaction buffer, RiboLock RNase inhibitor (20 U), 10 mM dNTP mix, and RevertAid RT (200 U) were added in sequence. Following a brief mix, the cDNA synthesis mixes were placed in a thermocycler, where they were incubated for 5 minutes at 25°C, followed be 60 minutes at 42°C before finally terminating the reaction by heating to 70°C for 5 minutes. cDNA samples were stored frozen at -20°C for up to 1 week or -80°C for longer.

Quantitative polymerase chain reaction

Quantitative polymerase chain reaction (qPCR) was used to assess levels of gene expression in PBMCs, using a StepOnePlus™ Real-Time PCR system, with PowerTrack™ SYBR Green PCR master mix (Thermo Scientific™, A46109). Primers for specific genes of interested (Table 2.2) were designed using the NCBI primer designer tool and purchased from Eurofins Genomics. Primer efficiencies were determined using a dilution series from a mix of cDNA samples, whereby a linear standard curve and coefficient of determination (R^2) of greater than 0.98 were required to "pass" any new primers.

To conduct the qPCR analysis, cDNA sample was added to PowerTrack™ SYBR Green PCR master mix and the forward and reverse primers in a 96-well qPCR plate. Blank reads were collected from wells containing water alone. qPCR samples were heated to 95°C for 10 minutes, followed by 40 cycles of 15 seconds at 95°C and 1 minute at 60°C.

Provided Ct values for each gene of interest were normalised to a housekeeping gene, such as GAPDH: $\Delta Ct_{Sample} = Ct_{Target} - Ct_{Reference}$. Next the ΔΔCt value was calculated by subtracting mean ΔCt of the control group from each sample: $\Delta\Delta Ct = \Delta Ct_{Sample} - \Delta Ct_{Control}$. Finally, relative gene expression (RGE) was calculated for each sample: $RGE = 2^{-\Delta\Delta Ct}$.

Table 2.2 qPCR primer information for PBMC gene expression analysis.

Gene of Interest	Sequence (5' to 3')	Tm (°C)	GC-Content
CXCL8 (IL-8)	Fwd – CTGATTTCTGCAGCTCTGT	57.3	50%
	Rev – GGGTGGAAAGGTTTGGAGTATG	60.3	50%
GAPDH	Fwd – TGCACCACCAACTGCTTAGC	59.4	55%
	Rev – GGCATGGACTGTGGTCATGAG	61.8	57%
IL6	Fwd – AGCCACTCACCTCTTCAGAAC	59.8	52%
	Rev – GCCTCTTTGCTGCTTTCACAC	59.8	52%
IL10	Fwd – GTGATGCCCCAAGCTGAGA	58.8	58%
	Rev – CACGGCCTTGCTCTTGTTTT	57.3	50%
NFKB1	Fwd – TGAGTCCTGCTCCTTCCA	56.0	56%
	Rev – GCTTCGGTGTAGCCCATT	56.0	56%
TNF	Fwd – CTGCTGCACTTTGGAGTGAT	57.3	50%
	Rev – AGATGATCTGACTGCCTGGG	59.4	55%

Rodent blood assay

Blood was collected from adult Sprague Dawley rats via cardiac puncture post-mortem into sodium heparin coated BD Vacutainer™ (BD, 367876) and used within 2 hours of collection. 800 µL of heparinised blood was added to 100 µL conditioned media or vehicle incubated for 1 hour at room temperature. Following the pre-incubation period, 100 µL of *E. coli* LPS (Invitrogen™, 00-4976-93) was added in RPMI media so that LPS had a final concentration of 50 µg/mL, or RPMI media alone as the unstimulated control. Blood cultures were further incubated for 5 hours at 37°C at 5% CO_2. Cultures were collected and centrifuged for 20 minutes at 2000 RCF, following which the supernatants were frozen at -80°C.

Blood supernatants were tested for levels of TNFα released using ELISA (Rat TNF-alpha DuoSet ELISA; R&D Systems, DY510)) following similar methods to the human ELISA described previously.

Intracellular organelle assessment

AB1190 mitochondria

AB1190 human myocytes were seeded into black-walled-clear-bottom 96 well plates at a density of 1000 cells per well and allowed to adhere overnight at 37°C with 5% CO_2 in normal culture media. Following attachment, culture media was aspirated and replaced with fresh culture media containing conditioned media or vehicle at a concentration of 10% v/v. AB1190 cells were subsequently incubated at 37°C with 5% CO_2 for either 24 or 48 hours. At the end of this incubation, treatment media was removed before cells were rinsed three times with EBSS (PAN Biotech, P04-43500). A cellular dye cocktail containing Hoechst 34580 (Invitrogen™, H21486), Calcein AM Green (Invitrogen™, C34852) and MitoTracker™ Deep Red (Invitrogen™, M22426) in EBSS for 30 minutes at 37°C with 5% CO_2. Vital dyes were imaged immediately using Revvity Operetta CLS High-Content Analysis System. MitoTracker™ Deep-Red intensity identified the mitochondrial mass with the cytoplasm region selected as the Calcein AM Green positive area.

AB1190 lysosome

AB1190 human myocytes were seeded into black-walled-clear-bottom 96 well plates at a density of 1000 cells per well and allowed to adhere overnight at 37°C with 5% CO_2 in normal culture media. Following attachment, culture media was aspirated and replaced with fresh culture media containing conditioned media or vehicle at a concentration of 10% v/v. AB1190 cells were subsequently incubated at 37°C with 5% CO_2 for either 24 or 48 hours. At the end of this incubation, treatment media was removed before cells were rinsed three times with EBSS (PAN Biotech, P04-43500). A cellular dye cocktail containing Hoechst 34580 (Invitrogen™, H21486), Calcein AM Green (Invitrogen™, C34852) and LysoTracker™ Red DND-99 (Invitrogen™, L7528) in EBSS for 30 minutes at 37°C with 5% CO_2. Vital dyes were imaged immediately using Revvity Operetta CLS High-Content Analysis System. LysoTracker™ Red DND-99 intensity identified the mitochondrial mass with the cytoplasm region selected as the Calcein AM Green positive area.

Enzyme modulation

Metalloproteinase

MP activity was determined by assessing the rate of digestion of a fluorescent substate, DQ™ Gelatin. *Bitis arietans* venom (BaV) was diluted in conditioned media or vehicle to give final venom concentrations of 4 µg/mL, 8 µg/mL, 16 µg/mL, 32 µg/mL. Then, 2 µL of 1 mg/mL DQ™ Gelatin (Invitrogen™, D12054) was added to a black-walled clear-bottom 96-well plate. Following incubation, 98 µL of BaV/conditioned media mixes were added and fluorescence (ex: 485 nm, em: 520 nm) was measured immediately using FLUOstar Omega (BMG LABTECH) plate reader. Fluorescence read outs were captured every 10 minutes for 90 minutes total. Wells containing only vehicle or conditioned media were used to normalise the baseline fluorescence.

Serine protease

SP activity was determined by assessing the rate of digestion of a fluorescent substrate, Nα-Benzoyl-L-Arginine-7-Amido-4-methylcoumarin hydrochloride (BAAM-C). BaV was diluted in conditioned media or vehicle to give final venom concentrations of 4 µg/mL, 8 µg/mL, 16 µg/mL, 32 µg/mL. Then, 2 µL of 2 nM/mL BAAM-C (Sigma Aldrich, B7260) was added to a black-walled clear-bottom 96-well plate. Following incubation, 98 µL of BaV/conditioned media mixes were added and fluorescence (ex: 355 nm, em: 460 nm) was measured immediately using FLUOstar Omega (BMG LABTECH) plate reader. Fluorescence read outs were captured every 10 minutes for 90 minutes total. Wells containing only vehicle or conditioned media were used to normalise the baseline fluorescence.

Phospholipase A2

PLA2 activity was determined by assessing the rate of digestion of a chromogenic substrate, NOB. BaV was diluted in conditioned media or vehicle to give final venom concentrations of 8 µg/mL, 16 µg/mL, 32 µg/mL, 64 µg/mL. In a clear 96-well plate, 20 µL of 3.1 mg/mL NOB (abcam, ab141769) dissolved in acetonitrile was added to 20 µL ddH_2O and 200 µL PLA2 reaction buffer (10 mM Tris-HCl, 10 mM $CaCl_2$, 100 mM NaCl). Lastly, 20 µL of BaV/conditioned media mix was added and absorbance at 425 nm was

measured immediately using FLUOstar Omega (BMG LABTECH) plate reader. Absorbance read outs were captured every 10 minutes for 120 minutes total. Wells containing only vehicle or conditioned media were used to normalise the baseline absorbance.

Myoblast differentiation

AB1190 fusion

AB1190 were seeded into 24-well TC plates and cultured until 80-90% confluence. Once at confluence, culture media was replaced with differentiation media (Skeletal Muscle Cell Growth Media (PromoCell®, C-23260), 5% horse serum (Gibco™, 26050-070), 1% Penicillin-Streptomycin (Gibco™, 15140-122)) and cultured 37°C with 5% CO_2 for 4 days. Conditioned media or vehicle was added to the differentiation media at 10% v/v at the start of the differentiation period. After four days, cells were fixed with 4% PFS for 15 minutes at room temperature, followed by three washes with PBS. Next cells were incubated for 15 minutes in permeabilization buffer (20 mM HEPES, 3 nM $MgCl_2$, 50 mM NaCl, 300 mM sucrose, 0.5% v/v Triton X-100 and 0.05% NaN_3), followed by three PBS rinses before incubating for 1 hour in blocking buffer (5% v/v foetal bovine serum, 0.05% v/v Triton X-100 in PBS) to prevent non-specific binding of antibodies. The primary antibody for pan-myosin (produced in house from mouse hybridoma cell line: A4.1025, Developmental Studies Hybridoma Bank), diluted 1:200 in blocking buffer, was incubated on the cells for 2 hours at room temperature. Following washing of slides thrice with blocking buffer (5 minutes each), an anti-mouse IgG fluorescent conjugated secondary antibody (Invitrogen, A11029), diluted 1:200, was incubated on cells for 1 hour at room temperature, in the dark. Following a series of washing in blocking buffer, 2x 5 minutes, followed by one PBS wash for 5 minutes, cells were incubated with DAPI (300 nM in PBS) for 10 minutes, before a final three PBS washes. Images were captured on Keyence BZ-X810 all-in-one fluorescence microscope. Fusion Index was determined using on open-source software called The Myotube Analyzer (github.com/SimonNoe/myotube-analyzer-app).

Development of Umbilical Cord Mesenchymal Stem Cell Adherent Conditioned Media

Generation of conditioned media – new buffers

Unless otherwise stated UCMSCs were used at passage 6-8 to produce conditioned media. Variations to the adherent conditioned media generation protocol were conducted. Following generation, conditioned media was pooled where appropriate and processed through two centrifugation cycles. Firstly, conditioned media was centrifuged at 300 RCF for 10 minutes for the removal of cells. Next, the supernatant was centrifuged at 2,000 RCF for 20 minutes to remove cellular debris and large vesicles. Conditioned media was then aliquoted and frozen at -80°C.

Phase 1: pilot of alternative buffers

UCMSCs were seeded [REDACTED] in Corning® CellBIND surface 6-well plates and allowed to adhere in culture media for 24 hours. Culture media was removed, and the cells washed 2x PBS (Gibco™ 20012-027) and once with the final generation buffer prior to addition of required generation vehicle at [REDACTED]. UCMSCs were incubated for 24 hours at 37°C with or without 5% CO_2 depending on the buffer used (Table 2.3). Conditioned supernatant was collected and processed via centrifugation.

Table 2.3 Catalogue and culture information on alternative conditioned media vehicles.

Buffer	Product Details	Generation Condition
Dulbecco's PBS (DPBS)	Gibco™, 14190-136	37°C, No supplemented CO_2
DPBS +$CaCl_2$ +$MgCl_2$	Gibco™, 14040-133	
DPBS +$CaCl_2$ +$MgCl_2$ +Glucose +Pyruvate	Gibco™, 14287-080	
Hanks' balanced salt solution (HBSS) +$CaCl_2$ +$MgCl_2$	Gibco™, 14025-092	
Earle's balanced salt solution (EBSS)	Gibco™, 14155-063	37°C, 5% supplemented CO_2
EBSS + $CaCl_2$ +$MgSO_4$	Gibco™, 14155-063	
Minimum essential media (MEM)	Gibco™, 51200-038	
ATCC basal media	ATCC, PCS-500-030™	

Phase 2: Medium scale generation of shortlisted buffers and timepoint optimisation of UCMSC conditioned media

UCMSCs were seeded [REDACTED] in Corning® CellBIND surface T75 flasks and allowed to adhere in culture media for 24 hours. Culture media was removed, and the cells washed 2x PBS (Gibco™ 20012-027) and once with the final generation buffer (EBSS with calcium and magnesium, MEM or ATCC basal media, Table 2.3) prior to addition of respective conditioning vehicle at [REDACTED]. UCMSCs were incubated for 24, 48 or 72 hours at 37°C at 5% CO_2. Conditioned supernatant was collected and processed via centrifugation.

Phase 3: Large scale generation of UCMSC conditioned media with selected buffer

EBSS with calcium and magnesium was selected as a suitable alternative for generating UCMSC ADH conditioned media. This new formulation has been termed UCMSC ADH-E. To generate a large batch of UCMSC ADH-E, UCMSCs were seeded [REDACTED] in Corning® CellBIND surface 10-layer CellStack and allowed to adhere in culture media for 24 hours. Culture media was removed, and the cells washed 3x in EBSS with calcium and magnesium (Elabscience, PB180336) prior to addition of [REDACTED] for conditioning. UCMSCs were incubated for [REDACTED] at 37°C at 5% CO_2 and the conditioned supernatant was collected and processed via centrifugation.

Storage and stability testing

The impact of different storage conditions on UCMSC conditioned media stability was assessed using a combination of content assessments (for protein, nucleic acid and EVs), bioactivity assays (whole blood inflammation) and European Pharmacopeial assays for medicinal product quality release (clarity, visual particles, and pH).

New batches of UCMSC ADH-E were generated and tested immediately for a "fresh" sample. UCMSC ADH-E was then aliquoted and placed into experimental storage conditions (-80°C frozen, 4°C refrigerated and ambient). EBSS with calcium and magnesium buffer was incubated without cells like-for-like as the UCMSC ADH-E protocol and stored in similar fashion to act as the most suitable vehicle controls and aliquots were taken for testing at different timepoints.

European pharmacopoeia 9.2 2.2.1 Clarity and degree of opalescence of liquids

According to European pharmacopoeia guidelines a solution can only be considered "clear" if it is visually the same as water or the solvent used. The guidance lays out accepted methodologies for assessing this property of a solution. One of the methods described, and the one used here, is to visually compare the solution against a series of opalescence standards. To create the reference standards, on the day of test, 4000 NTU formazin suspension (Sigma Aldrich, TURB4000-100ML) was diluted in ultrapure water (0.75 mL formazin in 49.25 mL water) to prepare a working solution at 60

NTU. Next the working solution was diluted in ultrapure water according to Table 2.4 to create four reference standards.

Table 2.4 Opalescent reference standards.

	0	**I**	**II**	**III**	**IV**
Volume of working solution (mL)	0	0.25	0.5	1.5	2.5
Volume of ultrapure water (mL)	5	4.75	4.5	3.5	2.5
Opalescent values (NTU)	0	3	6	18	30

To conduct the test, 5 mL of reference standards I – IV, along with ultrapure water (reference 0) were loaded into identical test tubes of colourless, transparent, neutral glass with a flat base and an internal diameter of 12-25 mm. The reference standards were positioned in front of black card in diffuse daylight, ensuring that reference standard I was distinguishable from water. Conditioned media was the added to a test tube and compared blind by three researchers against the reference standards. A score was awarded by each researcher based which reference standard its opalescence was most similar to, and the average score determined the clarity of the conditioned media.

European Pharmacopeia 6.0 2.9.20 Particulate contamination: visible particles

Contaminating particles within an injectable or infusion include any extraneous, mobile undissolved particles other than gas bubbles, which are unintentionally present in the solution. To assess for presence of visible particles, 5 mL of conditioned media was aliquoted into identical test tubes of colourless, transparent, neutral glass with a flat base and an internal diameter of 12-25 mm. Firstly, each test tube was positioned in front of black card, gentle swirled and then observe for 5 seconds. Next, this was repeated with the test tubes placed in front of white card. The presence or absence of particles was recorded.

European Pharmacopeia 9.0 2.2.4 Approximate pH of solutions.

The approximate pH of a solution was determined using MQuant® Supelco® pH 6.5 – 10.0 indicator strip (Merck, 109543).

Three-dimensional culture of umbilical cord mesenchymal stem cells

To prepare for a 50 mL 3D culture of UCMSCs, 0.63g Synthemax™ II microcarriers (Corning, 3781) were weighed into a sterile Erlenmeyer flask (Thermo Scientific™, 4115-0125) suspended in 10 mL of RoosterNourish™-MSC-XF culture media (RoosterBio, K82016) and equilibrated at 37°C at 5% CO_2 for at least 15 minutes. Meanwhile, UCMSCs were passaged from 2D T-flask cultures, counted and 1.125 $x10^6$ UCMSCs were added to each flask to give an initial seeding density of 5000 cells/cm^2. The culture media was adjusted to approximately 20 mL after which flasks were placed into a 37°C at 5% CO_2 incubator and left static overnight (18 hours) to allows cells to adhere to the microcarriers. The following morning, culture media was adjusted to 50 mL and 3D UCMSC cultures were placed on an orbital shaker set to 50 RPM for the remainder of their culture.

For full length cultures (4-5 days), a full media change was completed on day 2. Briefly, culture flasks were moved to the laminar flow cabinet and microcarriers were allowed to settle for 20 minutes. Culture media was carefully aspirated, so not to disturb the microcarriers, and discarded. Fresh, prewarmed culture media was added to the flasks equivalent to the volume removed. Flasks were placed back on the orbital shaker set to 50 RPM in the 37°C at 5% CO_2 incubator.

To passage a 3D culture, flasks were removed from the orbital shaker and allowed to settle for 20 minutes. culture media was aspirated carefully so not to disturb the microcarriers. Next, 50 mL of pre-warmed TrypLE™ Express dissociation enzyme solution (Gibco™, 12604-021) was added to the flasks, before placing them back on the orbital shaker set to 100 RPM in the 37°C at 5% CO_2 incubator for 20 minutes. Following the incubation, the cell suspension was aspirated and passed through a 40 µm cell strainer to remove the microcarriers. Culture flasks were rinsed with PBS, and the wash was passed

through the cell strainer as well. The filtered cell suspension was centrifuged at 300 RCF for 10 minutes and counted ahead of subsequent cultures.

Generation of conditioned media – three-dimensional culture

UCMSC 3D flasks were cultured as described above. At the end of the 5-day culture period, cells were collected and passed through a 70 µm reversible cell strainer to retain the microcarriers. The flask was rinsed with EBSS before passing over the microcarriers in the cell strainer. This was repeated twice more. Washed microcarriers were added to a fresh flask and EBSS with calcium and magnesium ([REDACTED]) was added at a volume of [REDACTED] of microcarrier surface area. Cells were incubated at 37°C at 5% CO_2 and gentle agitation (30 rpm) for [REDACTED]. Following generation, conditioned media was aspirated from the flask and passed through a 40 µm cell strainer to retain microcarriers, before subsequently processed through two centrifugation cycles. Firstly, conditioned media was centrifuged at 300 RCF for 10 minutes for the removal of cells. Next, the supernatant was centrifuged at 2,000 RCF for 20 minutes to remove cellular debris and large vesicles. Conditioned media was then aliquoted and stored at 4°C.

In Vivo Muscle Regeneration

Home Office licence and ethics statement for animal research

Animal research was conducted in accordance with 'ANIMALS (SCIENTIFIC PROCEDURES) ACT 1986' under a UK Home Office license (ref: PP8746932) at the University of Reading (establishment license: XF75DBBCB). Work under this license was reviewed and approved by the University of Reading's Animal Welfare and Ethics Review Board. Animals were received from a licensed UK breeder and maintained under standard husbandry conditions (controlled environment with *ad libitum* food and water).

Muscle regeneration model

A mouse model of muscle damage was used to test the effects of UCMSC conditioned media (UCMSC ADH-E) on muscle regeneration. C57BL/6 mice, aged 6-7 weeks old, were randomly assigned to

experimental groups. Muscle damage was induced with an intramuscular (IM) injection of 0.8 µg/g body weight *Bitis arietans* venom (BaV) (VenomTech Ltd), in 30 µL sterile normal saline, into the right tibialis anterior (TA) muscle under general anaesthesia (anaesthetised at 5% isoflurane 2 L/min oxygen, maintained at 2% isoflurane 2 L/min oxygen inhalation). UCMSC ADH-E was administered as a 5 µL/g body weight intraperitoneal (IP) bolus injection 1 hour prior to IM injection (day 0) and again daily until day 4 for both day 5 and day 15 cohorts. Further IP administration of UCMSC ADH-E followed on day 5, day 8, day 11 and day 14 to conclude the model for the day 15 cohort. Animals were euthanised via CO_2 asphyxiation with cervical dislocation, as recognised in Schedule One of the 'ANIMALS (SCIENTIFIC PROCEDURES) ACT 1986' as a humane method of killing.

Tissue harvest and processing

Following euthanasia of the mice, the damaged TA muscles were dissected from the hind limbs, weighed and immediately frozen on liquid nitrogen cooled isopentane before being stored at -80°C for further processing. Muscles were mounted in optimal cutting temperature (OCT) embedding media (Cell Path Ltd, KMA-0100-00A) ahead of cutting 15 µm cross sections from the mid-belly of the muscle using a cryo-microtome. Slides were stored at -80°C until required for further processing.

Haematoxylin and Eosin stain

Slides containing sections of TA muscles were removed from the -80°C storage and allow to equilibrate to room temperature for 15 minutes. Residual OCT embedding media was removed from the sections with a PBS wash, after which slides were immersed in Harris haematoxylin solution (Thermo Scientific™, 12627926) for 2 minutes. Subsequently washing twice with distilled water removed Harris haematoxylin solution from the slides, which were then dipped twice in acidic alcohol (70% v/v ethanol and 0.1% v/v HCl). Haematoxylin was "blued" under running tap water for 5 minutes before immersing slides in 1% w/v Eosin Y solution (Sigma Aldrich, 318906-500mL) for 2 minutes. Following a rinse with distilled water to remove excess stain, muscle sections were dehydrated with increasing concentrations of ethanol, firstly 2 minutes with 70% v/v ethanol, then 2 minutes with 90% v/v ethanol

and finally thrice with 100% ethanol for 2 minutes each. Following dehydration, sections were "cleared" with two washes, 3 minutes each, with xylene prior to mounting coverslips with DPX histological mounting media (Fisher Scientific, D/5330/05).

Picrosirius red stain

Fibrotic tissue can be identified through the use of picrosirius red staining. Slides containing sections of TA muscles were removed from the -80°C storage and allow to equilibrate to room temperature for 15 minutes. Slides were first immersed in Bouin's solution (Sigma Aldrich, SLCP7185) heated to 56°C for 15 minutes, followed by a wash in distilled water for a further 15 minutes. Next, sections were stained with picrosirius red staining solution (Abcam, ab246832) for 1 hour in the dark and subsequently washed twice with 0.5% v/v glacial acetic acid. Sections were finally dehydrated with ethanol and "cleared" with xylene prior to mounting with DPX mounting media and coverslip. The degree of fibrosis was determined via threshold analysis in ImageJ. A set area of 500 μm^2 was selected from the undamaged muscle to set a baseline for the threshold analysis tool. This value was compared to that from damaged muscles regions (200 μm^2 area) and presented as a relative percentage of picrosirius red coverage.

Immunohistochemistry stains

Slides containing sections of TA muscles were removed from the -80°C storage and allow to equilibrate to room temperature for 15 minutes, before a hydrophobic barrier was drawn around the sections to aid with the retention of staining solutions on the surface of the slide. Next, sections were washed with PBS to remove OCT embedding media residues. Tissue sections were incubated for 15 minutes in permeabilization buffer (20 mM HEPES, 3 nM $MgCl_2$, 50 mM NaCl, 300 mM sucrose, 0.5% v/v Triton X-100 and 0.05% NaN_3), followed by three PBS rinses before incubating for 1 hour in blocking buffer (5% v/v foetal bovine serum, 0.05% v/v Triton X-100 in PBS) to prevent non-specific binding of antibodies. Primary antibodies, diluted in blocking buffer (Table 2.5), were added to the slides and incubated overnight at 4°C. Following the washing of slides thrice for 10 minutes each with blocking

buffer, secondary antibodies with conjugated fluorophores (Table 2.6) were incubated on sections for 1 hour at room temperature, in the dark. Following a final series of washing in blocking buffer, three times 10 minutes, coverslips were mounted with DAKO fluorescent mounting media, containing 2.5 µg/mL DAPI.

Table 2.5 Primary antibodies used for immunohistochemical analysis of muscle.

Target	Host	Dilution	Catalogue information	Lot Number
Dystrophin	Rabbit IgG	1 in 400	Abcam, ab15277	GR3417779-1
Fibrinogen	Rabbit IgG-FITC	1 in 200	Dako, F0111	41693429
Laminin	Rabbit IgG	1 in 1000	Invitrogen, PA1-16730	ZH4441303
Myosin-3	Mouse IgG	1 in 200	Santa Cruz, sc-53091	H1518
PDGFRα	Rabbit IgG	1 in 500	Abcam, ab203491	1076010-16

Table 2.6 Secondary antibodies used for immunohistochemical analysis of muscle.

Target	Host	Dilution	Catalogue information	Lot Number
Anti-Rabbit IgG	Goat IgG – Alexa 488	1 in 200	Invitrogen, A11034	2018207
Anti-Rabbit IgG	Goat IgG – Alexa 594	1 in 200	Invitrogen, A11037	2005936
Anti-Mouse IgG	Goat IgG – Alexa 546	1 in 200	Invitrogen, A11003	1107499

Microscopy

Histology images (H&E and picrosirius stains) were capture on a Hamamatsu NanoZoomer-SQ microscope, at 40x magnification and autofocus. Collected images were stitched together for each section ready for downstream analysis. Immunohistochemistry images were captured using a Keyence BZ-X810 all-in-one fluorescence microscope. Briefly, using 2x magnification, the section of interest was located on the slide, and the image capture zone was selected. Switching to a 10x magnified objective, a sequence of images was taken until the full capture zone was collected. The focus was

adjusted by the software automatically. The appropriate filters were selected for the fluorophores present (Dapi – blue, 488 – green, 546/594 – red). The exposure time was adjusted to a suitable level for each stain; however, it remained at a consistent level within each set. The collected images were stitched together ready for each section ready for downstream analysis.

Statistical Analysis

Data was presented in the text as mean ± SEM unless otherwise stated. Statistical analysis was conducted with GraphPad Prism 10 software. Statistical analyses were performed using two-tailed t-tests and analysis of variance (ANOVA). Two-tailed t-tests were used to compare the means of two independent groups when a difference was expected but no directional hypothesis was specified. One-way or two-way ANOVA was used when more than two groups or more than one independent factor were compared, allowing assessment of main effects and interactions. Where ANOVA indicated a significant effect, appropriate post hoc multiple-comparison procedures were applied: Tukey's test was used to compare all pairs of group means; Dunnett's test was used when multiple treatment groups were compared to a single control; and Sidak's correction was used when a predefined subset of pairwise comparisons was of interest. Assumptions of normality and homogeneity of variance were checked prior to applying parametric tests, and a significance level of $\alpha=0.05$ was adopted for all analyses. Statistical significance was represented by asterixis: * p= <0.05; ** p= <0.01; *** p= <0.001; **** p= <0.0001.

Chapter 3 - Results: Characterisation of Umbilical Cord Mesenchymal Stem Cell Conditioned Media and Biological Activity.

Introduction

The International Society of Cellular Therapy (ISCT) released a position paper in 2006, outlining the minimal criteria for defining multipotent mesenchymal stem cells (MSC) (Dominici et al., 2006). In this statement the ISCT stated that for a cell to be classified as an MSC it must be capable of adhering to plastic, meet a specific expression profile of surface proteins (≥95% of MSC population must express CD105, CD73 and CD90, as measured by flow cytometry, and must lack expression (≤2% positive) of CD45, CD34, CD14 or CD11b, CD79α or CD19 and human leukocyte antigen-DR (HLA-DR)) and be capable of differentiating into three cell types under standard in vitro conditions (osteoblasts, adipocytes and chondrocytes demonstrated by staining of in vitro cell cultures) (Dominici et al., 2006). Plastic adherence has been well-described as a property of MSC (Colter et al., 2000), with cells demonstrating a spindle-shape morphology (Markov et al., 2021).

Surface antigen expression has been used extensively in immunology and haematology to rapidly identify a cell population (Dominici et al., 2006). As stated, MSCs should have positive expression of three key surface antigens. CD73, also known as ecto 5' nucleosidase and CD90, known as Thy-1, are mediators of immunostimulatory signals, such as extracellular adenosine triphosphate (ATP) (Wang et al., 2021), as well as cell-cell and cell-extracellular matrix signals (Barker and Hagood, 2009). CD105, also known as endoglin, is a component of the transforming growth factor-β receptor (TGF-βR) complex (Pierelli et al., 2001) and has a role in cell growth and differentiation. To ensure experimentation with heterogeneous population of MSCs are not contaminated by other cell types, the ISCT recommend a negative expression panel of antigens to detect common contaminating cells. These cells commonly include those from haemopoietic origin, therefore a negative expression profile for the following surface antigens give confidence of a pure MSC population: CD34, a marker for haematopoietic progenitors; CD45, a pan-leukocyte marker; CD14 or CD11b for monocytes and macrophages; and CD79α or CD19, for B cells (Dominici et al., 2006). Lastly, HLA-DR was included in the negative expression panel as it is an antigen which usually only presents itself on the surface of MSCs under stressful conditions, such as in response to IFNγ (Dominici et al., 2006).

The final criterion for MSC classification is the capability to form three mesodermal cell-lineages. ISCT states that MSCs must be shown to differentiate into osteoblasts, adipocytes, and chondrocytes (Dominici et al., 2006) which are typically identified histologically via Alizarin Red or von Kossa staining for osteogenic differentiation, Oil Red O for adipogenesis and Alcian blue or via immune-histologically detected via collagen type II for chondrogenic lineages. It was this inherent property of MSCs which first brought the attention of the regenerative medicine field (Zhou et al., 2021), however in recent years, it is the molecules MSCs release that have taken the spotlight (Liang et al., 2014). Umbilical cord-derived MSC (UCMSC) conditioned medias have had particular focus amongst researchers over recent years due to their ethical sourcing and potency (Rhatomy et al., 2023, Serafini et al., 2023, Tang et al., 2023, Wang et al., 2022, Wei et al., 2022, Zou et al., 2022), with a popular method of generating conditioned media consisting of the conditioning of culture media (Zou et al., 2022, Tang et al., 2023, Hyland et al., 2020, Ma et al., 2021) or nutrient-lacking basal media (Wei et al., 2022, Dong et al., 2020).

Micregen Ltd., the industrial collaborator of this project, have developed a method of generating conditioned media from MSCs, so far tested on adipose-derived MSCs (ADMSCs) (Mitchell et al., 2019) and amniotic fluid-derived MSCs (AFMSC) (Mellows et al., 2017), which involves the pelleting of cells in phosphate buffered saline (PBS) in a method translatable to clinical manufacture. This method uses a combination of stresses which have been shown previously to enhance conditioned medias (Ferreira et al., 2018), these being nutrient deprivation (Ishiuchi et al., 2021), hypoxia (Lambertini et al., 2018, Peltzer et al., 2020, Gnecchi et al., 2006) and a 3D environment (Bartosh et al., 2010).

In this chapter, the suitability of this novel method of generating conditioned media was explored on an alternative stem cell, UCMSCs. Firstly, the ISCT guidelines for MSC classification including plastic adherence and population doubling limits, MSC surface marker and panel tri-lineage differentiation was confirmed. Next, two methods of generating conditioned media were used to produced, one in basal media from adherent culture mimicking the literature and the other using Micregen Ltd.'s

method of pelleting cells in PBS. The resulting conditioned medias were treated as a 1x solution for the purpose of testing these drug products. Initially, the compositions of these conditioned medias were determined, beginning with the concentrations of key molecules such as proteins, nucleic acids, and extracellular vesicles.

Next the capability of these conditioned medias to alter biological systems was assessed. The specifications laid out for the test procedures and acceptance criteria for biotechnological/biological products by The International Council for Harmonisation of Technical Requirements for Pharmaceutics for Human Use (ICH) in ICH Topic Q 8B, states that a relevant and validated potency assay should be included as part of the specifications for release of a biotechnological/biological product to assess biological activity. Assessment of biological properties may include animal-based biological assays, measuring an organism's response to the product; cell culture-based assays, measuring biochemical or physiological responses at the cellular level; or biochemical assays, measuring properties such as immunological interactions or enzymatic reaction rates. The ICH define biological activity and potency as quoted below:

> *"**Biological Activity:** The specific ability or capacity of the product to achieve a defined biological effect. Potency is the quantitative measure of the biological activity."*

> *"**Potency:** The measure of the biological activity using a suitably quantitative biological assay (also called potency assay or bioassay), based on the attribute of the product which is linked to the relevant biological properties."*

Micregen Ltd. has developed biological assays specifically designed for the release of conditioned media therapeutic products. These potency assays have been developed with reliability and reproducibility in mind, making considerations such as the cell line used in these in vitro assays. Choosing cell lines, such as a cancer line, ensure that the assay can be conducted the same each time it is used. One such cell is HeLa, isolated in 1951 at John Hopkins Hospital, USA, from a cervical biopsy

of Henrietta Lack (Jones, 1997). These cells were found to grow indefinitely outside in body, within controlled culture conditions, deeming them immortal. Over the years, HeLa cells have been studied around the world, with research groups utilising them to study bioactivity of therapies from anti-cancer nanoparticles (Proboningrat et al., 2019) to small-molecule inhibitors (Madoux et al., 2010), to the effects of hypoxia preconditioning of human MSCs (Lambertini et al., 2018). After exploring several cell lines during assay development, Micregen Ltd.found that HeLa's were best suited for testing effects on cellular proliferation and migration (data not shown here).

In order to assess the effects of conditioned medias on inflammation, a new assay was developed. White blood cells such as monocytes and macrophages, play a major role in the body's immune response. Monocytes are a subset of circulating white blood cells which, in both haemostasis and inflammation, leave the bloodstream and differentiate into macrophages according to the local growth factor signals (Shi and Pamer, 2011). Monocytes and macrophages are central in the immune system and orchestrating inflammation (Jakubzick et al., 2017). They make up 5-10% of all blood immune cells and have a life span of 1-3 days (Austermann et al., 2022). During inflammation, monocyte activation and macrophage polarisation begins with the recognition of pathogens or tissue damage through pattern recognition receptors (PRRs) (Medzhitov and Janeway, 2000). PRRs recognise two classes of molecules, these being pathogen-associated molecular patterns (PAMPs) and damage-associated molecular patterns (DAMPs), and are divided between four families, the cytoplasmic proteins; Retinoic acid-inducible gene (RIG)-I-like receptors (RLRs) and NOD-like receptors (NLRs) and the transmembrane receptors Toll-like receptors (TLRs) and C-type lection receptors (CLRs) (Austermann et al., 2022). Out of these, TLRs are the most extensively characterised, of which there are 10 identified members in humans (Kawai and Akira, 2010). These receptors are involved in the early sensing of infection, initiating the inflammatory response through pathways including Myeloid differentiation primary response gene (88) (MyD88)-dependant pathway resulting in activation of nuclear factor kappa-light-chain-enhancer of activated B-cells (NF-κB), in turn initiating transcription of inflammatory cytokines such as tumour necrosis factor-alpha (TNFα), interleukin-6 (IL-6) and

interleukin-1 beta (IL-1β) (Austermann et al., 2022). These cytokines are released and can be in the circulation as biomarkers of the inflammatory response, and can be replicated ex vivo (Segre and Fullerton, 2016).

In this chapter, the initial proof-of-concept conditioned media work was conducted on a UCMSC donor procured from the American Type Culture Collection (ATCC) before being repeated on a second research-use only UCMSC procured from RoosterBio®. With this second donor, further characterisation was also conducted to identify the specific proteins, and nucleic acids present in the conditioned media using techniques such as mass spectrometry and RNA sequencing.

Results

Establishing culture characteristics of umbilical cord mesenchymal stem cells

The International Society of Cellular Therapy MSC criteria 1: plastic adherent culture, growth, and viability

With the culture of any new MSC population, it was important to determine the baseline culture characteristics of the cells, such as, the growth rate, expansion capabilities, and morphology of UCMSCs. Additionally, in relation to developing a translatable therapeutic, understanding these attributes can inform on manufacturing strategies (Pakzad et al., 2022). Therefore, UCMSCs were cultured on standard tissue culture plastic continuously from first revival to an advanced population doubling age and population doubling time was tracked at each passage, n=1 (Figure 3.1A). UCMSCs cultured over 60 days for approximately 10 to 12 passages, had a relatively linear growth phase for the initial 8-9 passages. However, after 43 days in culture the growth rate began to slow over the final 3 passages. Cell viability was measured at each passage, n=1-7 (Figure 3.1B), which unlike population double time, remained constant above 85.0% throughout culture. X-gal staining revealed that the increase in population doubling time correlated with an increase in cellular senescence and a change in morphology (Figure 3.1C).

The International Society of Cellular Therapy MSC criteria 2: surface antigen panel assessment by flow cytometry

To ensure UCMSCs conformed to the accepted criteria for MSCs, the positive expression MSC surface markers must be detected, as well as the lack of surface markers not attributed to MSCs but to common contaminating cell types. Flow cytometry analysis was carried out to assess the expression profile of positive (CD73; CD90; CD105) and negative (CD34; CD45; CD19; CD14; HLA-DR) MSC markers, n=1, 50,000 cell events (Figure 3.2). There was good to strong expression of the three positive markers, CD73 at 98.6%, CD90 at 42.7% and CD105 at 92.7%. The negative panel of markers had very low levels of expression, CD34 at 5.25%,

CD45 at 0.93%, CD19 at 1.1%, CD14 at 1.41% and HLA-DR at 1.7%. These expression levels within reasonable doubt conformed with the accepted expression levels for the cells to be considered as

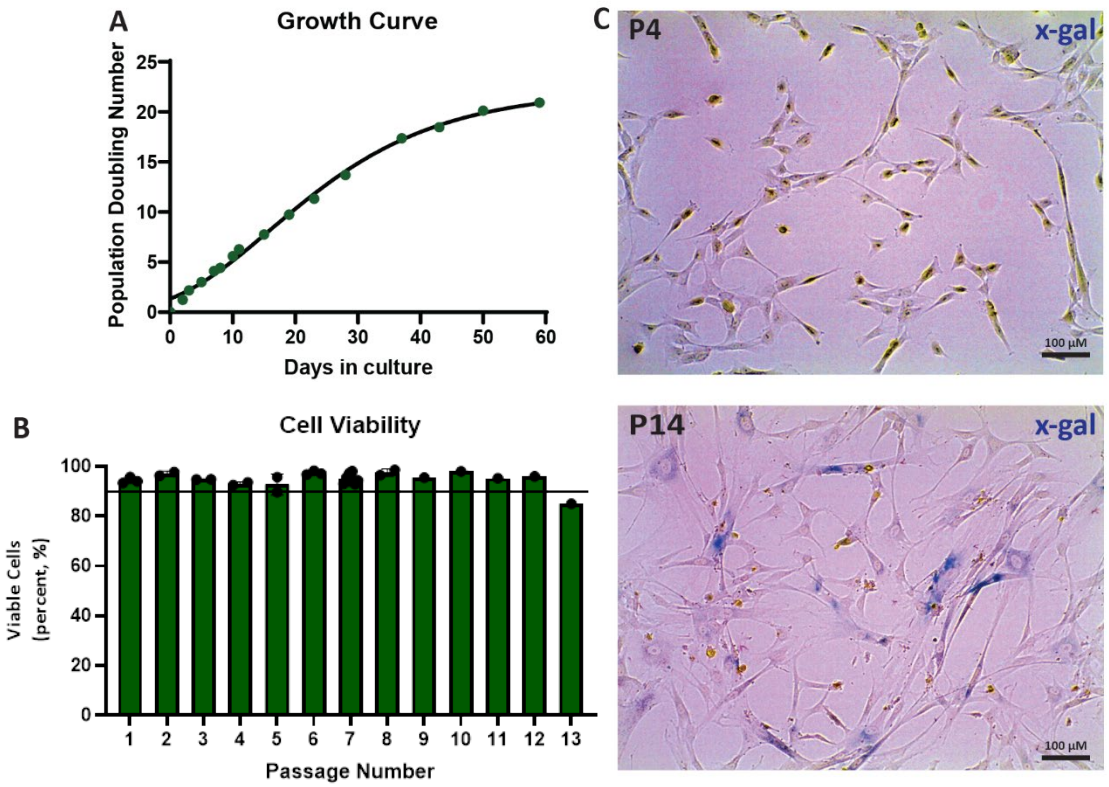

Figure 3.1 The International Society of Cellular Therapy MSC criteria 1: Growth and viability of UCMSCs.

(A) *Tracking of population doubling number of UCMSCs over 60 days of culture post revival from cryopreservation (n=1).* ***(B)*** *Cell viability of UCMSC measured using Trypan Blue exclusion over the duration of 13 passages, with a line indicating 90% viability (n=1 to 7).* ***(C)*** *UCMSCs at passage 4 (top) and passage 14 (bottom) following x-gal straining for β-galactosidase activity at pH 6.0.*

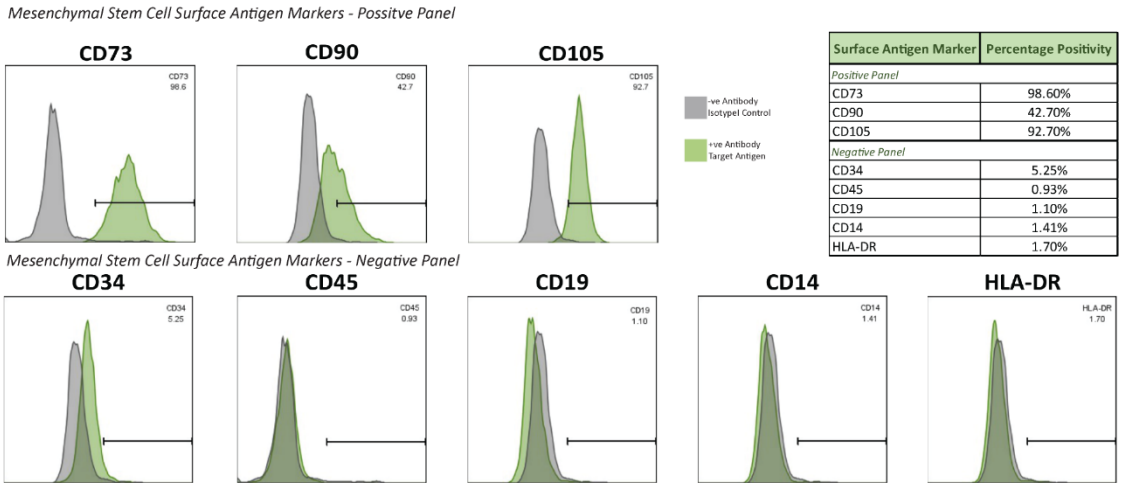

Surface Antigen Marker	Percentage Positivity
Positive Panel	
CD73	98.60%
CD90	42.70%
CD105	92.70%
Negative Panel	
CD34	5.25%
CD45	0.93%
CD19	1.10%
CD14	1.41%
HLA-DR	1.70%

Figure 3.2 The International Society of Cellular Therapy MSC criteria 2: Surface antigen panel.

Flow cytometry profiling of UCMSCs confirmed cells had positive expression of the CD73, CD90 and CD105 which have been internationally recognised as positive surface antigens for MSCs. Common contaminating cells, often present following MSC isolation can be identified by the surface antigen CD34, CD45, CD19, CD14 and HLA-DR which have been added as a panel of negatively expressed markers for MSCs. The UCMSC used to generated conditioned media for this study were confirmed to have negative expression for these five antigens. n=1, 50,000 cell events

The International Society of Cellular Therapy MSC criteria 3: trilineage differentiation proven by staining of in vitro culture.

In addition to this panel of surface markers, for a cell to be recognised as an MSC, they must show an ability to differentiate into a variety of cell types. Cultured UCMSCs (Figure 3.3A) were successfully differentiated into three mesodermal cell lineages, these being, adipogenic (Figure 3.3B), osteogenic (Figure 3.3C) and chondrogenic (Figure 3.3D), staining positive with Oil Red O, Alizarin Red S and Alcian Blue, respectively.

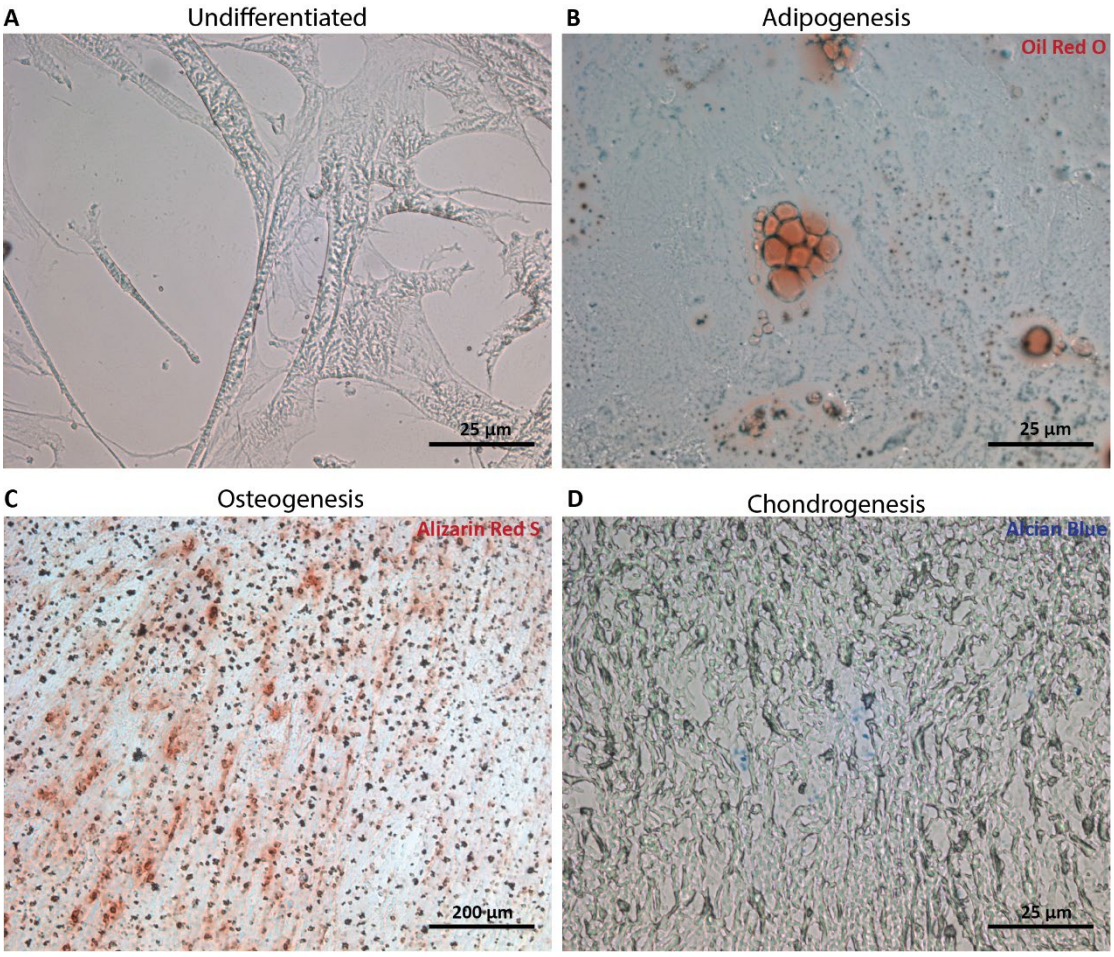

Figure 3.3 The International Society of Cellular Therapy MSC criteria 3: Tri-lineage differentiation.

Requirements for MSC laid out by the ISCT specify that MSCs should be proven to differentiate into three cell types. ***(A)*** *represents an undifferentiated UCMSC, showing the standard fibroblast-like morphology taken at 40x magnification.* ***(B)*** *Oil Red O positive lipid droplets present in UCMSCs following adipogenic differentiation taken at 40x magnification.* ***(C)*** *Positive straining with Alizarin Red S identifies calcium deposits following osteogenic differentiation of UCMSCs taken at 4x magnification.* ***(D)*** *Cross section of UCMSC chondrogenesis pellet stained with Alcian Blue for the glycosaminoglycans secreted by chondrocytes take at 40x magnification.*

Generating conditioned media from umbilical cord mesenchymal stem cells

In order to ensure the UCMSCs used for conditioned media generation were as healthy as possible, a cell bank was created at passage 3. When making conditioned media, UCMSCs were used between passage 5 and passage 8, with a minimum time in culture of two passages after revival from cryopreservation.

Conditioned media is multifactorial in action, comprising of components such as proteins, nucleic acids, and extracellular vesicles (EVs). Here, UCMSC conditioned media was generated with two methods, UCMSC PEL being pelleted cells in a PBS solution and UCMSC ADH being 2D adherent cells covered by basal media. Primary characterisation of conditioned media was conducted to determine total protein and nucleic acid concentrations, and extracellular vesicle profile within each conditioned media.

Conditioned media composition - protein

Total protein quantification revealed the UCMSC PEL conditioned media had an average protein concentration of 14.64 ±2.76 µg/mL SEM and UCMSC ADH conditioned media of 20.12 ±1.24 µg/mL SEM, which was not significantly different, p=0.1441, n=3 biological replicates (Figure 3.4A). Taking time to reflect on the difference in the generation methods used, one of the many differences is the ratio of cells to the volume conditioned. Reassessing this data to consider the concentration of protein secreted from equal numbers of cells (Figure 3.4B) revealed a very different picture. UCMSC ADH conditioned media had approximately 14x greater secreted protein than UCMSC PEL at 80.49 ±4.96 µg/10^6 cells SEM over 5.86 ±1.10 µg/10^6 cells SEM which was statistically significant, n=3 biological replicates (p=<0.0001). Further investigation into the protein content of UCMSC conditioned media through the use of gel electrophoresis for size separation and silver staining visualisation, revealed both conditioned medias had a broad size range of proteins (Figure 3.4C). The two conditioned medias shared many similar bands at approximately 120 and 110 kDa as well as three bands at 55 kDa and two bands at 30 and 28 kDa. However, there were discernible differences in intensity between the

two generation methods. Equally, there were clear bands present in UCMSC PEL that were not found in UCMSC ADH, of note bands located between 80 and 60 kDa, 40 kDa and several between 25 and 10 kDa. Bands at 100 kDa, 50 kDa and 20 kDa were present in UCMSC ADH conditioned media and not UCMSC PEL. Overall, the silver staining demonstrated that in equal volumes of conditioned media, UCMSC PEL had a greater overall intensity of all proteins compared to UCMSC ADH.

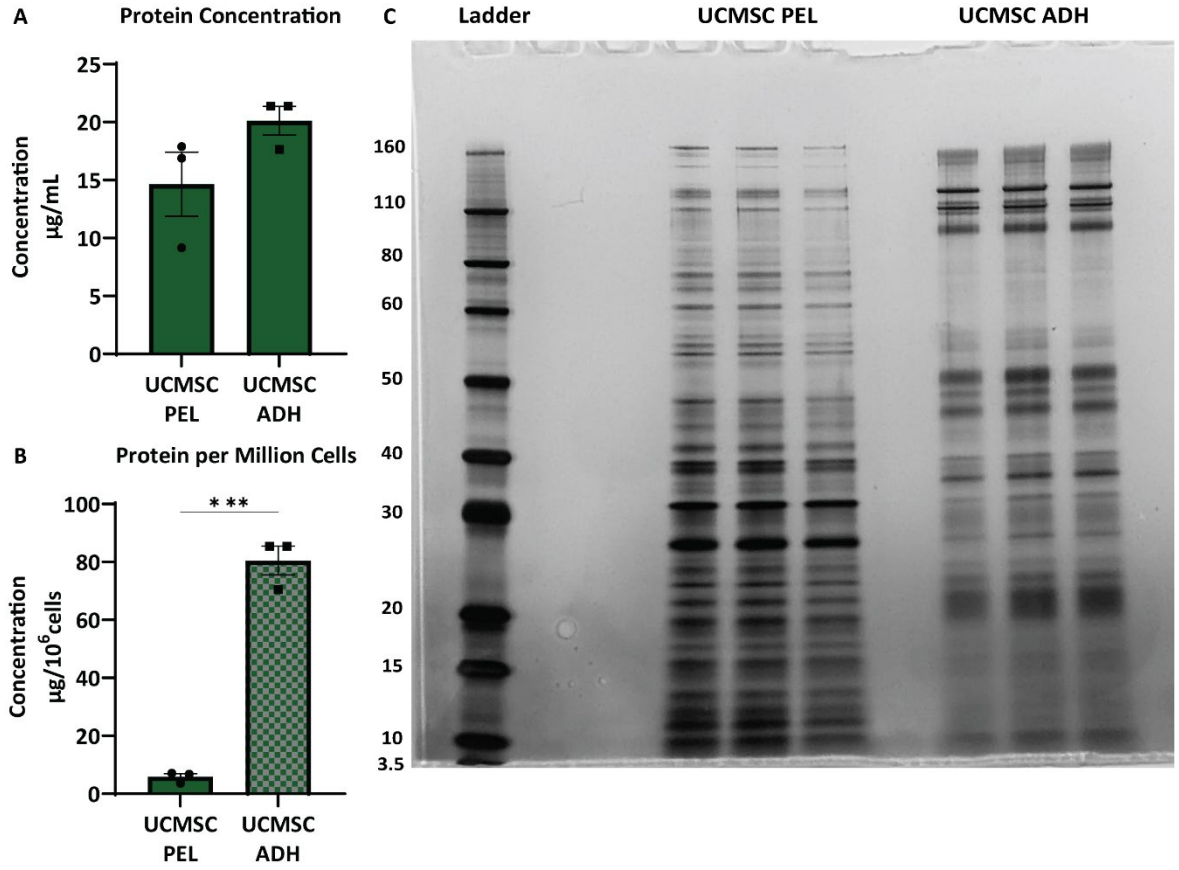

Figure 3.4 Protein content of UCMSC conditioned media.

(A) *Protein concentration of UCMSC PEL and UCMSC ADH conditioned media and* ***(B)*** *normalised secreted protein by number of cells used in production. Bars represent the mean of three batches (n=3). Statistical significance from t-test is represented by asterixis: * p= <0.05; ** p= <0.01; *** p= <0.001; **** p= <0.0001.* ***(C)*** *Silver stained SDS-page of UCMSC conditioned media.*

Conditioned media composition – Nucleic acids

In addition to protein, nucleic acids (specifically RNAs) are commonly secreted by stem cells (Vaiasicca et al., 2024). Total nucleic acid quantification revealed the average concentration of nucleic acid for UCSMC PEL had significantly more nucleic acids than UCMSC ADH (Figure 3.5A), 12.24 ±1.42 µg/mL SEM and 5.95 ±0.33 µg/mL SEM respectively, p=0.0193, n=3 biological replicates. Assessing the level of nucleic acid in relation to the number of cells used to generate the conditioned media (Figure 3.5B), UCMSC ADH conditioned media had significantly more nucleic acids, 23.79 ±1.34 µg/10^6 cells SEM, released per million cells than UCMSC PEL, 4.90 ±0.57 µg/10^6 cells SEM, p=<0.0001, n=3 biological replicates.

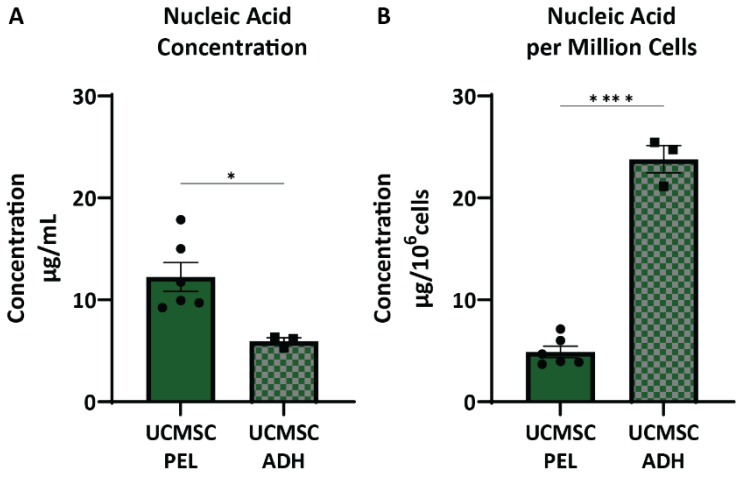

Figure 3.5 Nucleic acid content of UCMSC conditioned media.

(A) *Nucleic acid concentration of UCMSC PEL and UCMSC ADH conditioned media and* ***(B)*** *normalised secreted nucleic acid by number of cells used in production. Bars represent the mean of three batches (n=3-6). Statistical significance from t-test is represented by asterixis: * p= <0.05; ** p= <0.01; *** p= <0.001; **** p= <0.0001.*

Conditioned media composition – extracellular vesicles

The third component to be assessed was the extracellular vesicles (EVs). These nanoparticles are released from cells and are known to carry protein and RNA cargos. UCMSC PEL conditioned media had a mean particle concentration of 9.563 ±0.47 x10^8 particles/mL SEM and UCMSC ADH had a mean

concentration of 4.05 ±0.08 x10^8 particles/mL SEM (Figure 3.6A). The concentration EVs in UCMSC PEL was significantly higher than UCMSC ADH, p=0.0046, n=3 biological replicates. However, when compared as the number of particles released per million cells (Figure 3.6B), the significant difference was reversed. UCMSC ADH had approximately 4x greater EV particles than UCMSC PEL at 16.20 ± 3.37 x10^8 particles/10^6 cells SEM and 3.82 ±0.18 x10^8 particles/10^6 cells SEM, respectively. This difference was statistically significant (p=0.0216, n=3 biological replicates). Representative plots from nanoparticle tracking analysis (NTA) display the distribution of particle sizes. UCMSC PEL conditioned media (Figure 3.6C) had a more uniform size of particles between 100 nm and 200 nm, whereas UCMSC ADH (Figure 3.6D) showed a greater heterogeneous size of particle, ranging from 60 nm to

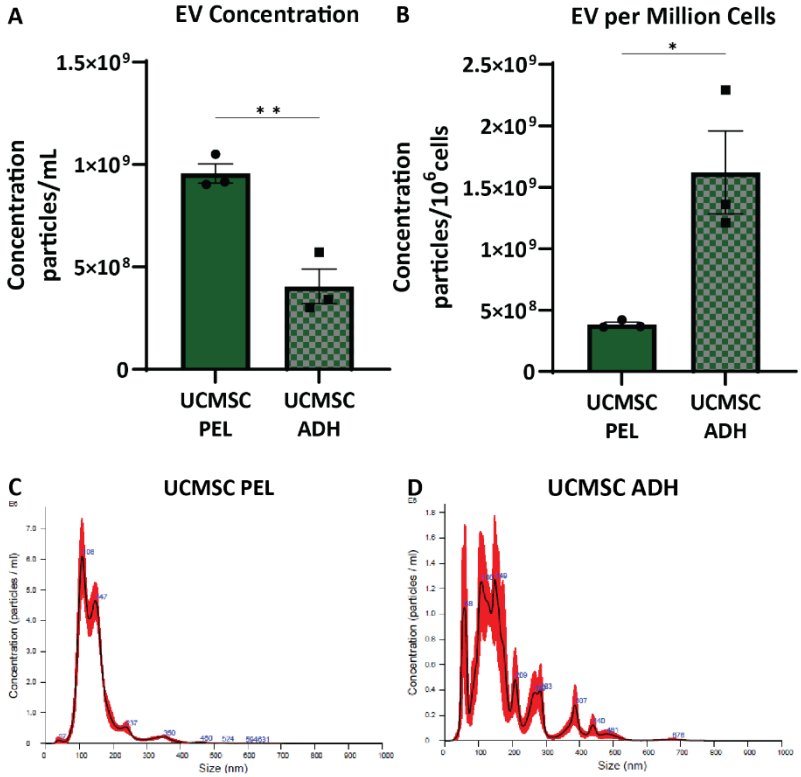

Figure 3.6 Extracellular vesicle component of UCMSC conditioned media.

(A) *Concentration extracellular vesicles from UCMSC PEL and UCMSC ADH conditioned media and* ***(B)*** *normalised extracellular vesicles to cells used in production. Bars represent the mean of three batches (n=3). Statistical significance from t-test is represented by asterixis: * p= <0.05; ** p= <0.01; *** p= <0.001; **** p= <0.0001.* ***(C, D)*** *representative nanoparticle tracking plots for UCMSC PEL and UCMSC ADH displaying the distribution of detected particles.*

500 nm. It is worth noting that the majority of particles analysed in UCMSC samples were still within the range of 100 nm and 200 nm, similar to UCMSC PEL conditioned media.

Testing bioactivity of umbilical cord-derived mesenchymal stem cell conditioned media on product release potency assays

UCMSC conditioned media potency - cellular proliferation assay.

To begin to assess the bioactivity and therapeutic potential of UCMSC conditioned media, both UCMSC PEL and UCMSC ADH were first tested for promotion of cellular proliferation. Both UCMSC PEL (Figure 3.7A) and UCMSC ADH (Figure 3.7B) conditioned medias were able to significantly increase HeLa cell number over the respective vehicle control at the higher concentrations. UCMSC PEL had a mean normalised proliferation rate with a 10% v/v treatment of 0.125x increasing cell numbers to 138.0 ±3.61% SEM; 0.25x to 161.3 ±14.75% SEM; 0.5x to 174.3 ±20.43% SEM; and 1x to 193.0 ±14.57% SEM compared to the vehicle control at 100.0%. One-way ANOVA with Dunnett's post testing, revealed that concentrations of 0.25x, 0.5x and 1x had a statistically significant increase in cell proliferation

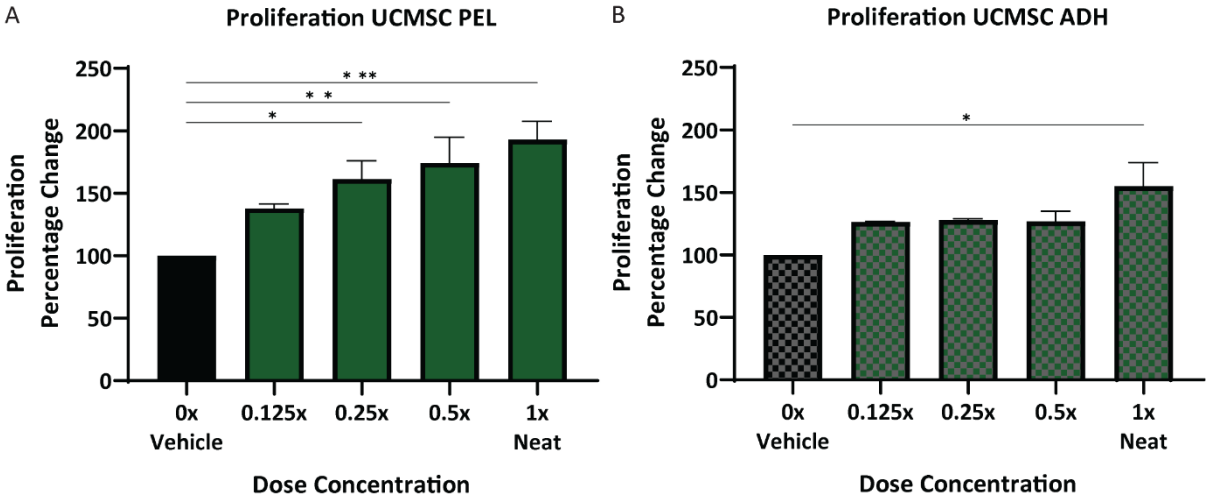

Figure 3.7 Bioactivity assessment of UCMSC conditioned media on cell proliferation.

*The effect of **(A)** UCMSC PEL and **(B)** UCMSC ADH conditioned media on HeLa cell proliferation. Bars represent the average of three repeat experiments (n=3). Statistical significance from ANOVA with Dunnett's post testing against the 0x vehicle group is represented by asterixis: * p= <0.05; ** p= <0.01; *** p= <0.001; **** p= <0.0001.*

compared to the vehicle control (p=0.0309, p=0.0088, and p=0.0008 respectively, n=3 biological replicates).

UCMSC ADH had a mean normalised proliferation rate at 10% v/v of 0.125x of 126.5 ±0.50% SEM; 0.25x of 128.0 ±1.00% SEM; 0.5x of 127.0 ±8.00% SEM; and 1x of 155.0 ±18.90% SEM compared to the vehicle control at 100.0%. One-way ANOVA with Dunnett's post testing, revealed that only a 1x treatment had a statistically significant increase in cell proliferation compared to the vehicle control (p=0.0411, n=3 biological replicates).

UCMSC conditioned media potency - cellular migration assay

Next, the two conditioned medias were tested for action on cell migration. Here, UCMSC PEL treatment (Figure 3.8A & B) had a mean normalised migration rate of 266.0 ±9.03% SEM compared to the vehicle control at 100.2 ±19.0% SEM. This was statistically significant when compared using an unpaired t-test at p=<0.0001, n=6 technical replicates. However, UCMSC ADH treatment (Figure 3.8C & D) had a mean normalised migration rate of 105.2 ±3.16% SEM which was not statistically different to the vehicle control at 100.0 ±9.71% SEM (unpaired t-test at p=0.6238, n=6 technical replicates).

UCMSC conditioned media potency - LPS-induced inflammatory response assay.

To identify any therapeutic activity on inflammation, a multicellular assay using freshly isolated human whole blood was established. Whole blood contains circulating leukocytes, which are integral to both the innate and humoral immune response, which mount an inflammatory and cellular response to damage or pathogens. Here, *E. coli* lipopolysaccharide (LPS), a well-documented pathogen-associated molecular pattern (PAMP) (Park and Lee, 2013) was used to initiate an inflammatory event with the intention of modifying this response with UCMSC conditioned media. Following stimulation with LPS, one of the ways leukocytes responded is with a release of cytokines and chemokines which can be quantified. An important and routinely assessed marker of the inflammatory response is tumour

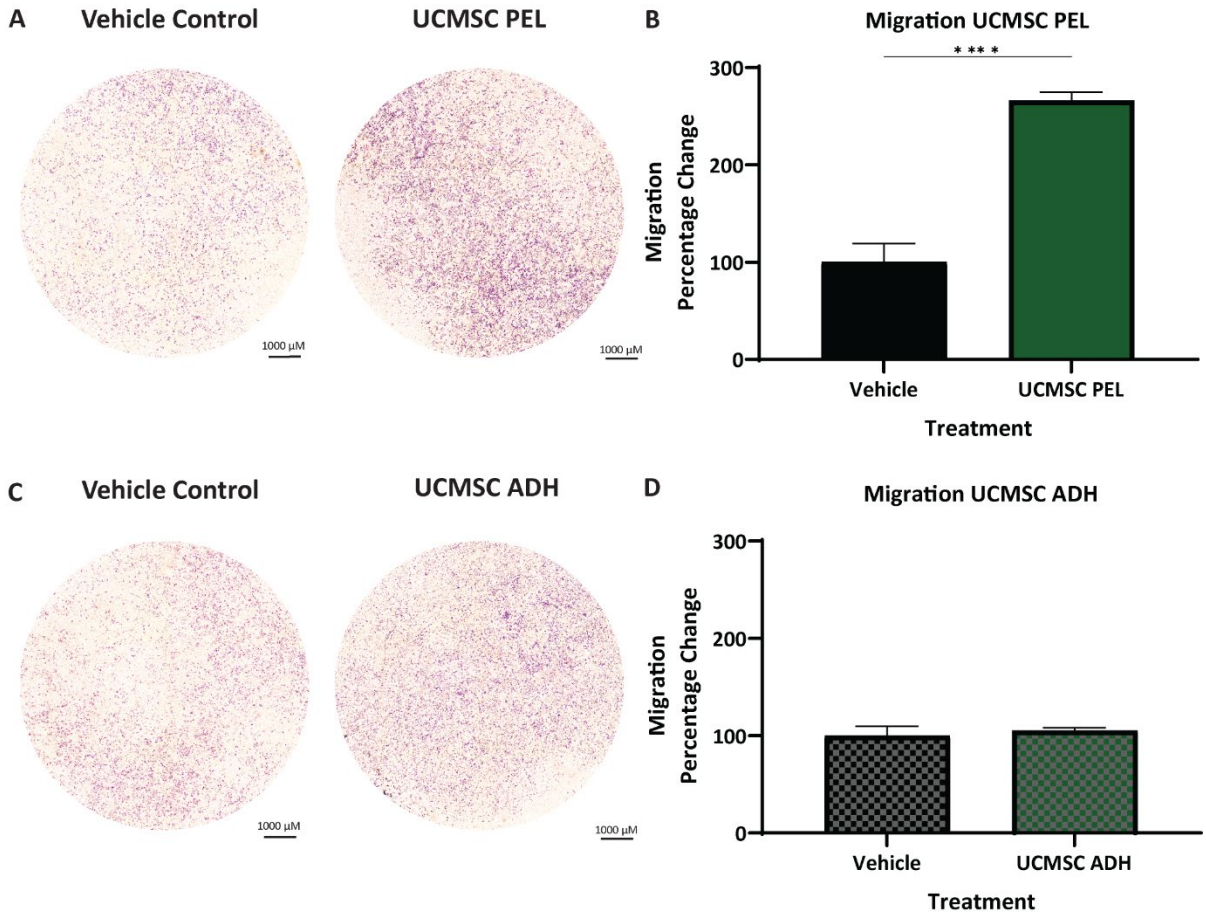

Figure 3.8 Bioactivity assessment of UCMSC conditioned media on cell migration.

The effect of ***(A, B)*** *UCMSC PEL and* ***(C, D)*** *UCMSC ADH conditioned media on HeLa cell migration. Bars represent average of average of six technical repeats (n=6). Statistical significance from t-test is represented by asterixis: * p= <0.05; ** p= <0.01; *** p= <0.001; **** p= <0.0001.* ***(A, C)*** *Representative images of conditioned media (right) or vehicle (left) treated transwell membranes following crystal violet staining.*

necrosis factor alpha (TNFα), which is strongly expressed following LPS stimulation. This assay uses the level of TNFα to evaluate the impact of UCMSC conditioned media on an inflammatory scenario.

As before, four concentrations of UCMSC conditioned medias were tested, and for both UCMSC PEL and UCMSC ADH all four concentrations significantly reduced TNFα levels following LPS stimulation. Results from the first blood donor found UCMSC PEL conditioned media decreased TNFα from 272.8 ±13.26 pg/mL (100.0 ±4.86%) SEM to 203.9 ±9.54 pg/mL (74.7 ±3.50%) SEM with 0.125x (p=0.0009), 174.5 ±8.37 pg/mL (64.0 ±3.07%) SEM with 0.25x (p=<0.0001), 140.3 ±6.75 pg/mL (51.4% ±2.48%) SEM

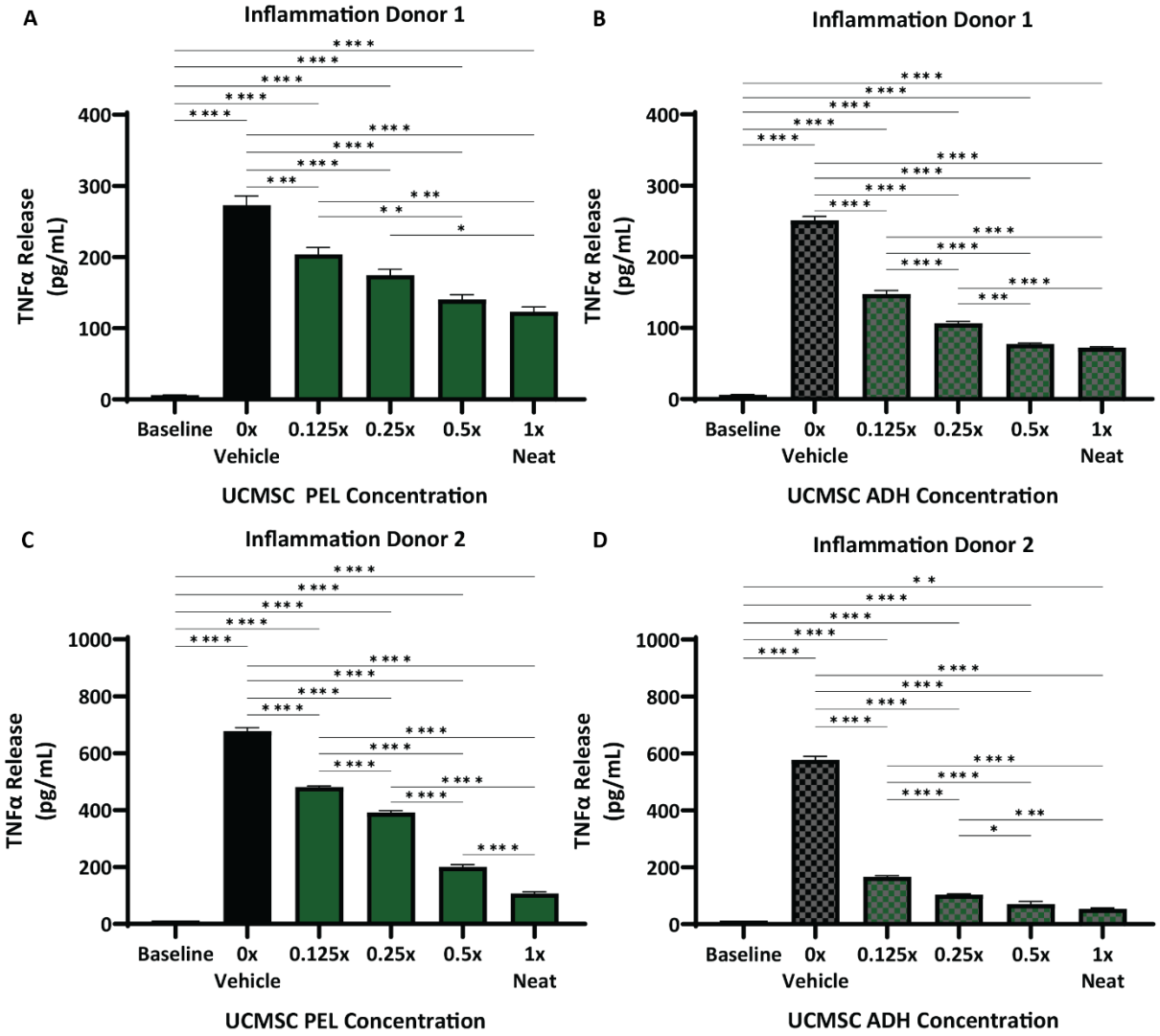

Figure 3.9 Bioactivity assessment of UCMSC conditioned media on inflammation.

*The effect of **(A, C)** UCMSC PEL and **(B, D)** UCMSC ADH conditioned media on TNFα levels release from human blood following LPS stress. (**A, B) and (C, D)** are paired from individual donor. Bars represent averages of 4 technical replicates (n=4). Statistical significance from ANOVA with Tukey's post testing is represented by asterixis: * p= <0.05; ** p= <0.01; *** p= <0.001; **** p= <0.0001.*

with 0.5x (p=<0.0001) and 123.5 ±6.52 pg/mL (45.3% ±2.39%) SEM with 1x (p=<0.0001) at 10% v/v treatment, n=4 technical replicates (Figure 3.9A). UCMSC ADH conditioned media had a greater overall decrease in TNFα levels, decreasing from 251.2 ±5.24 pg/mL (100.0 +2.08%) SEM with the vehicle to 147.5 ±4.92 pg/mL (58.7 ±1.96%) SEM with the lowest 0.125x treatment (p=<0.0001). TNFα was further reduced to 106.7 ±2.61 pg/mL (42.5 ±1.04%) SEM with 0.25x (p=<0.0001), 77.4 ±1.21 pg/mL

(30.8 ±0.48%) SEM with 0.5x (p=<0.0001) and 72.2 ±1.02 pg/mL (28.7 ±0.41%) SEM with the highest 1x concentration (p=<0.0001) at 10% v/v treatment, n=4 technical replicates (Figure 3.9B).

Similar results were found with a second donor. UCMSC PEL conditioned media decreased TNFα levels from the 677.5 ±12.21 pg/mL (100.0 ±1.80%) SEM of the vehicle to 481.3 ±3.40 pg/mL (71.0 ±0.50%) SEM with 0.125x (p=<0.0001), 391.4 ±6.96 pg/mL (57.8 ±1.03%) SEM with 0.25x (p=<0.0001), 200.8 ±8.06 pg/mL (26.6 ±1.19%) SEM with 0.5x (p=<0.0001) and 106.8 ±5.85 pg/mL (15.8 ±0.86%) SEM with 1x (p=<0.0001) at 10% v/v treatment, n=4 technical replicates (Figure 3.9C). As before, UCMSC ADH conditioned media had an overall greater reduction in TNFα level across all concentrations, with the lowest concentration of 0.125x already reducing the levels to 166.9 ±3.86 pg/mL (28.9 ±0.67%) (p=<0.0001) from 578.2 ±11.45 pg/mL (100.0 ±1.98%) SEM of the normalised vehicle control (Figure 3.9D). 0.25x further decreased TNFα levels to 103.5 ±2.92 pg/mL (17.9 ±0.51%) SEM (p=<0.0001), 0.5x to 70.4 ±9.63 pg/mL (12.2 ±1.67%) SEM (p=<0.0001) and finally 1x treatment of UCMSC ADH conditioned reduced TNFα to 54.7 ±2.80 pg/mL (9.5 ±0.48%) SEM (p=<0.0001), n=4 technical replicates.

Human cytokine/chemokine multiplex array

To further explore the effects of the UCMSC conditioned medias on inflammation further, plasma supernatants from the whole blood assays were profiled on a human cytokine/chemokine multiplex array to assess levels in forty-eight inflammation-associated markers, n=4 technical replicates (Tables 3.1 and 3.2). Out of these, seven cytokine/chemokines were not detectable in any sample (IL-2, IL-3, IL-4, IL-5, IL-7, IL-17A, and VEGF) and one (RANTES) was above the saturation limit of the array.

Although detectable, fourteen cytokine/chemokines (Fractalkine, GM-CSF, IFN-α2, IL-9, IL-12p70, IL-13, IL-15, IL-17E/IL-25, IL-17F, IL-22, IL-27, M-CSF, TGFα, and TNFβ) had no significant changes following stimulation with LPS compared against unstimulated baseline, nor were they altered by the addition of either UCMSC PEL (Table 3.1) or UCMSC ADH (Table 3.2) conditioned media treatments (Figure 3.10). Out of the remaining twenty-six markers, UCMSC PEL significantly decreased fourteen

(Eotaxin, FLT-3L, G-CSF, IFNγ, IL-1β, IL-6, IL-12p40, IL-18, IP-10, MCP-3, MDC, MIG/CXCL9, MIP-1α, and TNFα) and significantly increased seven (EGF, FGF-2, GROα, IL-1α, IL-10, PDGF-AA, PDGF-AB/BB). On the other hand, UCMSC ADH significantly decreased twelve (IFNγ, IL-1α, IL1β, IL-1RA, IL-6, IL-12p40, IL-18, IP-10, MDC, MIG/CXCL9, MIP-1α, and TNFα) and significantly increased nine (EGF, G-CSF, GROα, IL-8, IL-10, MCP-1, MCP-3, PDGF-AA, and PDGF-AB/BB) compared to the LPS stimulated vehicle controls. Across the board, cytokines/chemokines modified by both conditioned medias were often more greatly altered by UCMSC ADH conditioned media than UCMSC PEL conditioned, and often statistically significant changes were reached with lower concentrations of UCMSC ADH treatment

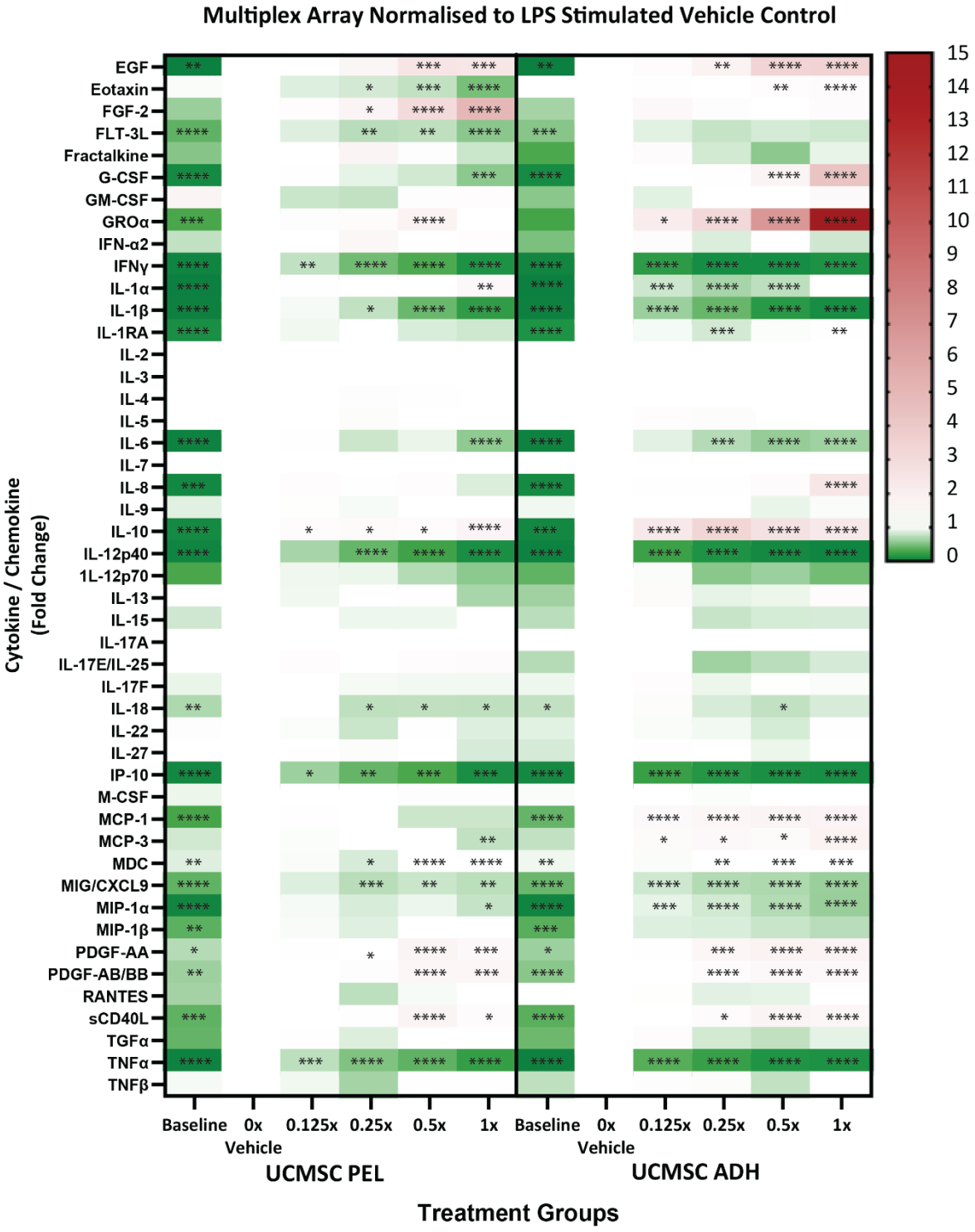

Figure 3.10 Cytokine/Chemokine release profile following UCMSC conditioned treatment of inflammation.

The effect of UCMSC PEL (left) and UCMSC ADH (right) conditioned media on levels of forty-eight markers of inflammation from LPS stimulated human blood. Heatmap depicts normalised levels where green represents values less than LPS stimulated vehicle controls, *[Continues on next page]*

Figure 3.10 continued: *white represents no change and red represents values greater than LPS stimulated vehicle controls (n=4). Statistical significance from ANOVA with Dunnett's post testing against the 0x vehicle group is represented by asterixis: * p= <0.05; ** p= <0.01; *** p= <0.001; **** p= <0.0001.*

Table 3.1 Results of multiplex array for UCMSC PEL conditioned media on inflammation.

A summary of the mean ±SEM levels of release of forty-eight cytokines and chemokines following UCMSC PEL conditioned media treatment of human blood after LPS stimulations.

Cytokine/Chemokine		Vehicle Control	Vehicle Control + LPS	0.125x UCMSC PEL + LPS	0.25x UCMSC PEL + LPS	0.5x UCMSC PEL + LPS	1x UCMSC PEL + LPS
EGF	pg/mL	0.0 ± 0.00	3.51 ± 0.04	3.61 ± 0.16	5.72 ± 1.19	8.64 ± 0.59	8.49 ± 0.37
Eotaxin	pg/mL	12.6 ± 0.22	12.95 ± 0.47	11.24 ± 0.42	10.67 ± 0.52	9.77 ± 0.32	6.13 ± 0.52
FGF-2	pg/mL	12.2 ± 3.33	20.23 ± 2.74	25.48 ± 4.24	34.16 ± 3.64	60.25 ± 2.99	100.09 ± 1.64
FLT-3L	pg/mL	0.6 ± 0.01	1.49 ± 0.05	1.30 ± 0.05	1.08 ± 0.06	1.11 ± 0.10	0.81 ± 0.04
Fractalkine	pg/mL	4.5 ± 0.84	8.60 ± 1.22	9.12 ± 3.91	14.52 ± 5.93	10.12 ± 2.31	6.81 ± 2.80
G-CSF	pg/mL	4.4 ± 0.33	66.63 ± 1.65	74.02 ± 0.85	59.96 ± 7.76	54.13 ± 2.28	36.88 ± 1.66
GM-CSF	pg/mL	2.3 ± 0.55	1.38 ± 0.27	1.08 ± 0.17	1.04 ± 0.44	1.63 ± 0.31	1.73 ± 0.39
GROα	pg/mL	2.8 ± 0.08	9.64 ± 0.35	11.67 ± 0.45	12.44 ± 1.56	17.86 ± 0.72	10.39 ± 0.61
IFN-α2	pg/mL	1.6 ± 0.06	2.16 ± 0.23	2.19 ± 0.36	3.45 ± 0.55	2.15 ± 0.08	2.73 ± 0.61
IFNγ	pg/mL	0.2 ± 0.03	6.35 ± 0.33	4.81 ± 0.25	2.84 ± 0.49	1.96 ± 0.10	0.79 ± 0.04
IL-1α	pg/mL	0.0 ± 0.00	120.54 ± 0.59	139.36 ± 4.02	120.22 ± 21.36	119.16 ± 3.68	180.15 ± 8.88
IL-1β	pg/mL	2.2 ± 0.22	993.93 ± 36.55	943.91 ± 19.67	749.90 ± 87.17	423.56 ± 21.61	198.67 ± 15.85
IL-1RA	pg/mL	2.2 ± 0.18	22.69 ± 0.63	21.15 ± 0.22	22.88 ± 3.03	19.37 ± 0.93	18.31 ± 1.07
IL-2	pg/mL	0.0 ± 0.00	0.00 ± 0.00	0.00 ± 0.00	0.00 ± 0.00	0.00 ± 0.00	0.00 ± 0.00
IL-3	pg/mL	0.0 ± 0.00	0.00 ± 0.00	0.00 ± 0.00	0.00 ± 0.00	0.00 ± 0.00	0.00 ± 0.00
IL-4	pg/mL	0.0 ± 0.01	0.06 ± 0.01	0.06 ± 0.01	0.07 ± 0.02	0.07 ± 0.01	0.04 ± 0.01
IL-5	pg/mL	0.1 ± 0.01	0.12 ± 0.01	0.12 ± 0.01	0.12 ± 0.02	0.13 ± 0.02	0.11 ± 0.01
IL-6	pg/mL	16.8 ± 1.43	1391.81 ± 49.49	1368.62 ± 60.25	1103.02 ± 177.62	1270.41 ± 32.56	785.89 ± 69.75
IL-7	pg/mL	0.0 ± 0.00	0.00 ± 0.00	0.00 ± 0.00	0.00 ± 0.00	0.00 ± 0.00	0.00 ± 0.00
IL-8	pg/mL	7.7 ± 0.26	186.46 ± 9.60	235.73 ± 11.37	216.64 ± 39.43	233.60 ± 11.13	159.60 ± 7.10
IL-9	pg/mL	3.2 ± 0.06	3.60 ± 0.06	3.55 ± 0.14	3.44 ± 0.15	3.74 ± 0.14	3.74 ± 0.16
IL-10	pg/mL	1.0 ± 0.09	16.94 ± 1.15	22.98 ± 0.78	24.21 ± 2.19	23.20 ± 0.81	29.10 ± 1.73
IL-12p40	pg/mL	11.6 ± 1.28	723.05 ± 27.95	474.52 ± 16.94	297.27 ± 52.01	181.72 ± 8.88	73.09 ± 5.01
1L-12p70	pg/mL	0.3 ± 0.01	0.87 ± 0.11	0.80 ± 0.07	0.80 ± 0.11	0.61 ± 0.05	0.48 ± 0.03
IL-13	pg/mL	14.3 ± 2.60	13.94 ± 0.91	13.00 ± 2.07	14.95 ± 3.43	15.68 ± 3.55	9.20 ± 1.97
IL-15	pg/mL	0.6 ± 0.04	0.70 ± 0.09	0.69 ± 0.09	0.64 ± 0.19	0.64 ± 0.08	0.70 ± 0.10
IL-17A	pg/mL	0.0 ± 0.00	0.00 ± 0.00	0.02 ± 0.02	0.06 ± 0.06	0.02 ± 0.02	0.09 ± 0.09
IL-17E/IL-25	pg/mL	10.6 ± 0.33	9.59 ± 0.97	11.96 ± 1.30	10.17 ± 1.56	12.11 ± 1.83	12.49 ± 1.29
IL-17F	pg/mL	4.2 ± 0.07	4.66 ± 0.27	4.79 ± 0.20	4.44 ± 0.27	4.38 ± 0.39	4.38 ± 0.27
IL-18	pg/mL	2.7 ± 0.14	3.98 ± 0.03	3.95 ± 0.18	2.95 ± 0.42	2.99 ± 0.11	3.01 ± 0.05
IL-22	pg/mL	151.4 ± 17.36	124.85 ± 12.44	121.47 ± 9.42	98.00 ± 24.08	139.34 ± 3.55	147.78 ± 9.53
IL-27	pg/mL	40.4 ± 2.08	39.33 ± 1.27	40.50 ± 1.38	38.46 ± 5.91	41.27 ± 2.73	33.06 ± 2.28
IP-10	pg/mL	33.7 ± 0.32	670.37 ± 30.85	411.95 ± 20.77	270.96 ± 35.63	198.68 ± 13.92	68.17 ± 2.29
M-CSF	pg/mL	5.7 ± 0.43	6.21 ± 0.28	6.69 ± 0.25	6.62 ± 0.79	7.30 ± 0.48	7.38 ± 0.68
MCP-1	pg/mL	61.3 ± 2.26	216.67 ± 3.13	243.86 ± 5.69	227.93 ± 31.84	172.26 ± 5.61	172.24 ± 5.98
MCP-3	pg/mL	5.3 ± 0.66	6.51 ± 0.40	6.36 ± 0.45	7.06 ± 0.53	6.85 ± 0.44	4.92 ± 0.58
MDC	pg/mL	13.9 ± 0.58	16.00 ± 0.43	15.44 ± 0.82	13.48 ± 1.83	17.21 ± 0.39	16.70 ± 0.50
MIG/CXCL9	pg/mL	33.4 ± 1.24	85.82 ± 2.66	74.51 ± 2.17	61.82 ± 4.06	67.44 ± 3.43	62.71 ± 1.35
MIP-1α	pg/mL	26.7 ± 0.37	969.69 ± 8.35	923.77 ± 45.73	823.46 ± 92.28	891.17 ± 31.57	745.86 ± 25.21
MIP-1β	pg/mL	105.3 ± 6.07	282.79 ± 13.51	270.93 ± 23.31	247.96 ± 40.72	292.02 ± 12.05	280.78 ± 11.15
PDGF-AA	pg/mL	115.0 ± 3.50	162.79 ± 7.78	183.95 ± 9.92	180.21 ± 34.01	286.92 ± 11.17	246.40 ± 9.32
PDGF-AB/BB	pg/mL	582.6 ± 53.38	940.07 ± 6.50	954.41 ± 26.62	1113.36 ± 66.35	1483.26 ± 60.41	1479.53 ± 77.30
RANTES	pg/mL	602.0 ± 47.82	935.76 ± 79.86	992.90 ± 53.92	687.08 ± 157.66	891.78 ± 107.08	954.52 ± 25.50
sCD40L	pg/mL	26.0 ± 0.79	68.35 ± 1.43	74.83 ± 2.89	76.07 ± 7.26	115.25 ± 6.07	92.29 ± 3.91
TGFα	pg/mL	0.9 ± 0.04	2.26 ± 0.06	2.58 ± 0.11	1.96 ± 0.17	2.32 ± 0.24	2.37 ± 0.15
TNFα	pg/mL	9.9 ± 0.62	1214.37 ± 34.50	893.29 ± 24.61	613.83 ± 94.54	467.48 ± 18.33	260.08 ± 16.85
TNFβ	pg/mL	31.6 ± 3.79	33.20 ± 1.83	30.87 ± 3.58	21.53 ± 6.78	38.38 ± 4.28	38.28 ± 6.22
VEGF-A	pg/mL	0.0 ± 0.00	0.00 ± 0.00	0.00 ± 0.00	0.00 ± 0.00	0.00 ± 0.00	0.00 ± 0.00

Table 3.2 Results of multiplex array for UCMSC ADH conditioned media on inflammation.

A summary of the mean ±SEM levels of release of forty-eight cytokines and chemokines following UCMSC ADH conditioned media treatment of human blood after LPS stimulations.

Cytokine/Chemokine		Vehicle Control	Vehicle Control + LPS	0.125x UCMSC ADH + LPS	0.25x UCMSC ADH + LPS	0.5x UCMSC ADH + LPS	1x UCMSC ADH + LPS
EGF	pg/mL	0.0 ± 0.00	3.38 ± 0.38	4.45 ± 1.00	6.29 ± 0.37	11.52 ± 0.44	11.65 ± 0.43
Eotaxin	pg/mL	11.4 ± 0.29	11.24 ± 0.24	12.63 ± 0.62	11.78 ± 0.30	13.80 ± 0.68	15.27 ± 0.33
FGF-2	pg/mL	12.9 ± 0.87	19.92 ± 5.01	30.23 ± 10.17	23.25 ± 1.81	22.07 ± 1.61	25.82 ± 3.19
FLT-3L	pg/mL	0.5 ± 0.04	0.92 ± 0.06	0.82 ± 0.12	0.71 ± 0.04	0.77 ± 0.04	0.75 ± 0.03
Fractalkine	pg/mL	3.5 ± 2.42	11.56 ± 0.82	15.34 ± 7.08	9.51 ± 1.98	6.46 ± 0.69	10.47 ± 2.00
G-CSF	pg/mL	4.4 ± 0.10	64.81 ± 3.90	69.44 ± 2.81	73.93 ± 2.91	110.86 ± 5.14	274.09 ± 4.23
GM-CSF	pg/mL	0.9 ± 0.20	1.70 ± 0.23	1.50 ± 0.38	1.72 ± 0.28	1.70 ± 0.41	2.50 ± 0.55
GROα	pg/mL	2.7 ± 0.08	10.23 ± 0.15	21.35 ± 1.10	32.39 ± 1.06	68.95 ± 2.66	150.97 ± 5.32
IFN-α2	pg/mL	1.4 ± 0.28	2.96 ± 0.21	3.86 ± 1.81	2.53 ± 0.29	2.95 ± 0.36	2.39 ± 0.55
IFNγ	pg/mL	0.1 ± 0.08	4.66 ± 0.21	0.86 ± 0.23	0.38 ± 0.03	0.38 ± 0.01	0.56 ± 0.06
IL-1α	pg/mL	0.0 ± 0.00	110.11 ± 4.36	87.90 ± 1.83	72.34 ± 1.23	81.22 ± 5.16	121.41 ± 3.74
IL-1β	pg/mL	1.8 ± 0.20	663.20 ± 22.31	404.83 ± 20.20	274.33 ± 18.33	116.33 ± 7.45	56.30 ± 2.34
IL-1RA	pg/mL	2.3 ± 0.19	18.05 ± 0.66	17.11 ± 0.65	14.87 ± 0.37	17.59 ± 0.46	20.49 ± 0.42
IL-2	pg/mL	0.0 ± 0.00	0.00 ± 0.00	0.00 ± 0.00	0.00 ± 0.00	0.00 ± 0.00	0.00 ± 0.00
IL-3	pg/mL	0.0 ± 0.00	0.00 ± 0.00	0.00 ± 0.00	0.00 ± 0.00	0.00 ± 0.00	0.00 ± 0.00
IL-4	pg/mL	0.0 ± 0.00	0.06 ± 0.00	0.10 ± 0.04	0.05 ± 0.01	0.06 ± 0.01	0.06 ± 0.01
IL-5	pg/mL	0.1 ± 0.00	0.12 ± 0.01	0.15 ± 0.05	0.12 ± 0.01	0.11 ± 0.00	0.13 ± 0.01
IL-6	pg/mL	15.1 ± 0.64	1348.49 ± 30.65	1200.25 ± 55.99	954.19 ± 55.97	788.33 ± 69.00	841.07 ± 58.55
IL-7	pg/mL	0.0 ± 0.00	0.00 ± 0.00	0.00 ± 0.00	0.00 ± 0.00	0.00 ± 0.00	0.00 ± 0.00
IL-8	pg/mL	18.0 ± 1.19	317.74 ± 8.63	358.68 ± 30.31	364.42 ± 8.89	422.21 ± 60.63	757.17 ± 49.61
IL-9	pg/mL	3.4 ± 0.13	3.60 ± 0.15	3.90 ± 0.53	3.71 ± 0.10	3.26 ± 0.17	3.49 ± 0.14
IL-10	pg/mL	1.3 ± 0.07	31.35 ± 1.31	71.74 ± 1.18	102.41 ± 7.97	82.56 ± 3.06	72.41 ± 3.41
IL-12p40	pg/mL	9.8 ± 0.94	633.12 ± 24.54	153.52 ± 9.59	82.91 ± 5.38	33.83 ± 1.48	15.26 ± 0.69
1L-12p70	pg/mL	0.4 ± 0.05	0.97 ± 0.07	0.93 ± 0.50	0.52 ± 0.08	0.59 ± 0.06	0.44 ± 0.10
IL-13	pg/mL	8.1 ± 2.57	12.90 ± 1.69	18.57 ± 6.75	11.63 ± 1.68	11.83 ± 2.27	17.39 ± 1.47
IL-15	pg/mL	0.6 ± 0.01	0.76 ± 0.10	0.79 ± 0.37	0.60 ± 0.05	0.64 ± 0.05	0.64 ± 0.04
IL-17A	pg/mL	0.0 ± 0.00	0.00 ± 0.00	0.77 ± 0.57	0.00 ± 0.00	0.08 ± 0.05	0.06 ± 0.06
IL-17E/IL-25	pg/mL	8.8 ± 0.97	12.40 ± 2.49	13.28 ± 2.78	7.76 ± 0.63	9.02 ± 0.83	10.37 ± 0.42
IL-17F	pg/mL	3.7 ± 0.22	4.03 ± 0.23	4.93 ± 0.99	3.69 ± 0.37	3.98 ± 0.37	3.89 ± 0.15
IL-18	pg/mL	2.1 ± 0.04	2.80 ± 0.05	2.74 ± 0.29	2.36 ± 0.05	2.11 ± 0.08	2.37 ± 0.14
IL-22	pg/mL	122.9 ± 16.29	139.24 ± 7.99	135.24 ± 20.30	130.74 ± 5.55	116.00 ± 22.57	162.00 ± 10.67
IL-27	pg/mL	32.2 ± 2.49	38.53 ± 2.96	43.22 ± 4.74	39.02 ± 1.68	35.24 ± 1.62	38.26 ± 2.19
IP-10	pg/mL	15.4 ± 0.37	280.90 ± 8.45	63.15 ± 2.81	43.34 ± 0.33	29.32 ± 2.26	23.79 ± 0.65
M-CSF	pg/mL	5.9 ± 0.33	6.14 ± 0.35	6.77 ± 1.41	5.98 ± 0.61	6.30 ± 0.69	6.77 ± 0.25
MCP-1	pg/mL	121.1 ± 3.84	299.36 ± 4.85	437.17 ± 7.90	475.41 ± 12.73	526.41 ± 11.06	516.45 ± 19.67
MCP-3	pg/mL	4.5 ± 0.29	5.99 ± 0.19	8.56 ± 1.10	9.01 ± 0.15	8.58 ± 0.85	10.96 ± 0.36
MDC	pg/mL	14.5 ± 0.36	15.61 ± 0.38	15.11 ± 0.28	15.91 ± 0.44	15.94 ± 0.65	16.22 ± 0.53
MIG/CXCL9	pg/mL	32.8 ± 0.74	77.73 ± 3.16	62.77 ± 1.59	54.23 ± 1.08	52.76 ± 1.23	46.84 ± 1.51
MIP-1α	pg/mL	26.1 ± 0.63	982.31 ± 18.50	882.55 ± 8.74	807.09 ± 7.09	689.03 ± 27.70	587.36 ± 7.64
MIP-1β	pg/mL	122.8 ± 4.18	347.43 ± 12.52	301.29 ± 57.25	295.69 ± 26.26	273.85 ± 20.34	251.31 ± 30.65
PDGF-AA	pg/mL	108.7 ± 9.11	175.43 ± 6.65	203.71 ± 2.63	273.93 ± 4.61	325.32 ± 24.01	316.15 ± 24.80
PDGF-AB/BB	pg/mL	595.8 ± 40.71	1112.64 ± 35.01	1185.82 ± 35.90	1447.24 ± 35.92	1718.84 ± 42.67	1664.14 ± 52.76
RANTES	pg/mL	942.3 ± 76.33	857.64 ± 66.30	846.02 ± 80.59	763.40 ± 46.64	770.35 ± 93.45	856.00 ± 82.14
sCD40L	pg/mL	24.3 ± 1.17	67.85 ± 4.54	72.82 ± 7.69	89.74 ± 2.52	114.65 ± 4.52	105.90 ± 3.36
TGFα	pg/mL	1.1 ± 0.08	2.47 ± 0.16	3.30 ± 1.00	2.03 ± 0.19	1.85 ± 0.24	2.21 ± 0.15
TNFα	pg/mL	8.3 ± 0.31	1081.03 ± 13.87	378.03 ± 11.26	248.32 ± 7.22	145.95 ± 7.77	127.93 ± 1.71
TNFβ	pg/mL	26.7 ± 3.13	35.81 ± 4.00	42.67 ± 9.03	35.05 ± 3.71	27.04 ± 5.39	37.76 ± 2.49
VEGF-A	pg/mL	0.0 ± 0.00	0.00 ± 0.00	0.00 ± 0.00	0.00 ± 0.00	0.00 ± 0.00	0.00 ± 0.00

.

Comparing a second umbilical cord mesenchymal stem cell line.

Following the initial investigation into UCMSC conditioned media, a new cell line was procured to determine if the results found would be conserved between UCMSC donors. The testing began as before with assessing the growth characteristics and limitations of this new UCMSC. Next three batches of both UCMSC PEL and UCMSC ADH conditioned medias were independently generated for characterisation and testing on the potency assays. These batches will be referred to as RUO1, RUO2 and RUO3 to signify they were produced from this second UCMSC cell line.

Assessment of growth characteristics – UCMSC RUO

As before, the cells were revived from cryopreservation and cultured over 60 days to assess expansion capability. Similarly, UCMSC cultured for approximately 10 to 12 passages with a relatively linear growth phase, n=3 biological replicate (Figure 3.11A). After 47 days of culture the growth rate began to reduce, however cell viability remained high, with the majority of measures being greater that 90% throughout culture, n=3 (Figure 3.11B). X-gal staining revealed that the increase in population double time correlated with an increase in cellular senescence and a change in morphology (Figure 3.11C).

As before, a cell bank was created at passage 3 and UCMSCs were used for generating conditioned media between passage 5 and passage 8, with a minimum time in culture of two passages after revival from cryopreservation.

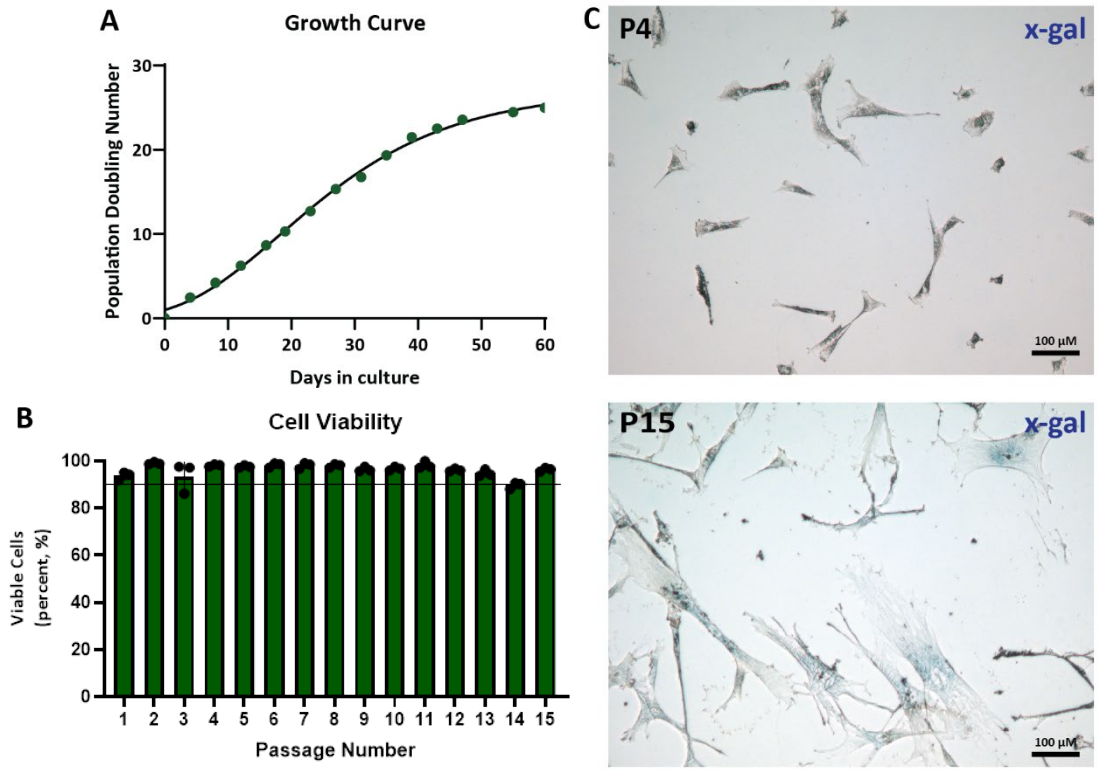

Figure 3.11 Assessment of growth and viability of UCMSC RUO cell line.

(A) *Tracking of population doubling number of UCMSC RUO cells over 60 days post revival from cryopreservation (n=3).* ***(B)*** *Trypan blue exclusion cell viability of UCMSC RUO cells over 15 passages, with a line indicating 90% viability (n=3).* ***(C)*** *Images of x-gal staining (blue) for pH 6.0 β-galactosidase activity of senescence cells and passage 4 (top) and passage 15 (bottom).*

Protein content of UCMSC RUO conditioned media

Total protein quantification revealed the UCMSC PEL conditioned media had an average protein concentration of 8.44 ±0.29 µg/mL SEM and UCMSC ADH conditioned media of 9.58 ±0.64 µg/mL SEM, which was not significantly different, p=0.1796, n=3 biological replicates (Figure 3.12A). When compared as the amount of secreted protein from a million cells (Figure 3.12B) showed UCMSC ADH conditioned media to have approximately 11x greater secreted protein than UCMSC PEL at 38.30 ±2.54 µg/10^6 cells SEM over 3.38 ±0.12 µg/10^6 cells SEM which was statistically significant, n=3 biological replicates (p=<0.0001). The silver staining visualisation revealed both conditioned medias

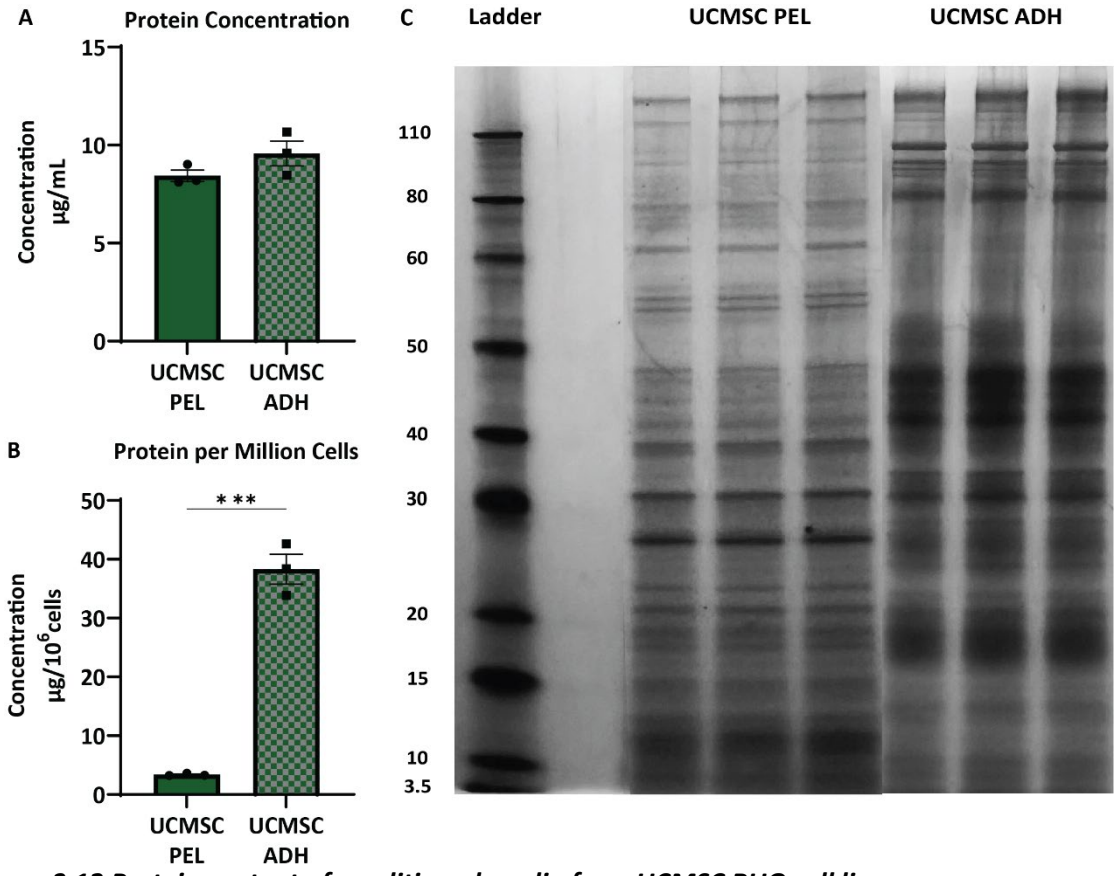

Figure 3.12 Protein content of conditioned media from UCMSC RUO cell line.

(A) *Protein concentration of UCMSC PEL and UCMSC ADH conditioned media and* ***(B)*** *normalised secreted protein by number of cells used in production. Bars represent the mean of three batches (n=3). Statistical significance from t-test is represented by asterixis: * p= <0.05; ** p= <0.01; *** p= <0.001; **** p= <0.0001.* ***(C)*** *Silver stained SDS-page of UCMSC conditioned media.*

had a broad size range of proteins, with the unique profile of each generation method being conserved with the new UCMSC RUO cells. (Figure 3.12C). The two conditioned medias shared many similar bands at approximately 120 kDa as well as bands at 80 and 30 kDa, however there were discernible differences in intensity between the two generation methods. Equally, there were clear bands present in UCMSC PEL that were not found in UCMSC ADH, of note a band located around 60 kDa, three bands around the 55 kDa location, 40 kDa and a clear band at 25 and 10 kDa. Bands at 100 kDa, 50 kDa and 20 kDa were present in UCMSC ADH conditioned media and not UCMSC PEL. Overall, the silver staining demonstrated that in equal volumes of conditioned media, UCMSC PEL and UCMSC ADH had an

equivalent overall intensity of all proteins which supported the results of the protein quantification assay.

To characterise the protein content of UCMSC conditioned media, samples were assessed by mass spectrometry analysis, n=3 biological replicates. In total 1,599 were identified, of which 856 proteins were uniquely identified in UCMSC PEL, 75 proteins were unique to UCMSC ADH, and 667 proteins were shared (Figure 3.13A). The heatmap of the detection intensity (Figure 3.13B) displayed the differences between UCMSC PEL and UCMSC ADH conditioned medias, as well as highlighting a number of differences between batches of the same conditioned media that were not resolved by silver stains. Principal component analysis (PCA), a statistical method which reduces multivariable data to key linear variables (principal components (PC)) to represent in a simpler package the most significant patterns and relationships in the data, determined that UCMSC PEL and USMSC ADH conditioned medias uniquely clustered along the first test dimension, PC1 which captured 65.99% of variance with an Eigenvalue of 124,379.3 (Figure 3.13C). In the next dimension, PC2, which only captured an additional 14.3% of the variance (Eigenvalue 26,950), revealed variation in the UCMSC PEL conditioned media with UCMSC PEL RUO2 and RUO3 batches being the most different from each other. On the other hand, the three UCMSC ADH batches clustered tightly in both dimensions indicating their greater uniformity.

Examining the proteins unique to UCMSC PEL through Gene Ontology (GO) enrichment analysis, many of these were found to be intracellular components related to proteosome regulation, focal adhesion, and translation initiation. The main group of proteins unique to UCMSC ADH conditioned media were revealed by Go enrichment to be extracellular matrix processing, specifically metalloendopeptidase inhibitor activity from proteins such as tissue metalloproteinase inhibitor 2. From the shared list of proteins key enrichment terms identified included neutrophil activity (aggregation and clearance), positive processing of protein processing, chronic inflammatory response, cell differentiation,

extracellular matrix assembly, positive regulation of wound healing, positive regulation of cell migration, leukocyte chemotaxis, muscle cell development, glial cell development, and angiogenesis.

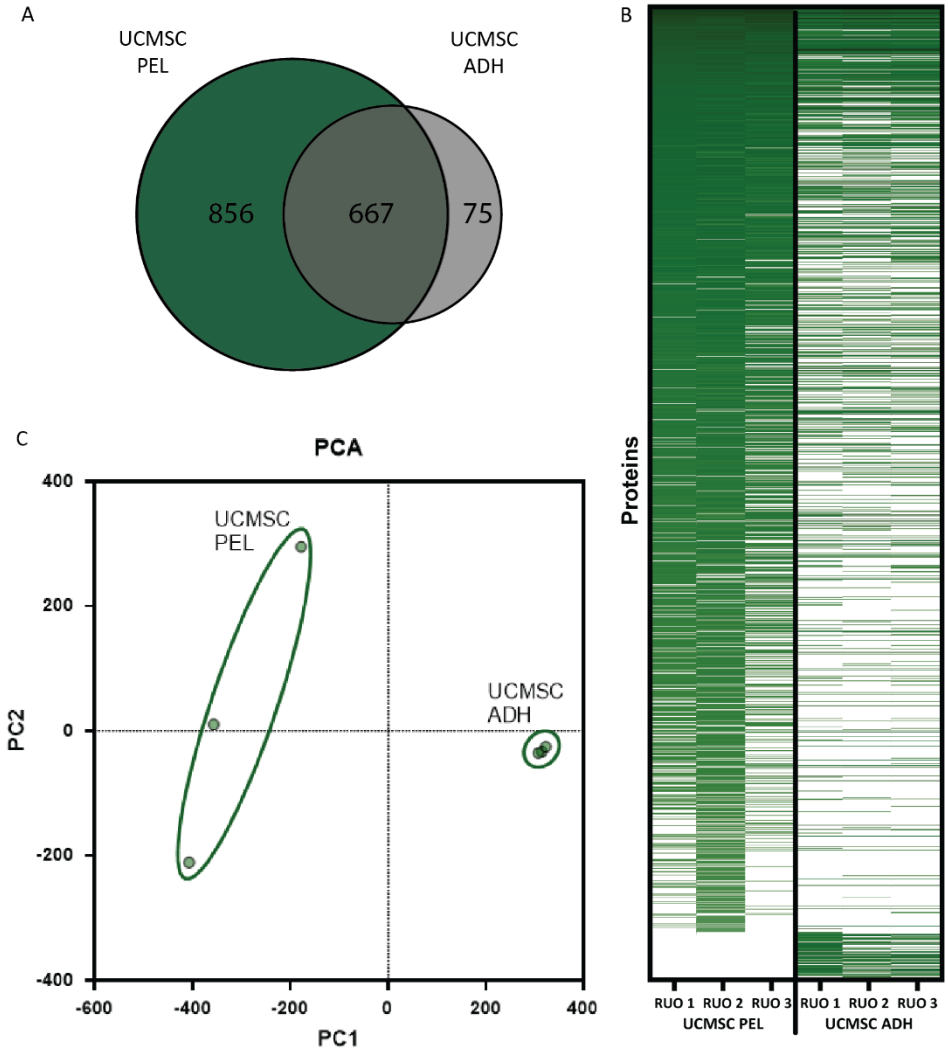

Figure 3.13 Mass spectrometry characterisation of UCMSC conditioned media.

(A) *Venn-diagram representing numbers of unique detected proteins across three batches of UCMSC PEL (green left) and UCMSC ADH (grey right) or non-unique shared proteins (overlap).* ***(B)*** *Heatmap depicting expression levels of proteins, where white is no expression and dark green is high expression.* ***(C)*** *Principal component analysis summarising the variance of all UCMSC conditioned media batches for all proteins, where PC1 axis represents the highest proportion of variance and PC2 the second highest. n=3 biological replicates.*

Nucleic acid content of UCMSC RUO conditioned media

Total Nucleic acid quantification revealed the average concentration of nucleic acid for UCSMC PEL had significantly more nucleic acids than UCMSC ADH (Figure 3.14A), 17.68 ±1.61 µg/mL SEM and 11.04 ±1.68 µg/mL SEM respectively, p=0.0465, n=3 biological replicates. However, secreted nucleic acid per one million cells (Figure 3.14B), showed UCMSC ADH conditioned media had significantly more nucleic acid, 44.15 ±6.74 µg/10^6 cells SEM, released than UCMSC PEL, 7.07 ±0.65 µg/10^6 cells SEM, p=0.0054, n=3 biological replicates.

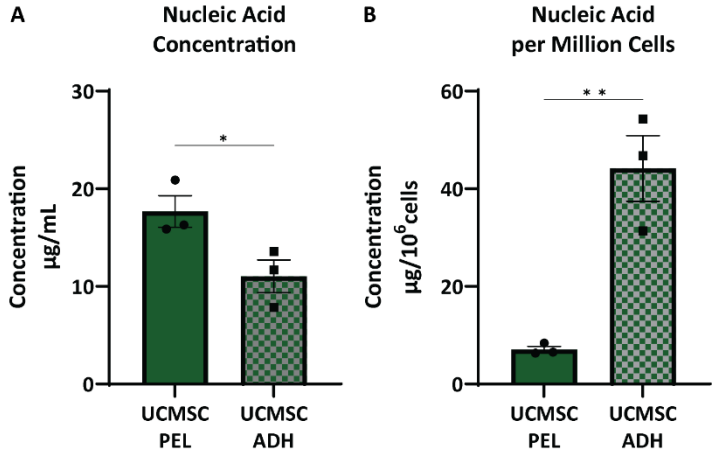

Figure 3.14 Nucleic acid content of conditioned media from UCMSC RUO cell line.

(A) *Nucleic acid concentration of UCMSC PEL and UCMSC ADH conditioned media and* ***(B)*** *normalised secreted nucleic acid by number of cells used in production. Bars represent the mean of three batches (n=3). Statistical significance from t-test is represented by asterixis: * p= <0.05; ** p= <0.01; *** p= <0.001; **** p= <0.0001.*

It is well documented that stem cell conditioned medias contain miRNA, which are often responsible for providing a biological response. To identify the miRNAs, present within these UCMSC conditioned medias, small RNA sequencing analysis was carried out, n=3 biological replicates. In total, 645 different miRNAs were identified, with 385 miRNAs shared by both conditioned medias (Figure 3.15A). UCMSC PEL conditioned media contained 258 unique miRNAs, whereas only 2 miRNAs were unique to UCMSC ADH. Similarly to the proteomics, a heatmap of read counts (Figure 3.15B) displays the difference between UCMSC PEL and UCMSC ADH conditioned medias. It also brings to light a degree of batch variation, particularly with UCMSC PEL conditioned media. A PCA test confirms along the PC1 axis (95.76% variance, Eigenvalue 727,934,849) that UCMSC PEL and UCMSC ADH statistically unique (Figure 3.15C). Along the PC2 axis (3.02% variance, Eigenvalue 2,293,423) identified some variations between UCMSC PEL batches, with batches RUO1 and RUO3 being the most different. UCMSC ADH conditioned media batches were clustered more tightly, however along the PC2 axis, RUO1 was found to be slightly different from the other two batches.

Inputting the top 200 miRNAs expressed for each UCMSC conditioned into GO enrichment analysis revealed a number of terms related to cell proliferation, such as “cell cycle”, “DNA replication”, “cell division” and “cell population proliferation”. Additionally, there were terms related to cell migration, angiogenesis, and inflammation with terms such as “Interleukin-1-mediated signally pathway” and “Interleukin-6-mediated signalling pathway”. Specifically, miRNAs including miR-21, miR-181, let-7b and miR-146a were found to be significantly upregulated in UCMSC ADH compared to UCMSC PEL.

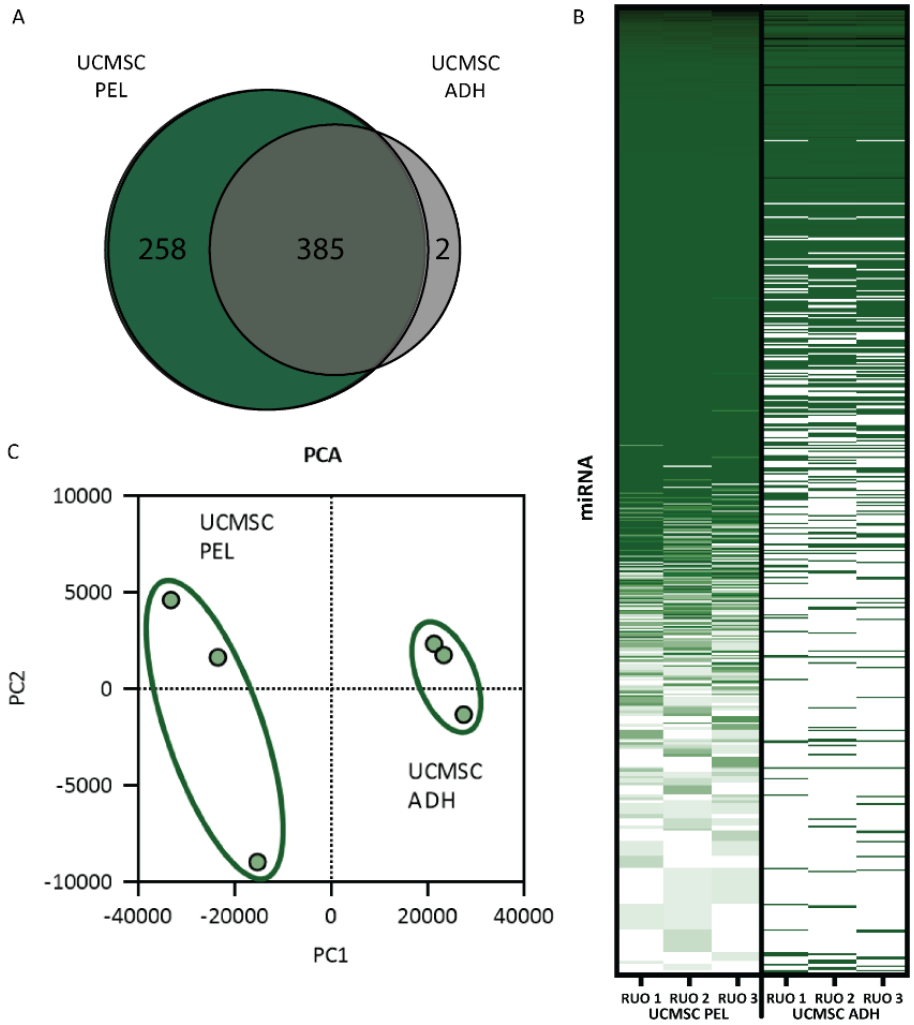

Figure 3.15 miRNA sequencing characterisation of UCMSC conditioned media.

(A) *Venn-diagram representing numbers of unique detected miRNAs across three batches of UCMSC PEL (green left) and UCMSC ADH (grey right) or non-unique shared miRNAs (overlap).* ***(B)*** *Heatmap depicting expression levels of miRNAs, where white is no expression and dark green is high expression.* ***(C)*** *Principal component analysis summarising the variance of all UCMSC conditioned media batches for all miRNAs, where PC1 axis represents the highest proportion of variance and PC2 the second highest.*

Extracellular vesicles of UCMSC RUO conditioned media

Lastly, nanoparticle tracking analysis found UCMSC PEL conditioned media had a mean particle concentration of 9.493 ±0.93 x10^8 particles/mL SEM and UCMSC ADH had a mean concentration of 1.863 ±0.42 x10^8 particles/mL SEM (Figure 3.16A). The concentration EVs in UCMSC PEL was significantly higher than UCMSC ADH, p=0.0018, n=3 biological replicates. However, as with both protein and nucleic acid concentrations, when compared as the number of particles released per million cells (Figure 3.16B), it revealed UCMSC ADH had approximately 4x greater EV particles than UCMSC PEL at 3.797 x10^8 ±0.37 x10^8 particles/10^6 cells SEM and 7.456 x10^8 ±0.17 x10^8 particles/10^6

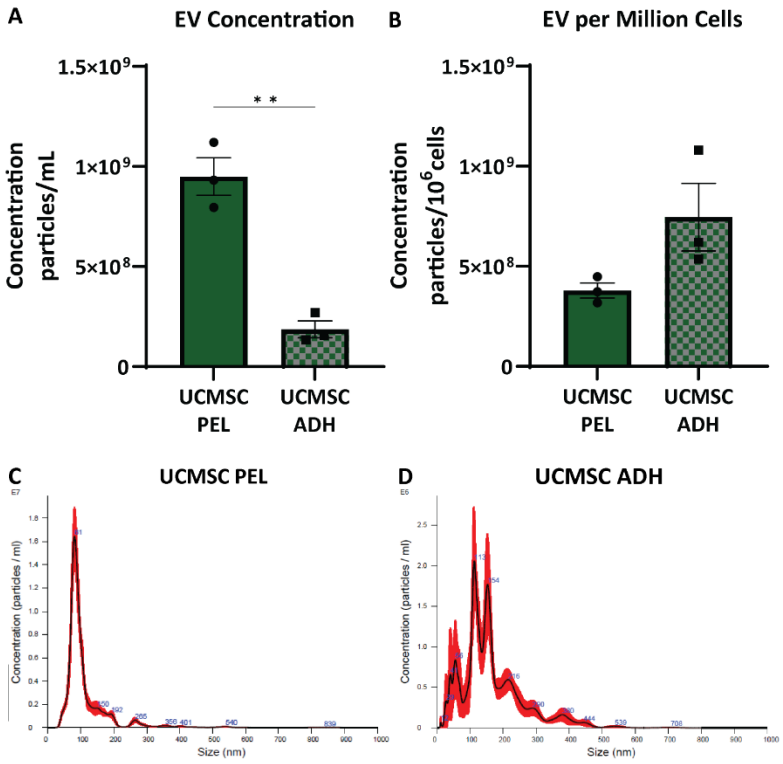

Figure 3.16 Extracellular vesicle component of conditioned media from UCMSC RUO cell line.

(A) *Concentration extracellular vesicles from UCMSC PEL and UCMSC ADH conditioned media and* ***(B)*** *normalised extracellular vesicles to cells used in production. Bars represent the mean of three batches (n=3). Statistical significance from t-test is represented by asterixis: * p= <0.05; ** p= <0.01; *** p= <0.001; **** p= <0.0001.* ***(C, D)*** *representative nanoparticle tracking plots for UCMSC PEL and UCMSC ADH displaying the distribution of detected particles.*

cells SEM respectively, although this difference was not statistically significant (p=0.1020, n=3 biological replicates). Representative plots from nanoparticle tracking analysis display the distribution of particle sizes. UCMSC PEL conditioned media (Figure 3.16C) had a more uniform size of particles between 100 nm and 200 nm, whereas UCMSC ADH (Figure 3.16D) showed a greater heterogeneous size of particle, ranging from 60 nm to 500 nm. It is worth noting again that the majority of particles analysed in UCMSC samples were still within the range of 100 nm and 200 nm, similar to UCMSC PEL conditioned media. These findings were in concurrent with the conditioned media generated form the first UCMSC cell line.

UCMSC RUO conditioned media potency – cellular proliferation

To begin assessing the efficacy of these UCMSC RUO conditioned medias, the three batches were tested on the proliferation potency assay. Beginning with UCMSC PEL conditioned media (Figure 3.17A), all three batches significantly increased proliferation compared to the vehicle control. Batch RUO1 had a normalised proliferation rate of 151.1 ±2.51% SEM; RUO2 of 140.4 ±2.42% SEM; and RUO3 of 143.6 ±0.34% SEM compared to the vehicle control at 100.0%. One-way ANOVA with Dunnett's post testing, found significance of p=<0.0001 across the board, n=3 biological replicates.

UCMSC ADH had similar results with the three batches also significantly increasing proliferation compared to the vehicle control (Figure 3.17B). Batch RUO1 had a normalised proliferation rate of 193.2 ±25.49% SEM; RUO2 of 179.6 ±4.71% SEM; and RUO3 of 177.0 ±7.57% SEM compared to the vehicle control at 100.0%. One-way ANOVA with Dunnett's post testing, found significance of p=0.0053, p=0.0133, and p=0.0160 respectively, n=3 biological replicates.

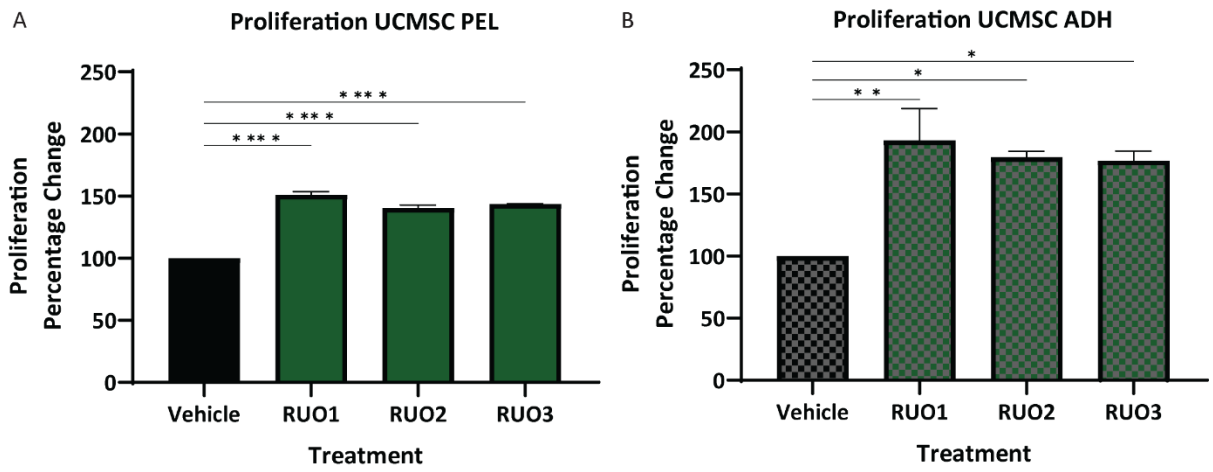

Figure 3.17 Bioactivity assessment of UMSC RUO conditioned media on cell proliferation.

The effect of ***(A)*** *UCMSC PEL and* ***(B)*** *UCMSC ADH conditioned media on HeLa cell proliferation. Bars represent the average of three repeat experiments (n=3). Statistical significance from ANOVA with Dunnett's post testing against the vehicle group is represented by asterixis: * p= <0.05; ** p= <0.01; *** p= <0.001; **** p= <0.0001.*

UCMSC RUO conditioned media potency – cellular migration

Testing of these conditioned medias on the migration assay revealed a similar picture to that of the proliferation assay, where all three batches of both UCMSC PEL and UCMSC ADH conditioned medias significantly increased migration compared to the respective vehicles. UCMSC PEL treatment (Figure 3.18A) had mean normalised migration rate for RUO1 of 174.7 ±4.08% SEM; RUO2 of 172.9 ±5.73% SEM; and RUO3 of 155.8 ±6.21% SEM compared to the vehicle control at 100.0 ±4.21% SEM. One-way ANOVA with Dunnett's post testing gave statistical significances of p=<0.0001, n=6 technical replicates. UCMSC ADH treatment (Figure 3.18B) had a mean normalised migration rate for RUO1 of 128.2 ±3.36% SEM; RUO2 of 129.2 ±3.93% SEM; and RUO3 of 120.2 ±6.45% SEM compared to the vehicle control at 100.0 ±2.57% SEM. One-way ANOVA with Dunnett's post testing gave statistical significances of p=0.0004, p=0.0003 and p=0.0147, respectively, n=6 technical replicates.

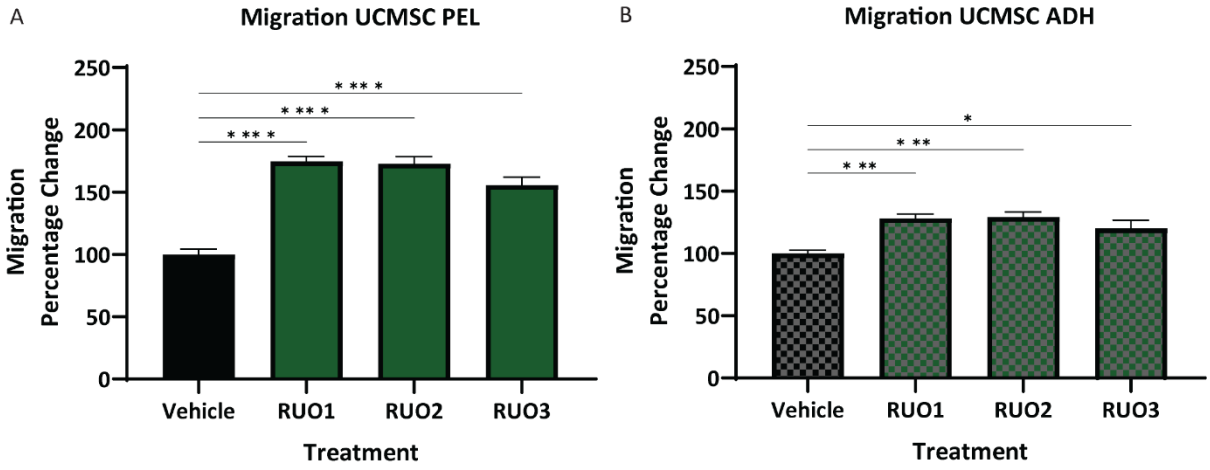

Figure 3.18 Bioactivity assessment of UCMSC conditioned media on cell migration.

*The effect of **(A, B)** UCMSC PEL and **(C, D)** UCMSC ADH conditioned media on HeLa cell migration. Bars represent average of average of six technical repeats (n=6). Statistical significance from ANOVA with Dunnett's post testing is represented by asterixis: * p= <0.05; ** p= <0.01; *** p= <0.001; **** p= <0.0001.*

<u>*UCMSC RUO conditioned media potency – inflammation*</u>

Finally, to complete the series of bioactivity assessments, the conditioned medias from this second cell line were tested on the whole blood inflammation assay. Initially, three batches of UCMSC PEL and UCMSC ADH conditioned media were tested at a single concentration of 1x. Here, one out of three UCMSC PEL batches had a statistically significant reduction in TNFα (Figure 3.19A). UCMSC PEL RUO1 and RUO2 non-significantly reduced TNFα to 85.4 ±8.04% SEM and 79.0 ±3.03% SEM respectively, whereas UCMSC RUO3 had the significant reduction to 74.6 ±0.19% SEM compared to the 100.0% maximum stimulation with the vehicle control, with a one-way ANOVA with Tukey's post testing gave statistical significances of p=0.0248, n=3 biological replicates. On the other hand, all three batches of UCMSC ADH conditioned media reduced TNFα levels with statistical significance (Figure 3.19B), with UCMSC RUO1 reducing to 45.1 ±4.99% SEM, UCMSC ADH RUO2 to 34.1 ±4.39% SEM and RUO3 to 37.0 ±6.51% SEM. One-way ANOVA with Tukey's post testing gave statistical significances of p=0.0004, p=<0.0001 and p=0.0001 respectively against the 100.0% maximum stimulation with the vehicle

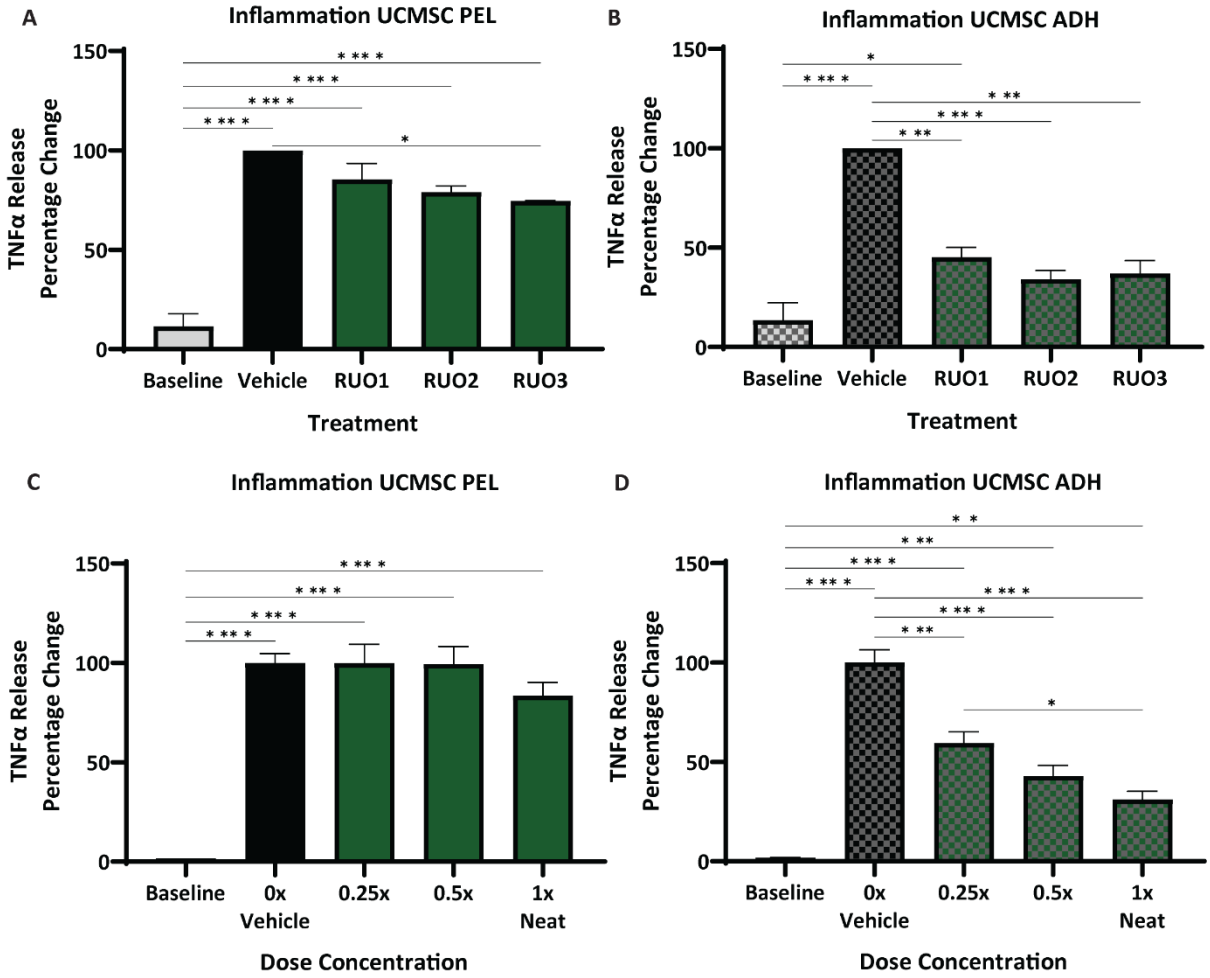

Figure 3.19 Bioactivity assessment of UCMSC conditioned media on inflammation.

The effect of three batches of ***(A)*** *UCMSC PEL and* ***(B)*** *UCMSC ADH conditioned media from UCMSC RUO cells on TNFα levels release from human blood following LPS stress. Bars represent the average of repeat experiments from three different blood donor (n=3). Dose series treatment with* ***(C)*** *UCMSC PEL and* ***(D)*** *UCMSC ADH conditioned media. Bars represent averages of three batches of UCMSC each conditioned media (n=3). Statistical significance from ANOVA with Tukey's post testing is represented by asterixis: * p= <0.05; ** p= <0.01; *** p= <0.001; **** p= <0.0001.*

treatment. Of note, UCMSC ADH RUO2 and RUO3 were non-significantly different to the baseline of 8.0% ±1.78% SEM.

Next the three batches of UCMSC conditioned medias were tested as a dose response. The average of the three batches was used to form a combined result for UCMSC PEL (Figure 3.19C) and UCMSC ADH

(Figure 3.19D) conditioned medias, n=3 biological replicates. There were no statistically significant changes in TNFα levels following UCMSC PEL treatment, whereas all three concentrations of UCMSC ADH had statistically significant decreases in TNFα levels. The lowest treatment of 0.25x UCMSC ADH reduced TNFα from the 100.0 ± 6.39% SEM vehicle level to 59.5 ±5.59% SEM (p=0.0005). This was further reduced to 42.8 ±5.36% SEM with 0.5x (p=<0.0001) and 31.0 ±4.28% SEM with 1x (p=<0.0001) UCMSC ADH, which was also statistically significant to 0.25x treatment on a one-way ANOVA with Tukey's post-test, p=0.0148, n=3 biological replicates.

Peripheral blood mononucleated cells inflammation assay.

So far, to assess the potency of these conditioned medias on inflammation, a whole blood assay has been used. Leukocytes are the primary responders to inflammatory molecules, with monocytes having the highest abundance of toll-like receptor-4 through which LPS stimulates the inflammatory response. Following stimulation, the monocyte family of cells respond by releasing a number of cytokines and chemokines which in turn signal other cells in the body. To refine the inflammation potency assay to focus on these primary responders, a sub-population of blood cells, peripheral blood mononucleated cells (PBMCs), can be isolated from whole blood. These cells include monocytes as well as lymphocytes without the presence of granulocytes, erythrocytes, and platelets.

Isolation of peripheral blood mononucleated cells and establishment of inflammation assay.

To begin, whole blood was separated using density gradient centrifugation and the different fractions were stimulated with LPS. Beginning with the PBMC population (Figure 3.20A), there was a 72.8 ±0.94 SEM fold increase in TNFα release, with an unpaired t test statistical significance of p=<0.0001, n=3 technical replicates. In contrast, the red blood cell and granulocyte population (Figure 3.20B) only had a 1.76 ±0.02 SEM fold increase in TNFα, p=<0.0001 and platelet rich plasma (Figure 3.20C) had no statistically significant changes, n=3 technical replicates.

The next steps in establishing this assay were to ensure that a UCMSC conditioned media could bring about changes in the inflammatory response. Here, a UCMSC ADH conditioned media from the first

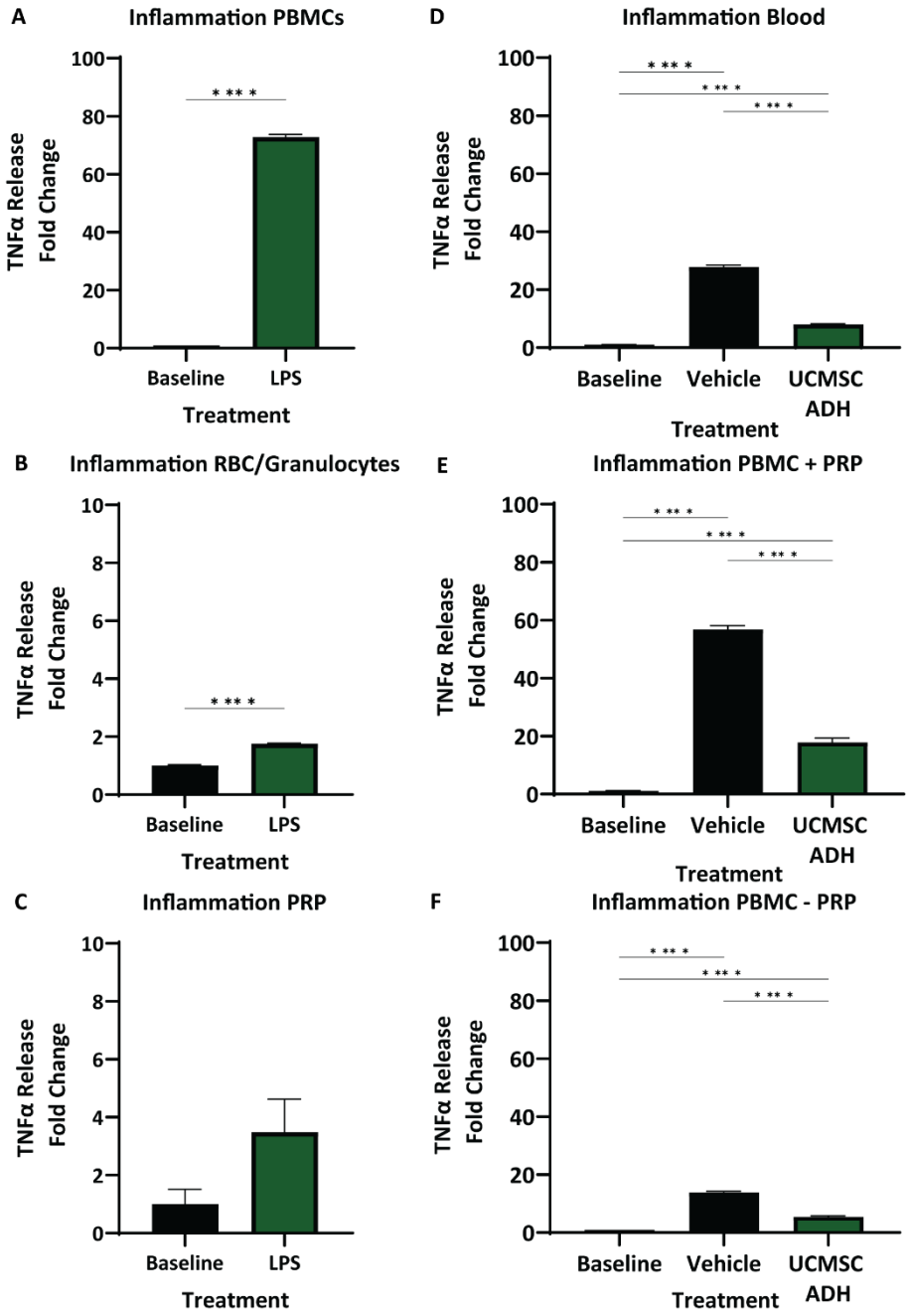

Figure 3.20 Establishment of a peripheral blood mononucleated cell inflammation assay.

Confirmation of sub-population of blood cells which respond to LPS stimulation through the release of TNFα. **(A)** peripheral blood mononucleated cells (PBMCs), **(B)** red blood cells (RBC) and Granulocytes, and **(C)** platelet rich plasma (PRP). Bars represent the average of three technical replicates (n=3), and statistical significance from t-test is represented *by asterixis: * p= <0.05; ** p= <0.01; *** p= <0.001; **** p= <0.0001.* ***(D)*** *Confirmation of effect from UCMSC ADH conditioned media treatment on whole blood for donor used for* *[Continues on next page]*

Figure 3.20 continued: (E) *unwashed PBMCs containing PRP and* ***(F)*** *washed PBMCs. Bars represent the average of four technical replicates (n=4) and statistical significance from ANOVA with Tukey's post testing is represented as by asterixis: * p= <0.05; ** p= <0.01; *** p= <0.001; **** p= <0.0001.*

cell line was used. A whole blood assay was conducted a control experiment (Figure 3.20D). As previously seen, LPS significantly increased TNFα by 27.9 ±0.61 SEM fold and a UCMSC ADH treatment reduced this increase to 8.0 ±0.27 SEM fold from baseline levels. One-way ANOVA with Tukey's post testing showed statistical significance of p=<0.0001 and p=<0.0001, respectively, n=4 technical replicates. PBMCs were isolated from the same blood and used at the original cell dilution, where LPS induced a 56.8 ±1.34 SEM fold statistically significant increase in TNFα, p=<0.0001, n=4 technical replicates (Figure 3.20E). The UCMSC ADH treatment reduced this increase to 17.8 ±1.54 SEM fold, with a statistical significance of p=<0.0001, n=4 technical replicates.

To determine if retaining the plasma during the isolation of PBMC had an impact on the responsiveness to LPS, some PBMCs were washed to remove the plasma and used at the equivalent cell dilutions with foetal bovine serum as a replacement. Here, LPS still induced a statistically significant (p=<0.0001), however lower, increase in TNFα, 13.8 ±0.50 SEM fold change (Figure 3.20F) and the UCMSC ADH treated significantly reduced the increase in TNFα to 5.4 ±0.35 SEM fold from the baseline, p=<0.0001, n=4 technical replicates.

UCMSC RUO conditioned media potency – PBMC inflammation.

Following the establishment of the assay protocol, three batches of UCMSC RUO conditioned medias were evaluated as with the whole blood assay previously. Initially, three batches of UCMSC PEL and UCMSC ADH conditioned media were tested at a single concentration of 1x. Beginning with UCMSC PEL, all three batches had a statistically significant reduction in TNFα (Figure 3.21A). UCMSC PEL RUO1 reduced TNFα levels to 59.7 ±0.4.08% SEM, RUO2 to 79.6% ±3.15% SEM and RUO3 64.9 ±4.28% SEM compared to the 100.0 ±3.47% SEM maximum stimulation with the vehicle control, with a one-way ANOVA with Tukey's post testing gave statistical significances of p=<0.0001, p=0.0051 and p=<0.0001

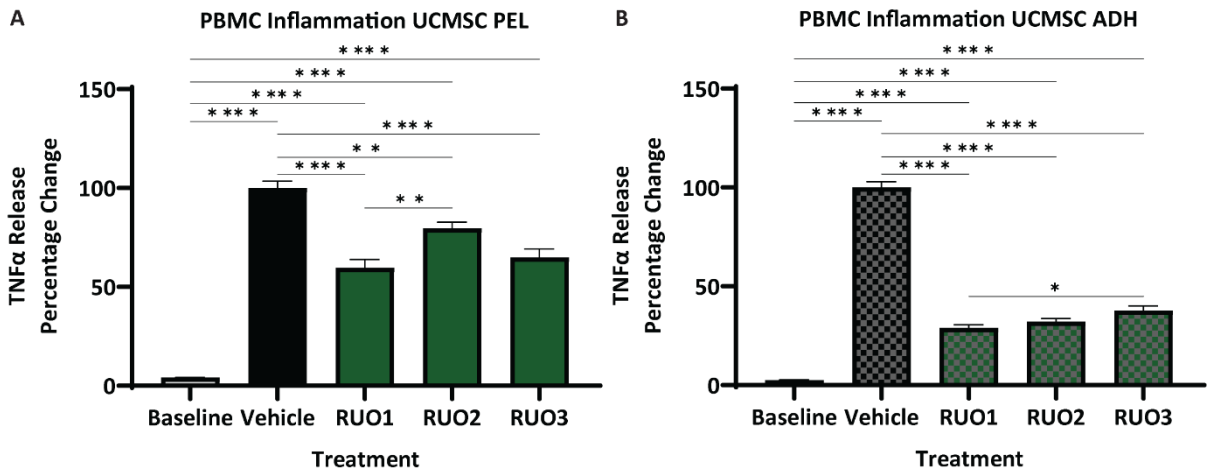

Figure 3.21 Bioactivity assessment of UCMSC conditioned media on PBMC inflammation.

The effect of ***(A)*** *UCMSC PEL and* ***(B)*** *UCMSC ADH conditioned media on TNFα levels from PBMCs stimulated with LPS. Bars represent average of four technical replicates (n=4) and statistical significance from ANOVA with Tukey's post testing is represented by asterixis: * p= <0.05; ** p= <0.01; *** p= <0.001; **** p= <0.0001.*

respectively, n=4 technical replicates. In addition, RUO 1 reduced TNFα significantly more so than RUO2, p=0.0062 however RUO1 was not statistically different to RUO3, which in turn was not statistically different from RUO2.

Similarly, however possibly to a greater extent, all three batches of UCMSC ADH conditioned media reduced TNFα levels with statistical significance (Figure 3.21B), with UCMSC RUO1 reducing to 29.0 ±1.55% SEM, UCMSC ADH RUO2 to 32.2 ±1.52% SEM and RUO3 to 37.9 ±2.25% SEM. One-way ANOVA with Tukey's post testing gave statistical significances of p=<0.0001 against the 100.0 ±2.93% SEM maximum stimulation with the vehicle treatment, n=4 technical replicates. As with UCMSC PEL, RUO1 also had a statistically greater reduction in TNFα than one of the other batches (p=0.0356), this time RUO3. However, as with the other case, RUO1 was not statistically different from RUO2 which in turn had no difference to RUO3.

Next, a dose series for each conditioned media was tested on PBMCs isolated from three donors, with the average response taken as the representative response for each concentration. All three batches

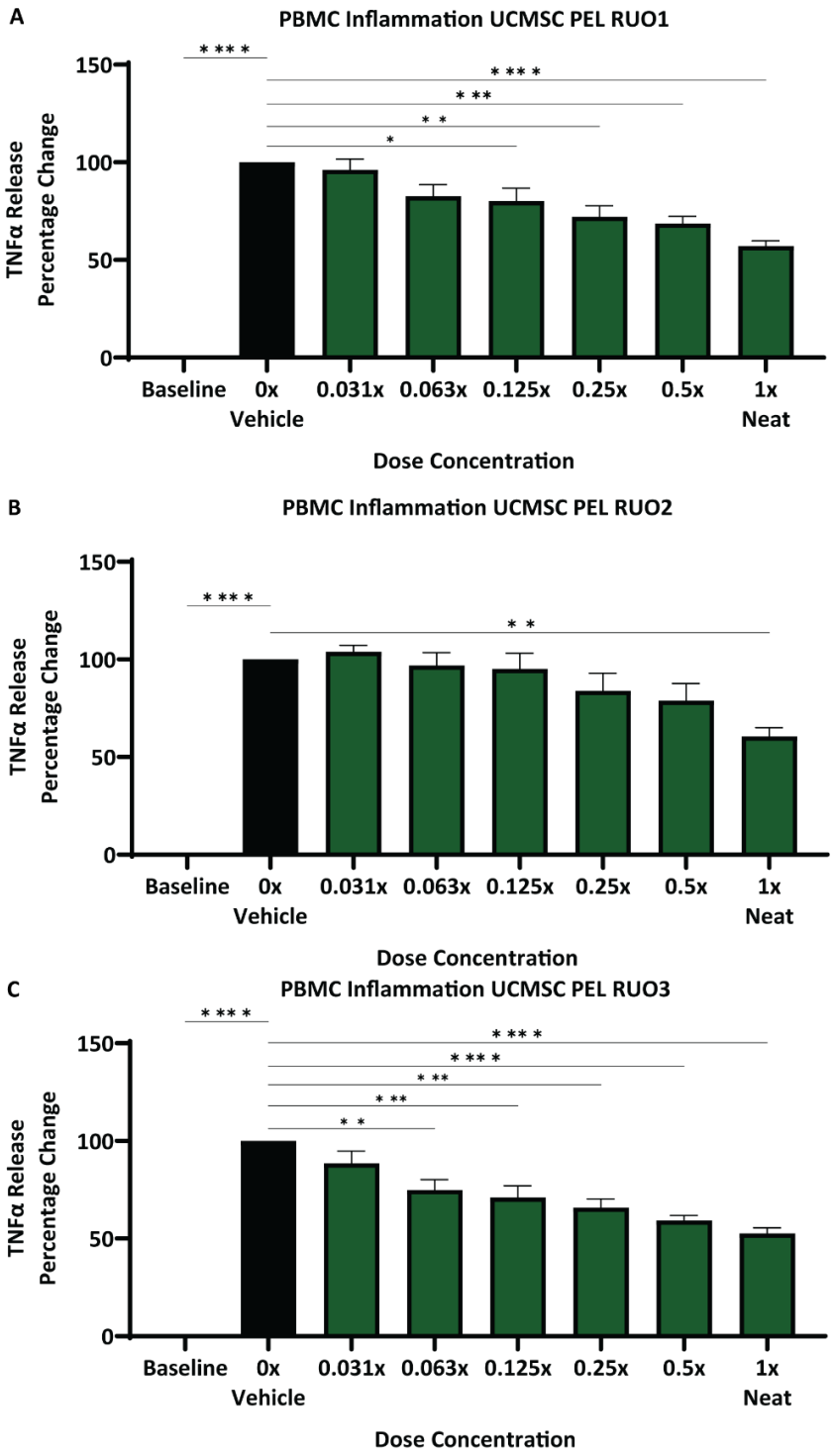

Figure 3.22 Bioactivity dose response for UCMSC PEL conditioned media on PBMC inflammation.

The effect of three batches of UCMSC PEL conditioned media on TNFα levels from human PBMCs after LPS stimulation. ***(A)*** *UCMSC PEL RUO1,* ***(B)*** *UCMSC PEL RUO2,* ***(C)*** *UCMSC PEL RUO3. Bars represent averages of three blood donors from repeated experiments (n=3). Statistical significance from ANOVA with Dunnett's post testing against the 0x vehicle control is represented by asterixis: * p= <0.05; ** p= <0.01; *** p= <0.001; **** p= <0.0001.*

of both conditioned medias (UCMSC PEL and UCMSC ADH) presented with the trend that the greater the concentration of conditioned media that greater the reduction in TNFα released from PBMCs. Beginning with UCMSC PEL RUO1 (Figure 3.22A), one-way ANOVA with Dunnet's post testing revealed that 0.125x, 0.25x, 0.5x and 1x had significantly reduced from the 100.0 ±0.00% SEM of the vehicle treatment to 80.2 ±6.57% SEM (p=0.0334), 72.2 ±5.67% SEM (p=0.0025), 68.7 ±3.69% SEM (p=0.0008) and 57.2 ±2.57% SEM (p=<0.0001) respectively, n=3 biological replicates. 0.031x and 0.063x concentrations had no statistical significance. UCMSC PEL RUO2 (Figure 3.22B) was only statistically significant for the 1x concentration, with TNFα levels reduced to 60.6 ±4.49% SEM (p=0.0018), n=3 biological replicates. Lastly, UCMSC PEL RUO3 (Figure 3.22C) had significant reductions in TNFα as low as 0.063x concentration, with a decrease from the 100.0% vehicle treatment to 75.0 ±5.28% SEM (p=0.0032). The high concentrations reduced TNFα, with 0.125x at 71.1 ±5.96% SEM (p=0.0009), 0.25x at 66.0 ±4.31% SEM (p=0.0002), 0.5x at 59.3 ±2.52% SEM (p=<0.0001) and 1x at 52.6 ±2.92% SEM (p=<0.0001), n=3 biological replicates.

Moving on to UCMSC ADH, despite a greater overall greater anti-inflammatory effect, due to greater variation between donors, statistical significance was limited to the top half of conditioned media concentrations. For UCMSC ADH RUO1, 0.5x and 1x concentrations had significance with 51.1 ±10.71% SEM (p=0.0172) and 42.4 ±7.20% SEM (p=0.0049) respectively (Figure 3.23A), n=3 biological replicates. UCMSC ADH RUO2 (Figure 3.23B) had significance at 0.25x with 57.3 ±12.57% SEM (p=0.0188) as well as 0.5x at 45.3 ±10.61% SEM (p=0.0027) and 1x at 41.6 ±6.93% SEM (p=0.0015), n=3 biological replicates. Lastly the third batch, RUO3 (Figure 3.23C), had significantly less TNFα level against the 100.0% maximum stimulation of the vehicle treatment with 0.5x at 48.2 ±9.47% SEM (p=0.0251) and 1x at 46.0 ±6.52% SEM (p=0.0188), n=3 biological replicates.

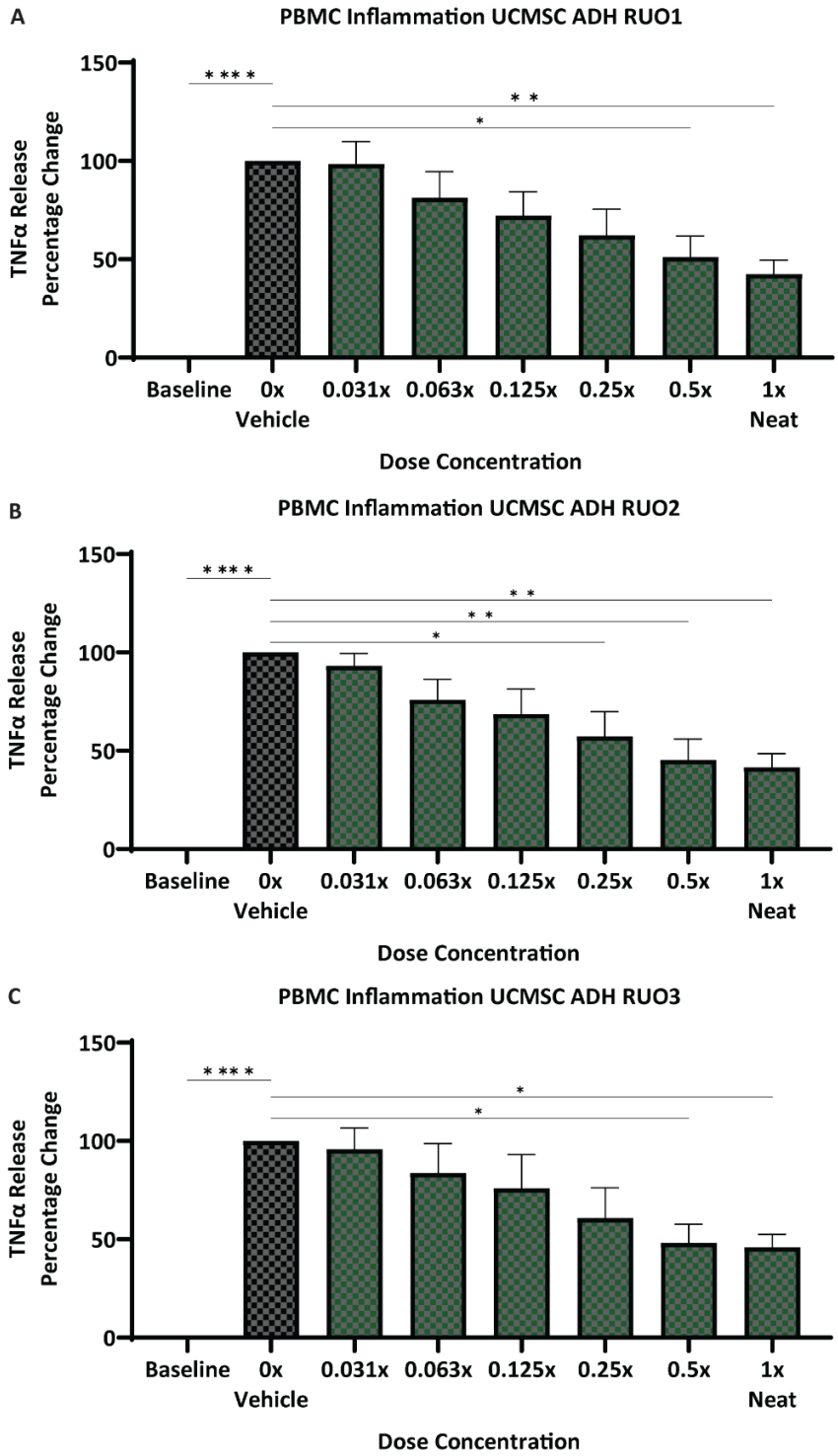

Figure 3.23 Bioactivity dose response for UCMSC PEL conditioned media on PBMC inflammation.

The effect of three batches of UCMSC PEL conditioned media on TNFα levels from human PBMCs after LPS stimulation. ***(A)*** *UCMSC PEL RUO1,* ***(B)*** *UCMSC PEL RUO2,* ***(C)*** *UCMSC PEL RUO3. Bars represent averages of three blood donors from repeated experiments (n=3). Statistical significance from ANOVA with Dunnett's post testing against the 0x vehicle control is represented by asterixis: * p= <0.05; ** p= <0.01; *** p= <0.001; **** p= <0.0001.*

Taking the average of the three batches, a representative dose response curve for UCMSC PEL and USMSC ADH was calculated, n=3 biological replicates (Figure 3.24). Exploring the dose curve metrics, revealed that the average maximal response at 1x treatment for the UCMSC PEL conditioned media was 56.8 ±2.31% SEM and UCMSC ADH was 43.3 ±1.34% SEM compared to the 0x vehicle treatment at 100.0%. The concentration at which half the maximum effect was achieved (EC50) was 0.235x for UCMSC PEL and 0.168x for UCMSC ADH. It can also be deduced that the maximum response for UCMSC PEL conditioned media can be achieved with a treatment of approximately 0.275x UCMSC ADH.

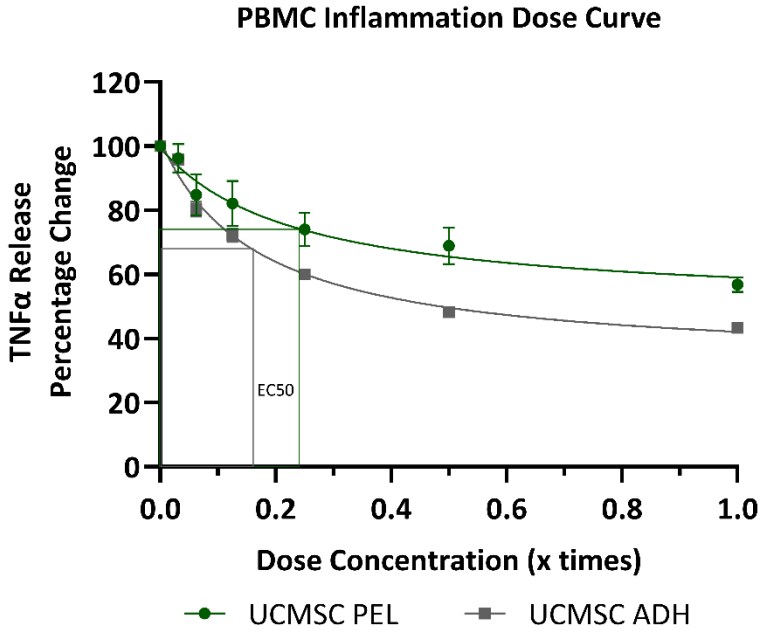

Figure 3.24 Dose response curve of UCMSC conditioned media on PBMC inflammation.

The effect of UCSMC conditioned media on TNFα levels from human PBMCs stimulated with LPS. Each data point represents the average of three UCMSC PEL (green) or UCMSC ADH (grey) conditioned media batches from three donor experiments (n=3). The half effective concentration (EC50) is marked by corresponding line.

Finally, a representative sample set was sent for cytokine/chemokine profiling on the multiplex array used previously for the whole blood assessment, n=3 biological replicates (Figure 2.25). From the forty-eight markers assessed, thirteen were either undetectable (GM-CSF, IL-3, IL-7, IL-17A, IL-22, and VEGF-A) or did not have any statistical changes with neither LPS-stimulation or UCMSC conditioned media treatment (eotaxin, IFNγ, IL-27, MCP-3, PDGF-AA, PDGF-AB/BB, and RANTES). Out of the remaining thirty-five markers, UCMSC PEL conditioned media treatment (10% v/v of 1x) significantly decreased five cytokine/chemokines (G-CSF, IL-1α, IL-1β, IL-1RA, and TNFα) and increased M-CSF compared to the vehicle treated group. UCMSC ADH conditioned media treatment (10% v/v of 1x) significantly decreased three cytokine/chemokines (IL-1β, MIP-1α and TNFα) whilst increasing M-CSF and MCP-1. Although the remaining cytokines and chemokines were not statistically altered with either conditioned media treatment, the overall landscape of changes suggests an anti-inflammatory activity of both UCMSC PEL and UCMSC ADH. In addition, as seen previously, cytokines such as TNFα had a greater reduction with UCMSC ADH conditioned media than UCMSC PEL and others such as IL-10 had a greater increase with UCMSC ADH than UCMSC PEL which supports an anti-inflammatory/pro-resolving picture.

Figure 3.25 continued: *white represents no change and red represents values greater than LPS stimulated vehicle controls (n=3). Statistical significance from ANOVA with Dunnett's post testing against the 0x vehicle group is represented by asterixis: * p= <0.05; ** p= <0.01; *** p= <0.001; **** p= <0.0001*

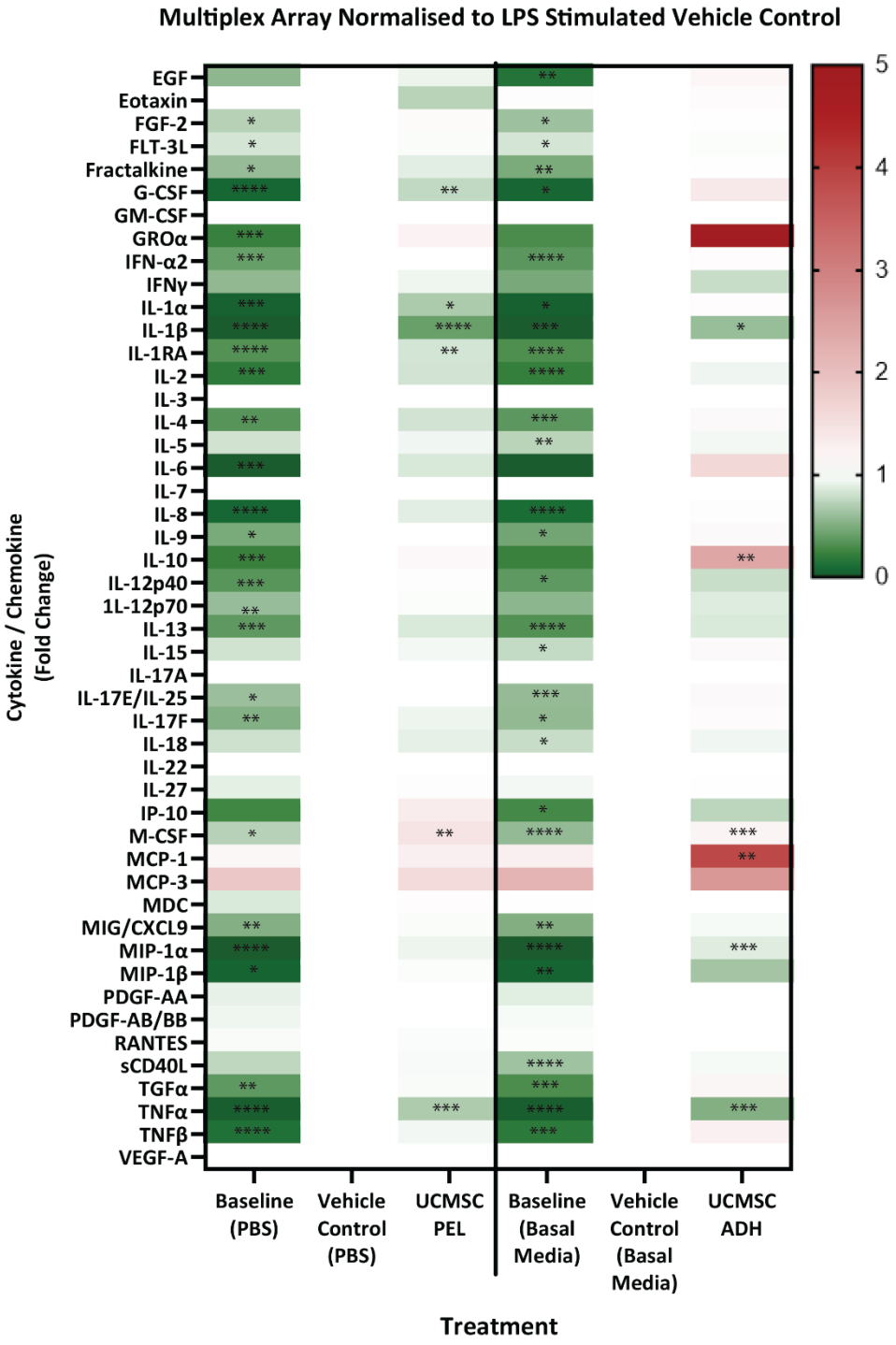

Figure 3.25 Cytokine/Chemokine release profile following UCMSC conditioned on PBMC inflammation.

The effect of UCMSC PEL (left) and UCMSC ADH (right) conditioned media on levels of forty-eight markers of inflammation from LPS stimulated human PBMCs. Heatmap depicts normalised levels where green represents values less than LPS stimulated vehicle controls, [Continues on previous page].

Discussion

This chapter's goal was to explore the utility of Micregen Ltd.'s novel method of generating conditioned media from mesenchymal stem cells (MSCs), on a previously untested MSC isolated from the Wharton's Jelly tissue of umbilical cords, whilst keeping regulatory compliance in mind. UCMSCs are of growing interest in therapeutic research. Easy, non-invasive insolation at relatively low cost provides ample opportunities to develop both autologous and allogenic therapies. Here, two different lines of UCMSC were tested on similar parameters; firstly, to understand their culture and secondly, to explore two methods of generating conditioned media using analysis of the secreted content and bioactivity.

Culture of umbilical cord mesenchymal stem cells.

The first UCMSC line was procured from the American Tissue Culture Collection (ATCC), a non-profit cell repository established to store and supply standard cell lines for research and development use. Most MSC papers, typically using primary cultures, limit the expansion to 3 or 4 passages. In order for human cells to be purchase outside of the requirements of the Human Tissue Act 2004, enough time in culture must be reached for all original cells to be replaced by new cells created within culture (typically at least one passage). The certificate of analysis from ATCC® provides details on the age of the UCMSC population which were obtained for this project. These UCMSCs were one passage old and had been proven to expand for at least 12 population doublings (approximately 4 passages). In order to work with these cells, firstly to research the conditioned media generation protocols and later to potentially produce large scale allogenic therapies, it would be necessary to culture these cells further than is common practice.

Therefore, two months continuous culture of these UCMSCs was conducted and it was found that the UCMSCs could be cultured for approximately 8-9 passages from the point of receipt. As well as understanding the growth rate trajectories of these cells, identifying the limit of growth was important to determine ahead of planning conditioned media research. As the population doubling time

increased, it was confirmed that the cells were entering senescence from approximately passage 10. Senescent cells have been extensively shown to produce a unique altered secretory profile, known as the senescence-associated secretory phenotype, which has been shown to be a driver of disease (Basisty et al., 2020). Therefore, it could be hypothesised that the inclusion of senescent UCMSCs during conditioned media generation would yield a less beneficial secretome (Kim et al., 2022). This information was used to set a threshold to limit the "age" of UCMSCs being used to generate conditioned media. When a second UCMSC line was tested, a similar growth rate was observed. It was found that over ten passages elapsed before senescence was reached. Upon securing this corresponding data, a level of confidence was gained; firstly, that the conditioned media generation threshold set from the first line would be appropriate for this cell and possible further lines, but also UCMSCs from commercial cell banks being a suitable source of cells for expanding to clinically desired numbers.

Returning to the initial ATCC UCMSC line, confirmation of ISCT criteria for MSC classification was conducted using flow cytometry to assess cell surfaces markers. The three positive markers, CD73, CD90 and CD105 were present on the cell surface, however, CD90 expression was lower than reported by the cell bank. These three antigens should be present in great than 95% of cells to MSC classification, however, the panel of negative markers, which detect common cell types which can contaminate the population with poor isolation, were lowly expressed in the population. This would suggest the low level of CD90 detected was not due to common cell contaminants. Optimisation of MSC surface marker profiling may be required to establish if the expression of CD90 was due to differentiation of MSC or technical errors. The Certificate of Analysis from the cell supplier recorded a CD90 value of 99.4%. Furthermore, another MSC line being researched on in this lab, which also presented with low CD90 levels, was later tested on a GMP validated MSC surface marker panel at a contract development and manufacturing organisation (CDMO) and shown to have >99% expression of CD90. Although not shown here, the antibodies used in the negative panel were validated on receipt using controls cells which positively express each marker.

To complete the classification of UCMSCs, successful differentiation in the adipogenic, osteogenic and chondrogenic lineages was confirmed by the positive staining of these cultures.

Generating conditioned media from umbilical cord-derived mesenchymal stem cells.

The focus of this project is on the generation of a translatable UCMSC conditioned media. To that end, two methods for generating conditioned media were utilized. Firstly, an adherent based conditioned media which mimics a common method used across the literature for UCMSCs and second method used was one established by this lab in partnership with Micregen Ltd.. This method was first developed for conditioned medias from two different MSCs, adipose-derived (Mitchell et al., 2019) and amniotic fluid-derived (Mellows et al., 2017), but until now has not been tested on UCMSCs.

The initial comparison of the major components of conditioned media revealed that the amount of total protein was non-significantly lower, but total nucleic acid and EV concentrations were greater in the novel UCMSC PEL conditioned media compared to UCMSC ADH. On the face of it, these findings matched predictions that the hypoxic conditions found within the cell pellet would induce the release of EVs and other molecules (Ishiuchi et al., 2021). However, these two conditioned medias were generated using vastly different methods, for example, both methods used equal numbers of cells but in different volumes of vehicle being conditioned. UCMSC ADH required a larger volume to be added to the flasks compared to what was needed for UCMSC PEL and thus may explain the more diluted components. To that end, when compared as a concentration of secreted molecules/particles per million cells used to generate the conditioned media, it revealed that the UCMSC ADH method resulted in the cells releasing approximately fourteen times the amount of protein, around five times the amount of nucleic acid and four times the levels of extracellular vesicles than UCMSC PEL conditioned media. Although in this study these conditioned medias are to be compared as individual drug products, these findings could be something to exploit during the further drug development.

When these conditioned medias were generated from the RoosterBio® UCMSCs, similar levels of content were recorded. As before total protein concentrations were equal, whereas total nucleic acid

and EV concentrations were greater in UCMSC PEL conditioned media compared to UCMSC ADH. On converting to secreted protein per million cells, protein from UCMSC ADH was again higher at eleven times that of UCMSC PEL, total nucleic acid six times greater and EVs were twice as many. Overall, the variance of batches within each conditioned media appeared relatively lower, particularly with the second UCMSC line. This could be due to a couple factors, one being the cell itself, but the most likely is that the technique in generating conditioned media became more refined and reproducible by the time the second UCMSC was used.

To assess the constituents of the conditioned media from a more qualitative approach, when the protein content was separated by molecular weight, the banding profiles on the silver stain gel revealed there were differences in the proteins profile and not only in total concentration. This suggests the cells have responded differently during the two generation methods and produce two unique drug products. Within each conditioned media variant, for both UCMSC lines, there was no major differences in the most prominent protein bands. When retrospectively compared UCMSC PEL and UCMSC ADH conditioned media profiles from the first UCMSC line against the second, the general banding patterns were identical, which suggests that the methods of generating conditioned media are capable of producing an equivalent conditioned media from different UCMSC lines and the UCMSC donor variation may not be a huge issue to address in later drug development.

Full characterisation of UCMSC conditioned media.

Superficial characterisation of the protein content highlighted differences not only in the concentration but also the type of proteins in UCMSC PEL compared to UCMSC ADH conditioned media. Mass spectrometry analysis of these conditioned media provided a comprehensive profile of the different proteins. This identified a number of proteins unique to each conditioned media. UCMSC PEL conditioned media had to most unique proteins. The Gene Ontology (GO) enrichment analysis, highlighted a number of pathways associated with intracellular components, including a number of proteins in UCMSC PEL which are associated with apoptosis, such as Caspase-3 and Annexin V. This

would indicate that cells were dying or pre-apoptotic during the conditioned media generation process. There is an emerging theory that during apoptosis, cells release a range of molecules and apoptotic-cell-derived EVs (ApoEVs) which influence surrounding cells to not only ensure proper clearance, but also initiate appropriate responses such as tissue repair, inflammation and other immune responses (Shi et al., 2025).

As well as understanding the potential relationship of the conditioned media proteins to biological processes, this in-depth characterisation also uncovered a degree of variation that the gel electrophoresis could not resolve. UCMSC PEL was found to carry the most variation between different preparations. Most of this variation was found in the proteins unique to UCMSC PEL, which would be present in only one or two of the batches.

In addition to the protein characterisation, small RNA sequencing was completed to identify the miRNAs present in the conditioned media. MicroRNAs play a crucial role in the regulation of a vast array of biological processes. Secreted miRNAs have been shown to act as key mediators on intercellular communication. Some of the noteworthy miRNAs found in both UCMSC conditioned media are implicated in the downplay of inflammation. miR-21 has been shown to modulate the NF-κB signalling pathway, through targeting genes such as IL1R1 (Zhang et al., 2020). miR-181 has been shown to negatively regulate TLR4 signalling via targeting TLR4 expression directly (Jiang et al., 2018) and similarly let-7b also targets TLR4 expression but also downstream signalling such as NF-κB (Guo et al., 2018). Finally, miR-146a is worth highlighting, out of the mentioned miRNAs this was the most different between UCMSC ADH and USMSC PEL conditioned media. Like the others, miR-146a has been shown to downregulate the NF-κB signalling pathway through targeting the expression of proteins such as IRAK1 and TRAF6 (Boldin et al., 2011) but it has also been linked to regulation of macrophage polarisation. Studies have shown that miR-146a, through interaction with Notch1 can inhibit M0 to M1 polarisation (pro-inflammatory) whilst promoting M0 to M2 polarisation (pro-resolving/anti-inflammatory) (Huang et al., 2016).

Umbilical cord-derived mesenchymal stem cell conditioned medias increase cellular proliferation.

An important mechanism in tissue repair is cell proliferation, whether it's the mature cells, the local precursor cell pool or distant stem cell niches such as the bone marrow. The enhancement of cell proliferation has been demonstrated as a biological action of different stem cell conditioned media and derivatives including UCMSC conditioned media made in the style of UCMSC ADH (Di et al., 2014, Lv et al., 2020, Sriramulu et al., 2020). The proliferative effect of UCMSC conditioned media made using the novel pelleting method alongside the traditional adherent conditioned media, was tested using Micregen Ltd.'s potency assay protocol. This revealed that both conditioned medias were able to increase proliferation of HeLa cells. The initial testing with the first UCMSC line suggested that the novel UCMSC PEL conditioned media may have a slightly greater effect on proliferation, since lower concentrations significantly increased the number of cells, whereas only the highest concentration of UCMSC ADH achieved this. However, conditioned media produced from the second UCMSC line, found that the overall increase in proliferation was slightly greater with UCMSC ADH then UCMSC PEL conditioned media. This second series of tests also demonstrated that the different batches of UCMSC conditioned media had similar efficacy, suggesting variation in the content quantification was not resolved in the mechanism of action.

Umbilical cord-derived mesenchymal stem cell pellet conditioned media increases cell migration.

As with cell proliferation, recruitment of cells to the site of damage or regeneration, whether its immune cells to clear damaged tissue or resident stem/progenitor cells to replace those lost, is key to disease resolution as well as haemostasis of tissue and is dependent on a cells ability to migrate. It is therefore thought that the ability to promote cell migration would be a desirable mechanism of action in a therapeutic. As with proliferation, UCMSC ADH style conditioned medias have been shown to promote migration of cells (Li et al., 2017). Using a transwell migration assay to explore the ability of the conditioned media to elicit a migratory response by possibly acting as a chemoattractant or signalling factors which influence the cell status such as changes in integrins and focal adhesion, did not find pro-migration action from the first UCMSC line. On the other hand, UCMSC PEL conditioned

media strongly promoted the movement of cells across the membrane. This activity was repeated by the second UCMSC line from RoosterBio®, with three batches bringing about a strong increase in cell movement. UCMSC ADH conditioned media from this second cell line, did promote cell migration, with all three batches having a significant effect. Although, the overall increase in migrated cells was lower than that of UCMSC PEL.

The differences seen in UCMSC ADH conditioned media between the two UCMSC lines could be attributed to donor variation, which has been studied in literature (Kang et al., 2018, Česnik and Švajger, 2024). However, interestingly, the levels of all three families of content (protein, nucleic acid and EVs) were measured lower in the second UCMSC line than the first, which would imply that the quality of content may be different.

LPS-induced inflammatory response in a whole blood which was attenuated by UCMSC conditioned media.

To determine if UCMSC conditioned medias have immunomodulating properties, a new assay was developed. Blood provides a source of immune cells which contribute to both homeostasis and disease. When stimulated with bacterial lipopolysaccharide (LPS), these cells release a variety of cytokines and chemokines, such as tumour necrosis factor alpha (TNFα) which is released during the initial response to stimuli.

UCMSC conditioned medias were tested in a dose wise manner on this assay. Both UCMSC PEL and UCMSC ADH showed strong statistically significant reductions in TNFα release. Interestingly, despite the differences in protein, nucleic acid and EV concentrations and the effects reported in the cellular proliferation and migration assays, UCMSC ADH had a seemingly greater activity in this assay than UCMSC PEL conditioned media. Both conditioned medias generated from the first UCMSC line were able to reduce the level of TNFα being released, however lower concentrations of UCMSC ADH had greater or equivalent effects as the highest UCMSC PEL concentration, demonstrating a more potent anti-inflammatory property on UCMSC ADH conditioned media. Similarly with the second UCMSC line,

UCMSC ADH had a greater reduction in TNFα levels than the corresponding UCMSC PEL conditioned media. However, in this instance, although all three batches of UCMSC PEL did reduce inflammation, only one reduced it significantly within an ANOVA test.

TNFα is released as a direct result of LPS stimulation, however, LPS induces a response in the canonical inflammatory pathway, which results in more than just TNFα release. The canonical LPS response often begins through toll-like receptors (TLRs), such as TLR-4, which in turn activates downstream nuclear factor-κB (NF-κB). NF-κB is an essential transcription factor for numerous genes, involved in cellular progression from cell cycle regulation to adhesion molecules, and importantly in this case, cytokines and chemokines including TNFα but also molecules such as interleukin (IL)-1, IL-6, IL-8, IL-12, MCP-1, MIP-1 and CXCL1 to name a few. With the inflammatory process being a vast multifactorial system, with numerous cells involved and even more related molecules, it is plausible that the two conditioned medias may work differently across inflammation.

A wider assessment of inflammatory cytokines and chemokines revealed a select number of molecules being altered, but not all. Changes in IL-1β, IL-6, IL-8, IL-10, IL-12p40, IP-10, MCP-1, MIP-1α and TNFα as a collection is indicative of a response from monocytes and macrophages. Molecules primarily related to other immune cells such as T-cells, T-helper cells and Neutrophils (for example IL-2, IL-4, and IL-5) were either unchanged following stimulation with LPS or unmodulated by UCMSC conditioned media. TLR4, a commonly involved receptor of PAMPs such as LPS (Park and Lee, 2013), is most abundantly expressed on the surface of monocytes and macrophages compared to the other immune cells (Austermann et al., 2022), along with these cells being crucial drivers of the initial response to bacterial infection, it is not surprising that the main group of cytokine/chemokines found to be increased following LPS stimulation are related to monocytes and macrophages. Comparing the two conditioned medias, UCMSC ADH conditioned media elicited an overall positive immunomodulated effect across this panel of cytokines and chemokines, with decreases measured in typical pro-inflammatory molecules such as IL-1β, IL-6, IL-12p40, IP-10, MIP-1α and TNFα, along with

increasing pro-resolving/mediation factors such as IL-8, IL-10 and MCP-1. Although UCMSC PEL conditioned media brought about statistically significant changes in a number of these cytokines, there were no effects measured in IL-8 and MCP-1. In addition, there were generally weaker changes measured following UCMSC PEL treatment in other markers.

LPS-induced inflammatory response in a PBMCs which was attenuated by UCMSC conditioned media.

As mentioned, LPS elicits and inflammatory response primarily through TLR4 present on the surface of cells, of which circulating monocytes have some of the highest expression of this receptor. Blood can be simply divided into subpopulations using density gradient centrifugation, which allowed study of these primary responders. When establishing the assay, it was important to verify that the PBMC population, which contains the monocytes, responded to LPS and that the other populations of cells were noteworthy of further study for this model. As predicted, the PBMC population had the greatest response to LPS. The method used in this initial isolation of PBMCs retained the plasma and platelets with the PMBCs, therefore the next phase of establishing the assay sought to further isolated the PBMCs via additional centrifugation. However, this found that the washed PBMCs, without PRP, exhibited a lower response to LPS than the unwashed cells. Upon reflection this finding is unsurprising. LPS binding protein (LBP), secreted by the liver is a circulating factor which binds with high affinity to LPS and accelerates the transfer of LPS to cell surface receptors such as CD14 and TLR4 (Hailman et al., 1994). Although not essential for LPS-CD14-TLR4 signalling, the presence of LBP noticeably reduces the amount of LPS required for cell activation (Su, 2002).

Following the establishment of the assay protocol, the UCMSC conditioned medias were tested on unwashed PBMCs. A comparison with three batches of UCMSC conditioned media from the second cell line found similar findings as the whole blood assay. Both UCMSC PEL and UCMSC ADH decreased levels of TNFα, with UCMSC ADH conditioned media demonstration a greater reduction in inflammation. Using a dose response curve to reflect on the potency of UCMSC PEL and UCMSC ADH,

the advantages of UCMSC ADH conditioned media as a therapeutic begin to come to light. Taking the EC50 value for UCMSC PEL conditioned media at 0.275x treatment, the amount of UCMSC ADH conditioned media to elicit the same level of response would only be approximately a 0.1x concentration. Taking this forward and bringing in the generation protocol, a 10% v/v treatment at 0.275x of UCMSC PEL conditioned media is 27.5 µL of conditioned media per 1 mL of culture (200 µL PBMCs) whereas only 10 µL of UCMSC ADH conditioned media would be required to bring about the same degree of treatment. Taking this one step further, relating this to the number of UCMSCs required to produce these volumes, the economy of the therapeutics becomes vastly different as 27.5 µL of UCMSC PEL requires almost 70,000 cells compared to 3,000 cells required for an equivalent treatment of UCMSC ADH conditioned media. Understanding these properties of a therapeutic candidate during early research and development enables the informed selection of which concepts would provide not only the best therapeutic outputs but also a balanced cost to value relationship. For example, once scaled up to a clinical size, treating patients with this degree of difference could result in a substantial difference in cost with little or no therapeutic benefit.

Finally, the effect of the UCMSC conditioned medias on a wider array of inflammatory molecules was explored. Compared to the whole blood, there was overall less significantly altered cytokines. UCMSC ADH still had greater increases in “resolving/anti-inflammatory” cytokines like GROα and IL10, and greater reduction in TNFα which aligns with the findings of the ELISAs. The difference in the response to LPS and UCMSC conditioned media across the board could reflect the involvement of other leukocytes which are removed during the PBMC preparation. Although TLR4 receptors are most abundant on monocytes/macrophages, the signally cascade that occurs once stimulated will undoubtedly stimulate the other cell present in the blood. Keeping this in mind, using the PBMC preparation was still a valuable tool to begin to observe the effect of UCMSC conditioned media on the primary responding cell population. However, it also highlights the importance of the complex system in when gathering the holistic mechanisms of action.

Chapter 4 - Results: Further Development of an Umbilical Cord Mesenchymal Stem Cell Conditioned Media Product.

Introduction.

The unique regenerative potential of stem cells continues to create excitement in the scientific and medical community with an increasingly heightened expectation among the public for this promising revolution in medicine. So far it has been demonstrated that a novel method of generating conditioned media from UCMSCs, through pelleting, was able to produce an active conditioned media. Yet in relative comparison with a conditioned media method commonly used throughout the literature, revealed it to be no more effective than this adherent counterpart. Due to this, along with the generally more inefficient use of cells, the project focus shifted toward developing a clinically compliant adherent conditioned media.

The process of creating a clinical-grade, allogenic, cell-free conditioned media from UCMSCs involves careful consideration of several key factors. Standardising the manufacturing process is vital, encompassing everything from material selection to cell culture conditions and the conditioned media generation, to ensure batch-to-batch consistency in both composition and potency (Chouaib et al., 2023, Phelps et al., 2018, Sagaradze et al., 2019, Gimona et al., 2017). The International Council for Harmonisation (ICH), established in 2015 as the over-arching governing body for global pharmaceutical regulation, align the requirements for medical products to demonstrate aspects of quality, safety, and efficacy. ICH guidelines for quality of biotechnical products outline the importance of a robust quality control strategy, including testing for stability and storage (Q1), contaminants/impurities (Q3), sterility and endotoxin assays (Q4), the quantification of essential bioactive components (Q6) and good manufacturing practice (Q7). Manufacturing considerations, such as the scale of the production to meet clinical needs, the optimisation of cell expansion and the conditioned media generation methods, and the source, grade and redundancy in supply for all the consumables and materials required for batch generation, should also be addressed early in a products development (Chouaib et al., 2023, Phelps et al., 2018).

There are also important considerations around which medias are suitable for generating conditioned media. Most of the scientific literature investigating different stem cell conditioned medias predominately use conditioned culture media (Hyland et al., 2020) or more commonly basal/serum free media (Yang et al., 2014, Choi et al., 2024a, Tang et al., 2023). Foetal bovine serum (FBS) is a common component of many culture medias, and the ones used for growing mesenchymal stem cells are no exception. There is an inherent risk of contamination from animal protein present in FBS (Panchalingam et al., 2015) as well as at greater risk of dangerous contaminants such as endotoxins, mycoplasma, viruses or prion proteins (Fang et al., 2017). Even in cases where GMP-grade FBS is used, these animal-derived components that are not used by the cells will be added to the secretions that are desired during the stem cell conditioning process. The next evolution is those known as serum-free or xeno-free media (Brunner et al., 2010), which replace the FBS component with either defined animal-derived components such as serum albumin and growth factors or human-derived alternatives such as human platelet lysate. The most acceptable alternative is chemically defined medium, which is not only serum/xeno free but is also without undefined lysates or supplements (Chouaib et al., 2023). This is not only considered the safest option but also presents with the greatest control for batch-to-batch reproducibility in GMP-compliant manufacture. However, no matter which media is utilised for the generation of conditioned media, there will still be inclusion of the components of the media in the final product. Here, it is our aim to identify not only the most GMP-appropriate vehicle for generating a stem cell conditioned media but one which will provide the fewest hurdles for clinical use. It is hoped that a salt buffer like PBS would be a suitable alternative to culture media for generating conditioned media from UCMSCs, which would be fully defined as well as widely available and on top of this, simplistic in composition.

For small-scale expansion to generate quantities of conditioned media for in vitro experiments or small rodent models the traditional two-dimensional monolayer cultures typically suffice. However, the demand for increased lot-size manufacturing for clinical use, large-scale alternatives are often required. Multi-layer flasks, offer higher capacity than the simpler T-flask, offering like-for-like culture

techniques. However, these vessels are cumbersome and time-consuming to handle and are ultimately still limited in their scale to the incubators that need to house them. Transitioning to a spinner flask or bioreactor three-dimensional culture, with the use of microcarriers, offers a wealth of benefits for both scaling up adherent cell culture and providing more opportunities to control the culture process. However, optimal conditions for expanding stem cells are still under investigation and will undoubtedly remain an integral part of process optimisation for each cell line, microcarrier, culture media and vessel combination being used for the foreseeable future.

Here, the hope is to use bioreactors to not only expand UCMSCs to the numbers required for clinical manufacture, but to also generate a conditioned media. A lot of focus has been given to the use of bioreactors for the production of GMP extracellular vesicles (Wiest and Zubair, 2025). Studies have shown that the type of culture influences quality of EVs produced by cells cultured in either 2D or 3D methods. Changes in EV-related gene expression from cells cultured in 3D reactors have been reported (Thippabhotla et al., 2019), as well as miRNA, EV surface markers and protein cargos differ in composition (Rocha et al., 2019). In addition to these possible changes to the conditioned media, the way in which cells and conditioned media are processed is also refined from 2D to 3D cultures. In 2D systems, it is hard to avoid opening the flask and manually replacing fluids, which increases the chance for contaminations. When cultures scale-out towards the required cell quantities for manufacture, the process becomes quite laborious. On the other hand, lots of investment has been made to develop GMP-compliant closed-system and automated 3D culture systems, which not only reduce the risk of contamination but also cut down time in expensive cleanrooms (Zhang et al., 2022). Taking these considerations in mind, highlights the importance of decision making around upstream culture methods early in a products development.

This chapter therefore focuses on these key areas of developing a clinical-relevant, GMP-ready therapeutic product from UCMSCs. Beginning with material selection a new GMP-compliant UCMSC cell line is tested against the previously used research-use-only cell line from Chapter 3, to determine

its suitability as a replacement UCMSC for the GMP product manufacture. The vehicle used for UCMSC ADH culture is also addressed, as the originally used ATCC basal media would not be suitable for GMP manufacture, ease of regulatory compliance nor material source security. ATCC basal media is undefined, non-GMP certified meaning there is not guarantee of its typicality, safety, and/or accuracy of the product. Although in some cases the use of non-GMP reagents can be used in GMP manufacture, with the appropriate risk assessments and additional testing by the user, being such as major component (the vehicle) for a product, it would be more appropriate to use a GMP-grade resource. In addition, ATCC have strict licensing rules on their products, which prohibit use outside of research. The impact of this change on the conditioned media stability will be investigated and finally a proof-of-concept for transitioning UCMSC adherent conditioned media to a 3D bioreactor-like system will be investigated.

Results

Following the procurement of an umbilical cord mesenchymal stem cell from a GMP-grade cell bank, with all the appropriate permissions for use in further manufacturing processing, this third cell line was tested against the UCMSC RUO cell line to confirm that it would be a similar or greater conditioned media generator. This cell line and its subsequent conditioned media will be referred to as UCMSC MUO.

GMP umbilical cord mesenchymal stem cell growth, conditioned media, and release testing.

Assessment of growth characteristics – UCMSC MUO

To begin, UCMSC MUO cells were revived from cryopreservation and cultured using GMP-grade materials, such as growth media and culture plastics for the first two passages. Once a GMP-like cell bank was created in house, normal research grade materials were used for subsequent cultures. Continuous culture over a 50-day period (n=1) revealed a similar culture lifespan as the UCMSCs in Chapter 3 (Figure 4.1A). A linear expansion rate was recorded for nine passages where, as previously reported, the growth rate for UCMSCs began to decline after 36 days of culture. A final passage on day 50 (passage 11) post-revival confirmed cell growth had dramatically slowed as there were only two population doublings since the previous passage 14 days prior, which had been occurring every 3 to 4 days otherwise. During this culture period, cell viability remained above 90% (Figure 4.1B). As before, the age of cells used for conditioned media generation was constrained to fall within the linear growth phase, and in this case between passage 3 and 6 were selected. To determine if these cells can produce an equivalent conditioned media as those previously used, both versions of conditioned media, UCMSC PEL and UCMSC ADH, were generated from the UCMSC MUO line. Following the collection of the secretome, cells were retained and/or passaged to assess their viability. A propidium iodide exclusion assay revealed that following UCMSC PEL conditioned media generations had 95.9% 'live' cells, and UCMSC ADH had 97.8% 'live' cells, n=3 biological replicates (Figure 4.1C).

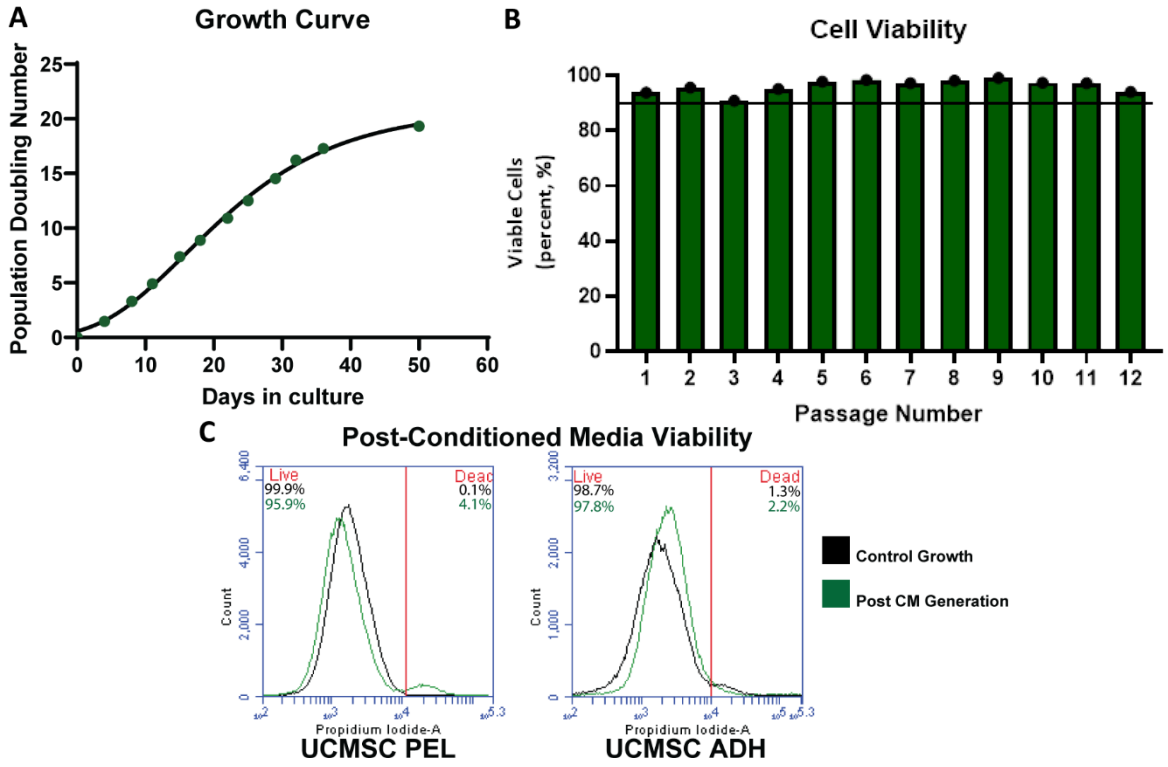

Figure 4.1 Growth and viability of UCMSC MUO cell line.

(A) *Tracking of population doubling number of UCMSC MUO cells over 50 days post revival from cryopreservation (n=1).* ***(B)*** *Trypan Blue exclusion cell viability of UCMSC MUO cells over the 12 passages, with a line indicating 90% viability (n=1).* ***(C)*** *Propidium Iodide exclusion cell viability post conditioned media generation, green (UCMSC PEL – left; UCMSC ADH – right) compared to cell cultured in number conditions, black (n=3).*

Assessment of UCMSC MUO conditioned media - UCMSC PEL

To confirm that the UCMSC MUO line can produce a UCMSC PEL conditioned media, three batches from UCMSC MUO were compared against UCMSC RUO. Comparing the constituent parts of the conditioned media revealed that there was no difference in the three major features of conditioned media. The protein concentration of UCMSC PEL derived from UCMSC MUO cells was 8.0 ±0.31 µg/mL SEM compared to 8.4 ±0.29 µg/mL SEM from the previous UCMSC RUO cells, n=3 (Figure 4.2A). The total nucleic acid concertation from UCMSC MUO was 20.0 ±0.71 µg/mL SEM compared to 17.7 ±1.61 µg/mL SEM form UCMSC RUO, n=3 biological replicates (Figure 4.2B), and finally, the EV concentration

form UCMSC MUO was $9.92x10^9$ ±$0.04x10^9$ particles/mL SEM compared to $9.49x10^8$ ±$0.94x10^8$ particles/mL SEM from UCMSC RUO cells, n=3-4 biological replicates (Figure 4.2C).

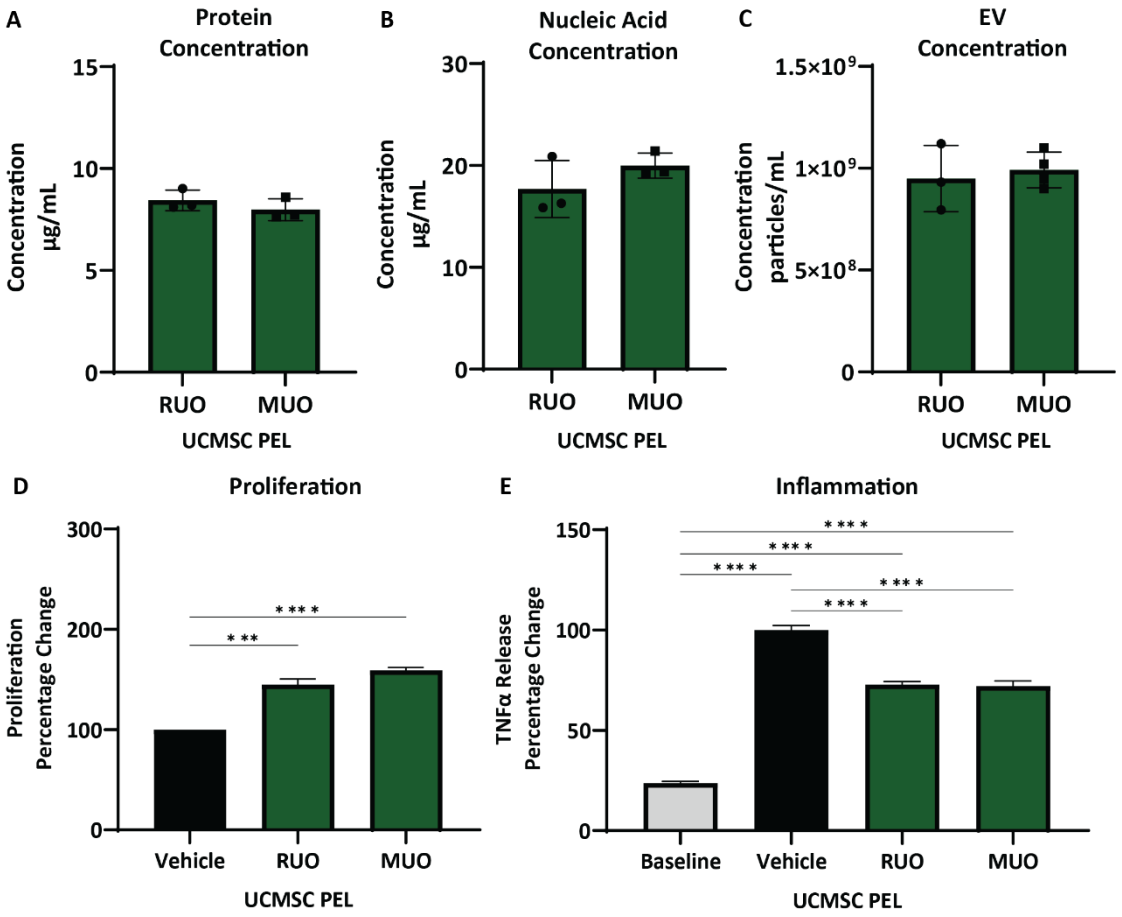

Figure 4.2 Content and bioactivity of UCMSC PEL conditioned media from UCMSC MUO cells compared to UCMSC RUO cells.

(A) *Quantification of protein,* ***(B)*** *total nucleic acid, and* ***(C)*** *extracellular vesicle concentrations from UCMSC RUO and UCMSC MUO derived UCMSC PEL conditioned media.* ***(D)*** *Effect of UCMSC PEL conditioned media from UCMSC RUO and MUO cells on HeLa cell proliferation. Bars represent an average response from three batches of conditioned media (n=3).* ***(E)*** *Effect of UCMSC PEL conditioned media from UCMSC RUO and MUO cells on TNFα levels release from human blood following LPS stress, Bars represent the average response from three batches of conditioned media (n=3). Statistical significance from ANOVA with Tukey's post testing is represented by asterixis: * p= <0.05; ** p= <0.01; *** p= <0.001; **** p= <0.0001.*

Next, the biological activity was assessed on the cellular proliferation assay. UCMSC PEL conditioned medias from both UCMSC RUO and UCMSC MUO (n=3 biological replicates) significantly increased proliferation to 144.9 ±5.65% SEM (p=0.0003) and 159.1 ±2.68% SEM (p=<0.0001) respectively, compared to the 100.0 ±0.00% SEM normal proliferative rate of the vehicle treatment (Figure 4.2D). Importantly, there was no significant statistical difference between the UCMSC PEL conditioned media from UCMSC RUO cells and that generated from UCMSC MUO cells (p=0.5043). Finally, the inflammation assay on whole blood (n=4 technical replicates) found that both UCMSC cells produced a UCMSC PEL conditioned media that reduced TNFα levels to 72.8 ±1.51% SEM with RUO and MUO to 72.1 ±2.60% SEM, with statistical significance of p=<0.0001 for both against the vehicle treatment at 100.0 ±2.36% SEM (Figure 4.2E). There was no statistical difference between the two conditioned medias (p=0.9932). Considering all the outlined results, UCMSC PEL conditioned media from UCMSC MUO cells was demonstrated to be similar to that previously generated from UCSMC RUO cell.

Assessment of UCMSC MUO conditioned media – UCMSC ADH

Whilst testing UCMSC PEL conditioned media, UCMSC ADH conditioned media from UCMSC MUO was also compared against that from UCMSC RUO cells. In a similar fashion, this comparison began with the content of the conditioned media, which likewise found no difference in the three components of the conditioned media. The protein concentration of UCMSC ADH derived from UCMSC MUO cells was 9.0 ±0.43 µg/mL SEM compared to 9.6 ±0.64 µg/mL SEM from the previous UCMSC RUO cells, n=3 biological replicates (Figure 4.2A). The total nucleic acid concentration from UCMSC MUO was 8.8 ±1.81 µg/mL SEM compared to 11.0 ±1.68 µg/mL SEM form UCMSC RUO, n=3 biological replicates (Figure 4.2B), and finally, the EV concentration form UCMSC MUO was $6.23x10^8$ ±$2.21x10^8$ particles/mL SEM which was not statistically different from UCMSC RUO quantified at $1.86x10^8$ ±$0.42x10^8$ particles/mL SEM, n=3 biological replicates (Figure 4.2C).

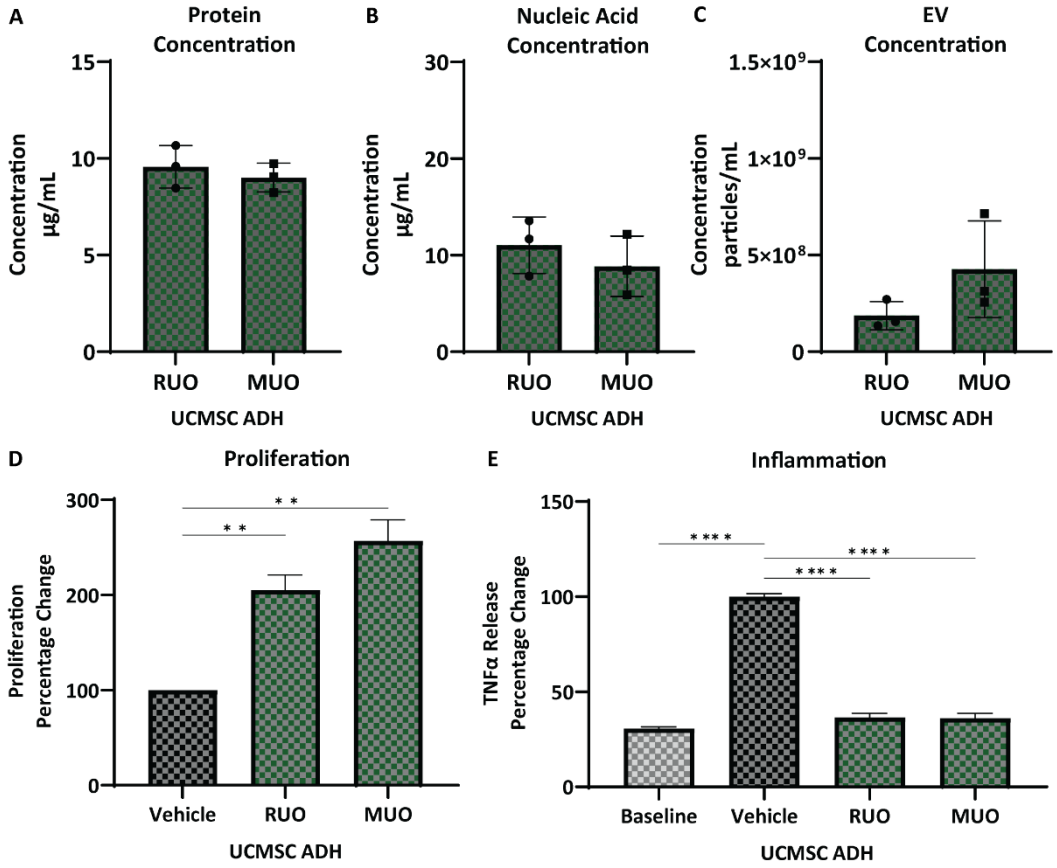

Figure 4.3 Content and bioactivity of UCMSC ADH conditioned media from UCMSC MUO cells compared to UCMSC RUO cells.

(A) *Quantification of protein,* ***(B)*** *total nucleic acid, and* ***(C)*** *extracellular vesicle concentrations from UCMSC RUO and UCMSC MUO derived UCMSC ADH conditioned media.* ***(D)*** *Effect of UCMSC ADH conditioned media from UCMSC RUO and MUO cells on HeLa cell proliferation. Bars represent an average response from three batches of conditioned media (n=3).* ***(E)*** *Effect of UCMSC ADH conditioned media from UCMSC RUO and MUO cells on TNFα levels release from human blood following LPS stress. Bars represent the average response from three batches of conditioned media (n=3). Statistical significance from ANOVA with Tukey's post testing is represented by asterixis: * p= <0.05; ** p= <0.01; *** p= <0.001; **** p= <0.0001.*

The assessment on the pro-proliferative activity of UCMSC ADH conditioned media, found there was no statistical difference (p=0.1289) between that generated from UCMSC RUO and UCMSC MUO cells (Figure 4.3D) and both sets of UCMSC ADH conditioned media demonstrated a statistically significant increase in proliferation, n=3 biological replicates. Comparing to normal proliferation rate of the vehicle (100.0 ±0.00% SEM), UCMSC ADH RUO increased to 205.1 ±16.17% SEM (p=0.0080) and UCMSC ADH MUO with a greater increased to 257.0 ±22.16% SEM (p=0.0010). As before, the final test to confirm equivalency of UCMSC MUO cells was the whole blood inflammation assay (Figure 4.3E). Here, both UCMSC ADH RUO and UCMSC ADH MUO significantly reduced TNFα levels from the 100.0 ±1.52% SEM vehicle maximum stimulation levels, down to 36.6 ±2.05% SEM (p=<0.0001) and 36.1 ±2.62% SEM (p=<0.0001) respectively. Both conditioned media treatments resulted in TNFα levels which were no longer significant to the baseline, n=4 technical replicates. Crucially, UCMSC ADH RUO and UCMSC ADH MUO had no difference in TNFα levels, as determined by a one-way ANOVA with Tukey's post-test (p=0.9976). Considering all the outlined results, UCMSC ADH conditioned media from UCMSC MUO cells was demonstrated to be similar to that previously generated from UCSMC RUO cells.

Development of UCMSC ADH conditioned media for clinical translation.

With the confirmation that the new UCMSC MUO cell line could produce conditioned media to a comparable level to those used in the initial research in Chapter 3, the next stage of this project was to focus on translating a UCMSC ADH conditioned media. The rationale behind the decision will be laid out in the discussion section later. Briefly, it was decided based on the results of biological activity assays and manufacturability that UCMSC ADH presented the most promising candidate for further development. The protocol used here to generate UCMSC ADH conditioned media used a vehicle of basal media from ATCC, with an unknown composition. It was identified that the most appropriate step in development would be to explore alternative vehicles for the collection of UCMSC secretome.

Identifying suitable buffers as a replacement of UCMSC ADH vehicle.

To begin the journey of exploration into alternative solutions for the collection UCMSC ADH conditioned media, a small-scale pilot study was conducted. Here, seven new solutions ranging in complexity from phosphate buffered saline (PBS) to widely available basal media were trialled. The full composition of each solution is outlined in appendix 1. UCMSCs were incubated for 24 hours at 37°C with or without CO_2 supplementation depending on the solution's buffering capacity. Following conditioned media generation, all cells were retained and counted with an assessment of viability. Statistical comparisons were made using a one-way ANOVA with Dunnet's post-test against the ATCC basal media, n=6 biological replicates.

The most simplistic buffer tested, Dulbecco's PBS (DPBS) had 112,717 ±18,021 SEM cells less than originally seeded. DPBS with the addition of calcium and magnesium salts had fewer cells still, 144,692 ±16.654 SEM less than seeded, but the worst loss of all was found with DPBS with calcium, magnesium, glucose, and pyruvate at 230,392 ±16,654 SEM below the seeding number. Hank's balanced salt solution (HBSS), a mild bicarbonate buffer commonly used in tissue culture for maintaining cells in non-CO_2 supplement environments, also resulted in a reduction in cell number after 24 hours, with 101,708 ±39,374 SEM cells below the number seeded.

The first solution to require 5% CO_2 supplementation was Earle's balance salt solution (EBSS), with a higher concentration of sodium bicarbonate, it is often used as the buffer base for common tissue culture media. EBSS buffer also had a large reduction in recovered cells compared to the starting number, a reduction of 198,158 ±13,950 SEM cells. However, unlike DPS, the addition of calcium and magnesium salts saw UCMSCs increase in number during the conditioned media collection period, to 91,750 ±18,938 SEM cells above the seeding number. The last new solution tested, was minimum essential medium (MEM), which has an EBSS base, with numerous additional amino acids, vitamins, and other nutrients. MEM also had an increase in cell number, 90,800 ±23,339 SEM cells more than seeding.

When compared to the original ATCC basal media, which had 152,417 ±38,990 SEM more cells at the end of the conditioned media generation period. EBSS with calcium and magnesium as well as MEM

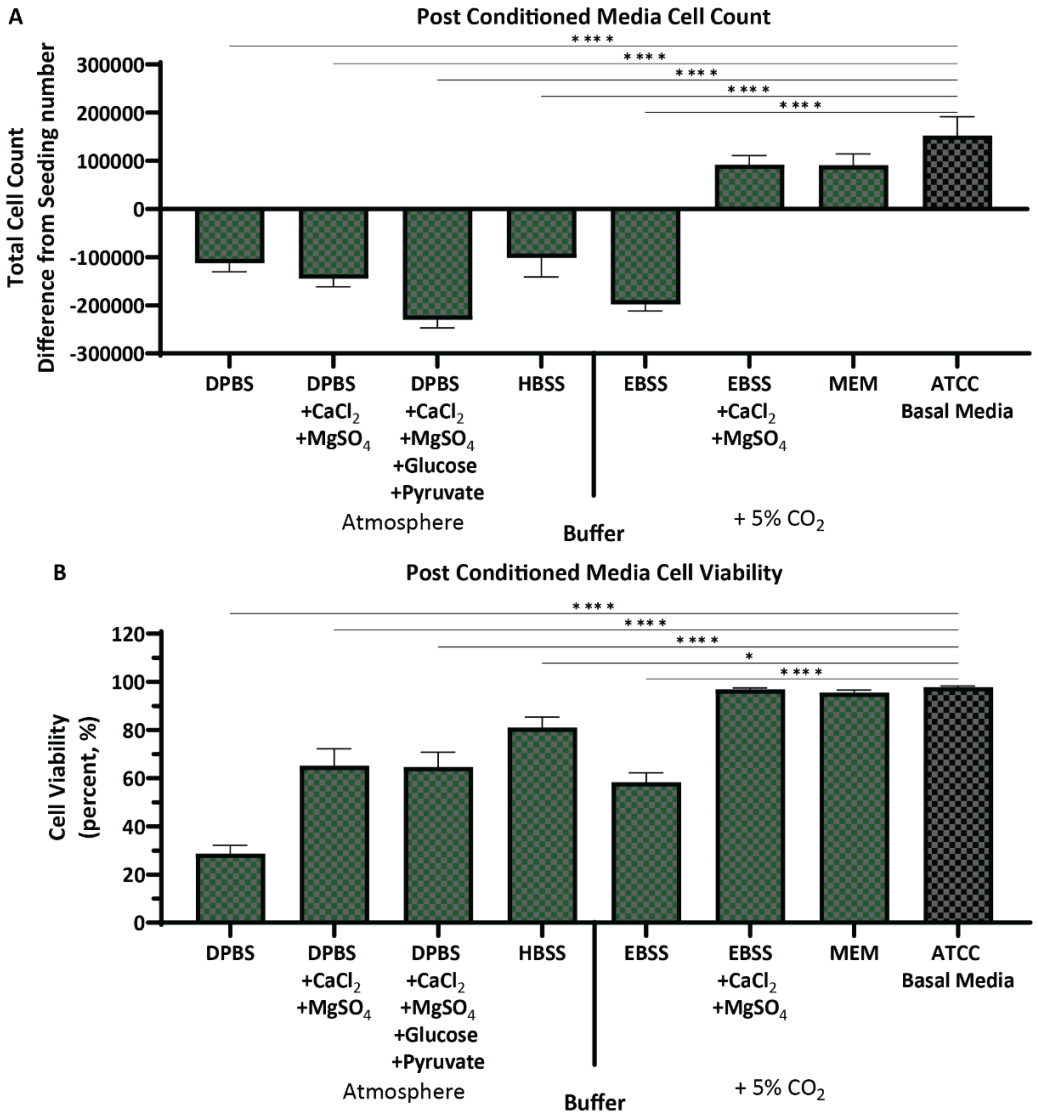

Figure 4.4 Impacted of different buffer solutions used for UCMSC ADH conditioned media generation for 24 hours on UCMSC survival post collection.

(A) *Cell count of UCMSCs at the end of the conditioned media generation in different buffers, presented as difference from the starting seeding number (0).* ***(B)*** *Trypan blue exclusion cell viability of recovered UCMSCs following conditioned media generation. Bars represent the average of six independent wells (n=6). Statistical significance from ANOVA with Dunnet's post testing against the original ATCC basal media is represented by asterixis: * p= <0.05; ** p= <0.01; *** p= <0.001; **** p= <0.0001.*

were not statistically different from the ATCC condition (p=0.3794 and p=0.4123 respectively), whereas all other conditions were significantly lower, at p=<0.0001.

Cell viability of the collected cells presented a similar picture, with the same five solutions having significantly lower viability of the recovered cells than the ATCC media (Figure 4.4B). DPBS had the lowest viability of 28.7 ±3.48% SEM (p=<0.0001), whereas DPBS with calcium and magnesium and DPBS with calcium, magnesium, glucose, and pyruvate had a viability of 65.8 ±7.03% SEM (p=<0.0001) and 64.6 ±6.08% SEM (p=<0.0001) respectively. EBSS had a viability of 58.3 ±3.86% SEM (p=<0.0001) and despite a reduction in cell number, the cells that were recovered from HBSS have an 81.0 ±4.41% SEM viability (p=0.0364. Lastly, EBSS with calcium and magnesium as well as MEM were found to be non-statistically different from ATCC media with all three having similar cell viability. EBSS with calcium and magnesium was 96.8 ±0.70% SEM viable (p=>0.9999), MEM was 95.6 ±1.03% SEM (p=0.9994) and ATCC was 97.8 ±0.48% SEM viable.

Based on the cell survival data, EBSS with calcium and magnesium and MEM were selected as possible alternatives to ATCC basal media. Next, it was prudent to determine if the biological activity of these conditioned medias were impacted by the change in vehicle. For this, the whole blood inflammation assay was selected as the pivotal mechanism of action for a UCMSC product. Both alternative solutions, along with the original formulation significantly reduced LPS-induced inflammation. Beginning with EBSS with calcium and magnesium conditioned media, TNFα levels were reduced to 55.3 ±0.82% SEM, p=<0.0001 (n=6 biological replicates) (Figure 4.5A) compared to its vehicle control at 100.0 ±0.27% SEM. Similarly, UCMSC adherent conditioned media generated in MEM reduced TNFα levels to 60.1 ±1.90% SEM, p=<0.0001 (n=6 biological replicates) compared to its vehicle at 100.0 ±3.14% SEM (Figure 4.5B). Finally, the original ATCC basal media reduced inflammatory TNFα to 58.2 ±2.53% SEM, p=<0.0001 (n=6 biological replicates) compared its vehicle at 100.0 ±2.95% SEM (Figure 4.5C).

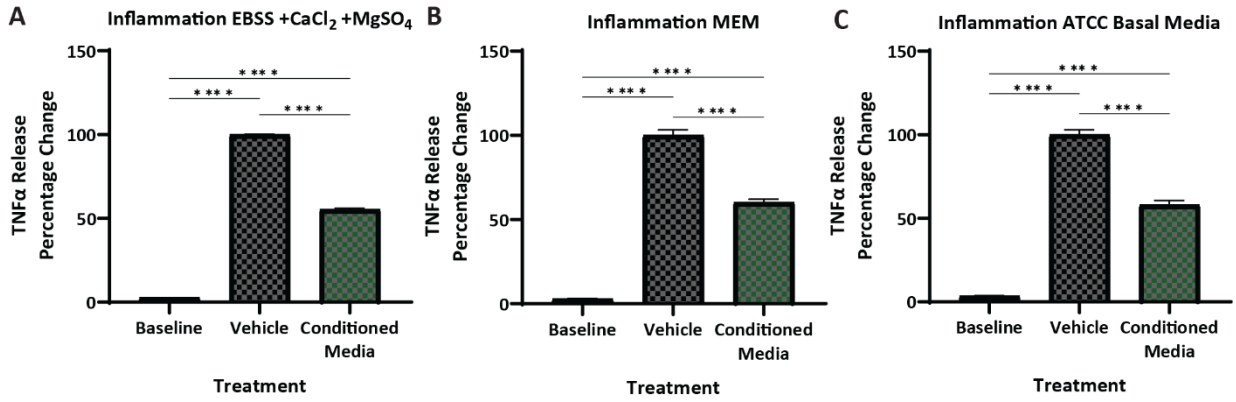

Figure 4.5 Potency assessment of UCMSC ADH conditioned media made with alternative buffers on inflammation.

Effect of conditioned media produced in buffers after 24 hours, with cell count and viability indifferent from the original media, on TNFα levels release from human blood following LPS stress. ***(A)*** *EBSS with Calcium and Magnesium,* ***(B)*** *Minimum Essential Media or* ***(C)*** *original ATCC basal media UCMSC ADH conditioned media. Bars represent the average response from six batches of conditioned media (n=6). Statistical significance from ANOVA with Tukey's post testing is represented by asterixis: * p= <0.05; ** p= <0.01; *** p= <0.001; **** p= <0.0001.*

<u>*Further exploration of shortlisted buffers with the extension of collection duration*</u>

Following the successful completion of the pilot study, an expanded investigation into the use of EBSS with calcium and magnesium (from herein referred to simply as EBSS) and MEM as an alternative ATCC's basal media for generating conditioned media from UCMSCs. The original formulation was generated from 24-hour incubation of UCMSCs, here extending the incubation period up to 48 hours and 72 hours was tested. As before, post-generation cell viability was assessed (n=3 biological replicates) (Figure 4.6A). Beginning with EBSS, cell viability was unchanged between 24 hours (92.8 ±1.59% SEM) and 48 hours (91.2 ±1.01% SEM), however the viability of UCMSCs decreased to 78.3 ±1.30% SEM after 72 hours, which was statistically significant to 24 hours (p=<0.0001) and 48 hours (p=0.0003). MEM, on the other hand, presented with a decrease in viability at 48 hours (87.2 ±0.73% SEM) from 24 hours (95.1 ±1.16% SEM), with significance of p=0.0340. In addition, after 72 hours, the

viability had significantly decreased to 73.2 ±2.67% SEM, p=<0.0001 compared to both 24 and 48 hours. Whereas the increase in incubation time had no detectable influence on the cell viability of UCMSCs incubated in ATCC basal media; 24 hours 95.0 ±0.58% SEM, 48 hours 94.8 ±1.97% SEM and 72 hours 91.2 ±1.76% SEM. Comparing between the solutions, there was no difference between the buffers at 24 hours. However, at 48 hours UCMSCs cultured in MEM were significantly less viable than the original ATCC (p=0.0444). In addition, both EBSS and MEM had significantly lower viability after 72 hours than ATCC basal media (p=0.0002 and p=<0.0001 respectively).

Quantification of protein content revealed that the increased duration of conditioning resulted in an increase in secreted proteins being collected; this was conserved across the three solutions (n=3 biological replicates) (Figure 4.6B). For EBSS made conditioned media, the protein concentration significantly increased from 7.2 ±1.12 µg/mL SEM after 24 hours to 32.7 ±3.31 µg/mL SEM at 48 hours (p=<0.0001) and 23.5 ±1.55 µg/mL SEM at 72 hours (p=<0.0001). There was also a significant difference between 48 hours and 72 hours (p=0.0054). For MEM made conditioned medias, the protein concentration significantly increased from 11.8 ±0.74 µg/mL SEM after 24 hours, to 23.9 ±0.71 µg/mL SEM at 48 hours (p=0.0003) and 27.8 ±1.44 µg/mL SEM at 72 hours (p=<0.0001). There was no statistically significant difference between 48-hour and 72-hour (p=0.6179). Conditioned media generated in ATCC basal media had significant increase in protein from 13.0 ±0.38 µg/mL SEM after 24 hours to 22.4 ±0.47 µg/mL SEM at 48 hours (p=0.0040) and 33.1 ±1.96 µg/mL SEM at 72 hours (p=<0.0012), which was also statistically greater than 48 hours (p=0.0012).

Quantification of the nucleic acid content revealed a similar pattern to that of the protein, where an extended collection time increased the amount of nucleic acid in the conditioned media (n=3 biological replicates) (Figure 4.6C). For conditioned media generated in EBSS, both 48 hours and 72 hours incubations had significantly more nucleic acid than 24 hours, increasing it from 14.0 ±0.33 µg/mL SEM to 20.8 ±0.63 µg/mL SEM (p=0.0023) and 21.0 ±0.72 µg/mL SEM

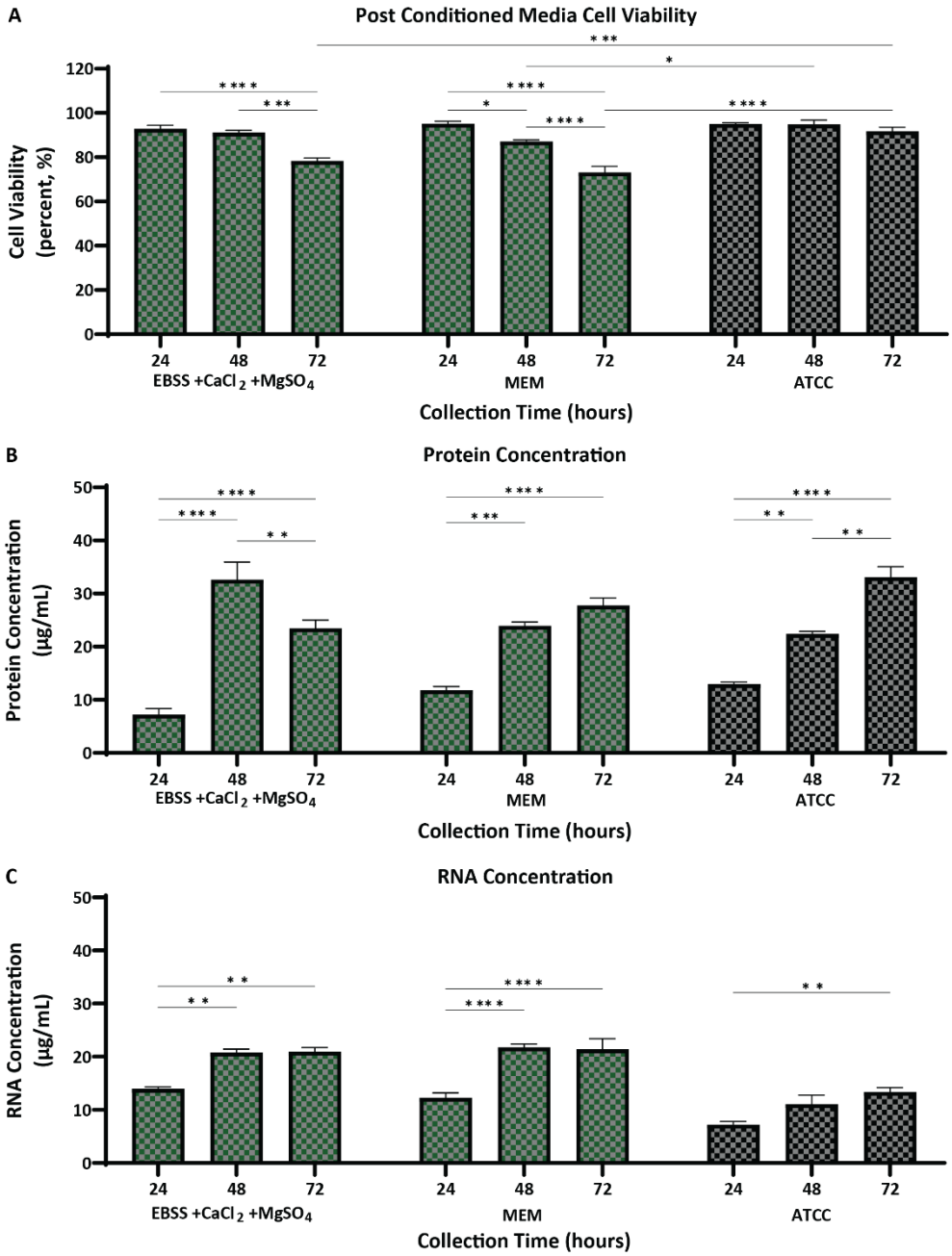

Figure 4.6 Assessment of viability and content from shortlisted alternative buffers for UCMSC ADH conditioned media generation with extended timepoints.

(A) *Trypan blue exclusion viability post UCMSC ADH conditioned media generation in EBSS with calcium and magnesium, minimum essential media or ATCC basal media at 24-hour, 48-hour and 72-hour incubation times.* ***(B)*** *Quantification of protein and* ***(C)*** *total nucleic acid concentrations from UCMSC ADH conditioned media variants. Bars represent the average of three conditioned media batches (n=3) and statistical significance from two-way ANOVA with Šídák's post testing is represented by asterixis: * p= <0.05; ** p= <0.01; *** p= <0.001; **** p= <0.0001.*

(p=0.0017) respectively. There was no difference between 48 hours and 72 hours (p=>0.9999). For MEM, the same was true. The 24-hour conditioned media had 12.3 ±0.92 µg/mL SEM which increased significantly to 21.8 ±0.63 µg/mL SEM at 48 hours (p=<0.0001) and 21.4 ±1.97 µg/mL SEM at 72 hours (p=<0.0001), and again, there was no significant difference between 48-hour and 72 hour (p=>0.9999). For the original ATCC basal media, there was only a significant (p=0.0059) difference between 24-hour and 72-hour generated conditioned media, although there was an increase between each incubation periods from 7.2 ±0.58 µg/mL SEM at 24 hours, to 11.1 ±1.71 µg/mL SEM at 48 hours and 13.4 ±0.80 µg/mL SEM at 72 hours.

Next these conditioned medias were tested on our developed potency assays, beginning with assessing the effect of UCMSC conditioned media on proliferation, where all conditioned media variations were found to increase the number of cells after 96 hours of culture (n=3 biological replicates). When compared to normalised vehicles at 100.0 ±3.06% SEM of cell proliferation, 24-hour EBSS conditioned media increased to 122.5 ±4.30% SEM (p=0.0076), 48-hour to 149.2 ±4.00% SEM (p=<0.0001) and 72-hour to 134.2 ±1.48% SEM (p=0.0001) (Figure 4.7A). Interestingly, the 48-hour generated conditioned media had significantly greater proliferation than the 24-hour (p=0.0126), however there was no statistical difference between 24-hour and 72-hour or 48-hour and 72-hour. The MEM made conditioned medias enhanced proliferation from 100.0 ±4.97% SEM to 136.8 ±4.03% SEM with the 24-hour (p=0.0063), 143.4 ±6.49% SEM with 48-hour (p=0.0015) and 151.4 ±4.45% SEM with 72-hour (p=0.0003) (Figure 4.7B); and ATCC basal media from 100.0 ±2.47% SEM to 126.0 ±7.13% SEM with 24-hour (p=0.0268), 128.0 ±11.59% SEM with 48-hour (p=0.0166) and 129.7 ±11.97% SEM with 72-hour (p=0.0108) conditioned media (Figure 4.7C). Unlike EBSS conditioned media, there was no statistical difference between any of the extended incubation times.

The final assessment was the whole blood inflammation assay. Here, all conditioned media significantly reduced the levels of TNFα from their respective vehicle controls (n=3 biological

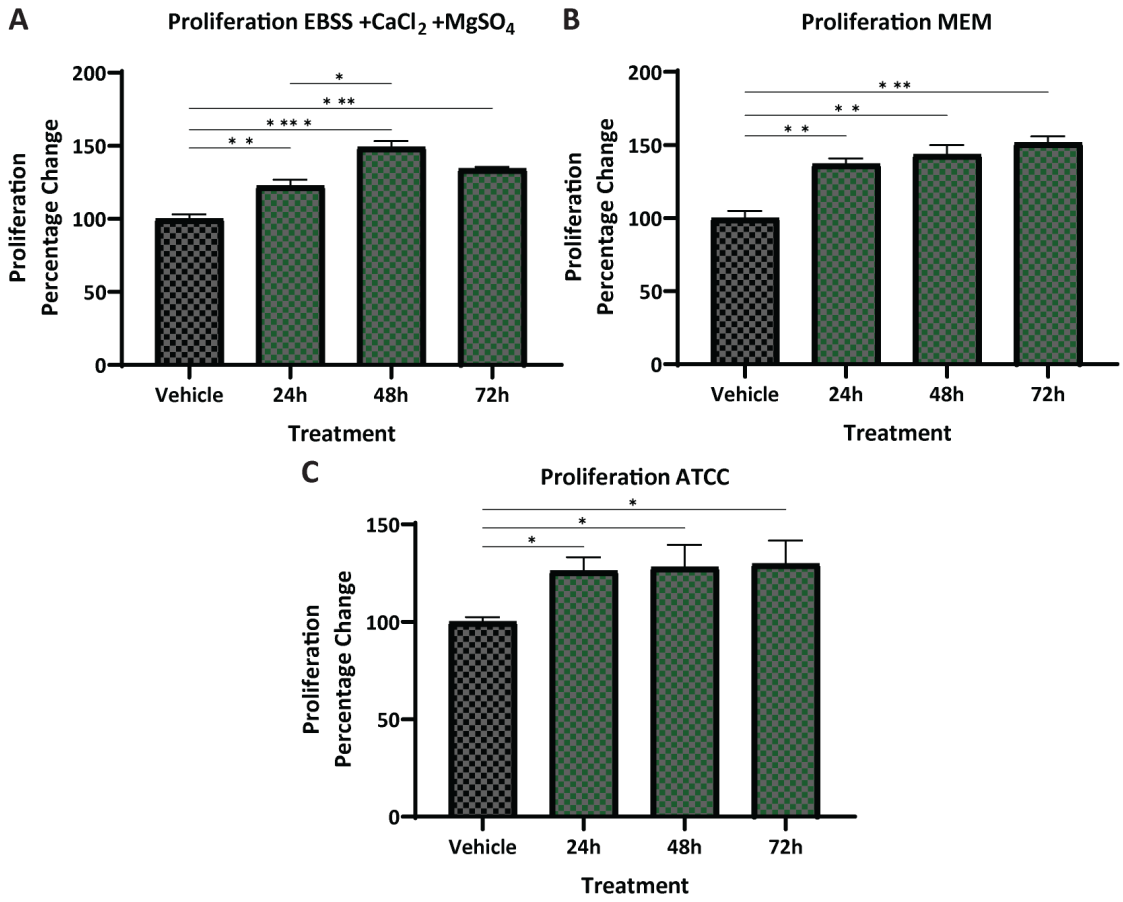

Figure 4.7 Impact of UCMSC ADH conditioned media produced in alternative buffers and timepoints on proliferation.

Assessment of modified UCMSC ADH conditioned medias on HeLa cell proliferation. ***(A)*** *EBSS with calcium and magnesium,* ***(B)*** *minimum essential media or* ***(C)*** *the original ATCC basal media, for 24-hoiur, 48-hour or72-hour incubation times. Bars represent the average of three conditioned media batches (n=3) and statistical significance from ANOVA with Tukey's post testing is represented by asterixis: * p= <0.05; ** p= <0.01; *** p= <0.001; **** p= <0.0001.*

replicates). EBSS conditioned media (Figure 4.8A) showed a reduction from 100.0 ±1.24% SEM to 40.4 ±2.71% SEM with the 24-hour (p=<0.0001), 30.2 ±0.58% SEM with 48-hour (p=<0.0001) and 16.1 ±1.61% SEM with 72-hour (p=<0.0001). In addition, 48-hour conditioned media was statistically significant to the 24-hour (p=0.0032), and 72-hour was significant to both 24-hour (p=<0.0001) and 48-hour (p=0.0002). Conditioned media generated in MEM for 24-hour reduced TNFα levels to 46.9 ±3.03% SEM (p=<0.0001) and 33.3 ±1.94% SEM with 48-hour (p=<0.0001) and 34.0 ±1.98% SEM with

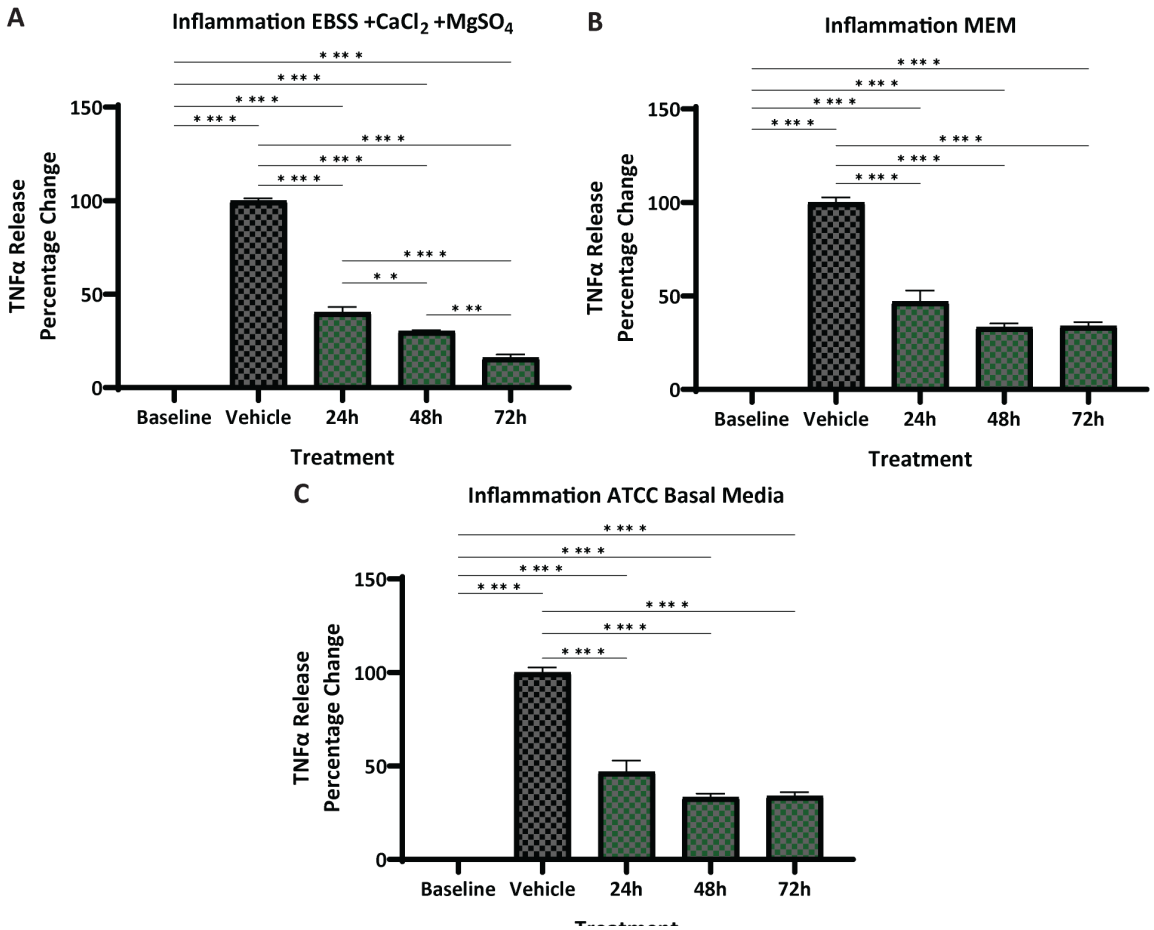

Figure 4.8 Impact of UCMSC ADH conditioned media produced in alternative buffers and timepoints on inflammation.

Assessment of modified UCMSC ADH conditioned medias on TNFα levels release from human blood following LPS stress. ***(A)*** *EBSS with calcium and magnesium,* ***(B)*** *minimum essential media or* ***(C)*** *the original ATCC basal media, for 24-hour, 48-hour or72-hour* incubation times. *Bars represent the average of three conditioned media batches (n=3) and statistical significance from ANOVA with Tukey's post testing is represented by asterixis: * p= <0.05; ** p= <0.01; *** p= <0.001; **** p= <0.0001.*

72-hour (p=<0.0001) conditioned media from the vehicle control, 100.0 ±2.64% SEM (Figure 4.8B). There was no statistical difference between the difference conditioned medias. Lastly, conditioned media generated in the original ATCC basal media (Figure 4.8C) had a reduction in TNFα from 100.0 ±2.64% SEM to 46.9 ±3.03% SEM following treatment with 24-hour conditioned media (p=<0.0001).

Additionally, the 48-hour and 72-hour conditioned medias also reduced TNFα levels to 33.3 ±1.94% SEM (p=<0.0001) and 34.0% ±1.99% SEM (p=<0.0001) respectively. As with MEM conditioned media, there was not statistically difference between the conditioned media durations.

Full scale production and assessment of selected UCMSC ADH formulation.

Using the information gathered from the first two phases of developing the UCMSC ADH conditioned media, it was decided that a UCMSC ADH conditioned media generated in EBSS with calcium and magnesium for 48 hours would provide the best chance of being clinically compliant, have the best manufacturability whilst being biologically potent. This conditioned media will be here on referred to as UCMSC ADH-E, and the full rationale for its selection will be discussed later in this chapter.

Here, three independent batches of UCMSC ADH-E conditioned media were generated in Corning® CellSTACK® multilayer flasks (batch numbers 2D001, 2D002 and 2D003). Using the release assays, the consistency of protein released from UCMSCs using this method of generating conditioned media was high, between 10.8 µg/mL and 15.3 µg/mL with the average being 12.9 ±1.33 µg/mL, n=3 biological replicates (Figure 4.9A). The consistency of nucleic acid secretion was also high, between 13.6 µg/mL and 19.4 µg/mL with the average at 15.7 ±1.87 µg/mL, n=3 biological replicates (Figure 4.9B). Lastly, looking at the subvisible particles with NTA revealed a good consistency of EV concentration, between $7.2x10^8$ particles/mL and $9.94x10^8$ particles/mL with the average at $8.57x10^8$ ±$1.37x10^8$, n=3 biological replicates (Figure 4.9C).

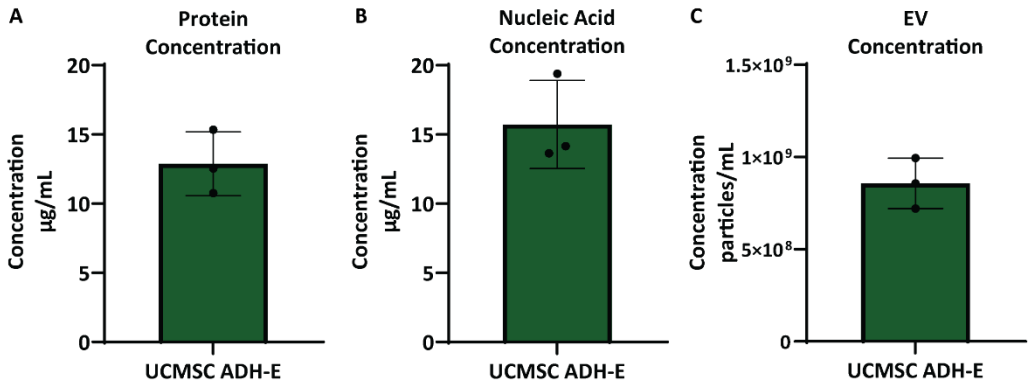

Figure 4.9 Quantification of UCMSC ADH-E content.

*Quantification of **(A)** protein, **(B)** total nucleic acid, and **(C)** extracellular vesicle concentrations for UCMSC ADH-E conditioned media. Bars represent the mean concentrations from three batches (n=3).*

Next, different concentrations of UCMSC ADH-E conditioned media were tested on inflammation. Beginning with batch 2D002, the previously used whole blood assay was adjusted to allow for up to 3x treatment (30% v/v instead of 10% v/v treatment) (Figure 4.10A). A two-fold dilution series was used to generate a treatment range from 0.006x up to the 3x maximum treatment, n=4 technical replicates. All concentrations of UCMSC ADH-E conditioned media reduced TNFα levels with statistical significance against the normalised vehicle control, 100.0 ±0.83% SEM as follows: 0.006x to 69.6 ±1.14% SEM (p=<0.0001); 0.012x to 44.8 ±1.22% SEM (p=<0.0001); 0.023x to 34.4 ±2.06% SEM (p=<0.0001); 0.047x to 24.6 ±0.31% SEM (p=<0.0001); 0.094x to 19.0 ±0.28% SEM (p=<0.0001); 0.188x to 13.9 ±0.17% SEM (p=<0.0001); 0.375x to 11.1 ±0.28% SEM (p=<0.0001); 0.75x to 9.7 ±0.18% SEM (p=<0.0001); 1.5x to 8.7 ±0.12% SEM (p=<0.0001); and 3x to 7.7 ±0.05% SEM (p=<0.0001). A maximal effect appeared to be reached with around 0.375x treatment, where there was no statistical significance on a one-way ANOVA with Tukey's post testing between this and all higher concentrations. 0.188x UCMSC ADH-E treatment was not significantly different from 0.375x, however it was when compared to 0.75x (p=0.0446) and all higher concentrations (vs 1.5x p=0.0049 and 3x p=0.0004). All other concentrations of UCMSC ADH-E conditioned media treatment were statistically different from all others.

The next batch of UCMSC ADH-E, 2D003, was tested using a ten-fold dilution series to generate treatments ranging from 0.001x and 1x (10% v/v) in the whole blood inflammation assay, n=4 technical replicates (Figure 4.10B). Here it was revealed that reducing the treatment down to 0.001x concentration lost the biological effect on LPS-induced inflammation when compared to the vehicle at 100.0 ±7.8% SEM, with TNFα levels remaining at 98.3 ±9.41% SEM (p=>0.9999). All other concentrations (0.01x, 0.1x, and 1x) of UCMSC ADH-E reduced TNFα levels significantly to 58.3 ±3.55% SEM (p=0.0003), 27.1% ±1.66% SEM (p=<0.0001), and 12.3 ±0.75% SEM (p=<0.0001) respectively. There was no statistical difference between the concentrations of 0.1x and 1x UCMSC ADH-E treatment.

Figure 4.10C presents a dose-response curve where both 2D002 and 2D003 UCMSC ADH-E treatments are presented as a ratio of conditioned media to blood volume, n=4 technical replicates. Firstly, statistical analysis confirmed that the generated curves have a 'Goodness of Fit' R^2 value of 0.9918 for 2D002 and 0.9218 for 2D003 demonstrating a strong confidence that the curves represent the data. The maximum effect of 2D002 was calculated with a 95% confidence interval to be between 7.4% and 9.8% TNFα with a best-fit value of 8.6%, whereas 2D003 would fall between 3.7% and 24.0% TNFα with a best-fit value of 14.2%. The EC50 values informs on the concentration where 50% of the maximum effect was achieved. The best-fit EC50 value for 2D002 was a treatment ratio of 0.0047 (95% confidence interval: 0.0043 to 0.0052), and the best-fit EC50 for 2D003 was at 0.0056 (95% confidence interval 0.0028 to 0.0117). A statistical comparison of fits determined that there was no statistical

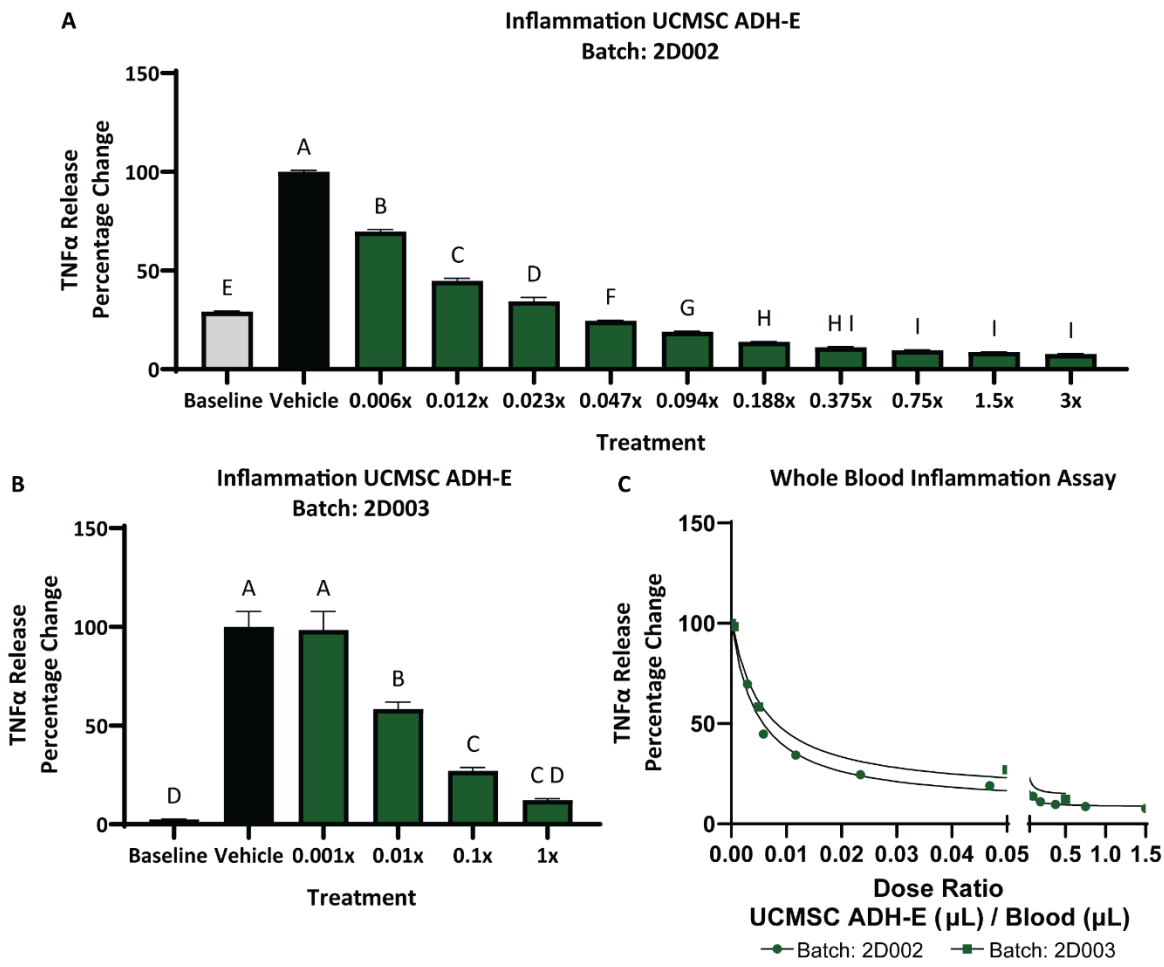

Figure 4.10 Anti-inflammatory potency of UCMSC ADH-E conditioned media.

UCMSC ADH-E conditioned media treatment on TNFα levels release from human blood following LPS stress. ***(A)*** *2-fold dilution series of UCMSC ADH-E Batch 2D002 treatment and* ***(B)*** *a 10-fold dilution series of UCMSC ADH-E batch 2D003. Bars represent the average of four technical replicates (n=4). Statistical significance from ANOVA with Tukey's post testing is displayed by grouping letters, where each bar is significantly different to any unmatched bar.* ***(C)*** *Dose response curve of UCMSC ADH-E conditioned media treatment. Dose adjusted to ratio of conditioned media volume to blood volume.*

difference between the EC50 values, p=0.4284. This provided confidence that these different batches of UCMSC ADH-E conditioned media had similar biological potency.

Storage and stability testing of UCMSC ADH-E conditioned media.

During the testing of the first batch UCMSC ADH-E conditioned media (2D001), became apparent that the method used to store conditioned media (frozen at -80°C) may not be suitable for this formulation,

as precipitates were observed on thawing. To investigate this further, following the generation of UCMSC ADH-E batch 2D002, the conditioned media was immediately aliquoted into 15 mL centrifuge tubes for storage in different conditions. To determine if this was an artifact of the conditioned media or of the vehicle, a flask of EBSS was put through the same process as the conditioned media generation but with the absence of cells.

Assessment of storage temperature

Following the generation and standard processing of conditioned media, the opacity of "fresh" UCMSC ADH-E and vehicle was assessed against known turbidity standards (Figure 4.10A-C) to give a baseline score of 0.0. There were no observable particles within either the vehicle or UCMSC ADH-E conditioned media. The standard storage condition of freezing conditioned media at -80°C is believed to provide the most stability of active components such as proteins and nucleic acids. However, upon freezing and thawing, both UCMSC ADH-E and the vehicle had an elevated turbidity score, of 1.0 or greater, n=3 technical replicates (Figure 4.11A). A huge number of visible particles were observed also, in both vehicle and the UCMSC ADH-E (as indicated by the arrows). Samples stored at +4°C had no observable change until the assessment on day 26, n=3 technical replicates (Figure 4.11B). Here, both the vehicle and UCMSC ADH-E conditioned media had become cloudy, with a score of 1.7 ±0.34 SEM and 2.34 ±0.34 SEM, respectively. However, only the conditioned media had visible particles observed. By day 56, the vehicle also presented with visible particles and a similar turbidity score as day 28, 1.3 ±0.34 SEM. UCMSC ADH-E on the other hand, had a significantly great score than the vehicle on day 56, 3.7 ±0.34 SEM ($p=<0.0001$), and still presented with particles. The final storage condition explored was ambient (approximately +20°C) n=3 technical replicates. Here, similarly to -80°C storage, visible particles were in both the vehicle and UCMSC ADH-E conditioned media as early as day 1 (Figure 4.11C). However, there was no opacity change in the vehicle until a non-statistically significant score of 0.7 ±0.34 SEM on day 28 (two scores of 0.0 vs one score of 1.0). On the other hand, UCMSC ADH-E had an elevated turbidity score of 2.7 ±0.67 SEM on day 28 ($p=<0.0001$ vs Fresh and $p=0.0016$ vs Day

28 vehicle) and 3.7 ±0.34 SEM on day 56 (p=<0.0001 vs Fresh and p=<0.0001 vs Day 56 vehicle). Of note, although the severity of visible particles was not quantified, it was observed that the number and size of particles seen in the ambient stored samples were greater than those in the +4°C storage samples.

In addition to the clarity and presence of visible particles, the pH of the samples was recorded at each timepoint, n=3 technical replicates. On day 0, fresh vehicle and UCMSC ADH-E conditioned media was

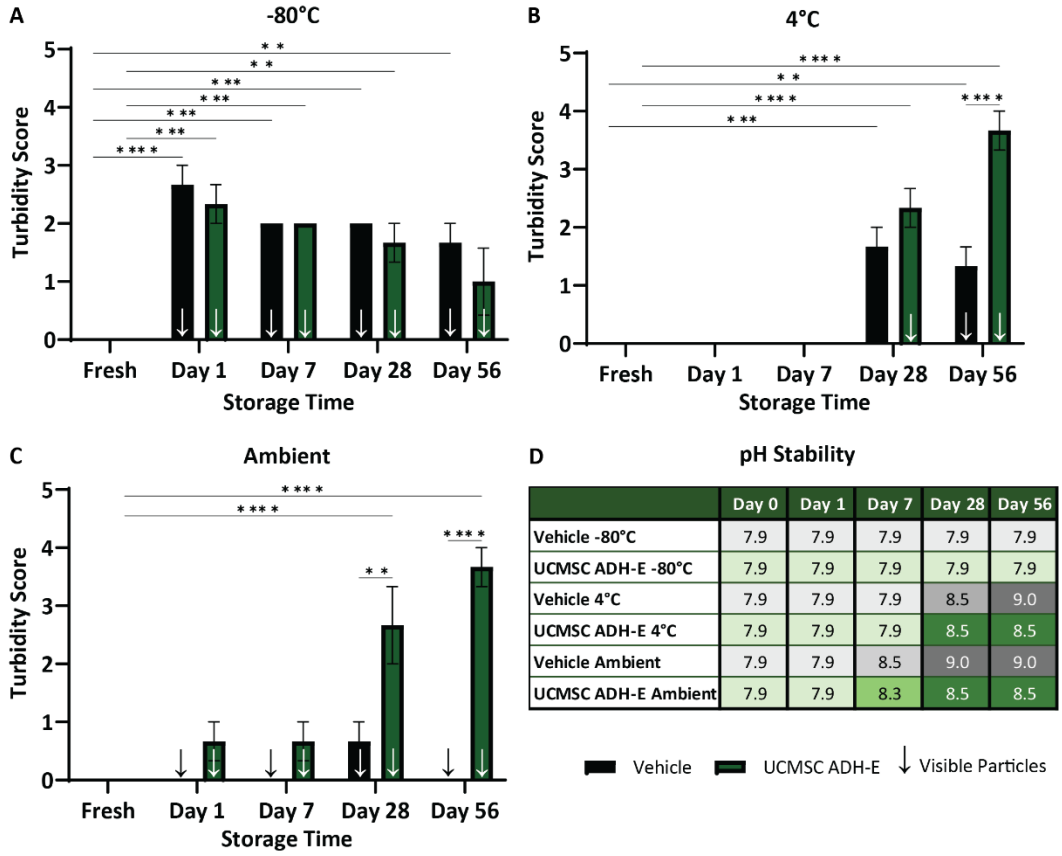

	Day 0	Day 1	Day 7	Day 28	Day 56
Vehicle -80°C	7.9	7.9	7.9	7.9	7.9
UCMSC ADH-E -80°C	7.9	7.9	7.9	7.9	7.9
Vehicle 4°C	7.9	7.9	7.9	8.5	9.0
UCMSC ADH-E 4°C	7.9	7.9	7.9	8.5	8.5
Vehicle Ambient	7.9	7.9	8.5	9.0	9.0
UCMSC ADH-E Ambient	7.9	7.9	8.3	8.5	8.5

Figure.4.11 Impact of storage temperature on pharmacopeial stability of UCMSC ADH-E conditioned media.

Assessment of clarity and visual particles following recommended European pharmacopeia assays of UCMSC ADH-E conditioned media stored **(A)** frozen at -80°C, **(B)** refrigerated at +4°C and **(C)** at an ambient temperature. Over a period of 8 weeks. Bars represent average clarity score from three blinded researchers (n=3) and arrows indicate presence of visual particles. S*tatistical significance from ANOVA with Dunnet's post testing is represented by asterixis: * p= <0.05; ** p= <0.01; *** p= <0.001; **** p= <0.0001.* ***(D)*** *Table of corresponding pH measurements.*

measured at pH 7.9 (Figure 4.11D). This remained unchanged for sample stored frozen at -80°C. Interestingly, for samples stored at +4°C had elevated pH levels on day 28 (vehicle pH 8.5; UCMSC ADH-E pH 8.5) and on day 56 (vehicle pH 9.0; UCMSC ADH-E pH 8.5), which corresponds to the changes in turbidity scores. For samples stored at an ambient temperature were found to have and increase pH level on day 7 (vehicle pH 8.5; UCMSC ADH-E pH 8.3), as well as day 28 (vehicle pH 9.0; UCMSC ADH-E pH 8.5) and day 56 (vehicle pH 9.0; UCMSC ADH-E pH 8.5).

Next, attention turned to impact on the content of UCMSC ADH-E conditioned media. A baseline measure of protein concentration and nucleic acid concentration was collected with from fresh conditioned media on the day of generation, n=2 technical replicates. The protein concentration was recorded as 10.8 ±0.04 µg/mL SEM (Figure 4.12A). On day 1 and day 7 samples stored frozen at -80°C were found to have a significantly lower amount of protein, 9.2 ±0.40 µg/mL SEM (p=0.0065) and 8.8 ±0.14 µg/mL SEM (p=0.0022) respectively, however there was no difference detected at the day 28 (10.8 ±0.06 µg/mL SEM) or day 56 (11.1 ±0.04 µg/mL) measures suggesting that this initial drop could be a result of assay to assay variation. There were no statistically significant changes in the protein concentration of refrigerated samples at +4°C. On the other hand, UCMSC ADH-E stored at an ambient temperature was found to have significantly lower protein on day 7 (8.4 ±0.04 µg/mL SEM, p=0.0011), day 28 (9.4 ±0.34 µg/mL SEM, p=0.0119) and day 56 (7.2 ±0.19 µg/mL SEM, p=0.0002) indicating that protein was being lost by this storage condition.

Storage at -80°C appeared not to alter the nucleic acid concentration either, however there was a non-significant trend towards a reduced nucleic acid concentration over time (Figure 4.12B). For samples stored at +4°C, there was a similar trend to reduced nucleic acid concentration as well, with day 28 reaching statistical significance (p=0.0131) with the nucleic acid concentration reduced to 10.6 ±0.70 µg/mL SEM compared to the 14.2 ±0.20 µg/mL SEM at generation. However, there was an unexpectant increase in nucleic acid concentration on day 56, 19.0 ±0.22 µg/mL SEM (p=0.0035). This phenomenon was also observed in UCMSC ADH-E stored ambient. There was no detectable change in nucleic acid concentration at day 1 and day 7, however at day 28 and day 56 there was a significantly greater amount of nucleic acids compared to the original concentration, 18.4 ±0.53 µg/mL SEM

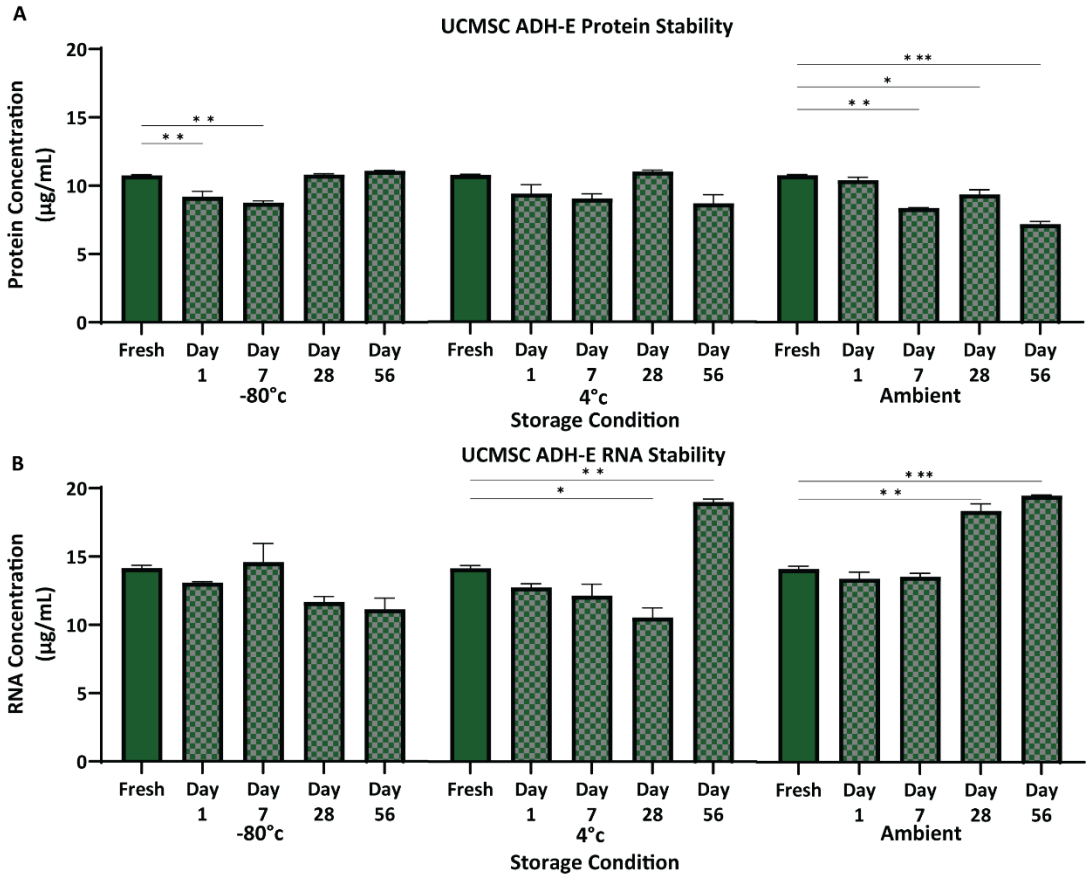

Figure 4.12 Impact of storage temperate on UCMSC ADH-E conditioned media content.

(A) *Quantification of protein and* ***(B)*** *total Nucleic acid concentration for UCMSC ADH-E conditioned media stored at -80°C, +4°C and ambient over an 8-week period. Bars represent average of two replicates (n=2) and statistical significance from ANOVA with Dunnet's post testing is represented by asterixis: * p= <0.05; ** p= <0.01; *** p= <0.001; **** p= <0.0001.*

(p=0.0011) and 19.5 ±0.05 µg/mL SEM (p=0.0004) respectively. This event aligned with a critical change in sample opacity recorded in Figure 4.11B and 4.11C.

Finally, the biological potency on LPS-induced inflammation was assessed after 1 week in storage. Using the human whole blood inflammation assay, each UCMSC ADH-E storage condition was compared against its respectively stored vehicle. Here it was shown that irrespective of the storage condition, UCMSC ADH-E reduced TNFα levels, n=4 technical replicates (Figure 4.13). Frozen -80°C UCMSC ADH-E conditioned media significantly reduced TNFα levels from 100.0 ±3.07% SEM in the vehicle to 24.4 ±1.27% SEM with treatment, a one-way ANOVA with Šídák's post testing revealed a significance of p=<0.0001. Refrigerated +4°C UCMSC ADH-E conditioned media significantly reduced TNFα levels from 100.0 ±3.32% SEM in the vehicle to 25.9 ±0.86% SEM after treatment, with a significance of p=<0.0001. Finally, UCMSC ADH-E stored at an ambient temperature (approximately +20°C), significantly reduced TNFα levels from 100.0 ±3.21% SEM in the vehicle to 26.7 ±0.48% SEM after treatment, with a significance of p=<0.0001. This indicates that the presence of particles and

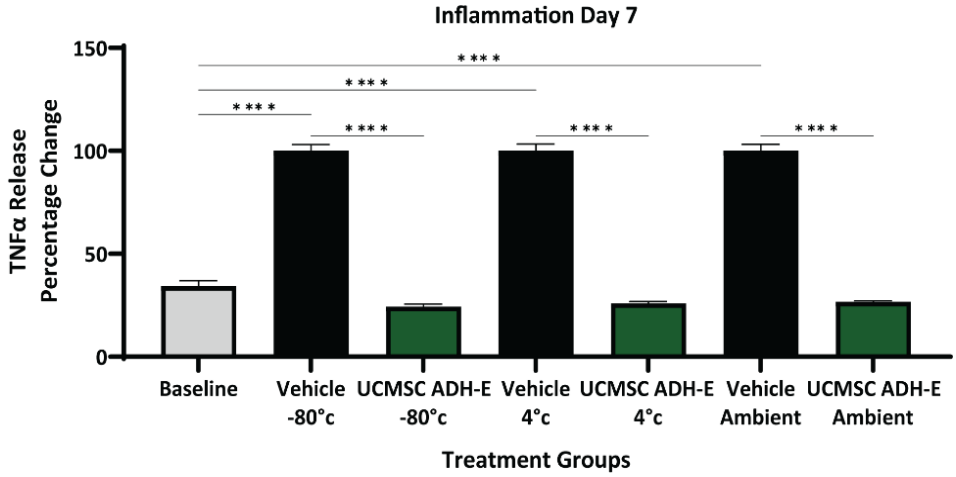

Figure 4.13 Biological potency inflammation assay one week of UCMSE ADH-E storage.

*UCMSC ADH-E conditioned media stored at -80°C, +4°C and ambient for 1 week on TNFα levels release from human blood following LPS stress. Bars represent the average of four replicates (n=4) and statistical significance from ANOVA with Šídák's post testing presented with asterixis: * p= <0.05; ** p= <0.01; *** p= <0.001; **** p= <0.0001.*

increase turbidity detected has not been detrimental to the biological activity of UCMSC ADH-E conditioned media.

UCMSC ADH-E storage in glass vials

Reflecting on the results from the initial storage and stability study and after discussions with chemists, it was deduced that the deterioration in clarity was likely due to the vehicle rather than the conditioned media. Additional investigations into the buffer, different suppliers suggested slight differences in storage conditions. From one alternative supplier, a document was uncovered explicitly stating that EBSS should not be frozen due to precipitation of the salts from solution. Considering this finding, it was concluded that the "crash-out" issues observed in the frozen samples were explained by this. However, as this buffer is recommended for storage at temperatures encompassing +4°C and ambient, the deterioration in turbidity and pH observed was still unexplained. A working theory was developed that there must be a chemical reaction initiated within the elevated CO_2 environment of the incubator, which created a less stable salt buffer solution which continues to react with gases in the air during storage. To put this theory to the test, a fresh UCMSC ADH-E conditioned media batch (2D003) was aliquoted into glass vials with a rubber bung providing a better air seal and stored at +4°C.

Beginning with the assessment of clarity, storing UCMSC ADH-E in this manner resulted in no change in turbidity scores by 4 months of storage (Figure 4.14A), however, there were some vials found to have visible particles at 4 months, n=3 technical replicates. The pH of these samples was found to remain at pH 7.9 throughout the 4 months of storage (Figure 4.14A). The protein concentration of this batch of UCMSC ADH-E conditioned media was quantified at 12.5 ±0.28 µg/mL SEM, which significantly decreased to 10.8 ±0.09 µg/mL SEM by 1 month of storage ($p=0.0098$, n=3 technical replicates) (Figure 4.14B). This level remained unchanged at 4 months, at 11.2 ±0.36 µg/mL SEM although this was still statistically different from the starting concentration ($p=0.0272$). The nucleic acid concentration was quantified at 13.6 ±0.28 µg/mL SEM at generation, which was unchanged after 1 month of storage at 13.8 ±0.29 µg/mL SEM (Figure 4.14C, n=3 technical replicates). When tested

after 4 months, the nucleic acid concentration was significantly lower than both the fresh and 1 month time points at 11.2 ±0.10 μg/mL SEM, p=0.0009 and p=0.0007, respectively.

The capability of UCMSC ADH-E to reduce LPS-induced TNFα levels in whole blood was also reviewed over the 4 months of storage in glass vials, n=4 technical replicates. Freshly made UCSMC ADH-E reduced TNFα from 100.0 ±7.77% SEM in with vehicle treatment to 12.3 ±0.75% SEM, which a one-way ANOVA with Tukey's post testing revealed a statistical significance of p=<0.0001 (Figure 14D). The levels of TNFα after treatment were not statistically different from the baseline value of 2.5 ±0.12% SEM (p=0.4061). After one month of storage at +4°C in glass vials, UCMSC ADH-E conditioned media retained bioactivity, reducing TNFα levels from 100.0 ±3.43% SEM to 20.8% ±1.08% SEM, with statistical significance of p=<0.0001. The post-treatment TNFα levels remained significantly higher than the baseline value of 0.0 ±0.07% SEM (p=0.0002). Lastly, after 4 months of storage, UCMSC ADH-E conditioned media was once again able to reduce TNFα levels in whole blood stimulated with LPS. The vehicle treatment control of 100.0 ±1.91% SEM was reduced to 31.3 ±0.81% SEM with treatment (p=<0.0001) which remained significantly higher than the baseline level of 6.2 ±0.15% SEM (p=<0.0001). Although, a direct comparison of storage timepoint is not possible, there was an overall trend towards a gradual loss of potency over the 4-month test period.

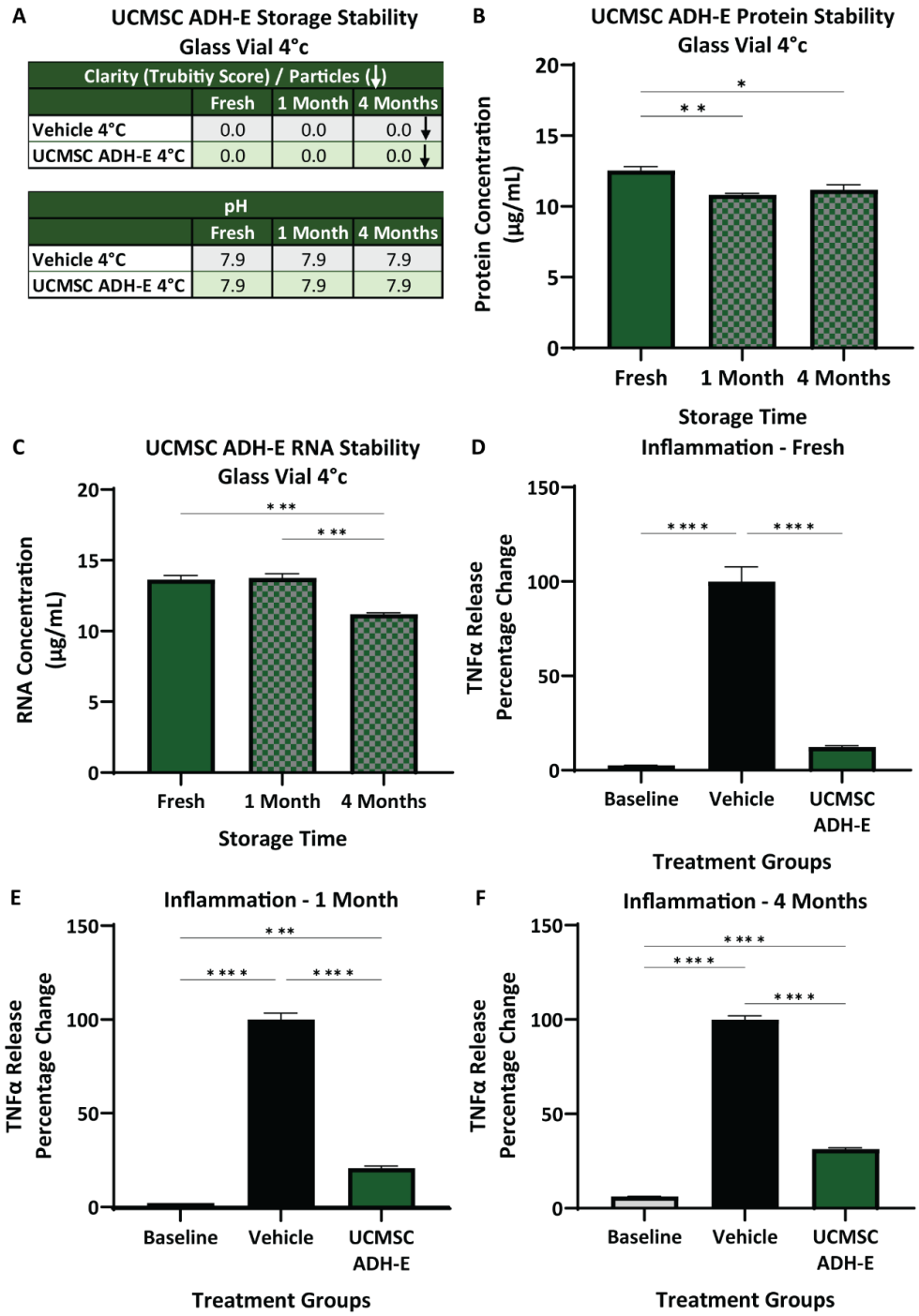

Figure 4.14 Glass vial storage of UCMSC ADH-E conditioned media.

UCMSC ADH-E conditioned media stored refrigerated at +4°C for a 4-month period in sealed glass vials. ***(A)*** *Table of European pharmacopeial clarity scores and visual particle observations. Scores are averages of three blinded researchers and arrows signify presence of visual particles.* ***(B)*** *Quantification of protein and* ***(C)*** *total nucleic acid concentration. Bars represent average of three repeat measures (n=3) and statistical significance from ANOVA with Dunnet's post testing presented by asterixis: * p= <0.05; ** p= <0.01; *** p= <0.001; **** p= <0.0001. [Continues on next page]*

Figure 14 continued: (D) *Effect of fresh,* ***(E)*** *one month old and* ***(F)*** *4 months old UCMSC ADH-E conditioned media on TNFα levels release from human blood following LPS stress. Bars represent the average of four replicates (n=4) and statistical significance from ANOVA with Tukey's post testing presented with asterixis: * p= <0.05; ** p= <0.01; *** p= <0.001; **** p= <0.0001.*

UCMSC ADH-E buffer exchange and sub-fractions

With the stability challenges of EBSS post-conditioned media generation experienced and alternative salt buffers proving unsuitable for conditioned media creation in mind, a small pilot study was conducted to investigate if the salts could be removed or replaced to leave a more stable buffer to store conditioned media in. A process step often used in analytical biochemistry and pharmaceutical formulation to remove low-molecular-weight materials that exceed desired/compatible levels. Methods commonly used for desalting or buffer exchange include dialysis and ultrafiltration. The former is often time consuming and requires multiple steps to remove components by diffusion. The most rapid method for dialysing large volumes is the use of ultrafiltration by tangential-flow filtration (TFF), where samples are recirculated under pressure though a semipermeable membrane until the retained volume has been suitably reduced. The last method considered, and the one used here was ultrafiltration by microscale centrifuge concentrators which is used in small-scale purification of samples. Here, volumes under 20 mL are loaded upon a low-molecular weight filter and spun in a standard laboratory centrifuged to force the volume across the filter. Once the volume was reduced to <200 µL, the filtrate was collected and set aside, and 0.9% normal saline was loaded on top of the concentrated UCMSC ADH-E CM to dilute back to the original volume.

Following the buffer exchange, the protein and nucleic acid concentrations were determined, n=3 technical replicates. The original UCMSC ADH-E conditioned media had a protein level of 12.5 ±0.28 µg/mL SEM (Figure 4.15A). In the filtrate, which passed through the 3 kDa MWCO membrane, there was no detectable protein 0.0 ±0.06 µg/mL SEM. On the other hand, in the 1x v/v retentate now in 0.9% sodium chloride (NaCl) had only 5.5 ±0.19 µg/mL SEM of protein which was statistically less than

the original concentration (p=<0.0001) suggesting that approximately 50% of the proteins were lost during the ultrafiltration process. The total nucleic acid concentration of the original UCMSC ADH-E conditioned media was 13.6 ±0.28 µg/mL SEM (Figure 4.15B). Following ultrafiltration, the filtrate contained 7.8 ±0.09 µg/mL SEM, which although significantly less than the original conditioned media (p=<0.0001), it was statistically significant over the retained nucleic acid with a lower concentration of 4.1 ±0.13 µg/mL SEM (p=<0.0001).

Next the NaCl retentate was tested on the whole blood LPS-induced inflammation assay, n=4 technical replicates. Here, despite having significantly less protein and nucleic acid than the original UCMSC ADH-E conditioned media, it reduced the levels of TNFα from 100.0 ±8.93% SEM of the NaCl vehicle to 37.7 ±3.25% SEM, with a one-way ANOVA with Tukey's post-test significance of p=<0.0001. (Figure 4.15C). Alongside this, the original UCMSC ADH-E was tested against its vehicle matched controls. As previously found, UCMSC ADH-E was capable of reducing TNFα to non-significant levels compared to the unstimulated baseline: UCMSC ADH-E conditioned media treatment at 12.3 ±0.75% SEM and baseline levels at 2.5 ±0.12% SEM of the maximum stimulated level of the vehicle treated (100.0 ±7.77% SEM). A one-way ANOVA with Tukey's post-test determined UCMSC ADH-E TNFα levels were significantly lower than the vehicle treated (p=<0.0001). The filtrate from the buffer exchange process was also tested and found to significantly reduce TNFα levels to 24.4 ±1.54% SEM (p=<0.0001), which was not significantly different to the whole UCMSC ADH-E conditioned media.

With the results from the pilot on exchanging the buffer using micro-concentrators suggesting that biologically relevant components were present in the low-molecular weight filtrate, a similar experiment was then conducted using the micro-concentrators, but without changing the buffer to NaCl. In this experiment, two different size filters were used to divide UCMSC ADH-E into three sub-fractions by MWCO. Firstly, UCMSC ADH-E was passed through a 1000 kDa filter, following which the filtrate was passed through a 3 kDa filter. The retentate from the first with was diluted in EBSS to the original starting volume to provide a >1000 kDa fraction. The retentate from the second filter was also

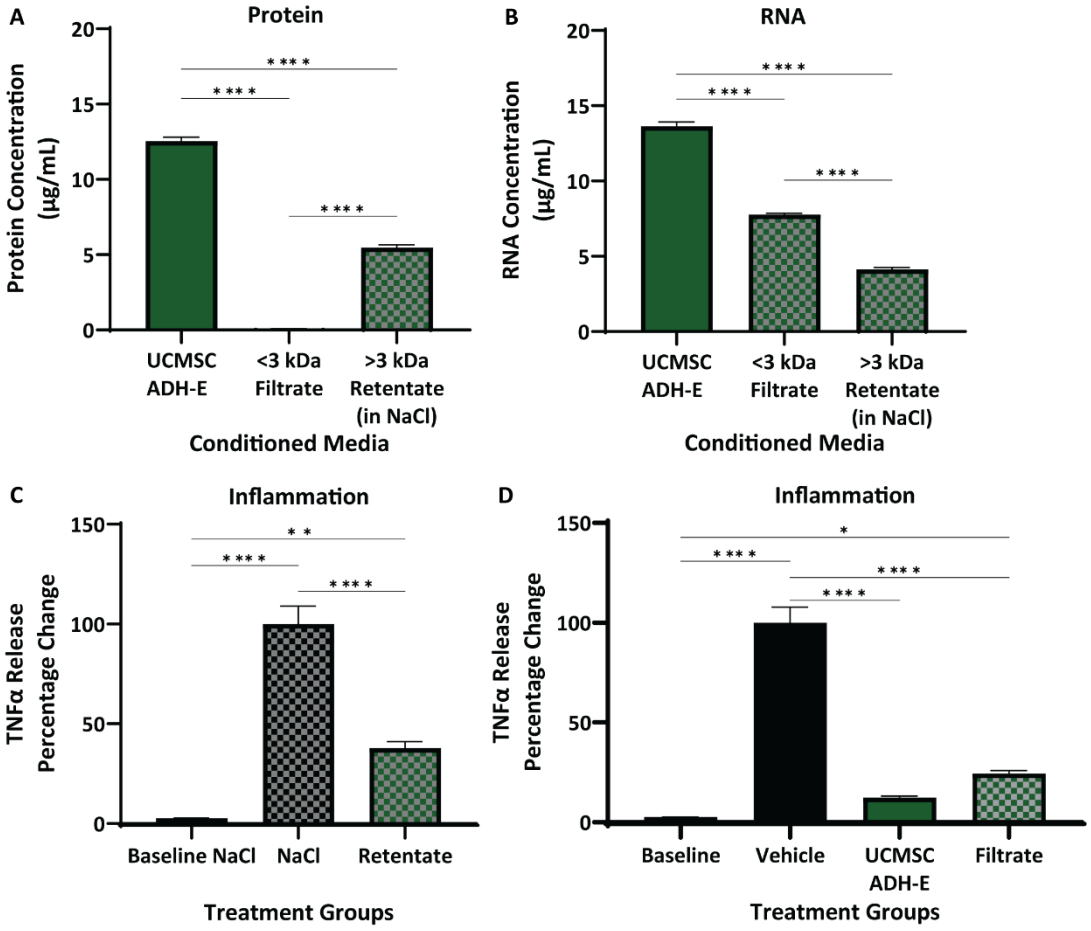

Figure 4.15 Impacted of exchanging buffer post collection of UCMSC ADH-E conditioned media.

(A) *quantification of protein and* ***(B)*** *total nucleic acid concentration following the exchange of salt solution via ultrafiltration. Bars represent average of three repeat measures (n=3).* ***(C)*** *Bioactivity of modified UCMSC ADH-E with NaCl buffer replacement and* ***(D)*** *original UCMSC ADH-E and ultrafiltrate in EBSS buffer on TNFα levels release from human blood following LPS stress. Bars represent the average of four replicates (n=4). Statistical significance from ANOVA with Tukey's post testing presented with asterixis: * p= <0.05; ** p= <0.01; *** p= <0.001; **** p= <0.0001.*

diluted in EBSS to the original starting volume to make a fraction between 3 kDa and 1000 kDa, and finally the filtrate from the 3 kDa filter formed remaining sub-fraction.

The protein concentration of the UCMSC ADH-E conditioned media used was 10.8 ±0.15 µg/mL SEM (Figure 4.16A). The highest amount of protein was found in the >1000 kDa sub-fraction with a concentration of 3.7 ±0.30 µg/mL SEM, however this was significantly lower than the original conditioned media (p=<0.0001) but significantly greater than the other two fractions (p=<0.0001

collectively), n=3 biological replicates. The other two sub-fractions were found to have undetectable levels of protein: 3-1000 kDa at 0.2 ±0.06 µg/mL SEM and <3 kDa at 0.1 ±0.03 µg/mL SEM, n=3 biological replicates. As before, the total protein from all sub-fractions was more than half that of the original concentration, suggesting a large proportion of proteins were lost during the ultrafiltration process.

The nucleic concentration of the original UCMSC ADH-E conditioned media was measured at 13.1 ±1.22 µg/mL SEM which was significantly greater than all sub fractions (>1000 kDa p=<0.0001; 3-1000 kDa p=<0.0001; and <3 kDa p=0.0291), n=3 biological replicates (Figure 4.16B). The most nucleic acid was detected in the smallest sub-fraction, with the <3 kDa having 10.2 ±0.40 µg/mL SEM, which was significantly greater than the >1000 kDa at 3.8 ±0.39 µg/mL SEM (p=0.0001) and 3-1000 kDa at 0.5 ±0.13 µg/mL SEM (p=<0.0001). The 3-1000 kDa sub-fraction had the lowest nucleic acid concentration, which was statistically lower than the >1000 kDa (p=0.0084). The total nucleic acid across the three sub-fractions totalled to a similar level as the original UCMSC ADH-E conditioned media, suggesting that unlike protein, nucleic acids may not be affected during the ultrafiltration process.

The concentration of EVs was also determined, with original UCMSC ADH-E conditioned media having 7.7 $x10^8$ ±1.15 $x10^8$ particles/mL SEM (Figure 4.16C). Most particles were retained as expected by the 1000 kDa filter, with a non-significantly different concentration of 7.6 $x10^8$ ±0.46 $x10^8$ particles/mL SEM being quantified in the >1000 kDa sub-fraction, n=3 biological replicates. Both remaining sub-fractions had significantly lower particle concentrations than both the original UCMSC ADH-E and the >1000 kDa sub-fraction, with 3-1000 kDa measured at 7.1$x10^7$ ±0.12$x10^7$ particles/mL SEM (p=0.0002 and p=0.0002 respectively) and <3 kDa at 4.2 $x10^7$ ±0.26 $x10^7$ particles/mL SEM (p=0.0001 and p=0.0002 respectively), n=3 biological replicates.

Finally, the bioactivity for all three sub-fractions was examined on the whole blood LPS-induced inflammation assay (Figure 4.16D). All three sub-fractions reduced TNFα levels from the vehicle control, at 100.0 ±3.43% SEM, with statistical significance to 59.8 ±3.12% SEM with >1000 kDa

(p=<0.0001), 73.8 ±5.07% SEM with 3-1000 kDa (p=0.0002), and 74.0 ±3.82% SEM with <3 kDa (p=0.0003), n=3 biological replicates. However, UCMSC ADH-E conditioned media treatment reduced TNFα the most to 20.8 ±1.08% SEM, which was statistically lower than the vehicle (p=<0.0001) as well as being significantly less than >1000 kDa (p=<0.0001), 3-1000 kDa (p=<0.0001) and <3 kDa (p=<0.0001). All treatment groups remained statistically different from the baseline TNFα levels, and there was no statistical significance between the sub-fractions.

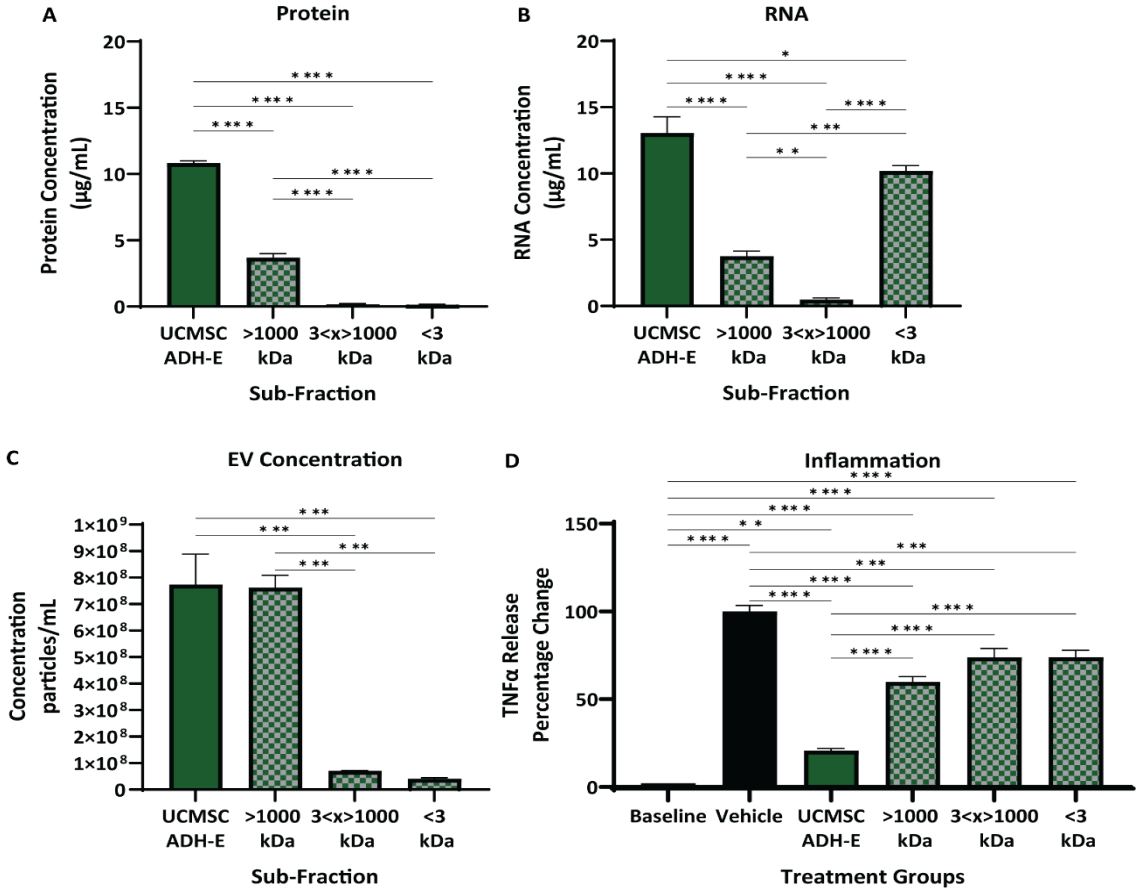

Figure 4.16 Impact of dividing UCMSC ADH-E conditioned media by molecular weight.

(A) *Quantification of protein,* ***(B)*** *total nucleic acid and* ***(C)*** *extracellular vesicle concentration of UCMSC ADH-E conditioned media sub-fractions divided by molecular weight with ultrafiltration.* ***(D)*** *Bioactivity of UCMSC ADH-E sub-fractions on TNFα levels release from human blood following LPS stress. Bars represent the average of three sets of sub-fractions (n=3) and statistical significance from ANOVA with Tukey's post testing presented with asterixis: * p= <0.05; ** p= <0.01; *** p= <0.001; **** p= <0.0001.*

Three-dimensional culture generated UCMSC conditioned media

One of the challenges for cell-derived therapeutics which has had tremendous advancements over the last few years is the lack of scalable, cost-effective systems to grow adherent cells to levels desired in an allogenic product. One approach would be to transition from the two-dimensional planar culture in T-flasks and CellSTACK® to monolayer microcarrier bead-based cultures in three-dimensional systems such as bioreactors. To that end, the next phase of UCMSC ADH-E development was to evaluate the potential for generating an equivalent conditioned media from a three-dimensional culture of UCMSCs. As mentioned, there have been many advancements in 3D culture systems including culturing of various mesenchymal stem cells. Therefore, using the information and resources available, a basic culture system was trialled.

Amalgamating information from the supplier and manufacturer of the UCMSCs and culture media (RoosterBio®), the manufacturer of the microcarriers (Corning®) and a protocol from Eppendorf for culturing bone marrow-derived MSCs in shaker flasks, an initial protocol was devised. To determine the most appropriate method to use for seeding UCMSCs, the benefit of agitation over static inoculation was explored. Equal numbers of cells were seeded into Erlenmeyer flasks and allowed to adhere for 24 hours. Agitation was provided by gently swirling the flask for 10 seconds every 20 minutes, with periods of rest for the first 2 hours of culture prior to placing on a low-speed (20 rpm) shaker, compared to the static method which was simply placed inside of the incubator for the duration of the time. At the end of the time, the cells were dissociated and counted to reveal that static method had a significantly greater number of cells recovered after 24 hours than the inclusion of agitation, $p=0.0014$, $n=3$ biological replicates (Figure 4.17A). However, both cultures had less cells than were seeded, with static inoculation recovering 41.8 ±3.94% SEM and with agitation only recovering 13.5 ±0.79% SEM. Compared to conventional 2D cultures in an equivalent sized T-flask, 119.8 ±3.35% SEM were covered after 24 hours, which as statistically significant above the agitated ($p=<0.0001$) and static ($p=<0.0001$) microcarrier-3D methods.

To determine if microcarrier-3D UCMSC cultures would expand, Erlenmeyer flasks were seeded with both inoculation methods as described above and cultured for three days of a shaker at 50 RPM. Upon passage, UCMSCs were counted and as expected the static method of inoculation yielded a higher number of UCMSCs, at 293.3 ±20.98% SEM of the seeded number compared to 152.9 ±10.62% SEM with agitation (Figure 4.17B). A two-way t-test gave a significance of p=0.0031, n=3-4 biological replicates. This confirmed that the static inoculation method would be used for further microcarrier-3D cultures of UCMSCs. Lastly, to compare the final cell density from microcarrier-3D culture to 2D flasks, sets of each culture were initiated. Once 2D cultures had reached confluency (approximately 80%) after three days, they are passaged and counted to reveal an average of 48,749 ±1,920 cells/cm^2 SEM (Figure 4.17C). With the experienced 50% attachment rate of UCMSC in the microcarrier-3D culture system, these cultures were grown on for an additional day. Even with this added time, microcarrier-3D cultures yielded on average 17,521 ±1,427 cells/cm^2 SEM in four days which was significantly lower than the 2D cultures (p=<0.0001), n=7-8 biological replicates.

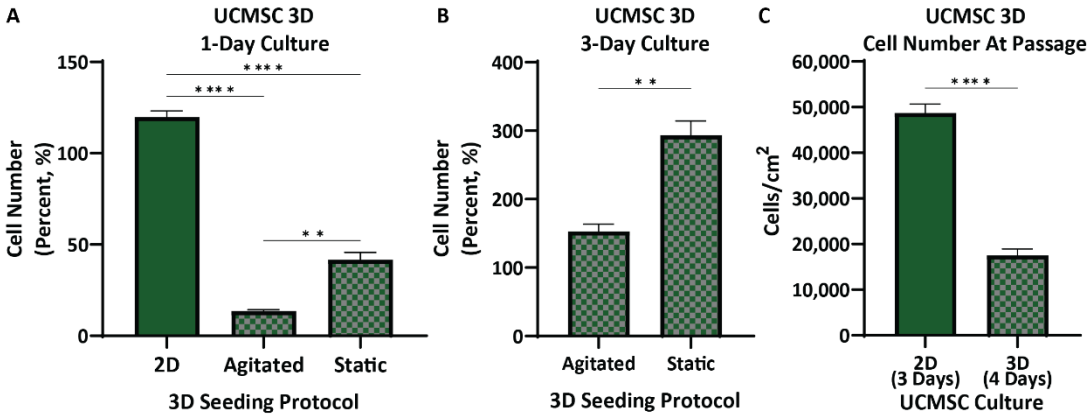

Figure 4.17 Establishing three-dimensional culture of UCMSCs

(A) *Percentage recovery of UCMSCs 24 hours following two seeding methods. Bars represent average of three flasks (n=3) and statistical significance for ANOVA with Tukey's post testing presented with asterixis: * p= <0.05; ** p= <0.01; *** p= <0.001; **** p= <0.0001.* ***(B)*** *Percentage recovery of UCMSCs following 3 days of 3D culture. Bars represent average of three agitated and four static flasks (n=3-4).* ***(C)*** *Cell density at passage for 3-day 2D cultures and 4-day 3D cultures of UCMSCs, where bars represent the average of eight 2D and seven 3D flasks (n=7-8). T-test statistical results present as asterixis: * p= <0.05; ** p= <0.01; *** p= <0.001; **** p= <0.0001.*

Generation of conditioned media from three-dimensional UCMSC cultures.

Based on the results from the initial cultures of UCMSCs in a microcarrier-shaker flask system, it was apparent that same approach to controlling the number of cells used to generate UCMSC ADH-E conditioned media would not be suitable due to the seemingly poor attachment. To that end, new UCMSC ADH-E-2D conditioned media was generated following the established protocol, whereas UCMSC ADH-E-3D conditioned media was generated from shaker flasks cultured for four days to reach a high confluency. The volume of EBSS buffer used was maintained in proportion to the culture surface area ([REDACTED]) when conditioned media was generated. On initial assessment of the content, UCMSC ADH-E-3D conditioned media had significantly lower protein concentration that UCMSC ADH-E-2D (Figure 4.18A), with only 20.7 ±1.62 µg/mL SEM compared to 37.8 ±0.79 µg/mL SEM (p=0.0003, n=3-4 biological replicates). Similarly, UCMSC ADH-E-3D conditioned media had significantly lower nucleic acid concentration than UCMSC ADH-E-2D (Figure 4.18B), with 14.5 ±1.03 µg/mL SEM compared to 30.7 ±0.45 µg/mL SEM (p=<0.0001, n=3-4 biological replicates). Conversely, UCMSC ADH-E-3D had a statistically significant (p=0.0017, n=3-4 biological replicates) greater concentration of particles quantified at 4.46 $x10^9$ ±0.33 $x10^9$ particles/mL SEM compared to 1.16 $x10^9$ ±0.29 $x10^9$ particles/mL SEM in the UCMSC ADH-E-2D conditioned media (Figure 4.18C).

As the cell number could not be controlled for microcarrier-3D conditioned media in the same way that was achieved with 2D conditioned media generation, the content was reassessed with normalisation. The protein, nucleic acid and EV concentrations were normalised to per million cells, using the seeding density for UCMSC ADH-E-2D and the average cell number after four days of culture (taken from Figure 4.17C). With reviewing the data in this configuration, it revealed that UCMSC ADH-E-3D had equivalent protein secreted per one million cells to the UCMSC ADH-E-2D conditioned media, at 92.9 ±7.27 µg/mL SEM and 89.0 ±1.96 µg/mL SEM respectively, n=3-4 biological replicates (Figure 4.18D). Total nucleic acid remained significantly lower in the UCMSC ADH-E-3D conditioned media at 64.8 ±4.62 µg/mL SEM compared to 76.3 ±1.13 µg/mL SEM of the UCMSC ADH-E-2D (p=0.0379, n=3-4 biological replicates), although the difference was less pronounced (Figure 4.18E). Lastly, the

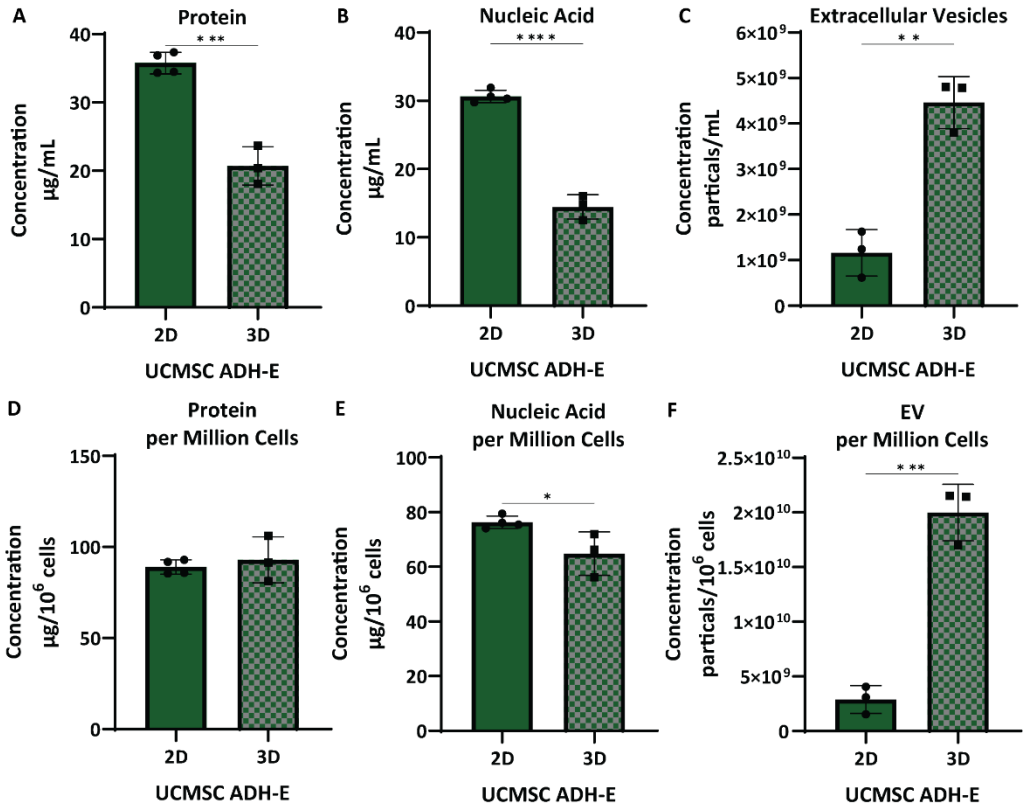

Figure 4.18 Evaluation of 3D conditioned media content.

UCMSC ADH-E conditioned media generated from 2D, and 3D culture systems quantified for ***(A)*** *protein,* ***(B)*** *total nucleic acid and* ***(C)*** *extracellular vesicle concentrations. Normalised results to concentration per one million cells, for* ***(D)*** *protein,* ***(E)*** *total nucleic acid and* ***(F)*** *extracellular vesicles. Bars represent the mean concentrations from four UCMSC ADH-E-2D and three UCMSC ADH-E-3D (n=3-4) conditioned media. T-test statistical significance presented as asterixis: * p= <0.05; ** p= <0.01; *** p= <0.001; **** p= <0.0001.*

difference in particle concentration was amplified with this normalisation, with the adjusted values for UCMSC ADH-E-3D at 2.0 $x10^{10}$ ±0.15 $x10^{10}$ particles/million cells SEM compared to 2.89 $x10^{9}$ ±0.74 $x10^{9}$ particles/million cells SEM in UCMSC ADH-E-2D, p=0.0005, n=3-4 biological replicates (Figure 4.18F).

Next the impact of generating conditioned media in this way on biological activity was explored. These conditioned medias were tested on developed assays for proliferation and inflammation modes of action. Beginning with a potency assay using HeLa cells, both UCMSC ADH-E-2D and 3D conditioned

medias significantly increased proliferation, n=3-4 biological replicates (Figure 4.19A), from 100.0 ±7.50% SEM in the vehicle to 171.9 ±11.46% SEM with 2D conditioned media treatment (p=0.0004) and 200.5 ±7.92% SEM with 3D conditioned media treatment (p=<0.0001). There was no statistical difference between the two conditioned media types (p=0.1713). A similar result was recorded on the whole blood LPS inflammation assay, n=3-4 biological replicates. Here, both UCMSC ADH-E-2D and 3D conditioned media significantly reduced TNFα levels from the vehicle treated control (p=<0.0001), from 100.0 ±3.63% SEM to 13.2 ±2.85% SEM and 20.6 ±2.31% SEM respectively (Figure 4.19B). There was no statistical significance between UCMSC ADH-E-2D and UCMSC ADH-E-3D treatments (p=0.2524).

To determine if an impact from differences in content concentration was being masked by a maximal effect threshold being reach with the 10% v/v 1x conditioned media treatment, a 10-fold dilution dose series was tested on the inflammation assay, n=3-4 biological replicates. If that was the case, lower treatment concentrations should differ between UCMSC ADH-E 2D and 3D conditioned media. As predicted, this was observed. For both conditioned medias there was no beneficial effect with 0.001x treatment compared to vehicle treatment of 100.0 ±4.49% SEM (Figure 4.18C). At 0.01x treatment UCMSC ADH-E-2D conditioned media reduced TNFα levels to 74.2 ±0.38% SEM (p=<0.0001), whereas UCMSC ADH-E-3D had no effect, 98.8 ±2.35% SEM (p=>0.9999). At 0.1x treatment UCMSC ADH-E-2D conditioned media further reduced TNFα levels to 31.9 ±0.83% SEM (p=<0.0001 vs vehicle and 0.001x treatment). A treatment of 0.1x UCMSC ADH-E-3D also significantly reduced TNFα levels from the vehicle group, to 57.3 ±1.03% SEM (p=<0.0001), however the levels of TNFα where significantly greater than the respective treatment of UCMSC ADH-E-2D (p=<0.0001). Finally, 1x treatment of UCMSC ADH-E-2D further reduced TNFα levels to 9.5 ±0.45% SEM (p=<0.0001 to the vehicle and lower treatment concentrations). UCMSC ADH-E-3D conditioned media at 1x treatment also reduced TNFα levels further, to 17.6 ±0.80% SEM, which was significantly lower than the 0.1x treatment (p=<0.0001 to vehicle and lower concentrations). However, the 1x treatment revealed a familiar result, where there was no statistical difference between UCMSC ADH-E-2D and UCMSC ADH-E-3D 1x treatments

(p=0.2966). Of note, 1x treatment with UCMSC ADH-E-2D was not significantly different to the baseline level of 2.5 ±0.03% SEM (p=0.9984) whereas UCMSC ADH-E-3D conditioned media treatment remained elevated about the baseline (p=0.0047).

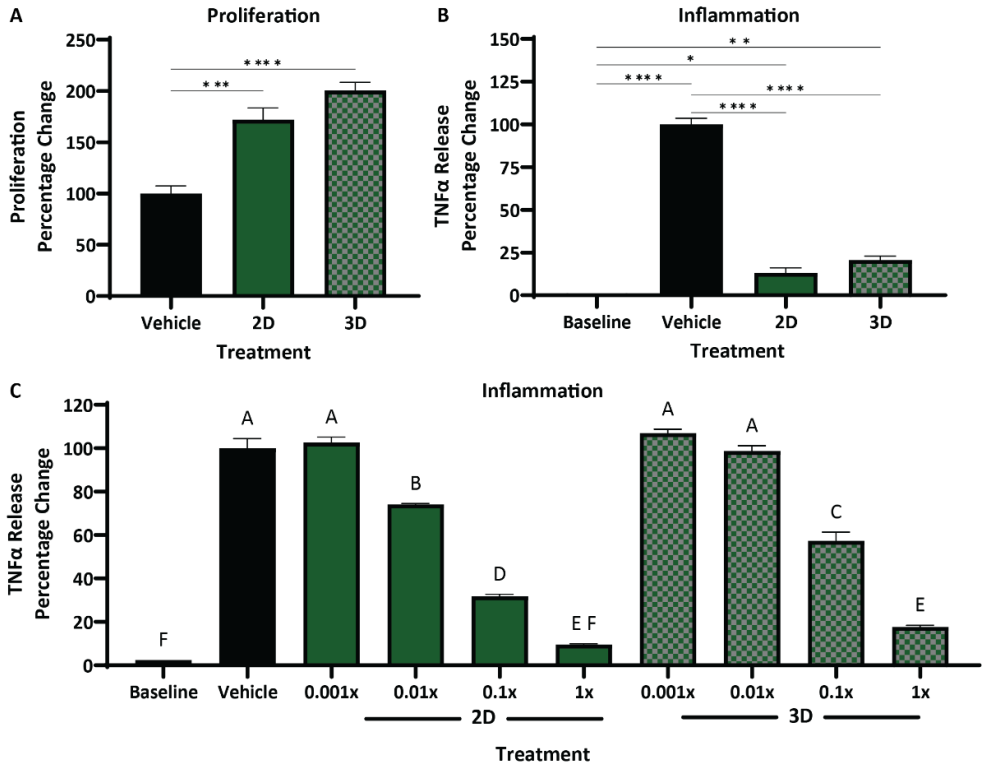

Figure 4.19 Bioactivity of three-dimensional generated UCMSC ADH-E conditioned media.

(A) *Assessment of 3D-derived UCMSC ADH-E conditioned media on HeLa cell proliferation compared to original 2D version.* ***(B)*** *Effect of UCMSC ADH-E 3D conditioned media on TNFα levels release from human blood following LPS stress compared to 2D conditioned media. Bars represent average of four UCMSC ADH-E-2D and three UCMSC ADH-E-3D (n=3-4) conditioned media. Statistical significance from ANOVA with Tukey's post testing presented as asterixis: * p= <0.05; ** p= <0.01; *** p= <0.001; **** p= <0.0001.* ***(C)*** *Effect of different concentrations of UCMSC ADH-E 2D and 3D conditioned media on TNFα levels release from human blood following LPS stress. Bars represent average of four UCMSC ADH-E-2D and three UCMSC ADH-E-3D (n=3-4) conditioned media. Statistical significance from ANOVA with Tukey's post testing is displayed by grouping letters, where each bar is significantly different to any unmatched bar.*

Discussion

GMP umbilical cord mesenchymal stem cell growth, conditioned media, and release testing.

In final product manufacture there are numerous considerations to meet quality and regulatory requirements, including the grade of starting materials. For this reason, the decision was made that before further development was to take place, the UCMSC line used should be from a GMP-compliant bank. Therefore, a new UCMSC line was procured from RoosterBio® at GMP-grade with the full permissions for use in further manufacture, which then required testing for compatibility to the previous lines. This provided valuable opportunity to assess a third donor, and a second line for one of the same suppliers. The growth of this line reflected what was previously recorded from UCMSCs, where the cells proliferated consistently well for over a month of continuous culture before rapidly dropping off into a plateau, all the while cell viability was found to be consistently high. This concurred with the cultures of the previous two UCMSCs utilised in Chapter 3, where after a period of liner expansion the cells turned senescent and ceased proliferating. This provides a level of confidence that whichever scale up/out manufacturing platform is selected would be adaptable and future proofed for replacement UCMSC lines, as three donors have already been shown similar growth characteristics and limitations within the less tightly control research and development (R&D) environment. Ensuring that this cell line would produce a biologically potent conditioned media, similar to those collected from the previous cell line, was vital for its viability for use in further product development, therefore both UCMSC PEL and UCMSC ADH conditioned medias were generated. UCMSCs remained highly viable through the generation process in both methods, which is thought to be important as batch-to-batch variability should be more controlled when collecting the actively secreted product from viable cells within a defined duration of stress, as opposed to reproducibly encouraging a level of cellular death.

Both conditioned media variants from this new cell line, UCMSC PEL MUO and UCMSC ADH MUO, when compared against their counterpart from UCMSC RUO cells, were found to have secreted the same quantities of protein, total nucleic acid, and extracellular vesicle. This demonstrated that not

only the methods of generating conditioned media are robust, but that they can be conserved across UCMSC donors. Building on this, the bioactivity effects were assessed on the proliferation potency assay, showing that within both conditioned media variants, there was no statistically conclusive difference in potency between the UCMSC lines used. Of note, the overall enhancement of proliferation appeared greater in both UCMSC ADH conditioned medias over the UCMSC PEL, something that was previously conflicted between the first UCMSC from ATCC and this RUO line from RoosterBio®. This has highlighted the importance of donor selection when working with cells such as MSCs, which has been something warned by the literature (Kang et al., 2018, Česnik and Švajger, 2024). Finally, the biological potency on LPS-induced inflammation confirmed there was no difference between conditioned medias from UCMSC RUO and UCMSC MUO cells in either pellet or adherent conditioned media as all conditioned medias successfully reduced levels of TNFα released from whole blood. The results from the biological potency assays on top of the quantification of content, provided sufficient evidence that the UCMSC MUO was equivalent to the previously tested UCMSC RUO line and thus suitable for use in further product development.

There are a few options used within the field to overcome donor-to-donor variation and securing the longevity of a therapeutic product. One option would be to create an immortalised-UCMSC cell line. To date, numerous immortalisation genes have been discovered, amongst which, Simian Virus 40 large T-antigen (SV40-LTA) immortalisation is the most widely studied. SV40-LTA acts through p53 to inactivate Retinoblastoma proteins (Rb) thereby activating E2F-dependant transcription and promoting S phase progression, therefore advancing cellular proliferation, which results in immortalisation (Chen et al., 2019). In addition to the prevention of cell senescence and apoptosis, SV40-LTA has also been recorded to mediate cell immortalisation through changes in telomerase activity (Foddis et al., 2002). However, SV40-LTA has been reported to induce chromosomal abnormalities and non-diploid cells, leading to possible genomic instability (Ray et al., 1990). There are of course alternatives to SV40-LTA, such as insertion of telomerase reverse transcriptase (TERT),

which restores the telomeres of ageing cells, without altering the cells responses to environmental stimuli. This could provide a potential option for creating a long-lasting cell bank.

However, UCMSCs are an abundant cell which can be easily isolated from the umbilical cord, with numbers reaching up to 4.7 million MSCs/cm of tissue (Stefańska et al., 2020). The results found thus far would indicate that UCMSCs have a relatively low donor-to-donor variation and based off the numbers of potential cells which could be isolated per donor and the identified expansion limit, the need for drastic genetic manipulation of the cells may not be necessary for development a clinical scale and commercially viable product.

Clinical development of UCMSC ADH conditioned media

So far, two conditioned media's have been generated and tested alongside one another, evaluating if a method of pelleting MSCs would generate a potent clinically compliant conditioned media from UCMSCs as it has from both adipose-derived and amniotic fluid-derived MSCs (Mitchell et al., 2019, Mellows et al., 2017). From the results collected throughout this project, it was becoming clear that UCMSC PEL conditioned media, although biologically active, was not an enhanced conditioned media compared to the UCMSC ADH. Exploring this further, parameters such as manufacturing complexity, larger scale-up requirements and associated higher costs of UCMSC PEL, lead the focus of clinical development on to UCMSC ADH conditioned media. UCMSC ADH conditioned media had demonstrated reproducibility as well as potent modifications of proliferation, migration, and inflammation, however the methods used are not fully clinically realised. The method used here, was devised from literature, where it is common to generate conditioned media with basal or serum free medias. Although these materials are not definitely non-compliant, the basal media used here was proprietary to the American Type Culture Collection (ATCC), and as such was not publicly defined and solely available from ATCC. To progress with this material could carry risk to the manufacture, with no redundancy in the supply change; risk to cost increases including the raw materials cost but also the

requirement to include specific vehicle safety trials; and risk to regulatory rejection if all raw materials were not defined sufficiently.

With the view to develop UCMSC ADH conditioned media further, the first parameter to address was the basal media used to collect the UCMSC secretions. With the mindset that simplicity would trump complexity for regulatory approval and safety concerns, common publicly defined and widely available culture buffers and media were tested. The first type of buffers tested were phosphate buffered saline (PBS) based, which were unable to maintain cells over the 24-hour period. The inclusion of calcium and magnesium ions marginally improved surviving cell viability, likely due to their importance in almost all cellular functions (Bagur and Hajnóczky, 2017) such as metabolism (McCormack and Denton, 1990), protein synthesis (Rubin et al., 1979) and cell-to-substrate adhesion (Takeichi and Okada, 1972). However, when the nutrients glucose and pyruvate were included, cell survival was worse than other PBS variants. This could have been a result of the limited buffering capacity of phosphate salts and with the availability of nutrients, the metabolism and accompanying CO_2 and lactic acid production may have been greater resulting in a reduced pH (Gstraunthaler et al., 1999). Hanks' Balanced Salt Solution (HBSS) was the next buffer compared, which was formulated to mimic the extracellular fluid to provide a stable environment for cells in culture. Like the PBS, it included both calcium and magnesium ions as well as glucose, but with the addition of sodium bicarbonate. The addition of bicarbonate ions improves the buffer system for use in cell culture, and HBSS is commonly used as a base for culture media for use in atmospheric conditions. This improved buffering capabilities is likely the reason the HBSS had the best cell survival and viability of all the atmospheric incubated solutions. Buffers intended for use in 5% CO_2 atmospheres were also included, the first being Earle's Balanced Salt Solution (EBSS) with and without calcium and magnesium ions. Like HBSS, EBSS contains bicarbonate but in at a higher molarity to provide it's stronger buffering capacity. As seen with PBS, the inclusion of calcium and magnesium improved cell survival and viability, but in this instance the composition of EBSS combined with these ions resulted in no loss of UCMSCs during the incubation. EBSS is commonly used as a base to culture medias, one being Minimal Essential Medium

(MEM), which in addition to EBSS contains essential amino acids and vitamins. MEM also had good survival and viability, and along with EBSS with calcium and magnesium performed similarly to the ATCC basal media originally used. In addition, both these buffers had similar anti-inflammatory activity which cemented them as candidates for further optimisation.

This optimisation came in the form of reviewing the incubation time. Extending the incubation time out to 48 hours had minimal impact on cell viability, whereas both EBSS and MEM failed to maintain cells for 72 hours. As could be expected increased conditioning time resulted in higher amounts of protein and nucleic acid across the three vehicles, however, this did not translate into an increase in potency, except for EBSS conditioned media, which found 48-hour conditioned media had a better proliferative and anti-inflammatory effect than the shorter 24-hour incubation timepoint. Differences may have been identified with a dose curve in case the maximal biological effect was reached within the assay, however, enough information was collected to identify that EBSS, with calcium and magnesium would be the suitable clinically optimal vehicle for conditioned media generation. The decision was based on the equivalent cell survival and biological potency to the original ATCC basal media, whilst being the simplest solution compared to MEM. [REDACTED] as there was evidence that this increased potency of the conditioned media, without being detrimental to the UCMSCs viability.

Storage and stability testing

Although EBSS had been identified as the most promising candidate to replace ATCC basal media use for generating UCMSC ADH conditioned media, a disruptive observation was made in all three of these vehicles, that had previously been missed. Upon thawing of conditioned media, visible precipitates were suddenly seen in the conditioned media. Reviewing product data sheets from additional manufactures identified that when EBSS (and EBSS based medias) is frozen there is a known problem of salt precipitation. The progressive deterioration of EBSS buffer found during the stability studies when stored at +4°C and ambient; the recommended storage temperature for EBSS buffer; was somewhat more puzzling.

The fact that the cloudy appearances and particulates were present in both the conditioned media and the vehicle gave reassurance that the UCMSCs nor their secretions were the cause. Comparing between refrigerated and ambient storage, the speed of deterioration appeared to be temperature dependant suggesting that cooler temperatures are beneficial for the stability of the conditioned media. Bicarbonate buffers work through a complex equilibrium of dissolved carbon dioxide (CO_2), carbonic acid (H_2CO_3), bicarbonate (HCO_3^-) and carbonate (CO_3^{2-}) (Shaw and Gregory, 2022).

$$CO_2 + H_2O \leftrightarrow H_2CO3 \leftrightarrow H^+ + HCO_3^- \leftrightarrow 2H^+ + CO_3^{2-}$$

Within the culture environment the level of supplemented 5% CO_2 atmosphere and the molarity of sodium bicarbonate dictates the physiological buffering range of the EBSS (pH 7.2 to 7.6). When the solution becomes too acidic, the bicarbonate ions neutralise the excess hydrogen ions by forming carbonic acid, which converts to carbon dioxide and water. When the solution becomes too alkaline, carbonic acid dissociates to release hydrogen ions which lowers the pH.

Sodium ions left over from the sodium bicarbonate in the EBSS may displace calcium and magnesium from their salts creating the presence of divalent ions and facilitating the precipitation of carbonate (Davenport et al., 2019).

$$Ca^{2+} + 2HCO_3^- \leftrightarrow Ca(HCO_3)_2 \rightarrow CaCO_3\downarrow + H_2O + CO_2$$

Here, calcium ions react with bicarbonate to form calcium bicarbonate. Upon returning to normal atmospheric carbon dioxide, the level of dissolved carbon dioxide begins to reduce, lowering the availability of carbonic acid, which in turn reduces the available hydrogen ions required to balance the pH with the bicarbonate, driving the reaction with calcium. In turn, the increase in pH results in calcium bicarbonate degradation to form calcium carbonate, an insoluble salt which precipitates. As gases such as carbon dioxide have higher solubility in cooler temperatures, this would also help explain why +4°C took longer to deteriorate than the ambient condition.

Reflecting on the impact of these storage conditions on the content would suggest that protein was stable at both -80°C and +4°C conditions, where there was detectable loss of protein when stored at ambient temperatures. This was somewhat expected as literature has reported that proteins are generally unstable at room temperature (Arakawa et al., 2001) and their degradation may have also been facilitate by the increased pH. Total nucleic acid on the other hand seemed relatively unaffected. However, being an absorbance-based assay, it is possible that the increased turbidity in ambient and later refrigerated samples has masked any true changes in nucleic acid concentration. This is supported by the unexpected increase in nucleic acid detected in later samples, which coincided with the elevation in opacity scores.

Storage of UCMSC ADH-E conditioned media at +4°C would be the best solution to this issue. To improve the longevity of the conditioned media, a fresh batch was storage in glass vials, sealed with a rubber bung. The reason to try this was to see whether limiting the rate that dissolved CO_2 was released could delay or prevent the onset of precipitation. Initially, the results looked promising, with the first signs of visible particles now at 4 months, without a change in turbidity score which had previously occurred by the first month when stored in 15 mL falcon tubes. There was an initial drop in protein at 1 month which remained stable to 4 months, and total nucleic acid was initially stable at 1 month (which had previously dropped by this time) but later decreased at 4 months. Although all timepoints were found to have strong effects on inflammation, there was a trend towards the conditioned media becoming less potent. Taking in to account all the results from the glass vial trial, there is certainly a pattern towards suitability for short time storage of conditioned media in this manner. For longer term, this may be unsuitable as biomolecules are generally recommended to store frozen for longer durations.

The bicarbonate-based buffers were found to be the best at maintaining UCMSCs during the conditioned media generation period compared to alternatives such as PBS, and the absence of calcium and magnesium ions resulting in poor cell survival, preventing this storage issue from the start

seemed improbable. To that end, the next solution explored as to remove the problematic salts after conditioned media was generated. Buffer exchanges have been used for years for antibody generation (Sarin et al., 2024) and during analytical methodologies such as mass spectrometry (Yang et al., 2024). The use of small-volume centrifuge filters at first seemed to be the most practical and viable option to test the feasibility of buffer exchange. However, upon quantifying the levels of retained and lost content it was found that a large proportion of protein was lost during the process, and a substantial amount of nucleic acid was found in the filtrate. As the protein was not detected in the filtrated, like the nucleic acid, it is likely that the protein was stuck to filter. As the nucleic acid was filtered out, it would suggest that it was not bound within the extracellular vesicles, which is what made the findings interesting when the filtrate had anti-inflammatory properties. EVs have been hailed as the next refinement of conditioned media, with an extensive list of publication finding these membrane-bound vesicles to have potent therapeutic actions (Gatti et al., 2011, Tang et al., 2017, Yin et al., 2016). The findings here, would suggest that there are potent molecules outside of EVs, and therefore exchanging the buffer could potentially lose these components too.

Repeating this fractionation without the change in vehicle (keeping all parts in EBSS), once again found that the protein was lost in the sample processing. Only a third of the protein was recovered from the process within the largest size fraction, whereas the total quantity of nucleic acids (a third in the largest size and two thirds in the smallest) and EVs (retained as expected by the largest filter) were present across the fractions. This work demonstrated that UCMSC conditioned media had a greater anti-inflammatory activity whole, than any of the sub fractions. In addition, no fraction was more efficacious than another. Therefore, if a method used to modify conditioned media post generation for better storage were to result in the loss of a particular collection of components, the resulting product would be less potent. Although, the final product may still be biologically active, this reduced potency may place additional pressure on the dosing criteria (volume required for therapeutic effect) and/or manufacturing scale.

Three-dimensional microcarrier culture of UCMSCs

This initial exploration into microcarrier culture of UCMSCs proved challenging. The use of microcarrier culture, which uses small beads to support adherent cells in bioreactors, offers vast potential for large-scale production and efficient cell yields compared to traditional 2D cultures (Lembong et al., 2020, Fernandes-Platzgummer et al., 2016, Rafiq et al., 2016). Establishing protocols of microcarrier-3D culture requires various considerations, from microcarrier material, bioreactor type, agitation speed, and cell harvesting methods (Rafiq et al., 2016). Working within the constraints of resource and costs, the microcarrier-3D culture of UCMSCs was established to a basic level. Although attachment of UCMSCs were relatively poor compared to traditional 2D culture, it was possible to expand the cells over several days. During the initial set up of the protocol, it was found agitation was detrimental to the success of inoculation, which resulted in the use of the static method for downstream conditioned media generation. However, literature does support that the methods with intermittent agitation can be successful for the attachment of UCMSCs (Soder et al., 2024).

Overall, the microcarrier-3D culture methods employed here, could benefit from the refined optimisation of bioreactors, where better environmental controls can be established for optimal cell expansion. UCMSCs have been demonstrated to culture efficiently in small and large scale stirred reactors (Zhang et al., 2022, Kurogi et al., 2022). The struggles with the attachment of UCMSCs in the shaker flask system used created a problem with being able to control the number of cells going into a conditioned media generation. Therefore, it was decided that the next best option for a proof-of-concept conditioned media generation would be to grow UCMSC microcarrier-3D cultures for a few days and estimate the cell numbers at the initiation of conditioned media collection. Using this method, the starting cell number was slightly above 50% of the cell number than what was used for the original 2D UCMSC ADH-E conditioned media. This difference in cell number could be the reason to between the lower levels of secreted proteins and nucleic acids quantified in 3D conditioned media, as once normalised to cell number, the levels were equivalent to 2D conditioned media. The numbers of EVs were found to be greater in the 3D conditioned media than 2D conditioned media despite the

lower cell number, which is a reported phenomenon (Kink et al., 2024). Despite these differences in concentration of content, the biological activity was not affected when initially tested. Both condition medias equally enhanced proliferation and reduced TNFα release with inflammation with no statistical difference. This could suggest that although total protein and nucleic acids were reduced, the key active molecules may have been secreted in greater amounts from the fewer cells in 3D culture resulting in equivalent total levels, or different more potent molecules may have been secreted by cells in the microcarrier-3D cultures. A comprehensive breakdown using mass spectrometry and RNA sequencing would be required to identify these changes. Alternatively, the biological limit may have been reached with in the assay. The explore this, a 10-fold dilution treatment series was tested on the inflammation assay, which revealed that both conditioned medias reached an equivalent maximum effect, lower concentrations of each conditioned media began to differ from each other. This identified that the differences in total content quantity had an overall impact on the potency of the conditioned media, but it's not being said that there would not be changes in the molecules secreted as well.

Overall, despite the challenges with the UCMSC microcarrier-3D cultures, which would hopefully be rectified by transition to full bioreactor systems, the premise of transitioning UCMSC ADH conditioned media to a scalable form was proven to be possible.

Chapter 5 - Results: Therapeutic Assessment of UCMSC ADH-E.

Introduction.

With the UCMSC conditioned media product development reaching key decision points in the translation journey, the final piece for the viability puzzle is the efficacy and identifying the clinical target. Before decisions can be made, it's important to build an understanding of the potential mechanisms of action through which UCMSC ADH-E conditioned media acts. Thus far, it has been demonstrated in vitro that UCMSC conditioned medias enhance cell proliferation and migration as well as having the capability to modulate an inflammatory response. This multi-action ability of conditioned media is the reason for the interest in regenerative medicine, as many clinical indications have a number of underlying pathologies (L et al., 2019).

To investigate the regenerative potential of UCMSC ADH-E conditioned media in a complex in vivo setting, an available model for use was venom-induced skeletal muscle damage. Skeletal muscle regeneration is a highly coordinated process involving a dynamic interplay between muscle stem cells, immune cells, and stromal populations in response to injury. Central to this process are satellite cells, the resident myogenic stem cells that activate, proliferate, and differentiate to form new myofibers (Yin et al., 2013). However, successful regeneration depends not only on the intrinsic potential of satellite cells but also on the regulatory microenvironment shaped by immune responses and mesenchymal progenitors (Tidball, 2017). The nature and severity of the muscle injury greatly influence the composition and timing of these cellular interactions, which in turn determine whether regeneration proceeds efficiently or results in fibrosis and chronic degeneration.

One widely used model of sterile muscle injury involves the administration of cardiotoxin (CTX), a myotoxin derived from *Naja* (cobra) venom. CTX induces rapid, localised necrosis of myofibres through membrane disruption while leaving the basement membrane, vasculature, and satellite cell niche largely intact (Hardy et al., 2016). This injury triggers a tightly regulated sequence of events: an initial infiltration of neutrophils, which in turn recruit pro-inflammatory M1 macrophages to clear necrotic debris and secrete cytokines like TNFα and IL-6, followed by a shift toward M2 macrophages, which

produce anti-inflammatory and pro-regenerative factors such as IL-10 and TGF-β1 (Arnold et al., 2007). In parallel, fibro-adipogenic progenitor (FAP) cells are transiently activated. These mesenchymal stromal cells provide structural and paracrine support to satellite cells but must be tightly regulated as persistent activation or dysregulation of FAPs can lead to fibrosis or fatty infiltration (Molina et al., 2021).

Due to its reproducibility and the preservation of a supportive regenerative microenvironment, the CTX model has become the gold standard for testing regenerative therapies, including stem cell derived conditioned media**.** As demonstrate and discussed previously, conditioned media contains a complex mixture of growth factors, cytokines, and extracellular vesicles that modulate key regenerative processes. Studies have shown that CM derived from mesenchymal stem cells such as those from adipose tissue (Mitchell et al., 2019), or amniotic fluid (Mellows et al., 2017) can enhance satellite cell proliferation and modulation of macrophage polarization towards the M2 phenotype using the CTX-injured muscle.

In contrast, the use of unpurified venoms such as from *Bitis arietans* (BaV), the puff adder, can induce a more pathological form of muscle damage. BaV contains a complex mix of metalloproteinases, phospholipases A2, and serine proteases (Calvete et al., 2007), which collectively cause not only extensive myonecrosis, but also damage to capillaries and extracellular matrix, and prolonged inflammation (Williams et al., 2019). The resulting environment is less permissive to satellite cell-mediated regeneration and more prone to fibrosis and tissue remodelling, mirroring clinical cases of severe envenomation or traumatic muscle injuries.

These fundamental differences underscore the limitations of the CTX model for evaluating regenerative therapies under pathological conditions. While CTX is useful for assessing the maximal regenerative potential of a therapeutic agent, it may overestimate efficacy by failing to capture the complexity of chronic or fibrotic injuries. Conversely, the use of a whole venom model, such as BaV, provides a more stringent and clinically relevant challenge, particularly for testing whether

regenerative therapies can modulate immune and stromal responses to overcome a hostile microenvironment. Therefore, in this chapter BaV-induced muscle injury has been used to assess the pro-regenerative effects of UCMSC ADH-E, by the evaluation of not only satellite cell activity but also on the reconstruction of the extracellular matrix and the behaviour of FAPs. By applying UCMSC ADH-E in a setting of complex, non-sterile muscle damage, this work aimed to determine its potential therapeutic action on restoring skeletal muscle under impaired regenerative conditions, which could also indicate other possible mechanisms of action and other potential clinical indications.

Results

Impact of UCMSC ADH-E on inflammation.

Peripheral blood mononucleated cell inflammation assay.

A strong inflammatory activity has been routinely observed from UCMSC ADH conditioned media and more so with UCMSC ADH-E in previous chapters. To continue to build the understanding of this property, the 2D formulation was tested on the LPS-induced peripheral blood mononucleated cells (PBMC) inflammation assay. As previously reported, TNFα was measured as a marker of the inflammatory response. On unstimulated PBMCs, there was no change in baseline TNFα levels with UCMSC ADH-E conditioned media treatment (Figure 5.1). In contrast, with LPS stimulation, UCMSC ADH-E significantly reduced TNFα to 35.6 ±4.57% SEM from the 100.0% normalised vehicle treatment (p=<0.0001, n=3 biological replicates).

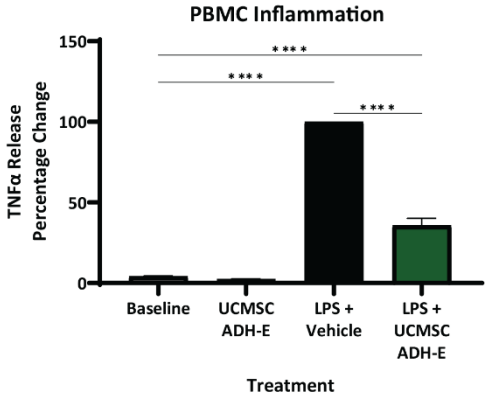

Figure 5.1 Bioactivity assessment of UCMSC ADH-E conditioned media on PBMC inflammation.

*The effect of UCMSC ADH-E conditioned media on TNFα levels from PBMCs stimulated with LPS. Bars represent average of three replicates (n=3) and statistical significance from ANOVA with Šídák's post testing is represented by asterixis: * p= <0.05; ** p= <0.01; *** p= <0.001; **** p= <0.0001.*

PBMC gene expression analysis of inflammatory markers.

To begin to understand how UCMSC ADH-E acts on the PBMCs, the cells from the inflammation assay were retained and gene expression analysis conducted for key inflammatory genes using quantitative polymerase chain reaction (qPCR), n=6 biological replicates. Beginning with NF-κB, a key transcription factor instrumental in numerous cell responses, in this case promoting the expression of cytokines

and the cells response to inflammation, the relative gene expression (RGE) was increased with LPS stimulation to 10.05 ±1.94 SEM from 2.00 ±0.67 SEM at baseline, p=<0.0012 (Figure 5.2A). UCMSC ADH-E treatment had no impact NF-κB in the absence of LPS (1.25 ±0.40 SEM), however UCMSC ADH-E conditioned media significantly reduced NF-κB gene expression to 4.69 ±1.07 SEM (p=0.0317). which was not significantly higher than the baseline level (p=0.5163). RGE of IL-1β increased to 12.03 ±1.12 SEM from 1.05 ±0.12 SEM with a one-way ANOVA with Šídák's post-test significance of p=<0.0001, which UCMSC ADH-E conditioned media significantly reduced IL-1β gene expression to 7.58 ±0.75 SEM (p=0.0014) (Figure 5.2B). RGE of IL-6 increased to 247.50 ±37.50 SEM from 1.36 ±0.41 SEM with a one-way ANOVA with Šídák's post-test significance of p=<0.0001, which UCMSC ADH-E conditioned media reduced to 170.60 ±29.97 SEM however, it was not statistically significant (p=0.1694) (Figure 5.2C). RGE of IL-8 increased to 12.18 ±1.74 SEM from 1.00 ±0.25 SEM (p=<0.0001), which UCMSC ADH-E conditioned media significantly reduced to 6.08 ±0.84 SEM (p=0.0021) (Figure 5.2D). RGE of IL-10 increased to 3.05 ±0.15 SEM from 1.00 ±0.03 SEM (p=0.0120), which UCMSC ADH-E conditioned media significantly increased IL-10 gene expression further to 5.04 ±0.74 SEM (p=0.0103) (Figure 5.2E). Finally, gene expression of TNFα was recorded to increase to 16.00 ±2.28 SEM from 1.05 ±0.09 SEM baseline levels (p=<0.0001) (Figure 5.2F). UCMSC ADH-E treatment significantly reduced to 3.14 ±0.28 SEM (p=<0.0001), which was not significantly different from the baseline (p=0.7018). Similarly to NF-κB gene expression, UCMSC ADH-E conditioned media treatment did not alter baseline gene expression of any of the cytokines assessed.

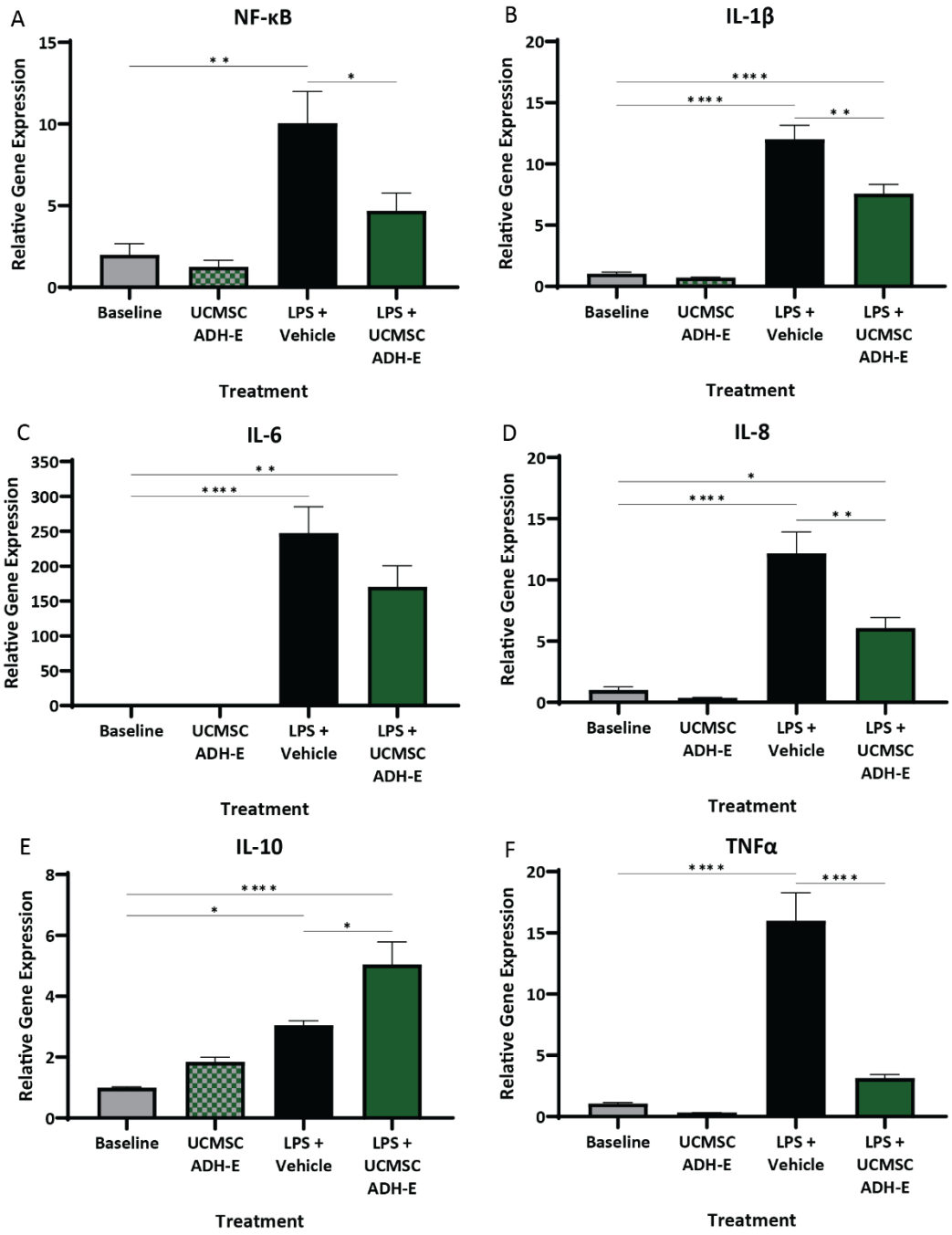

Figure 5.2 Expression levels of inflammatory genes from UCMSC ADH-E treated PBMCs

The effect of UCMSC ADH-E conditioned media on gene expression of ***(A)*** *NF-κB,* ***(B)*** *IL-1β,* ***(C)*** *IL-6,* ***(D)*** *IL-8,* ***(E)*** *IL-10 and* ***(F)*** *TNFα, from PBMCs stimulated with LPS. Bars represent average of six replicates (n=6) normalised to the housekeeping gene, GAPDH. Statistical significance from ANOVA with Šídák's post testing is represented by asterixis: * p= <0.05; ** p= <0.01; *** p= <0.001; **** p= <0.0001.*

Assessment of conserved bioactivity in rodent.

Ahead of any in vivo testing, which is still considered a vital step of medical product development (Domínguez-Oliva et al., 2023), the anti-inflammatory activity of UCMSC ADH-E was tested on rodent blood to determine if the effect was species specific. Therefore, a modified whole blood assay was developed to use rat blood instead of human blood. As rodents are more resistant to LPS than humans (Raduolovic et al., 2018) a greater concentration of LPS was required to stimulate a response. Nevertheless, UCMSC ADH-E significantly reduced the levels of TNFα to 71.7 ±2.62 SEM from 100.0 ±4.12% SEM of the normalised vehicle treated, p=0.0025, n=3 biological replicates (Figure 5.3).

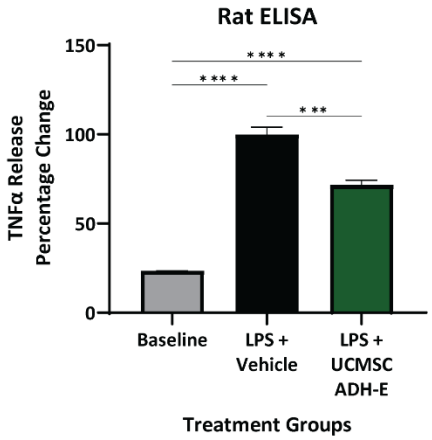

Figure 5.3 Bioactivity assessment of UCMSC ADH-E conditioned media on rat blood inflammation.

*The effect of UCMSC ADH-E conditioned media on TNFα levels from rat blood stimulated with LPS. Bars represent average of three replicates (n=3) and statistical significance from ANOVA with Šídák's post testing is represented by asterixis: * p= <0.05; ** p= <0.01; *** p= <0.001; **** p= <0.0001.*

Impact of UCMSC ADH-E on muscle regeneration.

In vitro assessment of bioactivity on myoblasts.

Previously, UCMSC ADH-E has been shown to promote changes in HeLa cells, such as increasing proliferation and migration. Myoblasts develop into muscle and are essential to the development, maintenance, and regeneration of skeletal muscle through a process called myogenesis. Immortalised-human myoblasts, AB1190 were used to investigate the effect of UCMSC ADH-E conditioned media

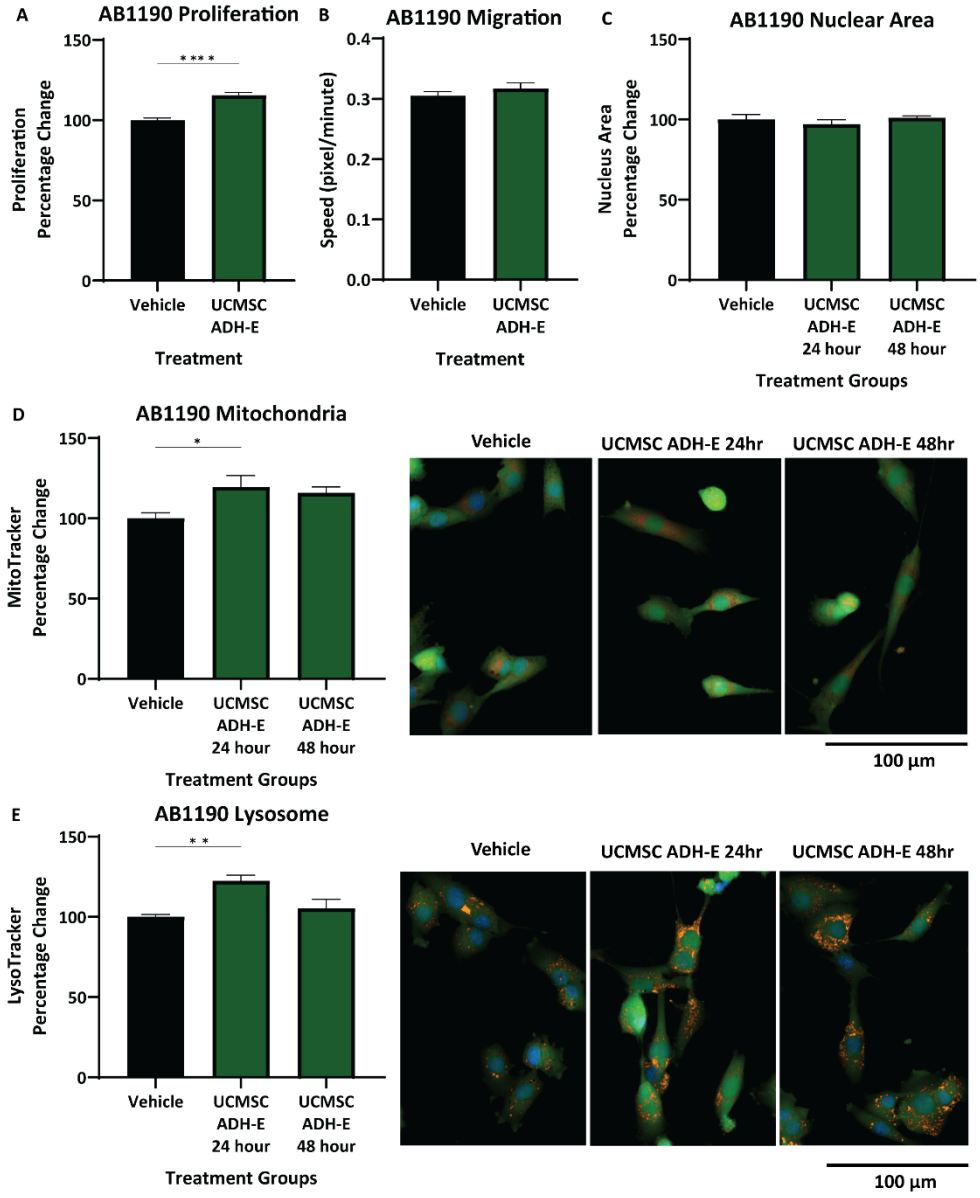

Figure 5.4 Bioactivity assessment of UCMSC ADH-E conditioned media on human myoblasts

(A) *The effect of UCMSC ADH-E conditioned media on human myoblast (AB1190) proliferation. Bars represent average of eight replicates (n=8).* ***(B)*** *The effect of UCMSC ADH-E on AB1190 migration. Bars represent average of twenty-five replicates (n=25). Statistical significance from two-way t-test is represented by asterixis: * p= <0.05; ** p= <0.01; *** p= <0.001; **** p= <0.0001.* ***(C)*** *Size of AB1190 nucleus following UCMSC ADH-E conditioned media treatment. Bars represent average of eight replicates (n=8).* ***(D)*** *Intensity of MitoTracker Deep-Red stain for AB1190 mitochondrial density following UCMSC ADH-E conditioned media treatment alongside representative images. Bars represent averages of four replicates (n=4). [Continues on next page]*

Figure 5.4 continued: (E) *Intensity of LysoTracker Red stain for density of AB1190 lysosomes following UCMSC ADH-E treatment, alongside representative images. Bars represent averages of four replicates (n=4). Statistical significance from ANOVA with Dunnett's post testing are represented by asterixis: * p= <0.05; ** p= <0.01; *** p= <0.001; **** p= <0.0001.*

on undifferentiated muscle cells. Firstly, UCMSC ADH-E conditioned media was found to increase proliferation of AB1190 cells to 115.6 ±1.66% SEM compared to 100.0 ±1.45% SEM of the vehicle treated controls, p=<0.0001, n=8 technical replicates (Figure 5.4A). Next, single cell tracking analysis of AB1190 found no difference in migration speed with UCMSC ADH-E conditioned media treatment (Figure 3.4B). Baseline cell speed was recorded at 0.31 ±0.007 px/min SEM, and following treatment, the speed was measured at 0.32 ±0.009 px/min SEM (p=0.3129, n=25 technical replicates).

Next, organelle specific dyes were used to evaluate intracellular changes as a result of UCMSC ADH-E conditioned media treatment. There was no alteration to nuclear size (n=8 technical replicates) (Figure 5.4C), however, UCMSC ADH-E increase the abundance of mitochondria (Figure 5.4D) and lysosomes (Figure 5.4E) after 24 hours of treatment, n=4 technical replicates. The mitochondria density, measured with MitoTracker significantly increased to 119.4 ±7.28% SEM above the 100.0 ±3.43% SEM (p=0.0439) baseline vehicle treated amount. At 48 hours, the mitochondria density remained elevated at 115.9 ±3.63% SEM, however this was no longer significantly higher (p=0.0950) than the vehicle baseline. A similar picture was found using LysoTracker dye to assess lysosome density. At 24 hours UCMSC ADH-E conditioned media increased lysosome density to 122.5 ±3.55% SEM above the 100.0 ±1.47% SEM (p=0.0054) of the vehicle treated baseline levels. At 48 hours, lysosome staining had returned to the original levels at 105.4 ±5.665 SEM.

In vitro assessment of modulating enzyme activity

Throughout the body enzymes play numerous important roles in homeostasis whereas in disease, dysfunction or dysregulation of the same enzymes can drive pathology. To assess for potential biochemical modifying properties of UCMSC ADH-E conditioned media, the activity of three enzymes

found in *Bitis arietans* venom (BaV) were examined, each n=3 biological replicates. The first was metalloproteinases (MP), which play a crucial role in tissue remodelling. Here, the enzyme kinetics over 90 minutes for a range of BaV concentrations were tested with and without the presence of UCMSC ADH-E conditioned media (Figure 5.5A). The reaction curves show to be no native MP activity from UCMSC ADH-E in the absence of BaV, in fact (Figure 5.5AB), UCMSC ADH-E decreased the MP activity of BaV. At the 90-minute endpoint, UCMSC ADH-E had significantly reduced MP activity of 4

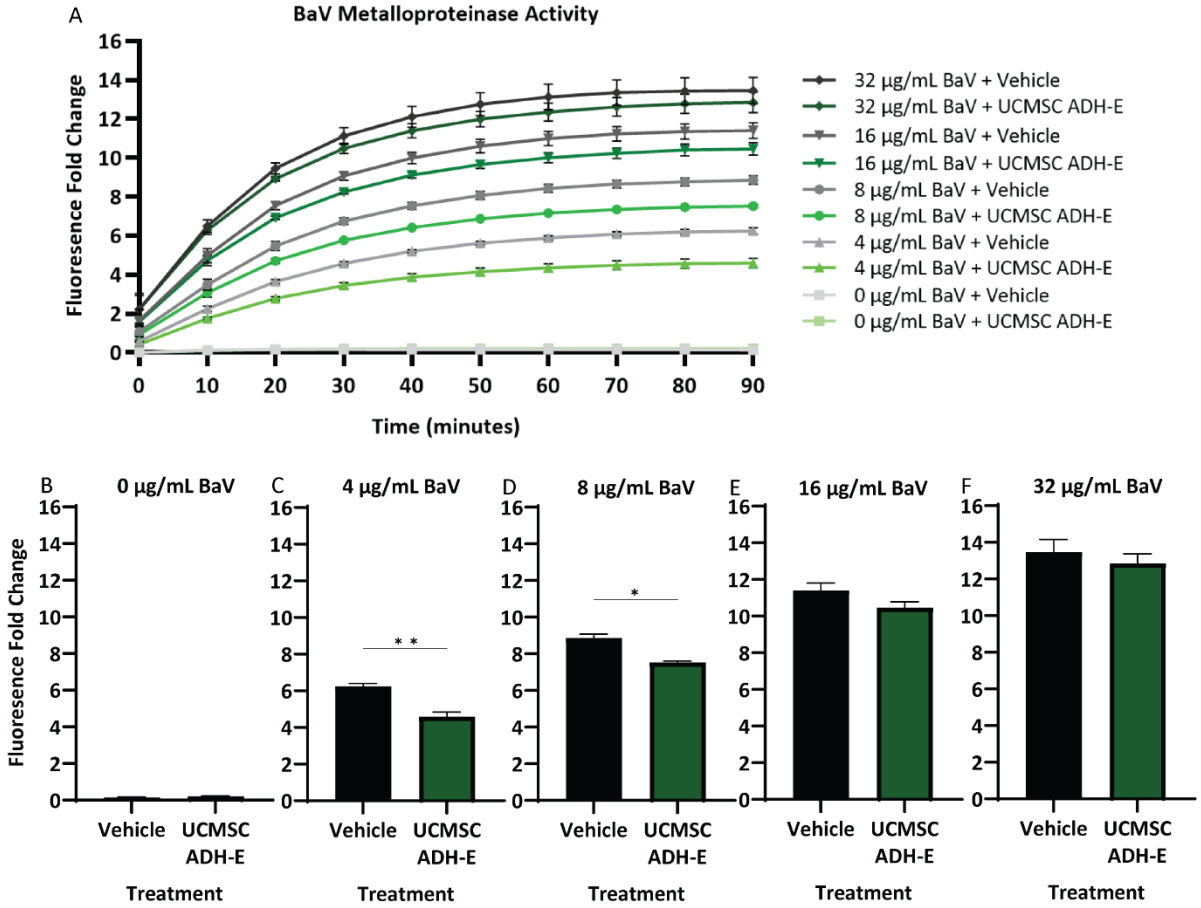

Figure 5.5 Assessment of UCMSC ADH-E conditioned media on metalloproteinase.

(A) *Enzyme kinetic plot of MP activity at different concentrations BaV in the presence of UCMSC ADH-E conditioned media, at intervals of 10 minutes for 1.5 hours. Each data point represents the average of three repeat assays (n=3).* ***(B)*** *Level of MP activity at 90-minute endpoint with 0 µg/mL and* ***(C)*** *4 µg/mL,* ***(D)*** *8 µg/mL,* ***(E)*** *16 µg/mL, and* ***(F)*** *32 µg/mL. Bars represent the average of three repeat assays (n=3) and statistical significance from two-way t-test are represented by asterixis: * p= <0.05; ** p= <0.01; *** p= <0.001; **** p= <0.0001.*

µg/mL BaV- compared to the vehicle (Figure 5.5B), from 6.3 ±0.17 fold down to 4.6 ±0.25 fold change (p=0.0082). Likewise, for 8 µg/mL BaV, UCMSC ADH-E reduced MP activity from 8.9 ±0.21 fold to 7.5 ±0.09 fold, with statistical significance of p=0.0127 (Figure 5.5C). At the higher BaV concentrations, UCMSC had a minor reduction in MP activity, from 11.4 ±0.4 to 10.5 ±0.32 for 16 µg/mL BaV (Figure 5.5E) and from 13.5 ±0.68 to 12.9 ±0.52 for 32 µg/mL, although these were not statistically significant, p=0.1436 and p=0.5164, respectively.

Next, serine protease (SP) activity was assessed. Overall, UCMSC ADH-E enhanced the BaV SP activity (Figure 5.6A). As with MP activity, UCMSC ADH-E had no detectable SP activity (Figure 5.6B). At the 90-minute endpoint with 4 µg/mL BaV there was no detectable SP activity with the venom alone, 0.0 ±0.01, however in the presences of UCMSC ADH-E there was a 0.23 ±0.10 fold increase in activity, although this was not statistically significant p=0.1164 (Figure 5.6B). At 8 µg/mL BaV a 0.15 ±0.02 fold change in SP activity with was significantly increase by UCMSC ADH-E to 0.35 ±0.01 fold, p=0.0034 (Figure 5.6D). Similarly at 16 µg/mL BaV (Figure 5.6E) UCMSC ADH-E conditioned media increased SP activity from 0.46 ±0.03 fold to 0.78 ±0.02 fold (p=0.0011) and at 32 µg/mL BaV (Figure 5.6F) it enhanced the activity even greater from 1.11 ±0.09 fold to 1.68 ±0.11 fold (p=0.0166).

The final biomolecule explored was Phospholipase A2 (PLA2). The overall PLA2 activity from BaV was minor (Figure 5.7A) and there was no PLA2 activity from UCMSC ADH-E (Figure 5.7B). Over the four concentrations of BaV used, UCMSC ADH-E conditioned media have no inhibitory nor stimulatory effect on PLA2 activity (Figure 5.7C-F).

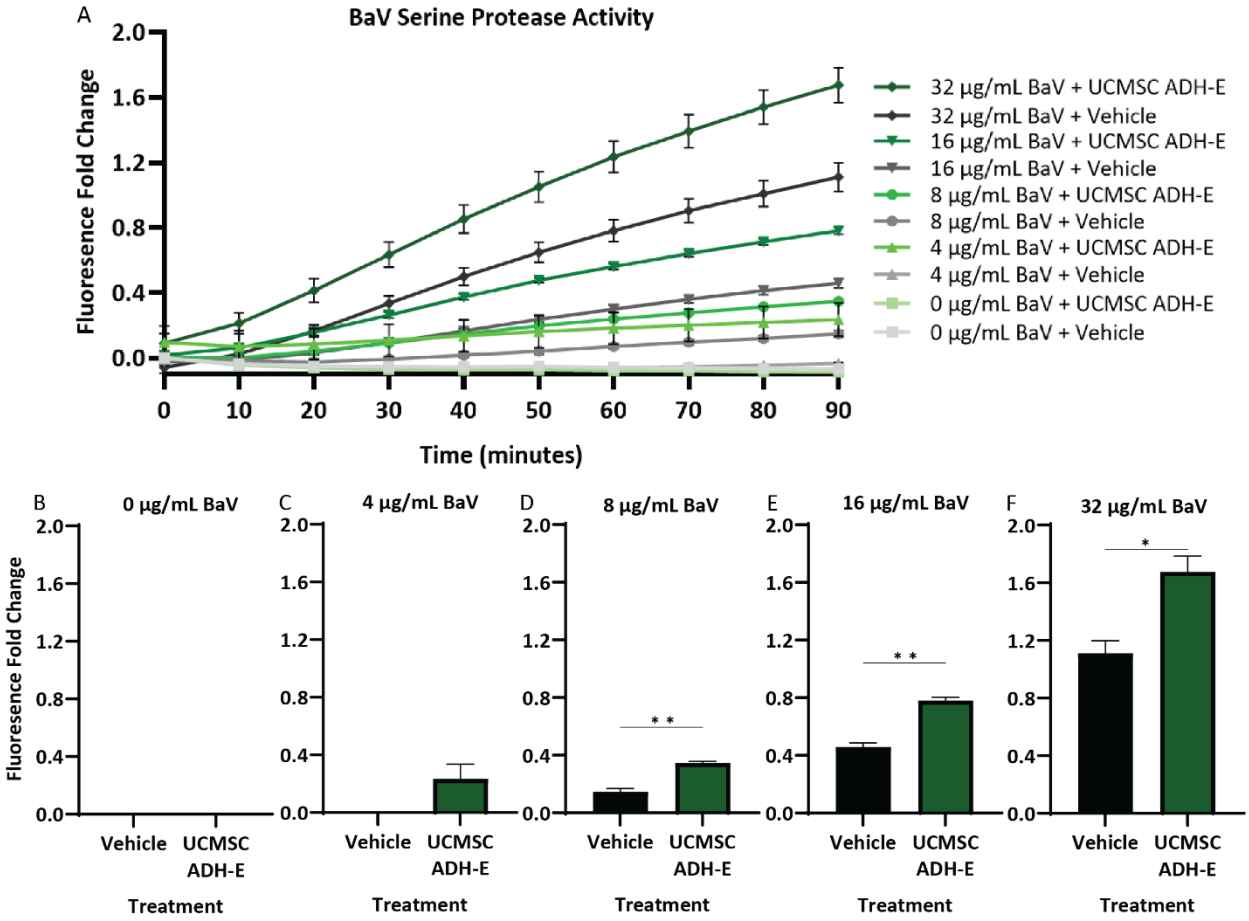

Figure 5.6 Assessment of UCMSC ADH-E conditioned media on serine protease.

(A) *Enzyme kinetic plot of SP activity at different concentrations BaV in the presence of UCMSC ADH-E conditioned media, at intervals of 10 minutes for 1.5 hours. Each data point represents the average of three repeat assays (n=3).* ***(B)*** *Level of SP activity at 90-minute endpoint with 0 µg/mL and* ***(C)*** *4 µg/mL,* ***(D)*** *8 µg/mL,* ***(E)*** *16 µg/mL, and* ***(F)*** *32 µg/mL. Bars represent the average of three repeat assays (n=3) and statistical significance from two-way t-test are represented by asterixis: * p= <0.05; ** p= <0.01; *** p= <0.001; **** p= <0.0001.*

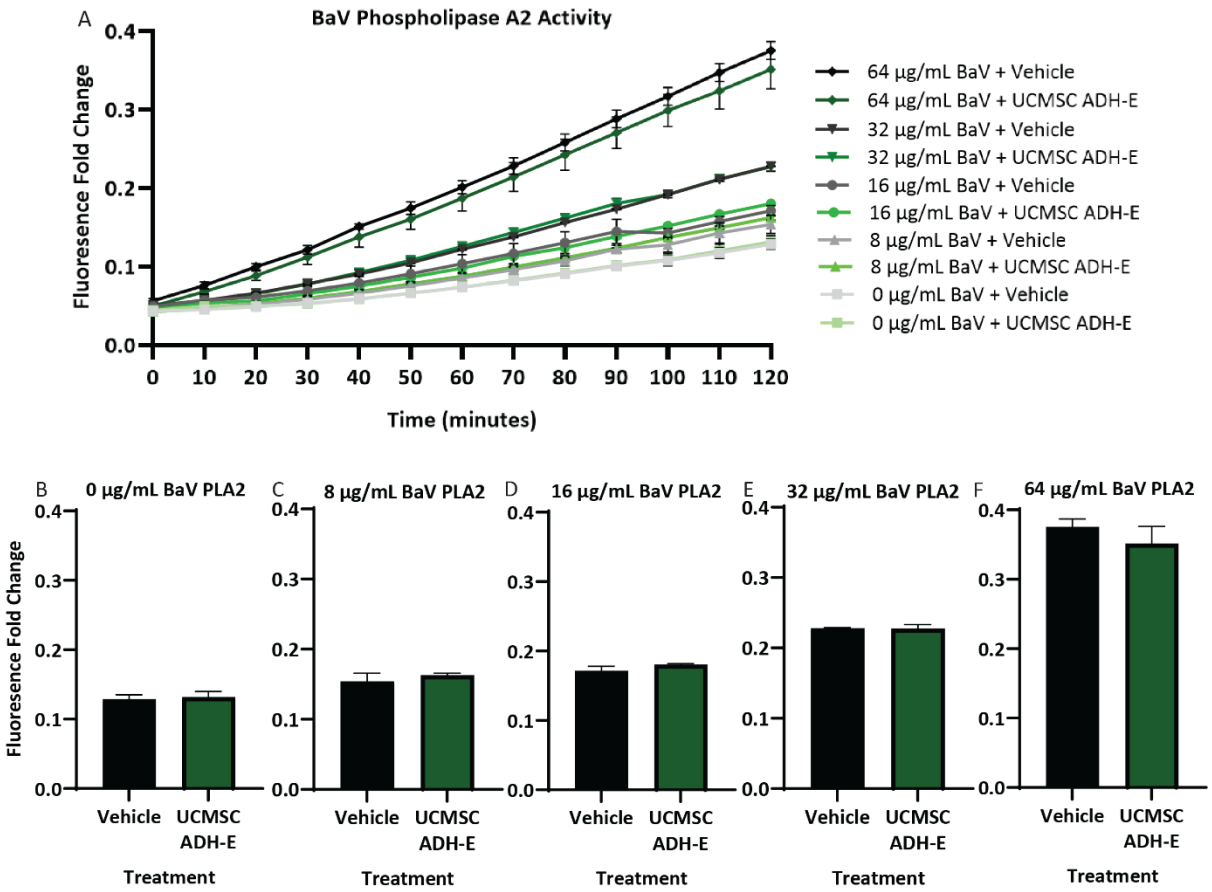

Figure 5.7 Assessment of UCMSC ADH-E conditioned media on phospholipase A2.

(A) *Enzyme kinetic plot of PLA2 activity at different concentrations of BaV in the presence of UCMSC ADH-E conditioned media, at interval of 10 minutes for 2 hours. Each data point represents the average of three repeat assays (n=3).* ***(B)*** *Level of PLA2 at 120-minute endpoint with 0 µg/mL and* ***(C)*** *8 µg/mL,* ***(D)*** *16 µg/mL,* ***(E)*** *32 µg/mL, and* ***(F)*** *64 µg/mL. Bars represent the average of three repeat assays (n=3) and statistical significance from two-way t-test are represented by asterixis: * p= <0.05; ** p= <0.01; *** p= <0.001; **** p= <0.0001.*

In vivo snake venom-induced muscle damage and regeneration model

To bring together a number of the therapeutic aspects of UCMSC ADH-E conditioned media, a venom-induced muscle damage model of skeletal muscle regeneration was employed to assess the efficacy in a complex system. Figure 5.8 aids as a reminder of the in vivo protocol, where an intramuscular injection of BaV into the tibialis anterior (TA) were followed by intraperitoneal injections of UCMSC ADH-E conditioned media.

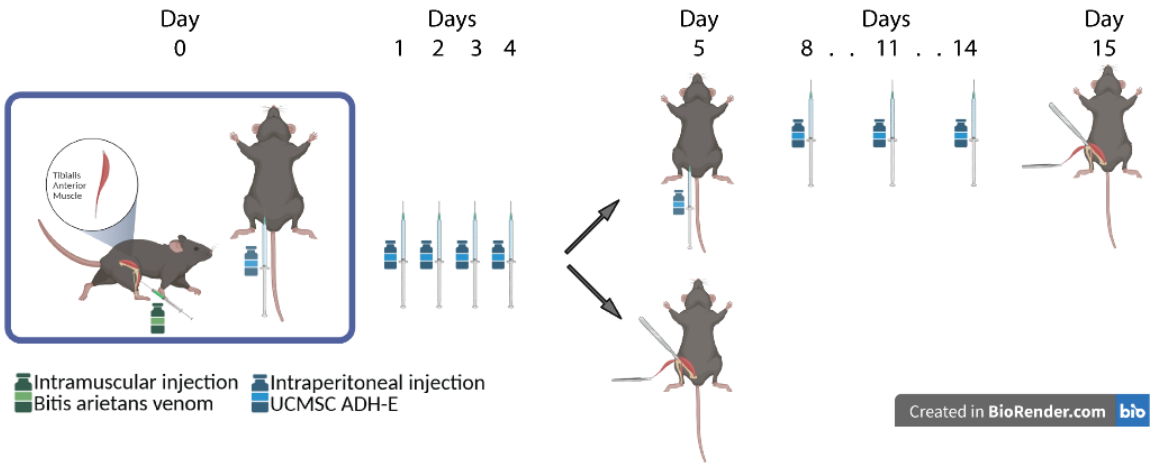

Figure 5.9 Timeline of in vivo BaV muscle damage model.

Schematic depiction of the procedures and timeline for BaV muscle damage model, from the intramuscular injection of venom marking day 0 and tissue harvesting to conclude the model on day 5 and day 15. Intraperitoneal injections of UCMSC ADH-E conditioned media administered daily from day 0 to day 4, and for the extended day 15 cohorts, additionally on day 5, 8, 11 and 14.

Upon dissection, TA muscles were weighed and normalised to the individual's body weight, n=8 biological replicates. There were no statistical differences in muscle weights at either day 5 (Figure 5.9A) or day 15 (Figure 5.9B) post BaV administration.

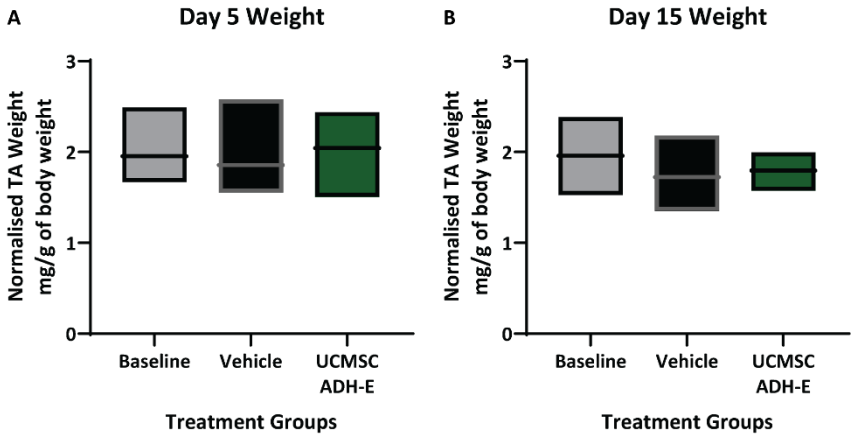

Figure 5.8 Muscle weights at harvest following BaV damage and UCMSC ADH-E treatment.

*Normalised TA weights to body weight from mouse BaV induced muscle damage and regeneration model at **(A)**, day 5 and **(B)** day 15 post injury. Box plots represent average mean, min and max weights of eight animals (n=8). Statistical significance from ANOVA with Tukey's post-test were non-significant.*

Initial histological assessment with haematoxylin and eosin (H&E) stain revealed the extent of the damage as well as the regeneration. Undamaged muscle has a uniform mosaic of myofibers with peripherally located myonuclei, bundled together with a thin extracellular matrix. Five days after damage with BaV, this architecture had almost completely been replaced by infiltrated leukocytes, such as macrophages and neutrophils, as indicated by the white arrows (Figure 5.10A). Some regenerated myofibres, small with centrally located nuclei, were present as indicated by the red arrows. By day fifteen the infiltrate leukocytes had mostly cleared, and more major myofibres were present with the classic centrally located nuclei feature of a regenerated fibre (red arrows). The size of these regenerated myofibres was measured to determine how advanced the regeneration was. Cross sectional area of the regenerated centrally located nucleated myofibres found no statistical difference between the vehicle treated (n=8 biological replicates), measuring 1147.0 ±84.45 μm^2 SEM, and UCMSC ADH-E treated animals measuring 1192.0 ±122.00 μm^2 SEM, n=8 biological replicates (Figure 5.10B). However, these fibres were significantly smaller than non-regenerated myofibres measuring 2451.0 ±212.6 μm^2 SEM. Additionally, the neat mosaic architecture had not been restored, with bands of non-myogenic cells marbling through the tissue (green arrows) indicative of fibrosis.

Next, the status of myofibre regeneration at the earlier timepoint of five days post injury was assessed. During the initial stages of regeneration, newly forming myofibres express myosin-3, aka embryonic myosin heavy chain, prior to switching to adult myosin heavy chain isoforms. Therefore, positive expression of myosin-3 can identify an actively regenerating myofibre, and the size can indicate how advanced the regeneration has progressed (Figure 5.11A). Analysis of these regenerating fibres revealed no difference in the size of myosin-3 positive fibres at day 5 post BaV injury, with untreated muscles having an average cross-section area of 304.8 ±38.76 μm^2 compared to UCMSC ADH-E treated at 341.3 ±53.94 μm^2, n=8 biological replicates (Figure 5.11B).

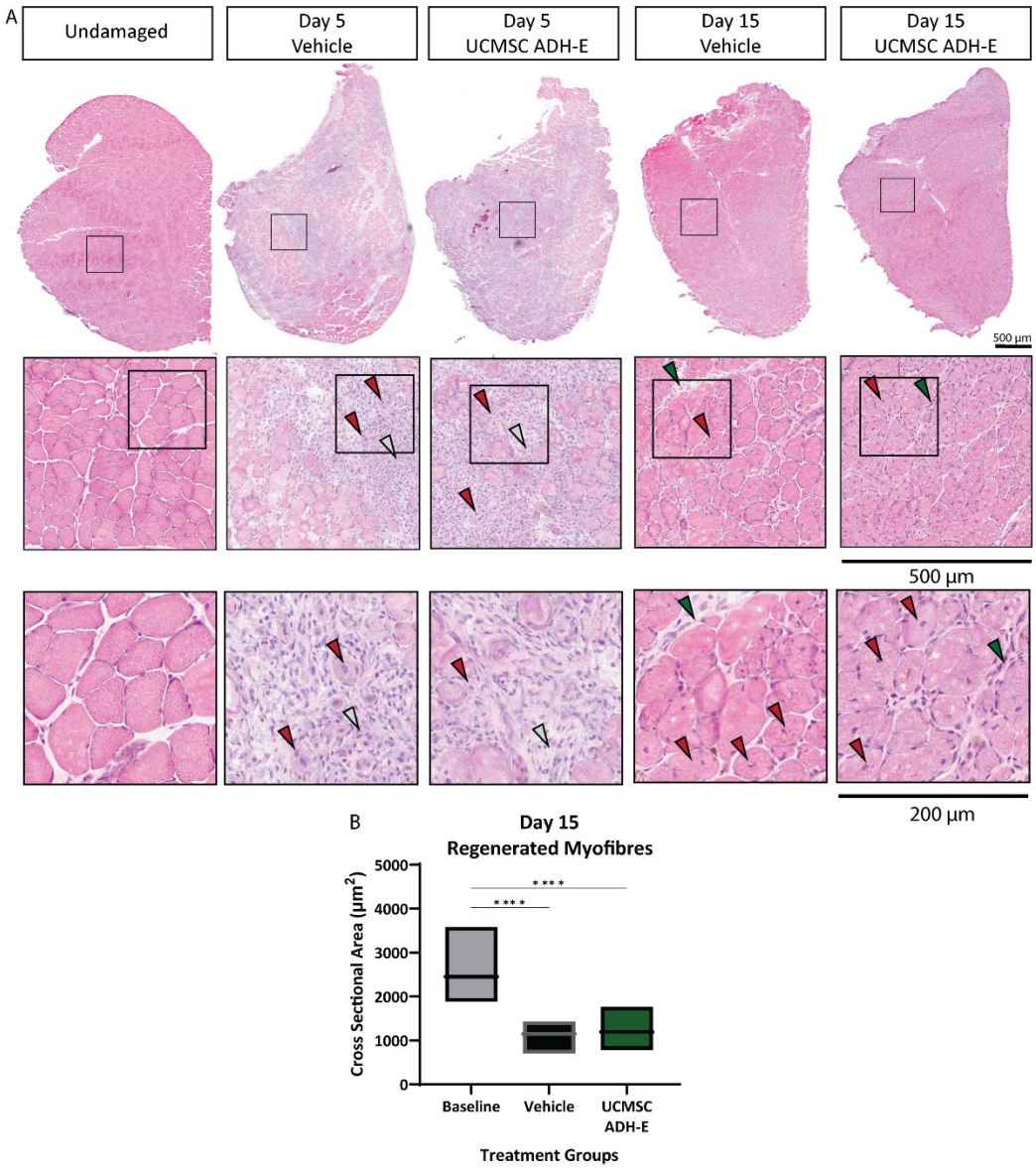

Figure 5.10 Haematoxylin and eosin stained BaV damaged TA sections following UCMSC ADH-E treatment.

(A) *Representative images of TA muscle sections stained with H&E, and 500 µm x 500 µm magnified region. Red arrows indicate myofibres with centrally located nuclei (regenerating myofibres). White arrows indicate immune cell inflation. Green arrows indicate non-myogenic cells.* ***(B)*** *Cross sectional area of regenerated myofibres (centrally nucleated). Box plots represent average mean, min and max from up to eight animals per cohort (n=5-8). Statistical significance from ANOVA with Tukey's post-test represent by asterixis: * p= <0.05; ** p= <0.01; *** p= <0.001; **** p= <0.0001.*

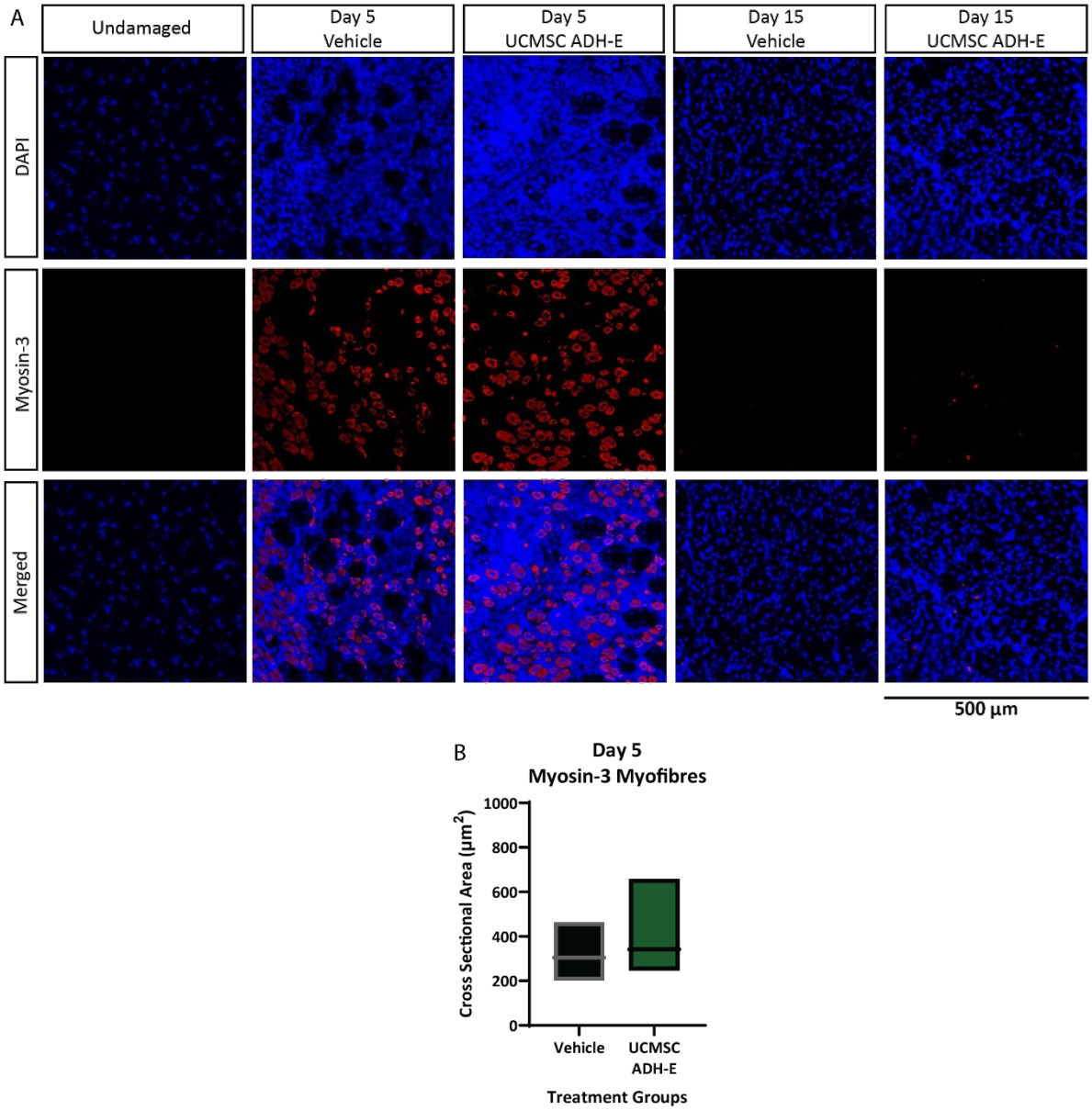

Figure 5.11 Myosin-3 positive regenerating myofibres in BaV damaged TA muscle following UCMSC ADH-E treatment.

(A) *Representative images of myosin-3 strained TA muscle sections, with nuclei in blue and regenerating myofibres in red. Images are a 500 µm x 500 µm area take from the damaged regions.* ***(B)*** *Cross sectional area of myosin-3 positive fibres. Box plots represent average mean, min and max from up to 7 animals (n= 6-7). T-test statistical analysis revealed non-significance.*

Dystrophin, a submembrane protein responsible for maintaining the structural integrity of myofibres, is expressed by mature fibres to act as a link between the cytoskeleton and the outer membrane. In healthy myofibres, it is ubiquitous around the membrane, however in compromised or poorly

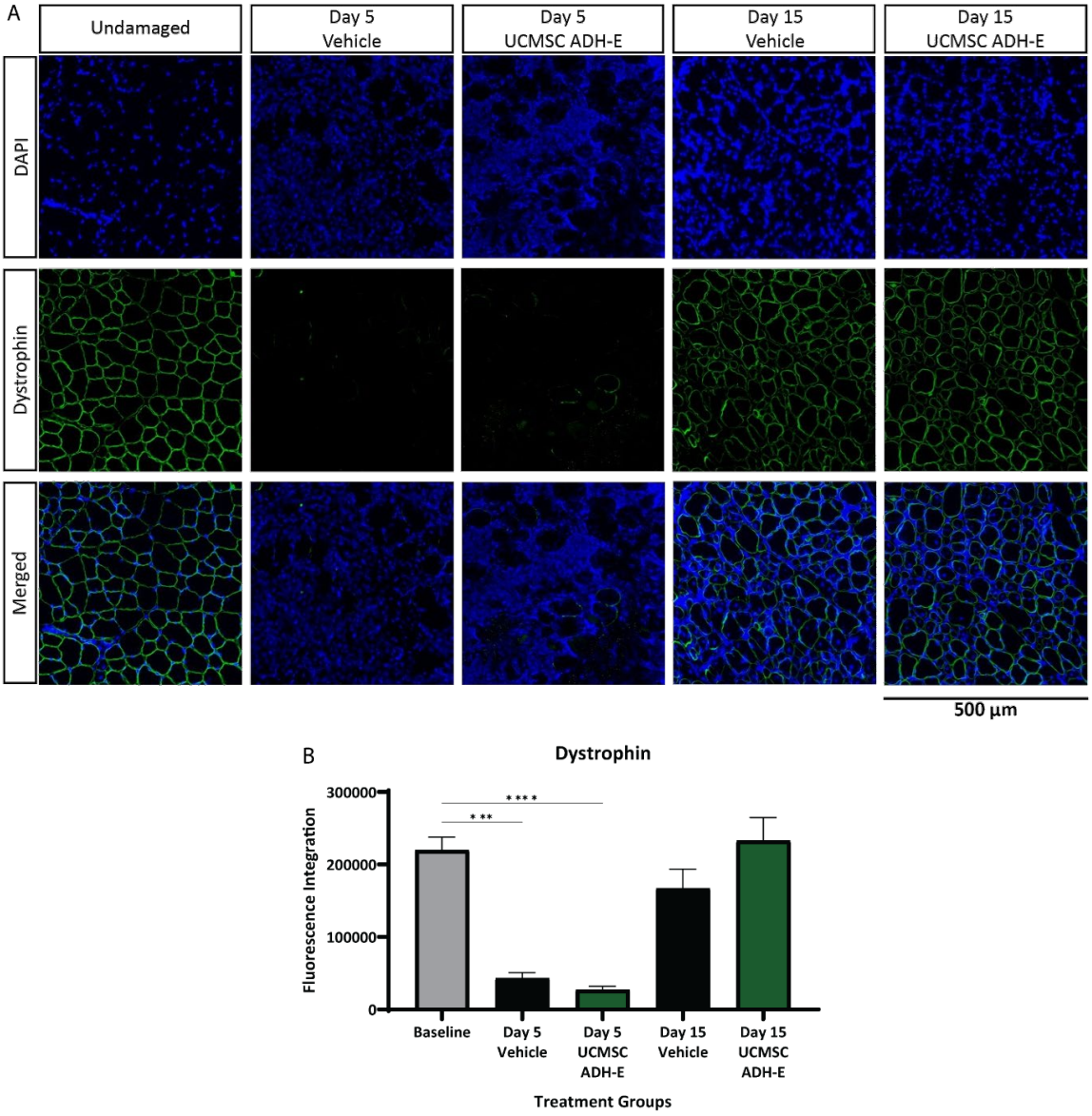

Figure 5.12 Dystrophin distribution in BaV damaged TA muscle following UCMSC ADH-E Treatment. ***(A)*** *Representative images of TA muscle sections stained for dystrophin (green) and nuclei (blue). Images are 500 µm x 500 µm areas from the damaged regions.* ***(B)*** *Fluorescence intensity by area integration of positive dystrophin throughout TA sections. Bars represent the average of up to eight animals (n= 5-8) and statistical significance from ANOVA with Šídák's post-testing is represent by asterixis: * p= <0.05; ** p= <0.01; *** p= <0.001; **** p= <0.0001.*

regenerated myofibres it is often expressed unevenly under the cell membrane (Figure 5.12A) and therefore can be used to assess the quality of the muscle fibres. On day five dystrophin expression was significantly reduced throughout the muscle. Undamaged muscle had on average an integrated fluorescence value of 219,810 ±17,909 SEM (n=5 biological replicates) which was reduced to 43,081 ±7,863 SEM in the day 5 vehicle treated mice (p=0.0002), and 27,088 ±4,680 SEM with UCMSC ADH-E treatment (p=<0.0001), n=8 biological replicates (Figure 5.12B). There was no statistical difference between the vehicle and UCMSC ADH-E treated mice at day five (p=0.9931). On day fifteen (n=8 biological replicates), dystrophin levels in vehicle treated muscles had increased to 166,924 ±26,760 SEM which was not statistically different to the undamaged levels. UCMSC ADH-E conditioned media treatment had a greater amount of dystrophin on day fifteen with an integrated fluorescence level of 232,976 ±31,860 SEM, although this was not statistically significant compared the vehicle treated mice.

The H&E stain suggested presence of non-myogenic cells remaining within the muscle at day fifteen, which is usually a sign of fibrosis. A large proportion of fibrosis is made up of collagen, which can be stained for with Picrosirius Red (Figure 5.13A). In undamaged muscle, collagen fibres made up 9.0 ±0.55% SEM of the muscle area, n=5 biological replicates (Figure 5.13B). At day five there was a large distribution of collagen through the damaged area of the muscle (white arrows) accounting for 58.7 ±3.23% SEM in vehicle treated mice and 59.3 ±5.21% SEM with UCMSC ADH-E treatment, n=8 biological replicates. At day fifteen, the collagen structure formed around the myofibres similar to the undamaged tissue, however the deposits were denser after regeneration, indicative of fibrosis (green arrows). Vehicle treated muscles had fibrotic lesions amounting to 51.1 ±1.66% SEM of the muscle area, which was significantly reduced by UCMSC ADH-E conditioned media to 33.6 ±1.56% SEM (p=0.0012, n=8 biological replicates).

Shortly after damage, fibro-adipogenic progenitors (FAPs) rapidly activate to modulate the regenerative process through communicating with both satellite cells and leukocytes, however,

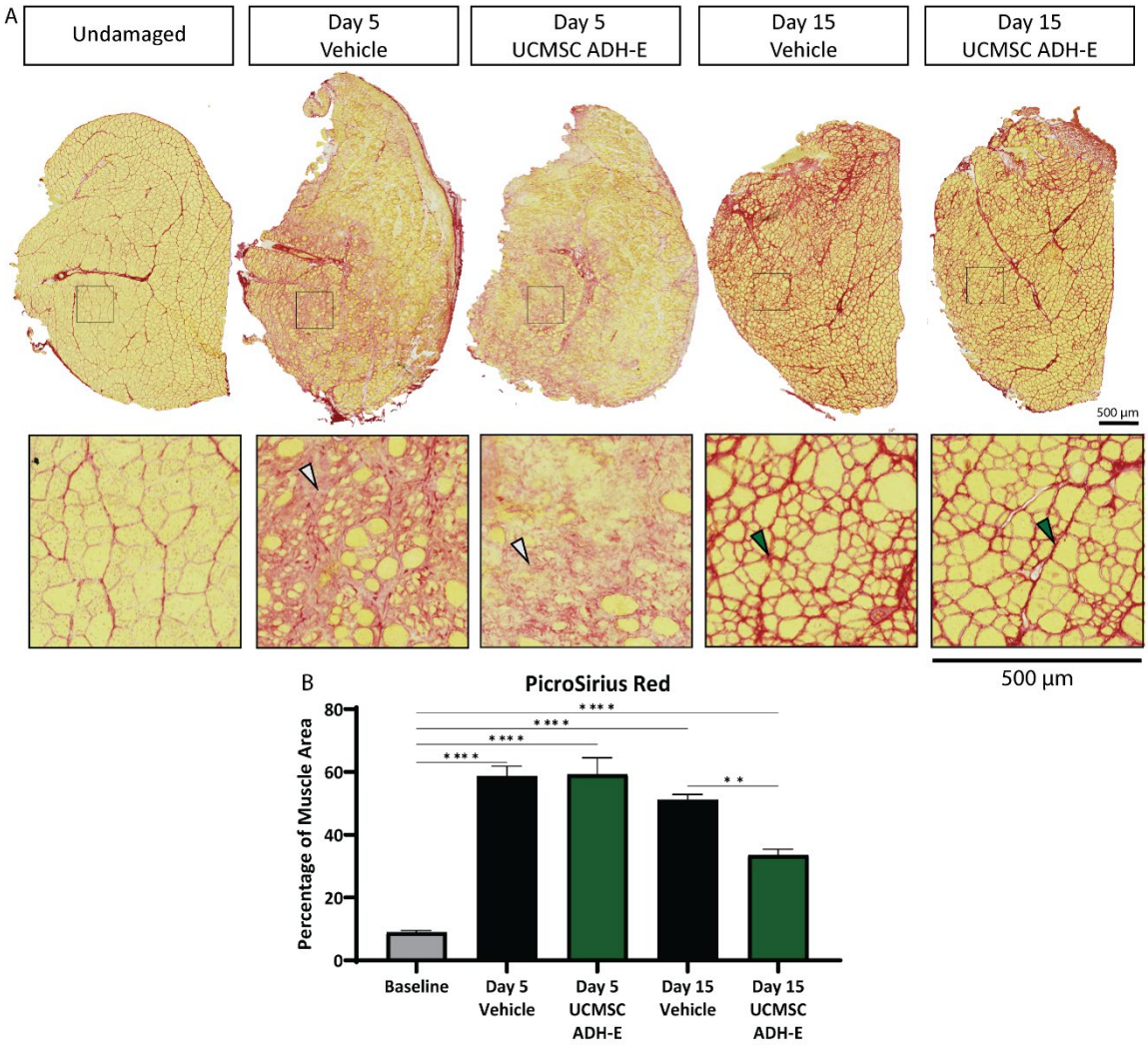

Figure 5.13 Picrosirius Red stained TA sections.

(A) *Representative images of TA muscle sections stained with Picrosirius Red of collagen, and 500 µm x 500 µm magnified region. White arrows indicate immune cell inflation. Green arrows indicate fibrotic lesions.* ***(B)*** *Area coverage of positive picrosirius red staining throughout TA sections. Bars represent the average of up to eight animals (n= 5-8) and statistical significance from ANOVA with Šídák's post-testing is represent by asterixis: * p= <0.05; ** p= <0.01; *** p= <0.001; **** p= <0.0001.*

dysregulation of FAP activity can lead to this kind of fibrotic repair. FAPs were identified by the expression of platelet-derived growth factor receptor-alpha (PDGFRα), where at day five post damage FAPs had increased in abundance within the muscle (Figure 5.14A). Baseline levels of FAPs in undamaged muscle were found to be around 2.1 ±0.31% SEM (n=5 biological replicates) which had increased 7.5 ±0.69% SEM in the vehicle day five muscles, n=8 biological replicates (Figure 5.14B).

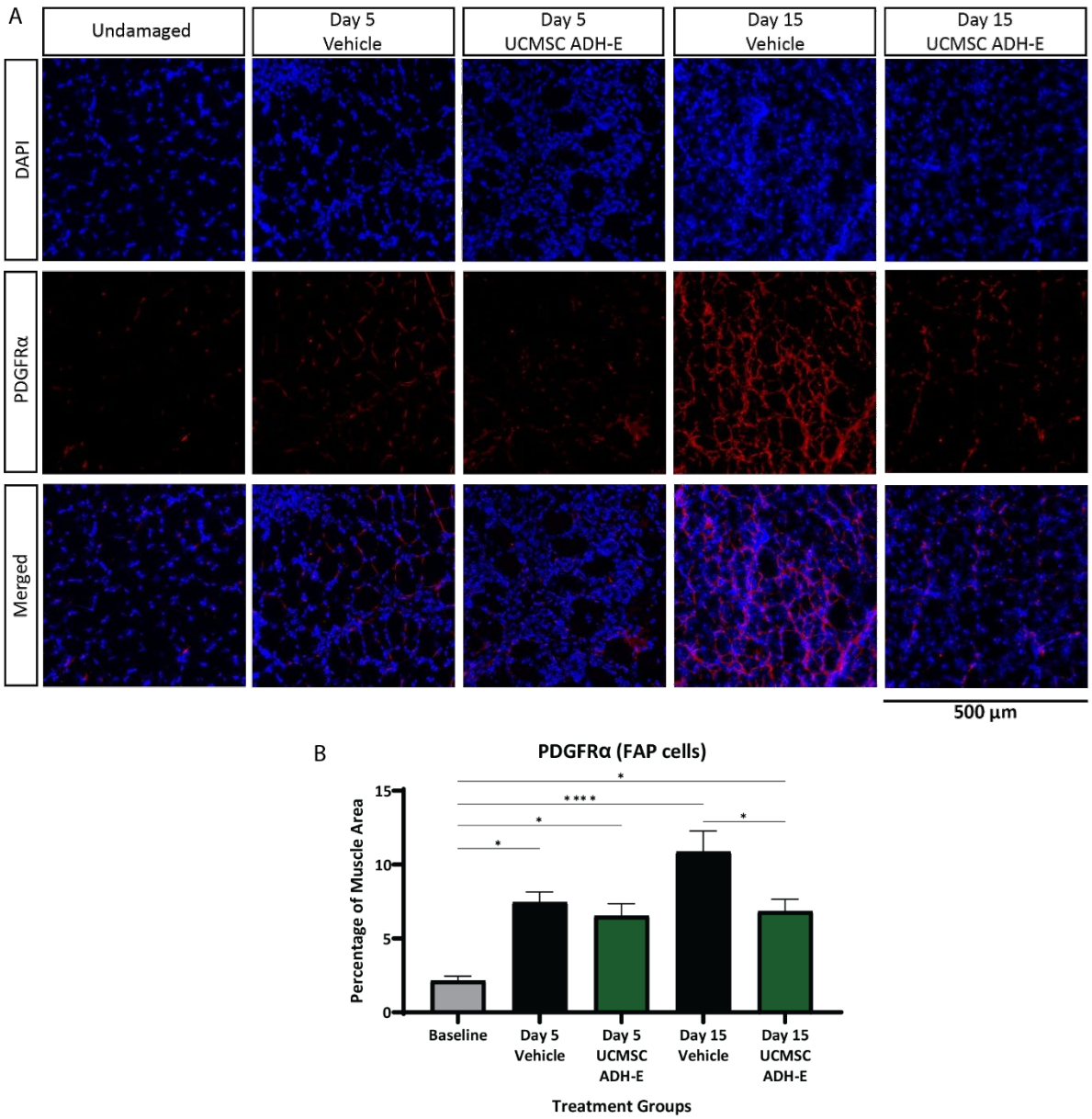

Figure 5.14 Fibro-adipogenic progenitor cell presence in BaV damaged TA muscle following UCMSC ADH-E treatment.

(A) *Representative images of TA muscle sections stained for platelet-derived growth factor alpha (PDGFRα) positive FAPs (red) and nuclei (blue). Images are 500 µm x 500 µm areas from the damaged regions.* ***(B)*** *Area coverage of FAPs throughout TA sections. Bars represent the average of up to eight animals (n= 5-8) and statistical significance from ANOVA with Šídák's post-testing is represent by asterixis: * p= <0.05; ** p= <0.01; *** p= <0.001; **** p= <0.0001.*

UCMSC ADH-E had no statistical difference at day five with FAPs abundances at 6.5 ±0.83% SEM, n=8 biological replicates. By day fifteen FAP abundance had risen to 10.9 ±1.40% SEM in the vehicle treated

mice, however, UCMSC ADH-E conditioned media treatment retained FAP abundance at a similar level to day five at 6.8 ±0.81% SEM, which was significantly lower the vehicle treated group (p=0.0396, n=8 biological replicates).

In vitro MP activity assays demonstrated inhibition of BaV MP activity with UCMSC ADH-E. Therefore next, the state of the extracellular matrix (ECM) was explored. Distribution of laminin, one of the major components of the ECM in skeletal muscle, uniformly surrounds the muscle fibres in healthy undamaged tissue (Figure 5.15A). At day five, the normal web of ECM was clearly disturbed following damage, with clear gaps of laminin in the region of damage with isolated single fibres. The fluorescence integration analysis revealed a reduction in laminin expression throughout the damaged muscle, from 858,886 ±543,390 in undamaged (n=5 biological replicates) to 333,332 ±69,835 at day five with the vehicle treatment and 173,979 ±65,245 with UCMSC ADH-E treatment, n=8 biological replicates (Figure 5.15B). However, statistical ANOVA test found these changes to be non-significant. At day fifteen, there was a greater abundance of laminin within the ECM, with a fluorescence integration of 2,387,320 ±346,681 (p=0.0144 vs undamaged muscle). UCMSC ADH-E treated muscle had less laminin at day fifteen with a fluorescence integration of 1,168,425 ±383,375, which was non-significant compared to the undamaged tissue (p=0.9872, n=8 biological replicates), however, it was also found to be just non-significantly different than the vehicle (p=0.0531).

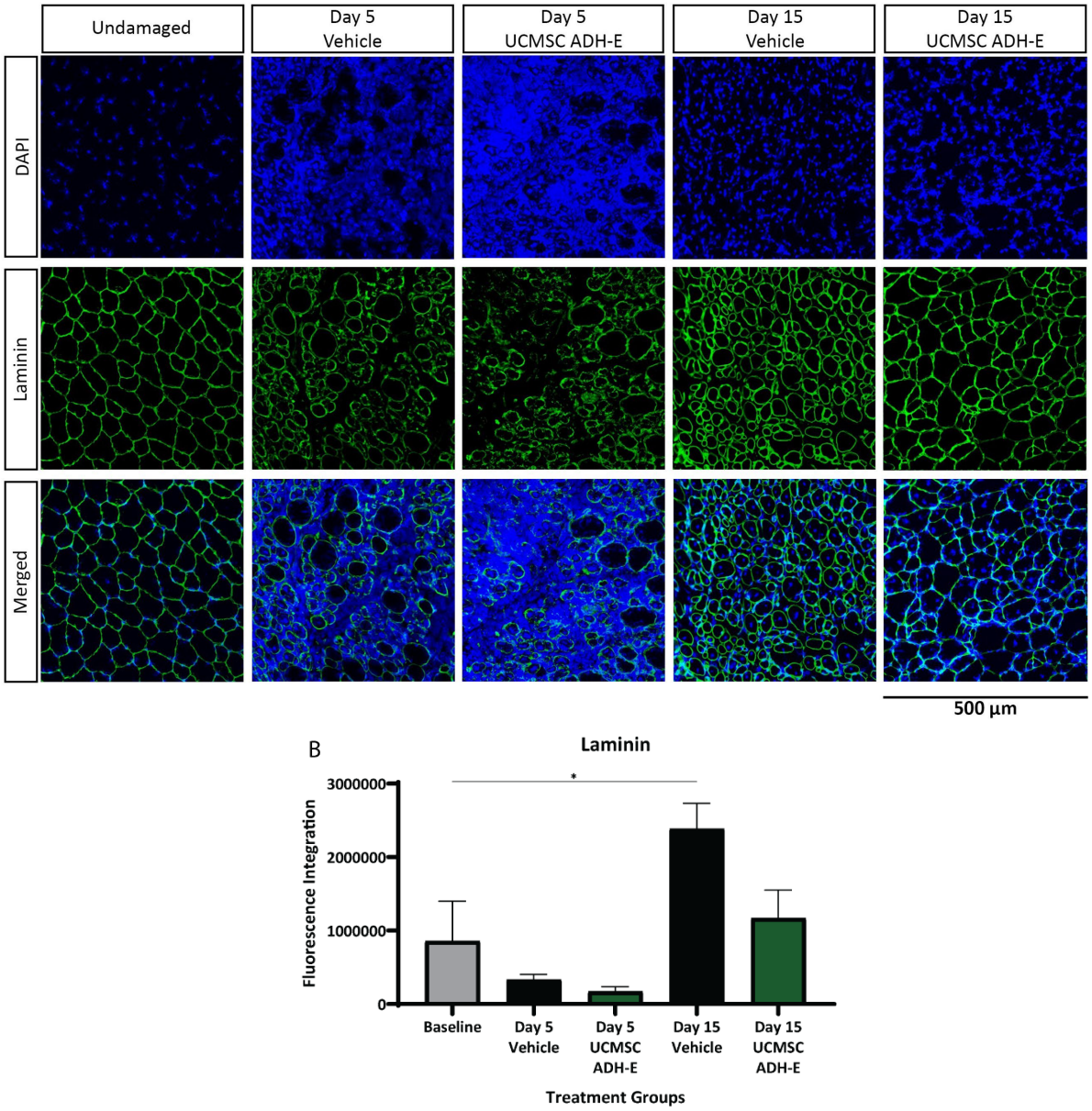

Figure 5.15 Extracellular matrix component laminin distribution in BaV damaged TA muscle following UCMSC ADH-E treatment.

(A) *Representative images of TA muscle sections stained for laminin (green) and nuclei (blue). Images are 500 µm x 500 µm areas from the damaged regions.* ***(B)*** *Fluorescence intensity by area integration of positive laminin throughout TA sections. Bars represent the average of up to eight animals (n= 5-8) and statistical significance from ANOVA with Šídák's post-testing is represent by asterixis: * p= <0.05; ** p= <0.01; *** p= <0.001; **** p= <0.0001.*

Finally, BaV is known to have haemorrhagic activity which is a commonly reported in the clinical setting (Godoi et al., 2023). To investigate if UCMSC ADH-E conditioned media had any impact on haemorrhage, the blood protein fibrinogen was immunostained to detect the presence of blood throughout the muscle (Figure 5.16A). The abundance of fibrinogen in undamaged muscles was measured at 0.6 ±0.04% SEM (n=5 biological replicates), which was significantly higher in day five vehicle muscles at 9.8 ±1.15% SEM (n=8 biological replicates), p=<0.0001 (Figure 5.16B). With UCMSC ADH-E conditioned media treatment there was significantly less fibrinogen detected, with the abundance at 6.1 ±1.66% SEM (p=0.0362, n=8 biological replicates). By day fifteen, there was no evidence of haemorrhage with the abundance of fibronectin returning the baseline levels, 0.6 ±0.11% SEM and 0.7 ±0.25% SEM for the vehicle and UCMSC ADH-E treated mice, respectively (n=8 biological replicates).

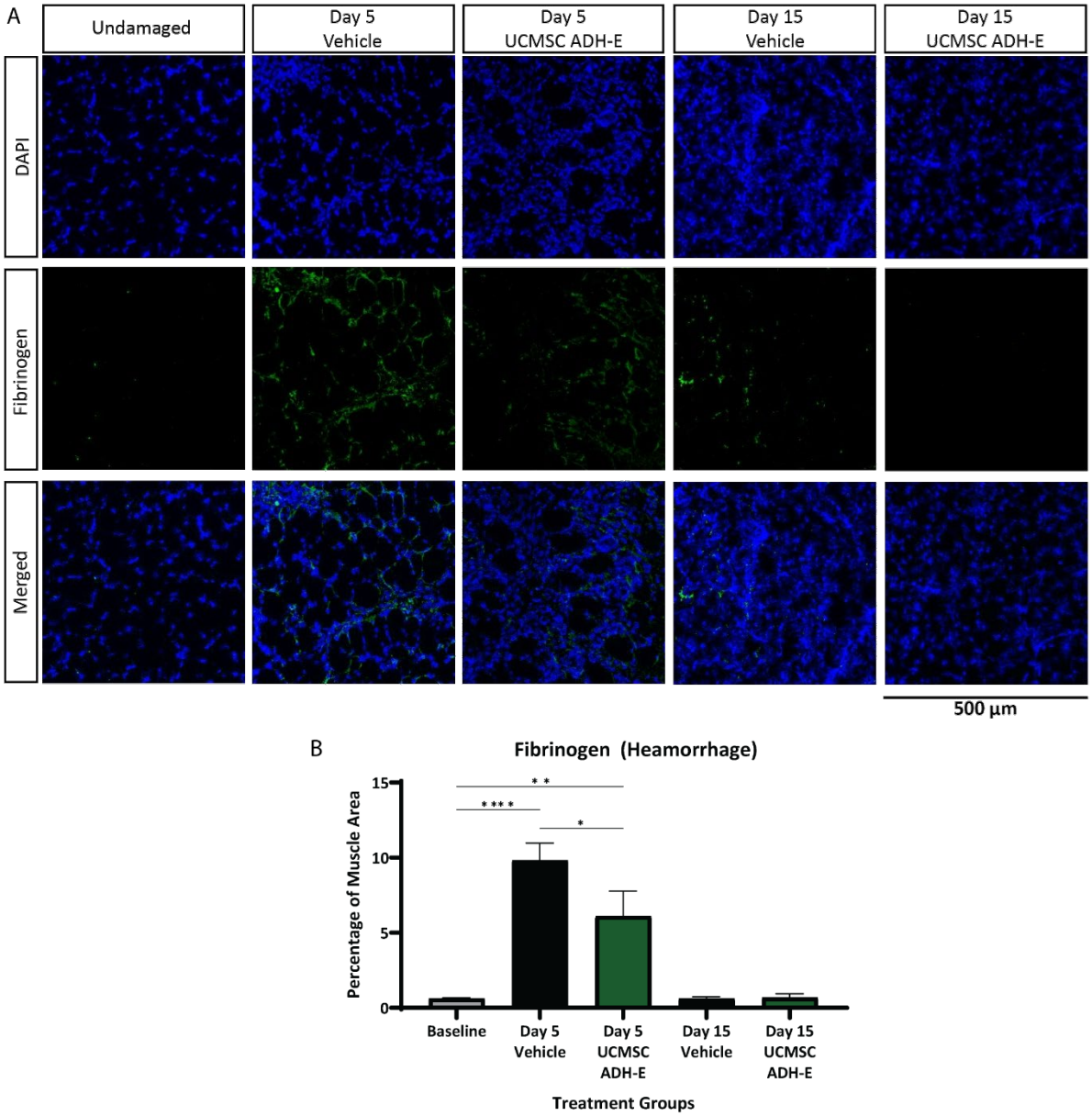

Figure 5.16 Fibrinogen distribution indicating haemorrhage in BaV damaged TA muscle following UCMSC ADH-E treatment.

(A) *Representative images of TA muscle sections stained for fibrinogen (green) and nuclei (blue). Images are 500 µm x 500 µm areas from the damaged regions.* ***(B)*** *Area of haemorrhage throughout TA sections. Bars represent the average of up to eight animals (n= 5-8) and statistical significance from ANOVA with Šídák's post-testing is represent by asterixis: * p= <0.05; ** p= <0.01; *** p= <0.001; **** p= <0.0001.*

In vitro myoblast fusion assay.

The absence of an effect on myofibre regeneration went against the predictions made from the original in vitro assessment. To investigate further the influence of UCMSC ADH-E on human myoblasts, the fusion index of myotubes was assayed (Figure 5.17A). The fusion index (FI: the number of nuclei per pan-myosin positive myofibre compared to total nuclei) was calculated to reveal at UCMSC ADH-E conditioned media reduced the fusion of myoblasts, FI: 0.084 ±0.002 SEM, from FI: 0.133 ±0.014 SEM for the vehicle control (Figure 5.17B). A Welch's t test revealed a statistical significance of p=0.0397, n=4 technical replicates.

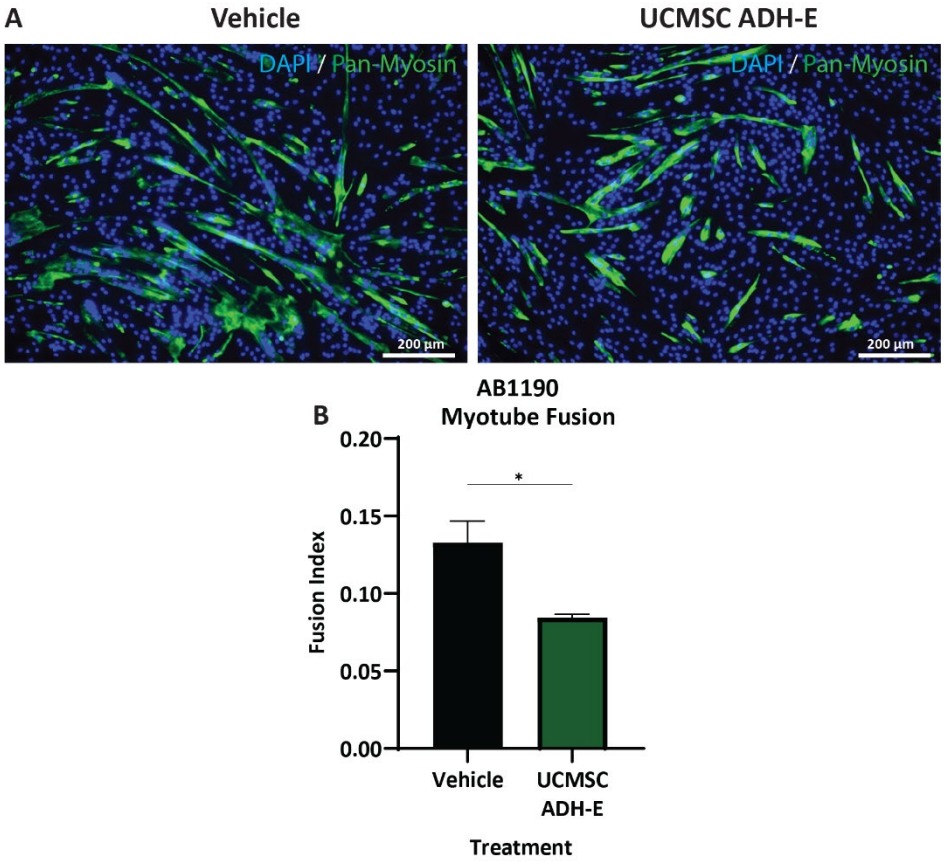

Figure 5.17 Assessment of myoblast fusion following UCMSC ADH-E treatment.

(A) *Representative images showing the effect of UCMSC ADH-E conditioned media on human myoblast fusion. Nuclei stained with DAPI in blue, myotubes stained with pan-myosin in green.* ***(B)*** *Fusion Index calculated from fussed cells (nuclei in pan-myosin positive cells) by total nuclei. Bars represent average of four repeats (n=4) with statistical significance from two-way t-test are represented by asterixis: * p= <0.05; ** p= <0.01; *** p= <0.001; **** p= <0.0001.*

Discussion

Stem cell conditioned medias have been demonstrated to have a multitude of biological activities and have been shown to be effective at treating research models of many diseases. In order to understand the potential of UCMSC ADH-E's therapeutic activity further, a number of biological assays were utilised to explore the different mechanisms of action.

UCMSC ADH-E effect on inflammation

This chapter began by exploring the impact of UCMSC ADH-E conditioned media on inflammation further. Using the developed PBMC assay, expressions of inflammatory-linked genes were assessed. The successful establishment of inflammation by LPS stimulation and reported UCMSC ADH-E conditioned media treatment was first confirmed prior to isolating RNA. Positively, the PBMC assay ran as expected, with LPS triggering an inflammatory responses and UCMSC ADH-E reduced the levels of TNFα.

Upon stimulation with LPS, interactions down the TLR4-NF-κB pathway initiates the expression of numerous genes, especially those regulated by NF-κB. NF-κB is the transcription factor for many genes, including IL-1, IL-8 and TNFα, which are documented to increase in expression following LPS insult (Lai et al., 2017). qPCR analysis revealed that treatment with UCMSC ADH-E conditioned media reduced expression of the above-mentioned cytokines. IL-6 can also be transcribed under the regulation of NF-κB; however, this gene was not reduced with UCMSC ADH-E. IL-6 is also expressed with the involvement of other transcription factors such as STAT3, which would provide rational as to why not all NF-κB regulated genes are downregulated. IL-10 is another cytokine which is not regulated by NF-κB, instead it is regulated by several transcription factors such as E4BP4, HIF-1α and STAT3 (Kubo and Motomura, 2012). IL-10 gene expression was increased with UCMSC ADH-E treatment. This cytokine is considered anti-inflammatory by inhibiting the expression of other inflammatory genes such as TNFα and IL-1β through interfering with pathways such as NF-κB activation (Driessler et al., 2004). Often the response to stimuli signalling through NF-κB, also stimulates the expression of NF-κB

initiating a positive feedback loop (Dorrington and Fraser, 2019). UCMSC ADH-E was found to decrease the expression of NF-κB as well, which would speak to its ability to dampen duration and/or intensity of the inflammatory response.

It is predicted that UCMSC ADH-E may reduce the inflammatory response by either reducing the response to LPS in the pre-gene expression cell signalling pathway or through the gene expression regulatory action of miRNAs. As conditioned medias are vastly multifactorial, it is highly likely that UCMSC ADH-E would act in both ways. Future investigations into the mechanism of action, would benefit from advanced approaches. Single nuclear sequencing would be invaluable to gather a holistic view of the biological activity of UCMSC ADH-E. Firstly, the effect of this conditioned media on the different subpopulations with the PBMCs could be explored. An advantage of single nuclear sequencing over single cell sequencing would be the capture of gene expression avoiding the activity of cytoplasmic miRNAs. Identification of how UCMSC ADH-E elicits the anti-inflammatory effect, with the addition of proteomics and full conditioned media characterisation, may also provide a value opportunity for further development of the conditioned media generation process, in an attempt to enhance this property further.

Lastly on the inflammation front, due to UCMSC ADH-E being derived from human cells, it was thought prudent to confirm cross-species activity prior to in vivo work. Although many biological molecules and activities are conserved in evolution, not only may the abundance of target molecules be different across species (Martens, 2015), but nucleic acid or amino acid sequences may vary to a point where they are no longer therapeutically compatible (Masubuchi et al., 2025). For example, rodents have been found to be less sensitive to LPS compared to humans (Gregory et al., 2024, Raduolovic et al., 2018). These evolutionary changes in species may create problems when modelling biological therapies, yet the use of rodent models are still considered a necessity in therapeutic development (Domínguez-Oliva et al., 2023). A short study using rat blood found that UCMSC ADH-E was able to reduce the inflammatory response to LPS. However, the reduction in TNFα released was not as

pronounced as the studies with human blood. This could be due to the differences between species or more generally the rat response to inflammation. This result provided a level of confidence that UCMSC ADH-E could elicit a therapeutic response in a rodent model, although dose comparison studies may be required before progressing into clinic.

UCMSC ADH-E effect on muscle progenitor cells

Muscle homeostasis and its regenerative capacity stems from the presence of resident progenitor stem cells known as satellite cells, which when required activate into myoblasts where they initially proliferate before undergoing myogenic differentiation. With it being demonstrated that UCMSC ADH-E had biological activity in promoting proliferation of HeLa cells, it was thought that a similar effect may happen with other cell types, and in the context of skeletal muscle regeneration, the myoblast would be a good starting point. UCMSC ADH-E was found to have a positive impact on myoblast proliferation, however single cell tracking analysis revealed there was no statistical change in baseline myoblast migration. Additionally, vital cell dyes provided tools to open up the examination of intracellular changes following UCMSC ADH-E conditioned media treatment. Firstly, nuclear size was examined. The size of a nucleus can provide a valuable indication of the status of a cell, for example nuclear size and shape changes are often associated with cell differentiation, development and disease (Jevtić et al., 2014). In this experiment UCMSC ADH-E was found not to influence nuclear size of human myoblasts.

However, UCMSC ADH-E was found to increase the abundance of mitochondria after 24-hours of treatment which remained elevated at 48 hours. Mitochondrial content of satellite cells, myoblasts, and myotubes vary, and have been shown to alter during myogenesis and skeletal muscle regeneration (Duguez et al., 2004). Mitochondrial reorganisation occurs early in myogenesis, with mitochondrial biogenesis-related genes having synchronous expression with myogenetic regulatory genes such as MyoD (Chernyavskij et al., 2024). Myogenesis is an energy demanding process which has been associated with an increase in mitochondrial mass and respiratory activity in order to

improve the oxidative phosphorylation necessary to meet the differentiation requirements (Duguez et al., 2002). Therefore, the increase in mitochondrial mass following UCMSC ADH-E suggest an improved cell state, which could facilitate not only the increased proliferation of myoblasts but also myogenic differentiation too. UCMSC ADH-E conditioned media also increased the mass of lysosomes in myoblasts. The increase in lysosomes could also suggest a priming of cells towards myogenesis. It has been demonstrated that an increase in lysosome formation occurs during myoblast differentiation, and lysosomal proteins, LAMP-1 and LAMP-2, have been demonstrated to play a role in this process (Sakane and Akasaki, 2018).

UCMSC ADH-E effect on enzyme activity

BaV, which was planned to be used to induce muscle damage in vivo, contains a vast array of bioactive molecules including the enzyme families of metalloproteinases, serine proteases, and phospholipase A2. Although snake venom forms of these enzymes are considered specialised for their deadly function, there are human versions of these which have important homeostatic roles. Additionally, in disease these enzymes are often implicated in the procession of pathologies. Here, BaV was used to explore the impact of UCMSC ADH-E on enzyme activity, from the point of view of interfering with the potential damage-inducing capacity of BaV and identifying other potential mechanisms of action against human diseases.

Beginning with the metalloproteinase activity (MP), UCMSC ADH-E conditioned media was found to reduce the MP activity of BaV. MPs make up 38.5% of BaV, as the most abundant molecules present (Juárez et al., 2006). Activity from all concentrations of BaV were reduced by UCMSC ADH-E, however, only 4 and 8 µg/mL were statistically different from the vehicle. These Zn^{2+}-MPs are responsible for causing damage to extracellular matrix through cleavage of collagens, laminin and other components (Olaoba et al., 2020) as well as directly damaging microvascular resulting in haemorrhage (Gutiérrez et al., 2016). In human homeostasis, MPs play an important role in regulation of the ECM, they are pivotal in wound healing (Caley et al., 2015) and haemostasis (Mastenbroek et al., 2015). In human

disease such as osteoarthritis, dysregulation of matrix-MPs (MMPS) drives a catabolic environment leading to the reduction of cartilage within the joints. The inhibitory action of UCMSC ADH-E on MPs would be a beneficial attribute as a therapy against a disease such as osteoarthritis. Proteomic analysis of the previous iteration of UCMSC ADH conditioned media (Chapter 3) found the presence of tissue inhibitor of metalloproteinases (TIMPs), which could explain this inhibitory action if they were found to be present in UCMSC ADH-E as well.

The second most abundant biomolecules in BaV are serine proteases (SPs) at 19.5% (Juárez et al., 2006). There are several types of SPs in biology, each with unique activity. Often in the case of snake venom SPs, serine proteases have a thrombin-like activity (Castro et al., 2004). UCMSC ADH-E conditioned media was found to increase the activity of BaV SPs, yet there was no underlying SP activity found in UCMSC ADH-E. This is interesting because, unlike thrombin, snake venom SPs do not require activation from protein cofactors, and there are no cells present in the assay to introduce additional enzymes. Therefore, the way in which UCMSC ADH-E could increase serine protease activity is intriguing. The presence of procoagulant phospholipids such as phosphatidylserine have been reported on the surface of EVs from numerous cells including MSCs (Silachev et al., 2019). These platforms, if present, could provide a site for the serine protease activity complex to form, and thus enhance the enzymatic activity. This interaction would be a fascinating avenue to explore in a future project.

Finally, phospholipase A2 (PLA2) activity was investigated. Although not very abundant, at 4.3% in BaV (Juárez et al., 2006), PLA2s are key toxins responsible to myotoxicity after envenomation. PLA2s disrupt the plasma membrane of myofibres leading to uncontrolled influx of ions and other molecules into a cell, resulting in the demise of the cell (Gutiérrez and Ownby, 2003, Xiao et al., 2017). In human physiology PLA2s predominantly play important role in lipid metabolism and inflammation (Khan and Hariprasad, 2020), however in disease PLA2s have been implicated in neuroinflammation (Li et al., 2025), cancer (Gu et al., 2025), respiratory diseases (Wang et al., 2025) and sepsis (Jin et al., 2024,

Tsao et al., 2024). Here, unlike with the other two enzymes explored, there was no direct action from UCMSC ADH-E on PLA2 activity. There is no strong evidence in literature that a direct effect on PLA2 activity should be expected from an MSC conditioned media, however, there are studies which report conditioned media can modulate the expression of PLA2s from the body's injury response (Souza-Moreira et al., 2019).

Effect of UCMSC ADH-E on regeneration in venom-induced muscle damage model

The BaV-induced muscle damage regeneration model provided a valuable tool for assessing a range of biological activities in a complex system. So far, UCMSC ADH-E conditioned media had demonstrated immunomodulatory properties, an ability to enhance cell proliferation and migration and enzyme modulation. All these are processes that underpin successful regeneration after tissue is damaged. The impact UCMSC ADH-E had on this severe snake venom-induced damage was overall positive. However, it was predicted based of the in vitro results that UCMSC ADH-E conditioned media could directly impact the speed of muscle fibre regeneration. When the size of new regenerated myofibres were measured there was no clear effect of UCMSC ADH-E treatment. At day 5 post injury in the more commonly utilised CTX model, MSC conditioned medias have been shown to increase the size of myosin-3 positive fibres (Mellows et al., 2017, Mitchell et al., 2003). Here, the absence of a similar effect may be attributed to the severity of injury. In CTX, the ECM remains relatively intact which facilitates a cleaner regeneration (Ahmad et al., 2023). In BaV, the enzyme content disrupts the ECM, therefore this lack of architecture would likely slow the regeneration of myofibres. Additionally, snake venom enzymes such as MP, SP and PLA2 have been reported to remain active for a few days post envenomation (Valenta et al., 2022) as well as instigating a greater leukocyte infiltration and inflammatory response than CTX damage (Rao et al., 2024). These factors contribute to a more hostile environment for regeneration, providing a greater challenge and regenerative timeline for a therapeutic to overcome. This aside, another possible explanation for the unexpected absence of a positive effect on myofiber regeneration was that UCMSC ADH-E had a negative impact on myofiber formation. To explore this potential effect, a human myoblast fusion assay was conducted in vitro.

This experiment revealed that UCMSC ADH-E reduced the fusion of myoblasts into myotubes over the five-day fusion period. The general findings within literature report MSC conditioned medias having a positive influence on myoblast differentiation (Bier et al., 2018), unless the conditioned media has been generated from senescent cells (Pundlik et al., 2024a, Pundlik et al., 2024b) which this project does not. A possible biological reason could come from interleukin-6 (IL-6). In Chapter 3, the proteomics identified IL-6 in the top 100 proteins of UCMSC ADH conditioned media, as well as finding it in a lower abundance in UCMSC PEL, therefore would plausible that IL-6 would be present in UCMSC ADH-E as well. IL-6 signalling has been associated with controlling hypertrophic muscle growth and myogenesis by regulating the proliferative capacity of muscle stem cells (Muñoz-Cánoves et al., 2013). Binding to the IL-6 receptor (IL-6R), at low concentrations IL-6 induces proliferation of myoblasts through activation of JAK1, increasing expression of markers such as proliferating cell nuclear antigen (PCNA). Whereas, at high concentrations IL-6 activates JAK2, which reduces PCNA expression, and instead increases differentiation through expression of MyoD and myogenin (Steyn et al., 2019). The concentration of IL-6 within UCMSC ADH-E used in the myoblast fusion assay, may have been at the levels which promote myoblast proliferation and inhibit differentiation, as supported by the increase in proliferation of AB1190 cells reported Figure 5.4A. To understand the impact that UCMSC ADH-E has on myoblast differentiation further, future work could look at this pathway in greater depth, beginning with exploring these markers of differentiation. Turning back to in vivo, the IL-6 present in UCMSC ADH-E is unlikely to be reason no augmentation of muscle fibre regeneration was observed, as IL-6 is released by cells in response to muscle damage (Tu and Li, 2023). Throughout this project, UCMSC conditioned media, including UCMSC ADH-E, has shown a remarkable ability to reduce inflammation, including TNFα and IL-6 released from leukocytes. Studies have shown the ablation of TNFα or IL-6 results in poor muscle regeneration (Yang and Hu, 2018).

In addition to the size of muscle fibres, the integrity of these cells is critical for avoiding damage during muscle contraction. At day five post injury, dystrophin was almost completely lost from the damaged region. At day fifteen regenerating fibres had matured and expressed dystrophin under the

membrane. UCMSC ADH-E treated mice, had a greater abundance of dystrophin, although statistically there was no difference from the vehicle administered mice. The results thus far suggest that despite the in vitro results demonstrating enhanced myoblast proliferation and intracellular changes, as well as the increased proliferation and migration of HeLa cells presented in Chapter 4, UCMSC ADH-E has no impact on the regeneration of new myofibres following BaV-induced muscle damage.

The initial histology of the TA muscle sections found the presence of non-myogenic cells still within the tissue at day fifteen. Picrosirius stain was used to identify whether this artifact was fibrosis. This stain identified a vast distribution of collagen throughout damage muscle at day five. Due to the extent of the damage and the number of infiltrated cells at this time point in the regeneration, the collagen stained by Picrosirius Red is likely to be the digested remnants of the ECM due to its disorganised nature around infiltrated leukocytes. At day fifteen, when immune cell presence had reduced, there were clear signs of fibrosis in the muscle. Following regeneration from BaV damage, skeletal muscle was unable to regenerate perfectly. The presence of fibrosis suggests dysregulation or imbalance in the regeneration process. UCMSC ADH-E conditioned media treatment was found to reduce the degree of fibrosis in the skeletal muscle. Preventing the formation of fibrosis is beneficial as it can lead to impaired muscle function, poor regeneration after injury and increased susceptibility to reinjury (Mahdy, 2019).

Fibrosis in skeletal muscle is the result of the dysregulation of fibro-adipogenic progenitor (FAPs) activity. Following damage, FAPs activate and rapidly proliferate with the function of facilitating myogenesis. Recruited leukocytes in response to damage signals promote the proliferation of FAPs, which produce a number of factors including IL-6 and follistatin which promotes the proliferation of satellite cells and myogenic differentiation (Nawaz et al., 2022). Infiltrated monocytes take on the M1 phenotype, in turn secreting TNFα. This cytokine promotes the apoptosis of FAPs whilst simultaneously preventing their differentiation. Once the phenotype of macrophages turns from proinflammatory M1 to regeneration M2, the levels of TNFα reduces and is succeeded by the release

of TGFβ. This factor now inhibits FAP apoptosis and along with IL-15 from maturing myofibres promotes the differentiation of FAPs into fibroblast. As expected, the levels of PDGFRα positive FAPs increase with BaV damage. At day five, during the proinflammatory stage, there was no difference with UCMSC ADH-E conditioned media treatment. This is promising to see, as an elevation or reduction in FAPs at this stage of regeneration would like result in impaired regeneration (Theret et al., 2021). By day fifteen the levels of FAPs had risen further without treatment, indicative of the mis-regulation from the macrophage population. With UCMSC ADH-E treatment the presence of FAPs remained a similar level to day five. This, along with the reduced fibrosis found with Picrosirius staining suggests that the conditioned media may be acting by preventing the differentiation of FAPs into fibroblasts and/or balancing the proliferation and apoptosis of FAPs.

The next parameter of muscle repair that was assessed looked at ECM glycoproteins known as laminins, which play a vital role in cell adhesions, as well as influencing differentiation and migration. At day five laminin was reduced in abundance and disorganised throughout the damaged regions. Again, there was no effect with UCMSC ADH-E treatment at day five. However, at day fifteen, laminin in untreated muscles had regenerated in greater abundance than undamaged muscle. UCMSC ADH-E conditioned media treated mice were found to have the same abundance of laminin in regenerated areas as the undamaged controls. In untreated muscle, the myofibres appeared more singular as opposed to latticed together like undamaged tissue. This is likely due to the presence of the non-myogenic cells present between the myofibres. This spacing of the myofibres requires lay down of additional basal lamina and ECM to facilitate the adhesion of the fibres.

The in vitro enzyme assays detected inhibitor actions from UCMSC ADH-E on the ECM degrading MP enzymes. The level of damage, and lack of difference in ECM disruption with UCMSC ADH-E conditioned media treatment suggests that the inhibitory action detected in vitro was not sufficient to inhibit the BaV activity in vivo. There are a couple of possible explanations. Firstly, the concentration of BaV injected intramuscularly was approximately 16 µg for an average 20g mouse, which was

approximately twenty-times greater than amount of BaV UCMSC ADH-E inhibited in vitro. Secondly, the indirect systemic administration of UCMSC ADH-E intraperitoneally would have diluted the active components further, and destruction of the blood vessel at the site of injury may have prevented adequate therapeutic access to the damage regions. A future consideration would be to explore possible administration at the site of envenomation, however, the injectable volume limitations in murine models would likely make this impossible to test without a larger animal model.

Finally, haemorrhagic injury was investigated. BaV injury caused a large amount of bleeding in the affected TA, which was still present and detectable at day five. UCMSC ADH-E conditioned media reduced the amount of bleeding by half. A potential mechanism of action could be linked to the serine protease activity result presented earlier. Snake venom serine proteases have thrombin like activity (Megale Â et al., 2018). Thrombin is a crucial enzyme involved in blood clotting. In vitro serine protease activity assays found that UCMSC ADH-E enhancing the activity. Therefore, it is not without reason to hypothesise that UCMSC ADH-E would enhance the natural thrombin clotting process. Alternatively, this conditioned media may have acted through repairing the damage to the vasculature reducing the leakiness by day five. By day fifteen, the haemorrhaging had resolved in both untreated and treated cohorts.

As discussed, the overall picture of UCMSC ADH-E treatment of BaV-induced muscle damage is positive. Although the conditioned media did not impact the myofibre regeneration directly in this model, the evidence of reduced fibrosis and FAP presence, similar myofibre integrity, and ECM architecture to undamaged skeletal muscle, as well as the reduction in haemorrhage, does support a therapeutic potential of UCMSC ADH-E in envenomation-induced muscle damage. Particularly, reflecting on real-world scenarios. Puff adders, such as *B. arietans*, inject 100-300 mg of venom in a single bite depending on the age and diet of the snake (Cloudsley-Thompson, 1988). For an average adult male (who are the highest risk category for snake bites in the native regions), for a body weight of 70kg this would amount to approximately 1.4 – 4.2 µg/g of venom per bite, which is not far above

the 0.8 μg/g modelled here. Adding the possibility of alternative administration regimens, such as injection to the site of envenomation, the benefits reported here may be possible to replicate in the clinic. Of course, further testing, such as in larger animal models, would be required as part of a pre-clinical package. Furthermore, a combinational therapeutic approach could be considered too. There are many small molecule therapies which target specific components of snake venom activity. One example would be Varesplasid which inhibits the activity of PLA2s (Lewin et al., 2022) or Batimastat and Marimastat which are being repurposed as anti-snake venom MP treatments (Layfield et al., 2020). Although these molecules could help prevent further damage to tissue, they have little to no benefit to the healing process. That's where a conditioned media therapy, such as UCMSC ADH-E would come in, and combined a more potent therapeutic effect may be possible. This would be an interesting avenue to explore in a future project.

Moving away from snake venom-induced muscle damage specifically, the results collected from this in vivo model provide invaluable insight into other potential mechanisms through which UCMSC ADH-E may work to combat disease. For example, the anti-fibrotic activity found here speaks to a number of diseases where fibrosis is a major component of the tissue's degeneration. Fibrosis can occur in any tissue, such as the lungs in the case of pulmonary fibrosis (Katzenstein and Myers, 1998), the liver with cirrhosis (Roehlen et al., 2020) and the skin in conditions such as scleroderma (Rosendahl et al., 2022) or scaring after wound closure (Peña and Martin, 2024). Factoring in the other potential mechanisms identified such as anti-haemorrhagic activity and anti-inflammatory activity, UCMSC ADH-E on paper has the potential to impact a number of diseases. This topic will be explored in more detail in the next chapter, the general discussion.

Chapter 6 - General Discussion

This project originally set out to investigate a novel method of generating a conditioned media from umbilical cord-derived mesenchymal stem cells, using a protocol of pelleting the cells. Mitchell and Mellows demonstrated that this method of producing conditioned media yielded a potent secretome from adipose-derived and amniotic fluid-derived MSCs (Mitchell et al., 2019, Mellows et al., 2017). This investigation into the utility of the method for umbilical cord-derived MSC (UCMSCs) found it to be biologically active, promoting proliferation, migration and reducing inflammation. Unlike the above-mentioned studies, this conditioned media preparation was compared to those produced by commonly used protocols. This revealed that although UCMSC PEL was bioactive, there was little evidence that this novel method of generating conditioned media resulted in any clear enhancement above traditional conditioned medias using adherent UCMSC cultures. Therefore, instead of continuing the investigation into the therapeutic capacity of UCMSC PEL, the focus of this project switch to the development of the adherent preparation (UCMSC ADH) which could be more easily manufactured at scale. Lastly, mechanisms of action were explored using blood and PBMC inflammatory assays and aspects of skeletal muscle regeneration as an investigatory platform both in vitro and in vivo.

Pelleting UCMSCs as method of generating conditioned media.

Reflecting on UCMSC PEL conditioned media as a standalone product, this project found the production method to be reproducible and biologically active. Multiple batches from three UCMSC lines were found to contain similar concentrations of protein, nucleic acid, and extracellular vesicles. Profiling by silver stained SDS-page showed reproducible protein profiles from each UCMSC PEL batch as well as between the three UCMSC lines. Reproducibility is an important attribute of any clinical product, and at the macroscopic level, this method was able to produce a similar conditioned media each time one was generated. The data collected here demonstrates that this method can be utilised to produce a stem cell conditioned media suitable for clinical manufacture, in a similar fashion to those reported by Mitchell and Mellows for adipose-derived and amniotic fluid-derived MSCs (Mitchell et al., 2019, Mellows et al., 2017).

Data from in vitro studies with UCMSC PEL conditioned media identified the same mechanisms of action being enacted on as other pellet conditioned medias. Increasing the proliferation of cells has been an associated activity of not only pelleted conditioned medias but is commonly demonstrated through secretome research (Napolitano et al., 2025). UCMSC PEL was no exception to this, with proliferation of HeLa cells as well as migration increasing with UCMSC PEL treatment. Additionally, UCMSC PEL conditioned media reduced the inflammatory response of human blood and primary PBMCs to LPS. All in all, UCMSC PEL exhibited many desirable aspects for a regenerative therapeutic.

The concept of the UCMSC PEL conditioned media method was derived from methods of enhancing secretomes in literature. Since the premise of the paracrine activity from stem cells was first conceptualised (Gnecchi et al., 2005), theorised methods of modifying the secretome have speckled the literature. Using a hypoxic environment was one of the earliest methods studied to augment conditioned media, promoting the release of trophic factors such as VEGF, FGF, HGF and IGF (Gnecchi et al., 2006). When investigating hypoxic preconditioning many maintain an adherent culture (Xu et al., 2022). An underlying mechanism of hypoxic preconditioning comes from activation of hypoxia-inducible factor-1 alpha (HIF-1α). HIF-1α is a transcription factor regulating responses to low oxygen levels, which has been reported to promote angiogenesis, oxidative to glycolytic metabolism switching, and anti-apoptosis properties (Pulido-Escribano et al., 2022, Razban et al., 2012). Any future work on pelleted conditioned media generation should look to include confirmation that the theorised conditioning was established. Specifically, assessing post-conditioned media cells for markers of hypoxia, such as hypoxia-inducible factor 1α (HIF-1α) would provide confidence that that hypothesised influence that pelleting has on these cells is correct (Mitchell, 2015). A study by Çiçek, demonstrated that hypoxic preconditioning of UCMSCs brought about an increase in HIF-1α levels in both cell lysate and conditioned media, which resulted in increased protein expression and larger nanoparticles (Çiçek et al., 2025). HIF-1α is considered a master regulator of the cellular response to hypoxia (Wang et al., 1995). Therefore, there is evidence to support that UCMSC conditioned media can be augmented by hypoxic preconditioning. When reviewing the mass spectrometry profile on

UCMSC PEL, HIF-1α was not identified in the conditioned media, suggesting that a state of hypoxia may not have been established, or at least to too fewer cells in the population were hypoxic. The notion of hypoxic preconditioning should still be considered as a potential alteration to the UCMSC conditioned media project and could form an interesting avenue to explore in the downstream development of a therapeutic product.

The nature of the cell pellet also incorporates a 3D-microenvironement. 3D-culture of MSCs as spheroids, has been shown to produce increased levels of molecules associated with cell survival, proliferation and vascularisation (Ferreira et al., 2018), such as angiogenin, FGF-2, angiopoietin 2, VEGF and HGF amongst others (Petrenko et al., 2017). Thus, it has been shown that spheroid culture can enhance these cells' immunomodulatory, angiogenic, anti-fibrotic and anti-apoptotic properties (Ferreira et al., 2018).

The above aside, the pelleting method did yield a biologically active conditioned media. In vitro experimentation demonstrated UCMSC PEL conditioned media promoted mechanisms that underpin tissue regeneration (an increase in cell proliferation and migration as well as reducing an inflammatory response to LPS). Work by Mitchell and Mellows demonstrated similar mechanisms of action from their secretomes collect from ADMSCs and AFMSCs respectively (Mitchell et al., 2019, Mellows et al., 2017). Furthermore, they both demonstrated that a pelleted conditioned media could reduce cellular senescence, a mechanism which was not explored in the project. Senescence is a cells emergency break in response to different stresses, including oncogenic activation, mitochondrial dysfunction and irreparable DNA damage (Herranz and Gil, 2018). In addition to its role in tumour prevention, senescence has been shown to be an important biological process for wound healing (Jun and Lau, 2010). However, poor removal of senescence cells is the primary driver of tissue ageing (van Deursen, 2014, Childs et al., 2015). Due to its important role in both health and disease, exploring the activity of UCMSC PEL and other UCMSC conditioned media preparations on senescence, could be a worthwhile avenue to explore for a future project.

Overall, a pelleted conditioned media from UCMSCs yielded results which were expected when this project began, from the robustness of its preparation to its biological action. However, what went against the predictions was how it compared to traditional adherent conditioned media. The original hypothesis was that pelleting MSCs to collect their secretions would yield a more potent conditioned media than adherently attached cells using a standard protocol. However, no enhancement was observed with the two conditioned media preparations demonstrating similar reproducibility in their generation, by way of quantifying protein, nucleic acid and EV concentration and also performing similarly in the bioassays. As discussed in Chapter 3 and 4, reflecting on biological output to the number of UCMSCs, the volume of conditioned media, and the more hands-on generation method, found UCMSC PEL to be a less viable commercial product than UCMSC ADH. For this reason, the attention of the project shifted to the further development of an adherent conditioned media protocol to be clinical translatable.

Development of adherent UCMSC conditioned media.

After uncovering the capped potential of a pelleted conditioned media from UCMSCs as a commercial therapeutic, this project pivoted to follow the development of the adherent conditioned media preparation. As mentioned, UCMSC conditioned media is commonly prepared by collecting the secretions of cells in standard culture media (Hyland et al., 2020) or basal/serum-free media (Yang et al., 2014, Choi et al., 2024a, Tang et al., 2023). Here, basal media was used to collect the secretions of adherent UCMSCs. The initial work, whilst being used as the comparator for UCMSC PEL, found this conditioned media to be reproducible, as several batches from three different UCMSC lines were quantified for secreted protein, nucleic acid and EVs. These conditioned medias were also biologically active, promoting cells to proliferate and migrate as well as reducing the inflammatory response to LPS. As with UCMSC PEL, these mechanisms of action had been previously reported by other research groups (Sriramulu et al., 2020, Vu et al., 2022, Li et al., 2017, Xu et al., 2022).

As this project progressed, several versions of UCMSC adherent conditioned medias were trialled. Initially identifying suitable solutions for conditioned media generation confirmed the importance of certain factors for maintaining a healthy cell population. Once viable conditioned medias were generated, using Earles Balanced Salt Solution (with calcium and magnesium salts) and Minimum Essential Media (MEM) as well as the originally used ATCC basal media, the biological activity was conserved. All three conditioned media preparations were equally capable at increasing proliferation and decreasing the inflammatory response to LPS. Overall, EBSS was selected over MEM, as the simplicity of the solution was an attractive quality for reducing the risk of downstream safety or regulatory complications. Unfortunately, there was a fundamental issue with the storage of these new conditioned media. EBSS, as well as EBSS based medias like MEM, are unable to be frozen due to the instability of salt solubility at sub-zero temperatures. This posed a potential concern over the storage lifespan of a product. As presented in Chapter 4, conditioned media generated in EBSS remained biologically active for at least 4 months when refrigerated. However, it was found that there were still some chemical instabilities with the buffer following long term storage. As discussed previously, resolving the shelf-life stability will be required to enhance its attractiveness for clinical manufacture and commercialisation.

As part of the Chemistry, Manufacturing and Controls (CMC) component of a medicinal products development, the regulators require GLP stability studies (ICH guidelines Q1A – Q1F Stability). During these studies, the shelf-life of a product is determined against the rigorously defined quality and potency criteria. Should a product be found to fail on any specification, it will be considered as expired. The longevity of a product's stability is an important consideration for its commercial appeal. Large batch sizes can often cut overall manufacturing costs, however, if the product cannot be stored long enough for clinical use, the benefit of large batches would be undone by wasted product. Therefore, smaller, more frequent manufacture may be required, would likely lead to a more expensive product to produce. This project concluded with the development of UCMSC ADH-E at a pivotal intersection, where the decisions on product stability and scale up begin to overlap. UCMSCs and other MSCs are

already being cultured in bioreactors (Kink et al., 2024, Mizukami et al., 2016) for the collection of EVs (Yan and Wu, 2020). Here, a proof-of-principle study demonstrated that microcarrier bound UCMSCs in a 3D culture system could be used in place of traditional planer culture to generate a similar conditioned media.

In order to round off this work into suitable buffers and culture conditions, ascertaining the complete characterisation of each secretome composition would have been valuable. Unfortunately, the scope, time frame and cost of this project did not allow for this. Therefore, should this project be taken forward, this could prove a valuable starting point. Especially, as the world of bioinformatics expands its analytical power with artificial intelligence (AI) programmes (Lin et al., 2025), there is a magnitude of data to explore. One aspiration has always been to use the data collected from the content characterisation of conditioned medias from different methods, along with next-generation analytics of the bioactivity to create a predictive model for ways to manipulate the production progress into generating a conditioned media with the desired biological effect. Continuing along this line, forming a greater understanding of the components of conditioned media could provide a platform for predicting the biological activity, potentially reducing the time and cost for a products development by avoiding dead end bioassay testing during pre-clinical data collection. Here, in Chapter 3, proteins and miRNAs were explored, like so many other research groups in the field of conditioned medias and their derivatives. An often-overlooked component present within the conditioned media are the lipids. An interesting avenue to explore for future work would identify and understand the involvement of lipids as part of the stem cell conditioned media action. The most abundant source of lipid are the EVs, which are bound by a phospholipid bilayer, which during EV biogenesis intracellular/cell membrane lipids are embedded within these membranes (Fyfe et al., 2023). Furthermore, the method of biogenesis influences the lipid content, for example exosomes have been shown to be enriched in glycolipids, phosphatidylserine and free fatty acids, whereas microvesicles from the same cell source were shown to be depleted (Haraszti et al., 2016). The lipid content should not be viewed as a static biochemical cargo, but rather a dynamic environment of signalling molecules.

Reactions within the vesicle, at the target cells microenvironment or upon uptake of EVs to the recipient cells, lipids can undergo alterations (e.g. oxidation, nitration, sulfation, and halogenation) which can alter the molecular structure and/or function (Melo et al., 2019). The resulting 'epilipids', which have been shown to play a significant role in regulating physiological and pathological conditions (Spickett, 2007, Fyfe et al., 2023). Which is why, taking an approach which incorporates all known molecules within conditioned media (multi-omics) would ultimately be a valid and impacting tactic to digitally explore the potential of these complex products for a future project.

The continued development of an allogenic UCMSC conditioned media therapeutic would follow a phased process encompassing cell sourcing and banking, controlled generation of conditioned media, and definition of quality, stability, and release frameworks of the final formulation under regulatory (FDA/MHRA/EMA) and ICH guidance. In practice, this might begin with establishing a well-characterised UCMSC master and working cell bank under GMP, with donor eligibility, viral safety and identity criteria consistent with expectations for ATMPs and biologicals, followed by selection of a manufacturing culture system (either 2D or saleable 3D bioreactors), as well as a simple, chemically-defined excipient that maintains cell characteristics while supporting secretion of the active secretome. The resulting conditioned media would be harvested aseptically, clarified (as described in this project), sterile-filtered, and filled, with process parameters (such as cell age, density, conditioning protocol, vehicle composition) locked as potential critical process parameters to ensure batch-to-batch reproducibility.

Downstream, the product would require a coherent panel of critical quality attributes and release tests, combining basic pharmacopeial criteria (such as appearance, pH/osmolality, sterility, endotoxin, mycoplasma) with quantitative measures of content (e.g. proteins, nucleic acid and EV concentrations, or specific surrogate biomarkers) and at least one robust functional potency assay that reflects a clinically relevant mechanism, such as modulation of inflammation. These assays would feed into a formal stability programme, designed under ICH Q1/Q5 principles, to define storage conditions, retest

intervals, and shelf-life. Ultimately, moving to patient use would require integrating this manufacturing and stability package into a full CMC dossier within an MHRA/FDA-authorised clinical programme, where indication, dose and regimen are justified by preclinical efficacy and mechanism data and supported by a scalable manufacturing strategy for an ATMP-class, cell-free UCMSC product.

Assessment of biological activity from UCMSC conditioned media.

Biological activity (potency) testing is required for all investigational medicinal products (IMP), including Advanced Therapy Medicinal Products (ATMP) and Cell and Gene Therapies (CGT) (Salmikangas et al., 2023, EMA, 2019). This requirement is legally mandated by many regulatory jurisdictions; for instance, Section 3.2.2.1 of Part I in Annex I of the EU Directive 2001/83/EC or Federal Regulation 21 CFR Part 600.3 in the USA. Regulatory expectations for ATMP potency testing vary according to the phase of product development. These potency assays are required to be validated for commercial production, with most guidelines recommending their implementation prior to pivotal clinical trials to enable correlation of potency results with clinical efficacy (Salmikangas et al., 2023). Due to the complexity of ATMPs and their often-multifaceted mechanisms of action, choosing suitable biological effect(s) to develop into a potency assay can be challenging. To this end, the European Medicines Agency (EMA) and U.S. Food and Drug Administration (FDA) recommend evaluating many potency assays for ATMPs during early development, as many functional assays may be difficult to validate. In particular, cell-based assays are intrinsically variable, which can prove problematic for release or comparability testing (EMA, 2019). This is why potency testing is one of the most challenging aspects of an ATMPs CMC development. Where there are concerns around potency when the time comes to submit the Market Authorisation Application (MAA), it can result in therapeutic rejection by regulatory authorities (Barkholt et al., 2019) and the accompanying detrimental effects this can cause to the biotechnology company could be substantial.

On the other hand, methods that are used for characterisation do not need to be fully validated, but undergo ‘phase-appropriate qualification’ to ensure reliable and repeatable results (EMA, 2019). As

mentioned, due to the multifaceted action of ATMPS, like the conditioned media in this project, one single marker or assay is unlikely to fully reflect the action of the product. This is why, many product developers opt for a panel of qualified characterisation assays to act as supplemental potency assays whilst their ATMPs are developing (Salmikangas et al., 2023). Only when the pivotal clinical studies (usually a Phase III clinical trial) are reached is the selection for a potency assay made. This approach allows both the collection of more data about an assays chance of validation (whilst the initial clinical batches are generated under GMP conditions), but selection of the ATMPs primary mechanism of action for potency testing using the initial clinical data in conjunction with the pre-clinical models.

Throughout this project, the initial assessment of biologically activity was conducted in the style of regulatory release potency assays, which were developed by Micregen Ltd., the industrial partner of this project, or as part of this project. The former, assays using HeLa cells for assessing the properties of conditioned media on cellular proliferation and migration, were designed to be robust, reliable and reproducible so that batch to batch variations can be identified. During their development, appropriate controls such as EGF, a biomolecule which stimulates proliferation (Riesco et al., 2017), were used to qualify the assay. HeLa cells were selected for use in this assay as they were amenable to stimulation by conditioned media. Furthermore, cancer lines such as HeLa, are well-characterised and immortal (Jones, 1997, Madoux et al., 2010, Lambertini et al., 2018), which allows for consistent use throughout the manufacturing lifespan of an ATMP. Furthermore, in comparison to primary cells, cancer lines are often less biologically variable (Mirabelli et al., 2019), which improves the reproducibility and reliability of an assay over time. Also, cancer cells lines are readily available, easy to culture (to de-risk operator variation) and can be expanded to large quantities if required. This makes them suitable for routine testing in quality control settings and high-throughput screening during ATMP development.

Cellular proliferation and migration assays were chosen as two of the proposed mechanisms of action that stem cell conditioned medias act through due to their importance as mechanisms of regeneration

(Iismaa et al., 2018). However, the use of HeLa cells, for all their benefit, do not specifically relate to a target tissue and thus are not necessarily a disease relevant model for the pre-clinical characterisation of a therapeutic product, such as the UCMSC conditioned medias explored here. Later in this project, these mechanisms were assessed in myoblasts, where the biological action of UCMSC conditioned media was conserved between test cells for proliferation alone. There is much evidence from the scientific community of MSC conditioned media having pro-proliferation and pro-migration effects. UCMSC conditioned media specifically has been demonstrated to act on cells such as dermal fibroblasts (Li et al., 2017), vascular endothelial cells, and MSCs (Shen et al., 2015).

The inflammation assays used in this project, consisting of human whole blood or PBMCs stimulated with LPS, were developed with pre-clinical adaptability and potency assay creation in mind. The use of LPS-induced inflammation in blood or PBMCs, quantified by ELISA, offers a robust and widely accepted approach to assessing immunomodulatory potency (Ngkelo et al., 2012, Talepoor et al., 2021). This assay was demonstrated to be highly responsive and reproducible. Throughout its use in this project, the LPS-induced inflammation assay has demonstrated its amenability to detecting changes in potency of conditioned media. In particular, its use in Chapter 4 demonstrated discrimination of different doses of UCMSC conditioned media evidencing its potential utility for identifying batch-to-batch quality.

LPS stimulates inflammation through TLR4 signalling, a receptor abundant on monocytes and macrophages (Austermann et al., 2022). In many cases, inflammation is not initiated in response to the presence of bacteria, which highlights a limitation of this assay in its current form. To broaden the scope of this assay, to capture a wider range of inflammatory responses for pre-clinical characterisation, alternative stimuli could be explored to relate to a chosen clinical target. For example, in response to damage, neutrophils as the first responders to damage-associated molecular patterns (DAMPs) amplify the inflammatory response through the release of pro-inflammatory cytokines, such as IL-1β, TNF-α and IL-6, which recruit additional immune cells (Castanheira and Kubes,

2019). Similarly, there are several autoimmune diseases where inflammation is orchestrated by lymphocytes. For example, in multiple sclerosis, Th1 and Th17 lymphocytes are reported to release cytokines such as IFNγ, IL-17, IL-1β and TNFα, leading to the recruitment and activation of microglia, macrophages and neutrophils (Lovett-Racke et al., 2011). Considering this, specific cytokines or mixes could be used in place of LPS to study the immunomodulatory capacity of conditioned media, in a more disease relevant variation of this assay. Additionally, molecules which selectively activate a specific cell type, paired with measuring the known response makers. An example of this would be using Resiquimod (R848), a potent TLR7/8 agonist, to active Th1 cells inducing the release of IL-12, IFNα and TNFα (Zhou et al., 2022).

Despite its versatility for pre-clinical biological assessment and demonstrated robustness and reliability, the qualities required for a phase-appropriate qualified assay still pose a challenge for this assay before GMP validation. When using primary cells, a key consideration includes accounting for donor variability. It would therefore be worthwhile exploring multiple donors, benchmarking potency against a reference anti-inflammatory agent or developing a panel of read outs to build a layer of redundancy should any donor response prove unpredictable.

Clinical targets for a UCMSC conditioned media product.

The earliest indication of stem cell paracrine activity was shown in the treatment of an ischemic heart condition (Gnecchi et al., 2005). Since then, stem cell conditioned medias have been tested in models of numerous disease indications (wound healing (Li et al., 2017), liver cirrhosis (Shi et al., 2024), neurodegenerative disease such as Alzheimer's (Kuo et al., 2021). Furthermore, there have been 2,207 (as of August 2025) clinical trials applications approved in the past 5 years, where a stem cell, their conditioned media, or derived product such as EVs have been tested (Internation Clinical Trial Registry Platform (ICTRP), World Health Organisation). The landscape where stem cell conditioned medias have been shown to be beneficial is broad, which raises the question to why there haven't been more therapies approved using this technology? The answer may lie more with the patient base than the

potency of stem cell conditioned medias. Emerging biotechnologies are often developed by start-up enterprises or university spinouts, who target niche, orphan-designated diseases to avoid competition with larger pharmaceutical companies, such as Novo Nordisk, GSK, Pfizer, or Astra Zenica to name a few. These rare diseases, although appealing for their gap in the market, carry the risk of low patient uptake. The reason is not just the scarcity of their occurrence, but the nature of these diseases being complex, with very ill patients who may not be willing to deviate from the standard care offered, which results in poor patient uptake to clinical trials. With this in mind, the selection of a clinical target for a new therapeutic product is not purely based on biological activity, but factors such as the market space, rarity of disease and the landscape for commercialisation which way heavily on the disease making process.

One condition for consideration is necrotising enterocolitis (NEC). NEC is a devastating disease affecting the immature intestine of newborns, especially preterm and low birth weight infants (LBWIs) (Hu et al., 2024). It has a prevalence beginning around 0.1% for LBWIs and increasing to 22% for neonates under 1 kg, extremely low birth weight infants (ELBWI). This rare disease carries a total mortality rate of 23.5%, which increases to approximately 51% for ELBWIs with NEC and the long-term prognosis for those infants who survive is poor (Hu et al., 2024). The most severe complications for surviving infants are neurodevelopmental disorders (24.8%) and intestinal failure (15.2%), leaving these children and their families to navigate lifelong health complications (Mutanen et al., 2018) and an expensive and complex aftercare for national healthcare systems. Current medical treatment tends to be limited to supportive measures, unless the patient deteriorates and requires surgical resection of the necrosing bowel (Zani and Pierro, 2015).

The immature neonate gut leaves it susceptible to NEC development. Unbalanced colonisation with bacteria, along with an undeveloped gastrointestinal immune system promotes a pro-inflammatory environment (Denning and Prince, 2018). Many groups have identified TLR4 signalling pathway as the mediator of this inflammatory imbalance. Approaches which target TLR4 signalling can reduce the

severity of NEC in animal models (Long et al., 2025, Gao et al., 2025). The data collected in this project demonstrated the anti-inflammatory properties of UCMSC conditioned media. More specifically, the investigation using PBMC cells, stimulated with LPS, found that UCMSC ADH-E conditioned media directly modulated the TLR4 signalling response. Furthermore, studies have shown that stem cell conditioned medias can attenuate in vivo models of NEC (O'Connell et al., 2021). In particular, amniotic fluid-derived MSC conditioned media has been frequently demonstrated to not only reduce inflammation but to also promote the proliferation of intestinal stem cells and angiogenesis (O'Connell et al., 2021, Zani et al., 2014). Poor perfusion of the intestine is also a key driver of the NEC pathology, which leads to ischemic damage and necrosis. Although this project has not explored angiogenic action directly, the enrichment analysis of the components in UCMSC PEL and UCMSC ADH in Chapter 3 suggested angiogenic potential. What this project did demonstrate was the augmentation of proliferation and migration of cells. Here it was shown that both HeLa cells and myoblasts were enhanced, and it would be reasonable to hypothesise that these conditioned medias would work to promote these processes in other cell types as well. Studies into other stem cell conditioned medias reported the ability to promote the expansion of residual cells to aid the regeneration of the intestine (O'Connell et al., 2021). Taking this mechanism of action, angiogenic potential and combine it with the potent anti-inflammatory effects reported in this project could form a valuable multi-action approach for the treatment of such a devasting disease.

Furthermore, haematological abnormalities have been reported in NEC (Hutter et al., 1976, Song et al., 2012). For most, defects remain mild, with no need for intervention, however for the more severe cases, patients can require blood product transfusion (Walsh and Kliegman, 1986). In particular, thrombocytopenia and coagulopathies have been reported in clinical cases of NEC (Hutter et al., 1976, Patel, 1977, Kenton et al., 2005, Sonntag et al., 1998). This is of interest as another potential mechanism of action for UCMSC ADH-E. From the data collected in Chapter 5, the conditioned media augmentation of snake venom serine protease activity and reduced haemorrhage in skeletal muscle following BaV damage demonstrates a potential benefit for haematological issues.

From a market and commercial perspective, NEC would be an appealing choice. As there is no current treatment for NEC, and its rarity suggests medicinal regulatory bodies including the FDA, MHRA and EMA may grant orphan designation status towards a clinical trial. This means that a promising therapeutic product can expedite through a clinical trial by combining phase I and phase IIa into a single 'combined' safety and efficacy trial. A search on the ICTRP using the search terms "Necrotising Enterocolitis OR Necrotizing Enterocolitis OR NEC" for the condition, and "Stem Cell OR Conditioned Media OR Secretome OR Extracellular Vesicles OR EVs OR exosomes OR MSC" for the intervention, revealed only one clinical trial: A pilot study using stem cell rich breast milk to treat early necrotizing enterocolitis (ID: ChiCTR2100042354), out of 191 NEC trials registered in the last 25 years for NEC. Further investigation into the other 190 trials found a more relevant clinical trial. Originally missed due to not directly registering as a stem cell derived intervention ST266 is a conditioned media style product from human amnion-derived cells, by Noveome® Biotherapeutics inc has started enrolling patients into a phase I/II combined clinical trial (ID: NCT06315738). In mice and pig animal models, ST266 was reported to restore gut architecture, improve gut barrier function, reduce TLR4-NF-κB-mediated inflammation and increase numbers of proliferating progenitor cells (Sodhi et al., 2022). Furthermore, a multidisciplinary initiative involving key stakeholders for the treatment of NEC (parents/caregivers, nurses, neonatologists, paediatric surgeons and scientists who specialise in stem cell biology, the intestine and immunology) have come together to establish the NEC-ACCELERATOR to harmonise and streamline the design and coordination of clinical trials in NEC, initially across Canada (Ganji et al., 2024). This goes to demonstrate how committed the field is in finding a treatment of NEC and how choosing NEC as the target disease of UCMSC ADH-E or similar conditioned media products would be of immense interest to both the scientific and medical communities. Additionally, what makes NEC commercially interesting are the similarities between NEC and adult inflammatory bowel disease (IBD), including Crohn's and enterocolitis. Research has shown that a number of genes identified to be modulated in NEC, have involvement in adult chronic inflammatory bowel disease. In particular, one study identified, 22% of differentially expressed genes (DEG) in NEC also appeared as

DEGs in Crohn's disease, including inflammatory cytokines and TLRs (Tremblay et al., 2016). With the prevalence estimated at approximately 1% of the global population living with IBD (Bruner et al., 2023), roughly 82 million people, the commercial reach of a licensed neonatal product for NEC used off label in adults with IBD would be vast.

Concluding remarks

This project has explored a number of aspects of developing a UCMSC conditioned towards a clinical product. The initial hypothesis that UCMSC PEL would be a more potent conditioned media than an adherent generated conditioned media (UCMSC ADH) was shown not to be the case. Although, the novel UCMSC PEL conditioned media was still found to be a potent and reproducible protocol for generating a clinically compliant conditioned media. However, the assessment of UCMSC PEL's ability to be scaled, and its commercial appeal, were found to be limited compared to an adherent approach. Therefore, this project developed a UCMSC conditioned media using an adherent culture, by focusing on the features important for regulatory approval and clinical manufacture beyond simply the biological potency. Herein, the second hypothesis, that a translatable adherent UCMSC conditioned could be generated (UCMSC ADH-E) was proven and accepted. Finally, the biological potency of the clinically adapted conditioned media was investigated. It was shown that this conditioned media could modulate cellular functions (proliferation and migration), biomolecule activity (MP and SP), and the inflammatory response. Furthermore, UCMSC ADH-E was shown to be biologically active in vivo. Here, utilising the BaV muscle injury model, it was shown that UCMSC ADH-E conditioned media improved ECM deposition, reduced fibrosis through modulating FAP presence, and reduced haemorrhage within the muscle. Additionally, animals were treated with a relatively high dose of conditioned media developed no adverse events (beyond the induced muscle damage), which demonstrated the safety of this conditioned media. This led to the acceptance of the final hypothesis, with the demonstration of potent biological activity.

UCMSC ADH-E is a promising conditioned media therapeutic candidate. It is easy to produce at scale, has minimal batch-to-batch variation, and uses GMP-available materials and processes. UCMSC ADH-E acts through augmenting cell proliferation and migration, regulating ECM modelling and has strong immunomodulatory properties. There are three development topics to address before UCMSC ADH-E would be ready for clinical applications: (1) stability of the EBSS buffer; (2) 3D generation in a bioreactor system; (3) collection of pre-clinical efficacy data for a selected target indication.

Chapter 7 - Appendices

Appendix 1: Composition of Conditioned Media Vehicles.

The components and their concentrations of the buffers and solutions used as vehicles for UCMSC ADH conditioned media generation in Chapter 4.

	Dulbecco's Phosphate Buffered Saline (DPBS)	**DPBS with calcium and magnesium**	**DPBS with calcium, magnesium, glucose and pyruvate**	**Hank's Balances Salt Solution (HBSS)**	**Earle's Balanced Salt Solution (EBSS)**	**EBSS with calcium, and magnesium**	**Minium Essential Medium (MEM)**
	mg/L	**mg/L**	**mg/L**	**mg/L**	**mg/L**	**mg/L**	**mg/L**
Inorganic Salts							
Calcium Chloride		100.0	100.0			100.0	200.0
Magnesium Chloride		100.0	100.0			100.0	
Magnesium Sulphate							97.67
Potassium Chloride	200.0	200.0	200.0	400.00	400.0	400.0	400.0
Potassium Phosphate Monobasic	200.0	200.0	200.0	60.0			
Sodium Bicarbonate				350.0	2200.0	2200.0	2200.0
Sodium Chloride	8000.0	8000.0	8000.0	8000.0	6800.0	6800.0	6800.0
Sodium Phosphate Monobasic					140.0	140.0	140.0
Sodium Phosphate Dibasic	2160.0	2160.0	2160.0	48.0			
Organic Compounds							
D-Glucose			1000.0	1000.0	1000.0	1000.0	1000.0
Sodium Pyruvate			36.0				
Amino Acids							
L-Arginine Hydrochloride							126.0
L-Cystine 2HCl							31.0
L-Histidine Hydrochloride-H_2O							42.0
L-Isoleucine							52.0
L-Leucine							52.0
L-Lysine Hydrochloride							73.0
L-Methionine							15.0
L-Phenylalanine							32.0
L-Threonine							48.0
L-Tryptophan							10.0
L-Tyrosine Disodium Salt Dihydrate							52.0
L-Valine							46.0
Vitamins							

Choline Chloride							1.0
D-Calcium Pantothenate							1.0
Folic Acid							1.0
Niacinamide							1.0
Pyridoxal Hydrochloride							1.0
Riboflavin							0.1
Thiamine hydrochloride							1.0
i-Inositol							2.0

Appendix 2: Solutions, Buffers, and Culture Media Recipes.

1x PBS buffer

Add one PBS tablet (Oxoid, BR0014G) per 100 mL distilled water and autoclave (20 minutes at 121°C).

4% PFA/PBS fixative solution

Add 20g of paraformaldehyde powder to 480 mL 1x PBS buffer and heat to 65°C overnight in a water bath to dissolve. Once cooled, adjust the final volume to 500 mL with 1x PBS buffer.

UCMSC culture media (ATCC)

To a fresh 500 mL bottle of mesenchymal stem cell basal media (ATCC PCS-500-030™) add the mesenchymal stem cell growth kit (ATCC, PCS-500-040™) and 5 mL of Penicillin-Streptomycin (Gibco™, 15140-122).

UCMSC culture media (RoosterBio®)

To a fresh 500 mL bottle of RoosterBasal™ (RoosterBio®, M22520) add the 10 mL RoosterBooster™-MSC-XF supplement (RoosterBio®, SU-016 (RUO) or SU3004 (MUO)) and 5 mL of Penicillin-Streptomycin (Gibco™, 15140-122).

HeLa culture media

To a fresh 500 mL bottle of high glucose, DMEM GlutaMax™ basal media (Gibco™, 10566-016) add 50 mL foetal bovine serum (Gibco™, 10500-064) and 5 mL Penicillin-Streptomycin (Gibco™, 15140-122).

AB1190 culture media

To a fresh 500 mL bottle of skeletal muscle cell basal media (PromoCell®, C-23260) add the 10 mL SupplementMix (PromoCell®, C-39365) and 5 mL Penicillin-Streptomycin (Gibco™, 15140-122).

MSC differentiation media - Adipogenic

To a fresh 225 mL bottle of MesenCult™ MSC basal medium (StemCell™ Technologies, 05413) add 25 mL of MesenCult™ 10x adipogenic differentiation supplement (StemCell™ Technologies, 05414), 0.5 mL of MesenCult™ 500x adipogenic differentiation supplement (StemCell™ Technologies, 05415) and 2.5 mL Penicillin-Streptomycin (Gibco™, 15140-122).

MSC differentiation media – Osteogenic

To 40 mL MesenCult™ osteogenic differentiation basal media (StemCell™ Technologies, 05466) add 10 mL MesenCult™ osteogenic differentiation 5x supplement (StemCell™ Technologies, 05467) and 0.5 mL Penicillin-Streptomycin (Gibco™, 15140-122). Stable for up to 1 week.

MSC differentiation media – Chondrogenic

To 19 mL MesenCult™-ACF chondrogenic differentiation basal medium (StemCell™ Technologies, 05456) add 1 mL MesenCult™-ACF 20x chondrogenic differentiation supplement and 0.2 mL Penicillin-Streptomycin (Gibco™, 15140-122).

Oil Red O stain

Stock: Add 0.5 g Oil Red O (Sigma Aldrich O0625) to 200 mL isopropyl alcohol, warmed to 56°C for 1 hour. Stable for 6 months.

Working: dilute Oil Red O stock 6 parts to 4 parts water and allow to settle for 10 minutes. Without disturbing any sediment, taking from the top, filter through a 0.2 µM filter. Stable for 2 hours.

Alizian Red S stain

Add 100 mg Alizarin Red S stain (Sigma-Aldrich A5533) to 90 mL distilled water. Adjust to pH 5.5 with ammonium hydroxide (Sigma-Aldrich 320145) and make the final volume up to 100 mL with water.

Alcian Blue stain

Add 100 mg Alcian blue (Sigma-Aldrich A3157) to 100 mL 0.1M hydrochloric acid and filter through a 0.2 µM filter.

Flow cytometry blocking buffer

Add 0.5 g bovine serum albumin (BSA) to 90 mL 1x PBS buffer and dissolve. Adjust volume to 100 mL with 1x PBS.

Senescence stain (x-gal)

5 mmol/L sodium phosphate solution pH 6.0, 5 mmol/L potassium ferricyanide, 5 mmol/L potassium ferrocyanide, 125 mmol/L sodium chloride, 50 mmol/L magnesium chloride, 2.5 mg/mL X-gal

Laemmli buffer

To 3.75 mL 1M Tria-HCl add 1.2 g sodium dodecyl sulphate (SDS), 0.93 g dithiothreitol (DTT), 6 mg 6 mg Bromophenol blue and 6 mL glycerol. Adjust volume up to 10 mL with ultrapure water.

Crystal violet stain

Stock: Add 1g of crystal violet to 50 mL of 20% methanol.

Working: Dilute stock 1 part to 3 parts 1x PBS solution.

Immunohistochemistry permeabilization buffer

Dissolve 0.954 g HEPES (20 mM), 0.260 g $MgCl_2$ (3 nM), 0.584 g NaCl (50 mM), 20.54 g sucrose (300 mM) and 0.1 g NaN_3 (0.05%), in 150 mL of distilled water. Add 250 µL Triton X-100 (0.5% v/v) and adjust the final volume to 200 mL with distilled water.

Immunohistochemistry blocking/wash buffer

To 475 mL 1x PBS buffer, add 25 mL foetal bovine serum, 0.2 g NaN_3 and 250 µL Triton X-100 for a 500 mL solution.

Chapter 8 - Bibliography

ABELS, E. R. & BREAKEFIELD, X. O. 2016. Introduction to Extracellular Vesicles: Biogenesis, RNA Cargo Selection, Content, Release, and Uptake. *Cell Mol Neurobiol,* 36**,** 301-12.

AHMAD, K., SHAIKH, S., CHUN, H. J., ALI, S., LIM, J. H., AHMAD, S. S., LEE, E. J. & CHOI, I. 2023. Extracellular matrix: the critical contributor to skeletal muscle regeneration-a comprehensive review. *Inflamm Regen,* 43**,** 58.

AL-NEDAWI, K., MEEHAN, B. & RAK, J. 2009. Microvesicles: messengers and mediators of tumor progression. *Cell Cycle,* 8**,** 2014-8.

ALIAGHAEI, A., GARDANEH, M., MAGHSOUDI, N., SALEHINEJAD, P. & GHARIB, E. 2016. Dopaminergic Induction of Umbilical Cord Mesenchymal Stem Cells by Conditioned Medium of Choroid Plexus Epithelial Cells Reduces Apomorphine-Induced Rotation in Parkinsonian Rats. *Arch Iran Med,* 19**,** 561-70.

ARAKAWA, T., PRESTRELSKI, S. J., KENNEY, W. C. & CARPENTER, J. F. 2001. Factors affecting short-term and long-term stabilities of proteins. *Advanced Drug Delivery Reviews,* 46**,** 307-326.

ARNOLD, L., HENRY, A., PORON, F., BABA-AMER, Y., VAN ROOIJEN, N., PLONQUET, A., GHERARDI, R. K. & CHAZAUD, B. 2007. Inflammatory monocytes recruited after skeletal muscle injury switch into antiinflammatory macrophages to support myogenesis. *J Exp Med,* 204**,** 1057-69.

ARUTYUNYAN, I., FATKHUDINOV, T., KANANYKHINA, E., USMAN, N., ELCHANINOV, A., MAKAROV, A., BOLSHAKOVA, G., GOLDSHTEIN, D. & SUKHIKH, G. 2016. Role of VEGF-A in angiogenesis promoted by umbilical cord-derived mesenchymal stromal/stem cells: in vitro study. *Stem Cell Res Ther,* 7**,** 46.

ARYA, S. B., COLLIE, S. P. & PARENT, C. A. 2023. The ins-and-outs of exosome biogenesis, secretion, and internalization. *Trends Cell Biol*.

AUSTERMANN, J., ROTH, J. & BARCZYK-KAHLERT, K. 2022. The Good and the Bad: Monocytes' and Macrophages' Diverse Functions in Inflammation. *Cells,* 11.

BAGUR, R. & HAJNÓCZKY, G. 2017. Intracellular Ca(2+) Sensing: Its Role in Calcium Homeostasis and Signaling. *Mol Cell,* 66**,** 780-788.

BALGI-AGARWAL, S., WINTER, C., CORRAL, A., MUSTAFA, S. B., HORNSBY, P. & MOREIRA, A. 2018. Comparison of Preterm and Term Wharton's Jelly-Derived Mesenchymal Stem Cell Properties in Different Oxygen Tensions. *Cells Tissues Organs,* 205**,** 137-150.

BARKHOLT, L., VOLTZ-GIROLT, C., RAINE, J., SALMONSON, T. & SCHÜSSLER-LENZ, M. 2019. Regulatory watch: European regulatory experience with advanced therapy medicinal products. *Nat Rev Drug Discov,* 18**,** 8-9.

BARTEL, D. P. 2004. MicroRNAs: genomics, biogenesis, mechanism, and function. *Cell,* 116**,** 281-97.

BARTENEVA, N. S., MALTSEV, N. & VOROBJEV, I. A. 2013. Microvesicles and intercellular communication in the context of parasitism. *Front Cell Infect Microbiol,* 3**,** 49.

BASISTY, N., KALE, A., JEON, O. H., KUEHNEMANN, C., PAYNE, T., RAO, C., HOLTZ, A., SHAH, S., SHARMA, V., FERRUCCI, L., CAMPISI, J. & SCHILLING, B. 2020. A proteomic atlas of senescence-associated secretomes for aging biomarker development. *PLoS Biol,* 18**,** e3000599.

BATSALI, A. K., KASTRINAKI, M. C., PAPADAKI, H. A. & PONTIKOGLOU, C. 2013. Mesenchymal stem cells derived from Wharton's Jelly of the umbilical cord: biological properties and emerging clinical applications. *Curr Stem Cell Res Ther,* 8**,** 144-55.

BERGMAN, P., LUNDIN, P. & MALMSTROM, T. 1961. Mucoid degeneration of Wharton's jelly. An umbilical cord anomaly threatening foetal life. *Acta Obstet Gynecol Scand,* 40**,** 372-8.

BIEHL, J. K. & RUSSELL, B. 2009. Introduction to stem cell therapy. *J Cardiovasc Nurs,* 24**,** 98-103; quiz 104-5.

BIER, A., BERENSTEIN, P., KRONFELD, N., MORGOULIS, D., ZIV-AV, A., GOLDSTEIN, H., KAZIMIRSKY, G., CAZACU, S., MEIR, R., POPOVTZER, R., DORI, A. & BRODIE, C. 2018. Placenta-derived mesenchymal stromal cells and their exosomes exert therapeutic effects in Duchenne muscular dystrophy. *Biomaterials,* 174**,** 67-78.

BIZZARRI, A., KOEHLER, H., CAJLAKOVIC, M., PASIC, A., SCHAUPP, L., KLIMANT, I. & RIBITSCH, V. 2006. Continuous oxygen monitoring in subcutaneous adipose tissue using microdialysis. *Analytica Chimica Acta,* 573-574**,** 48-56.

BOLDIN, M. P., TAGANOV, K. D., RAO, D. S., YANG, L., ZHAO, J. L., KALWANI, M., GARCIA-FLORES, Y., LUONG, M., DEVREKANLI, A., XU, J., SUN, G., TAY, J., LINSLEY, P. S. & BALTIMORE, D. 2011. miR-146a is a significant brake on autoimmunity, myeloproliferation, and cancer in mice. *J Exp Med,* 208**,** 1189-201.

BONIFACINO, J. S. & GLICK, B. S. 2004. The mechanisms of vesicle budding and fusion. *Cell,* 116**,** 153-66.

BRUNER, L. P., WHITE, A. M. & PROKSELL, S. 2023. Inflammatory Bowel Disease. *Prim Care,* 50**,** 411-427.

BRUNNER, D., FRANK, J., APPL, H., SCHÖFFL, H., PFALLER, W. & GSTRAUNTHALER, G. 2010. Serum-free cell culture: the serum-free media interactive online database. *Altex,* 27**,** 53-62.

CALEY, M. P., MARTINS, V. L. & O'TOOLE, E. A. 2015. Metalloproteinases and Wound Healing. *Adv Wound Care (New Rochelle),* 4**,** 225-234.

CALVETE, J. J., ESCOLANO, J. & SANZ, L. 2007. Snake venomics of Bitis species reveals large intragenus venom toxin composition variation: application to taxonomy of congeneric taxa. *J Proteome Res,* 6**,** 2732-45.

CASTANHEIRA, F. V. S. & KUBES, P. 2019. Neutrophils and NETs in modulating acute and chronic inflammation. *Blood,* 133**,** 2178-2185.

CASTRO, H. C., ZINGALI, R. B., ALBUQUERQUE, M. G., PUJOL-LUZ, M. & RODRIGUES, C. R. 2004. Snake venom thrombin-like enzymes: from reptilase to now. *Cell Mol Life Sci,* 61**,** 843-56.

ČESNIK, A. B. & ŠVAJGER, U. 2024. The issue of heterogeneity of MSC-based advanced therapy medicinal products-a review. *Front Cell Dev Biol,* 12**,** 1400347.

CHEN, Y., HU, S., WANG, M., ZHAO, B., YANG, N., LI, J., CHEN, Q., LIU, M., ZHOU, J., BAO, G. & WU, X. 2019. Characterization and Establishment of an Immortalized Rabbit Melanocyte Cell Line Using the SV40 Large T Antigen. *Int J Mol Sci,* 20.

CHENG, A., CHOI, D., LORA, M., SHUM-TIM, D., RAK, J. & COLMEGNA, I. 2020. Human multipotent mesenchymal stromal cells cytokine priming promotes RAB27B-regulated secretion of small extracellular vesicles with immunomodulatory cargo. *Stem Cell Res Ther,* 11**,** 539.

CHERNYAVSKIJ, D. A., LYAMZAEV, K. G., PLETJUSHKINA, O. Y., CHEN, F., KARPUKHINA, A., VASSETZKY, Y. S., CHERNYAK, B. V. & POPOVA, E. N. 2024. Mitochondrial fragmentation in early differentiation of human MB135 myoblasts: Role of mitochondrial ROS production in the absence of depolarization. *Life Sciences,* 354**,** 122941.

CHILDS, B. G., DURIK, M., BAKER, D. J. & VAN DEURSEN, J. M. 2015. Cellular senescence in aging and age-related disease: from mechanisms to therapy. *Nat Med,* 21**,** 1424-35.

CHOI, Y. J., KIM, J. H., LEE, Y., PYEON, H. J., YOO, I. K. & YOO, J. H. 2024a. Anti-fibrogenic effect of umbilical cord-derived mesenchymal stem cell-conditioned media in human esophageal fibroblasts. *Sci Rep,* 14**,** 22233.

CHOI, Y. J., KIM, W. R., KIM, D. H., KIM, J. H. & YOO, J. H. 2024b. Human umbilical cord/placenta mesenchymal stem cell conditioned medium attenuates intestinal fibrosis in vivo and in vitro. *Stem Cell Research & Therapy,* 15**,** 69.

CHOUAIB, B., HAACK-SØRENSEN, M., CHAUBRON, F., CUISINIER, F. & COLLART-DUTILLEUL, P. Y. 2023. Towards the Standardization of Mesenchymal Stem Cell Secretome-Derived Product Manufacturing for Tissue Regeneration. *Int J Mol Sci,* 24.

ÇIÇEK, G., BAĞCI, F., FILIZFIDAN, M., DUMAN, S. & AKTAN, T. M. 2025. Physicochemical and Biological Modifications in Mesenchymal Stem Cells-Derived Conditioned Media Under Hypoxic Preconditioning: Impact on Oxidative Stress and Nanoparticle Stability. *Life (Basel),* 15.

CLOUDSLEY-THOMPSON, J. L. 1988. THE PUFF ADDER (BITIS ARIETANS). *British Herpetological Society Bulletin.*

CONCONI, M. T., BURRA, P., DI LIDDO, R., CALORE, C., TURETTA, M., BELLINI, S., BO, P., NUSSDORFER, G. G. & PARNIGOTTO, P. P. 2006. CD105(+) cells from Wharton's jelly show in vitro and in vivo myogenic differentiative potential. *Int J Mol Med,* 18**,** 1089-96.

COTSARELIS, G. 2006. Epithelial stem cells: a folliculocentric view. *J Invest Dermatol,* 126**,** 1459-68.

CUMMINS, E. P., BERRA, E., COMERFORD, K. M., GINOUVES, A., FITZGERALD, K. T., SEEBALLUCK, F., GODSON, C., NIELSEN, J. E., MOYNAGH, P., POUYSSEGUR, J. & TAYLOR, C. T. 2006. Prolyl hydroxylase-1 negatively regulates IκB kinase-β, giving insight into hypoxia-induced NFκB activity. *Proceedings of the National Academy of Sciences,* 103**,** 18154-18159.

D'SOUZA-SCHOREY, C. & CHAVRIER, P. 2006. ARF proteins: roles in membrane traffic and beyond. *Nat Rev Mol Cell Biol,* 7**,** 347-58.

D'SOUZA-SCHOREY, C. & CLANCY, J. W. 2012. Tumor-derived microvesicles: shedding light on novel microenvironment modulators and prospective cancer biomarkers. *Genes Dev,* 26**,** 1287-99.

DAVENPORT, A., VERBINE, A. & RONCO, C. 2019. Chapter 152 - Composition of Hemodialysis Fluid. *In:* RONCO, C., BELLOMO, R., KELLUM, J. A. & RICCI, Z. (eds.) *Critical Care Nephrology (Third Edition).* Philadelphia: Elsevier.

DAVIES, J. E., WALKER, J. T. & KEATING, A. 2017. Concise Review: Wharton's Jelly: The Rich, but Enigmatic, Source of Mesenchymal Stromal Cells. *Stem Cells Transl Med,* 6**,** 1620-1630.

DEL CONDE, I., SHRIMPTON, C. N., THIAGARAJAN, P. & LÓPEZ, J. A. 2005. Tissue-factor-bearing microvesicles arise from lipid rafts and fuse with activated platelets to initiate coagulation. *Blood,* 106**,** 1604-11.

DEL PESO, L., CASTELLANOS, M. C., TEMES, E., MARTÍN-PUIG, S., CUEVAS, Y., OLMOS, G. & LANDÁZURI, M. O. 2003. The von Hippel Lindau/hypoxia-inducible factor (HIF) pathway regulates the transcription of the

HIF-proline hydroxylase genes in response to low oxygen. *Journal of Biological Chemistry,* 278**,** 48690-48695.

DENG, Y., YI, S., WANG, G., CHENG, J., ZHANG, Y., CHEN, W., TAI, Y., CHEN, S., CHEN, G., LIU, W., ZHANG, Q. & YANG, Y. 2014. Umbilical Cord-Derived Mesenchymal Stem Cells Instruct Dendritic Cells to Acquire Tolerogenic Phenotypes Through the IL-6-Mediated Upregulation of SOCS1. *Stem Cells and Development,* 23**,** 2080-2092.

DENNING, N. L. & PRINCE, J. M. 2018. Neonatal intestinal dysbiosis in necrotizing enterocolitis. *Mol Med,* 24**,** 4.

DENZER, K., KLEIJMEER, M. J., HEIJNEN, H. F., STOORVOGEL, W. & GEUZE, H. J. 2000. Exosome: from internal vesicle of the multivesicular body to intercellular signaling device. *J Cell Sci,* 113 Pt 19**,** 3365-74.

DESZCZ, I. 2023. Stem Cell-Based Therapy and Cell-Free Therapy as an Alternative Approach for Cardiac Regeneration. *Stem Cells Int,* 2023**,** 2729377.

DI, G. H., LIU, Y., LU, Y., LIU, J., WU, C. & DUAN, H. F. 2014. IL-6 secreted from senescent mesenchymal stem cells promotes proliferation and migration of breast cancer cells. *PLoS One,* 9**,** e113572.

DOMÍNGUEZ-OLIVA, A., HERNÁNDEZ-ÁVALOS, I., MARTÍNEZ-BURNES, J., OLMOS-HERNÁNDEZ, A., VERDUZCO-MENDOZA, A. & MOTA-ROJAS, D. 2023. The Importance of Animal Models in Biomedical Research: Current Insights and Applications. *Animals (Basel),* 13.

DOMINICI, M., LE BLANC, K., MUELLER, I., SLAPER-CORTENBACH, I., MARINI, F., KRAUSE, D., DEANS, R., KEATING, A., PROCKOP, D. & HORWITZ, E. 2006. Minimal criteria for defining multipotent mesenchymal stromal cells. The International Society for Cellular Therapy position statement. *Cytotherapy,* 8**,** 315-7.

DONG, L., PU, Y., CHEN, X., QI, X., ZHANG, L., XU, L., LI, W., MA, Y., ZHOU, S., ZHU, J., LI, Y., WANG, X. & SU, C. 2020. hUCMSC-extracellular vesicles downregulated hepatic stellate cell activation and reduced liver injury in S. japonicum-infected mice. *Stem Cell Res Ther,* 11**,** 21.

DONOVAN, P. J. & GEARHART, J. 2001. The end of the beginning for pluripotent stem cells. *Nature,* 414**,** 92-7.

DORRINGTON, M. G. & FRASER, I. D. C. 2019. NF-κB Signaling in Macrophages: Dynamics, Crosstalk, and Signal Integration. *Frontiers in Immunology,* Volume 10 - 2019.

DRIESSLER, F., VENSTROM, K., SABAT, R., ASADULLAH, K. & SCHOTTELIUS, A. J. 2004. Molecular mechanisms of interleukin-10-mediated inhibition of NF-kappaB activity: a role for p50. *Clin Exp Immunol,* 135**,** 64-73.

DUGUEZ, S., FÉASSON, L., DENIS, C. & FREYSSENET, D. 2002. Mitochondrial biogenesis during skeletal muscle regeneration. *Am J Physiol Endocrinol Metab,* 282**,** E802-9.

DUGUEZ, S., SABIDO, O. & FREYSSENET, D. 2004. Mitochondrial-dependent regulation of myoblast proliferation. *Experimental Cell Research,* 299**,** 27-35.

DZIERZAK, E. & PHILIPSEN, S. 2013. Erythropoiesis: development and differentiation. *Cold Spring Harb Perspect Med,* 3**,** a011601.

EMA 2019. Guideline on quality, non-clinical and clinical requirements for investigational advanced therapy medicinal products in clinical trails (Draft). *In:* (CAT), C. F. A. T. (ed.).

ESKANDANI, M., VANDGHANOONI, S., BARAR, J., NAZEMIYEH, H. & OMIDI, Y. 2017. Cell physiology regulation by hypoxia inducible factor-1: Targeting oxygen-related nanomachineries of hypoxic cells. *International Journal of Biological Macromolecules,* 99**,** 46-62.

FAN, J., XU, G., CHANG, Z., ZHU, L. & YAO, J. 2020. miR-210 transferred by lung cancer cell-derived exosomes may act as proangiogenic factor in cancer-associated fibroblasts by modulating JAK2/STAT3 pathway. *Clin Sci (Lond),* 134**,** 807-825.

FANG, C. Y., WU, C. C., FANG, C. L., CHEN, W. Y. & CHEN, C. L. 2017. Long-term growth comparison studies of FBS and FBS alternatives in six head and neck cell lines. *PLoS One,* 12**,** e0178960.

FERNANDES-PLATZGUMMER, A., CARMELO, J. G., DA SILVA, C. L. & CABRAL, J. M. 2016. Clinical-Grade Manufacturing of Therapeutic Human Mesenchymal Stem/Stromal Cells in Microcarrier-Based Culture Systems. *Methods Mol Biol,* 1416**,** 375-88.

FERREIRA, J. R., TEIXEIRA, G. Q., SANTOS, S. G., BARBOSA, M. A., ALMEIDA-PORADA, G. & GONÇALVES, R. M. 2018. Mesenchymal Stromal Cell Secretome: Influencing Therapeutic Potential by Cellular Pre-conditioning. *Front Immunol,* 9**,** 2837.

FISH, J. E., SANTORO, M. M., MORTON, S. U., YU, S., YEH, R.-F., WYTHE, J. D., IVEY, K. N., BRUNEAU, B. G., STAINIER, D. Y. R. & SRIVASTAVA, D. 2008. miR-126 Regulates Angiogenic Signaling and Vascular Integrity. *Developmental Cell,* 15**,** 272-284.

FODDIS, R., DE RIENZO, A., BROCCOLI, D., BOCCHETTA, M., STEKALA, E., RIZZO, P., TOSOLINI, A., GROBELNY, J. V., JHANWAR, S. C., PASS, H. I., TESTA, J. R. & CARBONE, M. 2002. SV40 infection induces telomerase activity in human mesothelial cells. *Oncogene,* 21**,** 1434-42.

FONG, C. Y., RICHARDS, M., MANASI, N., BISWAS, A. & BONGSO, A. 2007. Comparative growth behaviour and characterization of stem cells from human Wharton's jelly. *Reprod Biomed Online,* 15**,** 708-18.

FRÜHBEIS, C., FRÖHLICH, D. & KRÄMER-ALBERS, E. M. 2012. Emerging roles of exosomes in neuron-glia communication. *Front Physiol,* 3**,** 119.

FRÜHBEIS, C., FRÖHLICH, D., KUO, W. P., AMPHORNRAT, J., THILEMANN, S., SAAB, A. S., KIRCHHOFF, F., MÖBIUS, W., GOEBBELS, S., NAVE, K. A., SCHNEIDER, A., SIMONS, M., KLUGMANN, M., TROTTER, J. & KRÄMER-ALBERS, E. M. 2013. Neurotransmitter-triggered transfer of exosomes mediates oligodendrocyte-neuron communication. *PLoS Biol,* 11**,** e1001604.

FUJII, S., MIURA, Y., FUJISHIRO, A., SHINDO, T., SHIMAZU, Y., HIRAI, H., TAHARA, H., TAKAORI-KONDO, A., ICHINOHE, T. & MAEKAWA, T. 2017. Graft-Versus-Host Disease Amelioration by Human Bone Marrow Mesenchymal Stromal/Stem Cell-Derived Extracellular Vesicles Is Associated with Peripheral Preservation of Naive T Cell Populations. *Stem Cells,* 36**,** 434-445.

FYFE, J., CASARI, I., MANFREDI, M. & FALASCA, M. 2023. Role of lipid signalling in extracellular vesicles-mediated cell-to-cell communication. *Cytokine Growth Factor Rev,* 73**,** 20-26.

GANJI, N., KALISH, B., OFFRINGA, M., LI, B., ANDERSON, J., BARUCHEL, S., BLAKELY, M., DE COPPI, P., EATON, S., GAUDA, E., HALL, N., HEATH, A., LIVINGSTON, M. H., MCNAIR, C., MITCHELL, R., PATEL, K., PECHLIVANOGLOU, P., PLEASANTS-TERASHITA, H., PRYOR, E., RADISIC, M., SHAH, P. S., THÉBAUD, B., WANG, K., ZANI, A. & PIERRO, A. 2024. Translating regenerative medicine therapies in neonatal necrotizing enterocolitis. *Pediatric Research,* 96**,** 1609-1615.

GAO, Y., YANG, L., WU, H., YAO, Q., WANG, J. & ZHENG, N. 2025. Sodium butyrate attenuates experimental neonatal necrotizing enterocolitis by suppressing TLR4-mediated NLRP3 inflammasome-dependent pyroptosis. *Food Funct,* 16**,** 3508-3524.

GATTI, S., BRUNO, S., DEREGIBUS, M. C., SORDI, A., CANTALUPPI, V., TETTA, C. & CAMUSSI, G. 2011. Microvesicles derived from human adult mesenchymal stem cells protect against ischaemia-reperfusion-induced acute and chronic kidney injury. *Nephrol Dial Transplant,* 26**,** 1474-83.

GENBACEV, O., ZHOU, Y., LUDLOW, J. W. & FISHER, S. J. 1997. Regulation of human placental development by oxygen tension. *Science,* 277**,** 1669-72.

GIMONA, M., PACHLER, K., LANER-PLAMBERGER, S., SCHALLMOSER, K. & ROHDE, E. 2017. Manufacturing of Human Extracellular Vesicle-Based Therapeutics for Clinical Use. *Int J Mol Sci,* 18.

GIUSTI, S., ADRIANI, E., SAMUELSSON, K., LAUDISIO, A., HORVATH, A., ZAMPOGNA, B. & PAPALIA, R. 2025. The role of arthroscopy in intra-articular adipose tissue-derived mesenchymal stem cells for the treatment of early-stage knee osteoarthritis: A bicentric retrospective comparative study. *J Exp Orthop,* 12**,** e70368.

GNECCHI, M., HE, H., LIANG, O. D., MELO, L. G., MORELLO, F., MU, H., NOISEUX, N., ZHANG, L., PRATT, R. E., INGWALL, J. S. & DZAU, V. J. 2005. Paracrine action accounts for marked protection of ischemic heart by Akt-modified mesenchymal stem cells. *Nat Med,* 11**,** 367-8.

GNECCHI, M., HE, H., NOISEUX, N., LIANG, O. D., ZHANG, L., MORELLO, F., MU, H., MELO, L. G., PRATT, R. E., INGWALL, J. S. & DZAU, V. J. 2006. Evidence supporting paracrine hypothesis for Akt-modified mesenchymal stem cell-mediated cardiac protection and functional improvement. *Faseb j,* 20**,** 661-9.

GODOI, K. S., GUIDOLIN, F. R., PORTARO, F. C. V., SPENCER, P. J. & DA SILVA, W. D. 2023. Anti-Metalloproteases: Production and Characterization of Polyclonal IgG Anti-F2 Fraction Antibodies Purified from the Venom of the Snake Bitis arietans. *Toxins (Basel),* 15.

GONZÁLEZ-GONZÁLEZ, A., GARCÍA-SÁNCHEZ, D., DOTTA, M., RODRÍGUEZ-REY, J. C. & PÉREZ-CAMPO, F. M. 2020. Mesenchymal stem cells secretome: The cornerstone of cell-free regenerative medicine. *World J Stem Cells,* 12**,** 1529-1552.

GREGORY, D. J., HAN, F., LI, P., GRITSENKO, M. A., KYLE, J., RILEY, F. E., CHAVEZ, D., YOTOVA, V., SINDEAUX, R. H. M., HAWASH, M. B. F., XU, F., HUNG, L.-Y., HAYDEN, D. L., TOMPKINS, R. G., LANFORD, R. E., KOBZIK, L., HELLMAN, J., JACOBS, J. M., BARREIRO, L. B., XIAO, W. & WARREN, H. S. 2024. Molecular profiles of blood from numerous species that differ in sensitivity to acute inflammation. *Molecular Medicine,* 30**,** 280.

GSTRAUNTHALER, G., SEPPI, T. & PFALLER, W. 1999. Impact of culture conditions, culture media volumes, and glucose content on metabolic properties of renal epithelial cell cultures. Are renal cells in tissue culture hypoxic? *Cell Physiol Biochem,* 9**,** 150-72.

GU, J., RUAN, J., GUO, C., LI, Z., FU, H., XIE, Y., XIE, H., GONG, X. & SHI, H. 2025. Organelles Ca(2+) redistribution contributes to cadmium-induced EMT of renal cancer cells through p-cPLA(2)-mediated arachidonic acid release. *Ecotoxicol Environ Saf,* 298**,** 118317.

GUDURIC-FUCHS, J., PEDRINI, E., LECHNER, J., CHAMBERS, S. E. J., O'NEILL, C. L., MENDES LOPES DE MELO, J., PATHAK, V., CHURCH, R. H., MCKEOWN, S., BOJDO, J., MCLOUGHLIN, K. J., STITT, A. W. & MEDINA, R. J.

2021. miR-130a activates the VEGFR2/STAT3/HIF1α axis to potentiate the vasoregenerative capacity of endothelial colony-forming cells in hypoxia. *Mol Ther Nucleic Acids,* 23**,** 968-981.

GUO, Z., CAI, X., GUO, X., XU, Y., GONG, J., LI, Y. & ZHU, W. 2018. Let-7b ameliorates Crohn's disease-associated adherent-invasive E coli induced intestinal inflammation via modulating Toll-Like Receptor 4 expression in intestinal epithelial cells. *Biochem Pharmacol,* 156**,** 196-203.

GUTIÉRREZ, J. M., ESCALANTE, T., RUCAVADO, A. & HERRERA, C. 2016. Hemorrhage Caused by Snake Venom Metalloproteinases: A Journey of Discovery and Understanding. *Toxins (Basel),* 8**,** 93.

GUTIÉRREZ, J. M. A. & OWNBY, C. L. 2003. Skeletal muscle degeneration induced by venom phospholipases A2: insights into the mechanisms of local and systemic myotoxicity. *Toxicon,* 42**,** 915-931.

GYÖRGY, B., SZABÓ, T. G., PÁSZTÓI, M., PÁL, Z., MISJÁK, P., ARADI, B., LÁSZLÓ, V., PÁLLINGER, E., PAP, E., KITTEL, A., NAGY, G., FALUS, A. & BUZÁS, E. I. 2011. Membrane vesicles, current state-of-the-art: emerging role of extracellular vesicles. *Cell Mol Life Sci,* 68**,** 2667-88.

HAILMAN, E., LICHENSTEIN, H. S., WURFEL, M. M., MILLER, D. S., JOHNSON, D. A., KELLEY, M., BUSSE, L. A., ZUKOWSKI, M. M. & WRIGHT, S. D. 1994. Lipopolysaccharide (LPS)-binding protein accelerates the binding of LPS to CD14. *J Exp Med,* 179**,** 269-77.

HARASZTI, R. A., DIDIOT, M. C., SAPP, E., LESZYK, J., SHAFFER, S. A., ROCKWELL, H. E., GAO, F., NARAIN, N. R., DIFIGLIA, M., KIEBISH, M. A., ARONIN, N. & KHVOROVA, A. 2016. High-resolution proteomic and lipidomic analysis of exosomes and microvesicles from different cell sources. *J Extracell Vesicles,* 5**,** 32570.

HARDY, D., BESNARD, A., LATIL, M., JOUVION, G., BRIAND, D., THÉPENIER, C., PASCAL, Q., GUGUIN, A., GAYRAUD-MOREL, B., CAVAILLON, J. M., TAJBAKHSH, S., ROCHETEAU, P. & CHRÉTIEN, F. 2016. Comparative Study of Injury Models for Studying Muscle Regeneration in Mice. *PLoS One,* 11**,** e0147198.

HARRISON, J. S., RAMESHWAR, P., CHANG, V. & BANDARI, P. 2002. Oxygen saturation in the bone marrow of healthy volunteers. *Blood,* 99**,** 394-394.

HE, J. G., WU, X. X., LI, S., YAN, D., XIAO, G. P. & MAO, F. G. 2024. Exosomes derived from microRNA-540-3p overexpressing mesenchymal stem cells promote immune tolerance via the CD74/nuclear factor-kappaB pathway in cardiac allograft. *World J Stem Cells,* 16**,** 1022-1046.

HENDRAWAN, S., KUSNADI, Y., LAGONDA, C. A., FAUZA, D., LHEMAN, J., BUDI, E., MANURUNG, B. S., BAER, H. U. & TANSIL TAN, S. 2021. Wound healing potential of human umbilical cord mesenchymal stem cell conditioned medium: An in vitro and in vivo study in diabetes-induced rats. *Vet World,* 14**,** 2109-2117.

HENNE, W. M., BUCHKOVICH, N. J. & EMR, S. D. 2011. The ESCRT pathway. *Dev Cell,* 21**,** 77-91.

HERRANZ, N. & GIL, J. 2018. Mechanisms and functions of cellular senescence. *J Clin Invest,* 128**,** 1238-1246.

HERRMANN, J. L., WANG, Y., ABARBANELL, A. M., WEIL, B. R., TAN, J. & MELDRUM, D. R. 2010. Preconditioning mesenchymal stem cells with transforming growth factor-alpha improves mesenchymal stem cell-mediated cardioprotection. *Shock,* 33**,** 24-30.

HESSVIK, N. P., SAGINI, K., ROMERO, S., RAMIREZ-GARRASTACHO, M., RODRIGUEZ, M., TUTTUREN, A. E. V., KVALVAAG, A., STANG, E., BRECH, A., SANDVIG, K. & LLORENTE, A. 2023. siRNA screening reveals that SNAP29 contributes to exosome release. *Cell Mol Life Sci,* 80**,** 177.

HOLIUK, Y., BIRSA, R., BUKREIEVA, T., NEMTINOV, P., KYRYK, V., USTYMENKO, A., MAZEVYCH, V., SOKOLOV, M., LOBYNTSEVA, G. & SHABLII, V. 2025. Effectiveness and safety of multiple injections of human placenta-derived MSCs for knee osteoarthritis: a nonrandomized phase I trial. *BMC Musculoskelet Disord,* 26**,** 418.

HU, S., HUANG, M., LI, Z., JIA, F., GHOSH, Z., LIJKWAN, M. A., FASANARO, P., SUN, N., WANG, X., MARTELLI, F., ROBBINS, R. C. & WU, J. C. 2010. MicroRNA-210 as a novel therapy for treatment of ischemic heart disease. *Circulation,* 122**,** S124-31.

HU, X., LIANG, H., LI, F., ZHANG, R., ZHU, Y., ZHU, X. & XU, Y. 2024. Necrotizing enterocolitis: current understanding of the prevention and management. *Pediatr Surg Int,* 40**,** 32.

HUANG, C., LIU, X.-J., QUNZHOU, XIE, J., MA, T.-T., MENG, X.-M. & LI, J. 2016. MiR-146a modulates macrophage polarization by inhibiting Notch1 pathway in RAW264.7 macrophages. *International Immunopharmacology,* 32**,** 46-54.

HUANG, X., LE, Q. T. & GIACCIA, A. J. 2010. MiR-210--micromanager of the hypoxia pathway. *Trends Mol Med,* 16**,** 230-7.

HUTTER, J. J., JR., HATHAWAY, W. E. & WAYNE, E. R. 1976. Hematologic abnormalities in severe neonatal necrotizing enterocolitis. *J Pediatr,* 88**,** 1026-31.

HYLAND, M., MENNAN, C., WILSON, E., CLAYTON, A. & KEHOE, O. 2020. Pro-Inflammatory Priming of Umbilical Cord Mesenchymal Stromal Cells Alters the Protein Cargo of Their Extracellular Vesicles. *Cells,* 9.

IISMAA, S. E., KAIDONIS, X., NICKS, A. M., BOGUSH, N., KIKUCHI, K., NAQVI, N., HARVEY, R. P., HUSAIN, A. & GRAHAM, R. M. 2018. Comparative regenerative mechanisms across different mammalian tissues. *NPJ Regen Med,* 3**,** 6.

ISHIUCHI, N., NAKASHIMA, A., DOI, S., KANAI, R., MAEDA, S., TAKAHASHI, S., NAGAO, M. & MASAKI, T. 2021. Serum-free medium and hypoxic preconditioning synergistically enhance the therapeutic effects of mesenchymal stem cells on experimental renal fibrosis. *Stem Cell Res Ther,* 12**,** 472.

JAKUBZICK, C. V., RANDOLPH, G. J. & HENSON, P. M. 2017. Monocyte differentiation and antigen-presenting functions. *Nat Rev Immunol,* 17**,** 349-362.

JEVTIĆ, P., EDENS, L. J., VUKOVIĆ, L. D. & LEVY, D. L. 2014. Sizing and shaping the nucleus: mechanisms and significance. *Curr Opin Cell Biol,* 28**,** 16-27.

JIANG, K., GUO, S., ZHANG, T., YANG, Y., ZHAO, G., SHAUKAT, A., WU, H. & DENG, G. 2018. Downregulation of TLR4 by miR-181a Provides Negative Feedback Regulation to Lipopolysaccharide-Induced Inflammation. *Frontiers in Pharmacology,* Volume 9 - 2018.

JIN, L., JIANG, M., QIAN, J., GE, Z., XU, F. & LIAO, W. 2024. The role of lipoprotein-associated phospholipase A2 in inflammatory response and macrophage infiltration in sepsis and the regulatory mechanisms. *Funct Integr Genomics,* 24**,** 178.

JONES, H. W., JR. 1997. Record of the first physician to see Henrietta Lacks at the Johns Hopkins Hospital: history of the beginning of the HeLa cell line. *Am J Obstet Gynecol,* 176**,** S227-8.

JOTHIMANI, G., PATHAK, S., DUTTA, S., DUTTAROY, A. K. & BANERJEE, A. 2022. A Comprehensive Cancer-Associated MicroRNA Expression Profiling and Proteomic Analysis of Human Umbilical Cord Mesenchymal Stem Cell-Derived Exosomes. *Tissue Eng Regen Med,* 19**,** 1013-1031.

JUÁREZ, P., WAGSTAFF, S. C., OLIVER, J., SANZ, L., HARRISON, R. A. & CALVETE, J. J. 2006. Molecular Cloning of Disintegrin-like Transcript BA-5A from a Bitis arietans Venom Gland cDNA Library: A Putative Intermediate in the Evolution of the Long-Chain Disintegrin Bitistatin. *Journal of Molecular Evolution,* 63**,** 142-152.

JUN, J. I. & LAU, L. F. 2010. The matricellular protein CCN1 induces fibroblast senescence and restricts fibrosis in cutaneous wound healing. *Nat Cell Biol,* 12**,** 676-85.

KANG, I., LEE, B. C., CHOI, S. W., LEE, J. Y., KIM, J. J., KIM, B. E., KIM, D. H., LEE, S. E., SHIN, N., SEO, Y., KIM, H. S., KIM, D. I. & KANG, K. S. 2018. Donor-dependent variation of human umbilical cord blood mesenchymal stem cells in response to hypoxic preconditioning and amelioration of limb ischemia. *Exp Mol Med,* 50**,** 1-15.

KATZENSTEIN, A. L. & MYERS, J. L. 1998. Idiopathic pulmonary fibrosis: clinical relevance of pathologic classification. *Am J Respir Crit Care Med,* 157**,** 1301-15.

KAWAI, T. & AKIRA, S. 2010. The role of pattern-recognition receptors in innate immunity: update on Toll-like receptors. *Nat Immunol,* 11**,** 373-84.

KE, Q. & COSTA, M. 2006. Hypoxia-Inducible Factor-1 (HIF-1). *Molecular Pharmacology,* 70**,** 1469-1480.

KENTON, A. B., O'DONOVAN, D., CASS, D. L., HELMRATH, M. A., SMITH, E. O., FERNANDES, C. J., WASHBURN, K., WEIHE, E. K. & BRANDT, M. L. 2005. Severe thrombocytopenia predicts outcome in neonates with necrotizing enterocolitis. *J Perinatol,* 25**,** 14-20.

KHAN, M. I. & HARIPRASAD, G. 2020. Human Secretary Phospholipase A2 Mutations and Their Clinical Implications. *J Inflamm Res,* 13**,** 551-561.

KIM, C. G., LEE, J. K., CHO, G. J., SHIN, O. S. & GIM, J. A. 2022. Small RNA sequencing of small extracellular vesicles secreted by umbilical cord mesenchymal stem cells following replicative senescence. *Genes Genomics*.

KINK, J. A., BELLIO, M. A., FORSBERG, M. H., LOBO, A., THICKENS, A. S., LEWIS, B. M., ONG, I. M., KHAN, A., CAPITINI, C. M. & HEMATTI, P. 2024. Large-scale bioreactor production of extracellular vesicles from mesenchymal stromal cells for treatment of acute radiation syndrome. *Stem Cell Res Ther,* 15**,** 72.

KOZADINOS, A., MYLONAKIS, A., BEKOS, F., KYDONAKIS, N., KOROVESIS, G., KASTANAKI, P., DESPOTIDIS, M., CHRYSIKOS, D. & TROUPIS, T. 2025. The Development of the Umbilical Vein and Its Anatomical and Clinical Significance. *Cureus,* 17**,** e79712.

KUBO, M. & MOTOMURA, Y. 2012. Transcriptional regulation of the anti-inflammatory cytokine IL-10 in acquired immune cells. *Frontiers in Immunology,* Volume 3 - 2012.

KUCHROO, P., DAVE, V., VIJAYAN, A., VISWANATHAN, C. & GHOSH, D. 2015. Paracrine factors secreted by umbilical cord-derived mesenchymal stem cells induce angiogenesis in vitro by a VEGF-independent pathway. *Stem Cells Dev,* 24**,** 437-50.

KUNCOROJAKTI, S., PRATAMA, A. Z. A., ANTUJALA, C. A., HARIJANTO, C. T. B., ARSY, R. K., KURNIAWAN, P. A., TJAHJONO, Y., HENDRIATI, L., WIDODO, T., ASWIN, A., DIYANTORO, D., WIJAYA, A. Y., RODPRASERT, W. & SUSILOWATI, H. 2024. Acceleration of wound healing using adipose mesenchymal stem cell

secretome hydrogel on partial-thickness cutaneous thermal burn wounds: An in vivo study in rats. *Vet World,* 17**,** 1545-1554.

KUO, S. C., CHIO, C. C., YEH, C. H., MA, J. T., LIU, W. P., LIN, M. T., LIN, K. C. & CHANG, C. P. 2021. Mesenchymal stem cell-conditioned medium attenuates the retinal pathology in amyloid-β-induced rat model of Alzheimer's disease: Underlying mechanisms. *Aging Cell,* 20**,** e13340.

KUROGI, H., TAKIJIRI, T., SAKUMOTO, M., ISOGAI, M., TAKAHASHI, A., OKUBO, T., KOIKE, T., YAMADA, T., NAGAMURA-INOUE, T. & SAKAKI-YUMOTO, M. 2022. Study on the Umbilical Cord-Mesenchymal Stem Cell Manufacturing Using Clinical-Grade Culture Medium. *Tissue Eng Part C Methods,* 28**,** 23-33.

L, P. K., KANDOI, S., MISRA, R., S, V., K, R. & VERMA, R. S. 2019. The mesenchymal stem cell secretome: A new paradigm towards cell-free therapeutic mode in regenerative medicine. *Cytokine Growth Factor Rev,* 46**,** 1-9.

LAI, J. L., LIU, Y. H., LIU, C., QI, M. P., LIU, R. N., ZHU, X. F., ZHOU, Q. G., CHEN, Y. Y., GUO, A. Z. & HU, C. M. 2017. Indirubin Inhibits LPS-Induced Inflammation via TLR4 Abrogation Mediated by the NF-kB and MAPK Signaling Pathways. *Inflammation,* 40**,** 1-12.

LAMBERTINI, E., PENOLAZZI, L., ANGELOZZI, M., BERGAMIN, L. S., MANFERDINI, C., VIECELI DALLA SEGA, F., PAOLELLA, F., LISIGNOLI, G. & PIVA, R. 2018. Hypoxia Preconditioning of Human MSCs: a Direct Evidence of HIF-1α and Collagen Type XV Correlation. *Cell Physiol Biochem,* 51**,** 2237-2249.

LANDO, D., PEET, D. J., WHELAN, D. A., GORMAN, J. J. & WHITELAW, M. L. 2002. Asparagine Hydroxylation of the HIF Transactivation Domain: A Hypoxic Switch. *Science,* 295**,** 858-861.

LAVRENTIEVA, A., MAJORE, I., KASPER, C. & HASS, R. 2010. Effects of hypoxic culture conditions on umbilical cord-derived human mesenchymal stem cells. *Cell Communication and Signaling,* 8**,** 18.

LAYFIELD, H. J., WILLIAMS, H. F., RAVISHANKAR, D., MEHMI, A., SONAVANE, M., SALIM, A., VAIYAPURI, R., LAKSHMINARAYANAN, K., VALLANCE, T. M., BICKNELL, A. B., TRIM, S. A., PATEL, K. & VAIYAPURI, S. 2020. Repurposing Cancer Drugs Batimastat and Marimastat to Inhibit the Activity of a Group I Metalloprotease from the Venom of the Western Diamondback Rattlesnake, Crotalus atrox. *Toxins (Basel),* 12.

LEE, E., LIM, G. H., AN, J. H., RYU, M. O., SEO, K. W. & YOUN, H. Y. 2025a. Enhanced immunomodulatory effects of canine adipose tissue-derived mesenchymal stem cells in 3D culture. *Front Vet Sci,* 12**,** 1500267.

LEE, J., JOSEPH, S., MANOHAR, K., MESFIN, F., HUNTER, C., BROKAW, J., SHELLEY, W. C., LIU, J., MCCAIN, R., CRAIN, C. J., LESCUN, T. & MARKEL, T. A. 2025b. Mesenchymal Stromal Cell Therapy Restores Intestinal Integrity and Attentuates Inflammation in a Preterm Piglet Model of Necrotizing Enterocolitis. *Res Sq*.

LEMBONG, J., KIRIAN, R., TAKACS, J. D., OLSEN, T. R., LOCK, L. T., ROWLEY, J. A. & AHSAN, T. 2020. Bioreactor Parameters for Microcarrier-Based Human MSC Expansion under Xeno-Free Conditions in a Vertical-Wheel System. *Bioengineering (Basel),* 7.

LEWIN, M. R., CARTER, R. W., MATTEO, I. A., SAMUEL, S. P., RAO, S., FRY, B. G. & BICKLER, P. E. 2022. Varespladib in the Treatment of Snakebite Envenoming: Development History and Preclinical Evidence Supporting Advancement to Clinical Trials in Patients Bitten by Venomous Snakes. *Toxins (Basel),* 14.

LI, M., LUAN, F., ZHAO, Y., HAO, H., LIU, J., DONG, L., FU, X. & HAN, W. 2017. Mesenchymal stem cell-conditioned medium accelerates wound healing with fewer scars. *Int Wound J,* 14**,** 64-73.

LI, T., LIU, J., HUANG, X., XIE, Y., HU, Y., XU, Q., TANG, B., TAN, J. & GUO, J. 2025. Deficiency of PLA2G6 Induces Ferroptosis in Dopaminergic Neurons and Contributes to Parkinson's Disease Pathogenesis via Disruption of PRDX6/FTH1/GPX4 Axis. *Mol Neurobiol*.

LI, X., ZHANG, D., YU, Y., WANG, L. & ZHAO, M. 2024. Umbilical cord-derived mesenchymal stem cell secretome promotes skin regeneration and rejuvenation: From mechanism to therapeutics. *Cell Prolif,* 57**,** e13586.

LIANG, X., DING, Y., ZHANG, Y., TSE, H. F. & LIAN, Q. 2014. Paracrine mechanisms of mesenchymal stem cell-based therapy: current status and perspectives. *Cell Transplant,* 23**,** 1045-59.

LIN, A., YE, J., QI, C., ZHU, L., MOU, W., GAN, W., ZENG, D., TANG, B., XIAO, M., CHU, G., PENG, S., WONG, H. Z. H., ZHANG, L., ZHANG, H., DENG, X., LI, K., ZHANG, J., JIANG, A., LI, Z. & LUO, P. 2025. Bridging artificial intelligence and biological sciences: a comprehensive review of large language models in bioinformatics. *Brief Bioinform,* 26.

LINDE, P., CHOW, L., SABINO, I., WILLIAMS, Z., IMPASTATO, R., DOW, S. & PEZZANITE, L. 2025. Innate immune pathway activation to modulate mesenchymal stromal cell (MSC) interactions with synovium and cartilage. *Front Bioeng Biotechnol,* 13**,** 1605148.

LIU, L., GAO, J., YUAN, Y., CHANG, Q., LIAO, Y. & LU, F. 2013. Hypoxia preconditioned human adipose derived mesenchymal stem cells enhance angiogenic potential via secretion of increased VEGF and bFGF. *Cell Biology International,* 37**,** 551-560.

LIU, X. Y., WEI, M. G., LIANG, J., XU, H. H., WANG, J. J., WANG, J., YANG, X. P., LV, F. F., WANG, K. Q., DUAN, J. H., TU, Y., ZHANG, S., CHEN, C. & LI, X. H. 2020. Injury-preconditioning secretome of umbilical cord mesenchymal stem cells amplified the neurogenesis and cognitive recovery after severe traumatic brain injury in rats. *J Neurochem,* 153**,** 230-251.

LONG, R., LU, S., CHEN, X., YE, W., WANG, T., WANG, X., XU, F. & LI, N. 2025. Human milk peptide MAMP-1 alleviates necrotizing enterocolitis via inhibition of the TLR4-mediated PI3K-AKT-NF-κB signaling pathway. *Food Funct,* 16**,** 3904-3917.

LOVETT-RACKE, A. E., YANG, Y. & RACKE, M. K. 2011. Th1 versus Th17: are T cell cytokines relevant in multiple sclerosis? *Biochim Biophys Acta,* 1812**,** 246-51.

LUBIS, A. M., LUTHFI, A., PAWITAN, J. A., PRIOSOERYANTO, B. P. & CANINTIKA, A. F. 2022. The Effect of Injection of Secretome of Umbilical Cord Mesenchymal Stem Cells in Articular Cartilage Repair in Sheep Model. *Curr Stem Cell Res Ther*.

LUGA, V., ZHANG, L., VILORIA-PETIT, A. M., OGUNJIMI, A. A., INANLOU, M. R., CHIU, E., BUCHANAN, M., HOSEIN, A. N., BASIK, M. & WRANA, J. L. 2012. Exosomes mediate stromal mobilization of autocrine Wnt-PCP signaling in breast cancer cell migration. *Cell,* 151**,** 1542-56.

LV, C. X., DUAN, H., WANG, S., GAN, L. & XU, Q. 2020. Exosomes Derived from Human Umbilical Cord Mesenchymal Stem Cells Promote Proliferation of Allogeneic Endometrial Stromal Cells. *Reprod Sci,* 27**,** 1372-1381.

MADOUX, F., MISHRA, J., MERCER, B. A., AYAD, N., ROUSH, W., HODDER, P. & ROSEN, H. R. 2010. Small Molecule Inhibitors of Wee1 Degradation and Mitotic Entry. *Probe Reports from the NIH Molecular Libraries Program.* Bethesda (MD): National Center for Biotechnology Information (US).

MAGUIRE, G. 2013. Stem cell therapy without the cells. *Communicative & Integrative Biology,* 6**,** e26631.

MAHDY, M. A. A. 2019. Skeletal muscle fibrosis: an overview. *Cell Tissue Res,* 375**,** 575-588.

MARCILLA, A., TRELIS, M., CORTÉS, A., SOTILLO, J., CANTALAPIEDRA, F., MINGUEZ, M. T., VALERO, M. L., SÁNCHEZ DEL PINO, M. M., MUÑOZ-ANTOLI, C., TOLEDO, R. & BERNAL, D. 2012. Extracellular vesicles from parasitic helminths contain specific excretory/secretory proteins and are internalized in intestinal host cells. *PLoS One,* 7**,** e45974.

MARTENS, G. A. 2015. Species-Related Differences in the Proteome of Rat and Human Pancreatic Beta Cells. *J Diabetes Res,* 2015**,** 549818.

MASTENBROEK, T. G., FEIJGE, M. A. H., KREMERS, R. M. W., VAN DEN BOSCH, M. T. J., SWIERINGA, F., DE GROEF, L., MOONS, L., BENNETT, C., GHEVAERT, C., JOHNSON, J. L., VAN DER MEIJDEN, P. E. J. & COSEMANS, J. M. E. M. 2015. Platelet-Associated Matrix Metalloproteinases Regulate Thrombus Formation and Exert Local Collagenolytic Activity. *Arteriosclerosis, Thrombosis, and Vascular Biology,* 35**,** 2554-2561.

MASUBUCHI, T., CHEN, L., MARCEL, N., WEN, G. A., CARON, C., ZHANG, J., ZHAO, Y., MORRIS, G. P., CHEN, X., HEDRICK, S. M., LU, L. F., WU, C., ZOU, Z., BUI, J. D. & HUI, E. 2025. Functional differences between rodent and human PD-1 linked to evolutionary divergence. *Sci Immunol,* 10**,** eads6295.

MATHÉ, G., AMIEL, J. L., SCHWARZENBERG, L., CATTAN, A., SCHNEIDER, M., DE VRIES, M. J., TUBIANA, M., LALANNE, C., BINET, J. L., PAPIERNIK, M., SEMAN, G., MATSUKURA, M., MERY, A. M., SCHWARZMANN, V. & FLAISLER, A. 1965. Successful Allogenic Bone Marrow Transplantation in Man: Chimerism, Induced Specific Tolerance and Possible Anti-Leukemic Effects. *Blood,* 25**,** 179-196.

MATHIEU, M., NÉVO, N., JOUVE, M., VALENZUELA, J. I., MAURIN, M., VERWEIJ, F. J., PALMULLI, R., LANKAR, D., DINGLI, F., LOEW, D., RUBINSTEIN, E., BONCOMPAIN, G., PEREZ, F. & THÉRY, C. 2021. Specificities of exosome versus small ectosome secretion revealed by live intracellular tracking of CD63 and CD9. *Nat Commun,* 12**,** 4389.

MCCORMACK, J. G. & DENTON, R. M. 1990. Intracellular calcium ions and intramitochondrial Ca2+ in the regulation of energy metabolism in mammalian tissues. *Proc Nutr Soc,* 49**,** 57-75.

MCCULLOUGH, J., FISHER, R. D., WHITBY, F. G., SUNDQUIST, W. I. & HILL, C. P. 2008. ALIX-CHMP4 interactions in the human ESCRT pathway. *Proc Natl Acad Sci U S A,* 105**,** 7687-91.

MEDZHITOV, R. & JANEWAY, C., JR. 2000. Innate immune recognition: mechanisms and pathways. *Immunol Rev,* 173**,** 89-97.

MEGALE Â, A. A., MAGNOLI, F. C., KUNIYOSHI, A. K., IWAI, L. K., TAMBOURGI, D. V., PORTARO, F. C. V. & DA SILVA, W. D. 2018. Kn-Ba: a novel serine protease isolated from Bitis arietans snake venom with fibrinogenolytic and kinin-releasing activities. *J Venom Anim Toxins Incl Trop Dis,* 24**,** 38.

MELLOWS, B. 2018. *Investigation into the Therapeutic Potential of a Clinically Compliant Amniotic Fluid-Derived Stem Cell Conditioned Media.* PhD, University of Reading.

MELLOWS, B., MITCHELL, R., ANTONIOLI, M., KRETZ, O., CHAMBERS, D., ZEUNER, M. T., DENECKE, B., MUSANTE, L., RAMACHANDRA, D. L., DEBACQ-CHAINIAUX, F., HOLTHOFER, H., JOCH, B., RAY, S., WIDERA, D.,

DAVID, A. L., HUBER, T. B., DENGJEL, J., DE COPPI, P. & PATEL, K. 2017. Protein and Molecular Characterization of a Clinically Compliant Amniotic Fluid Stem Cell-Derived Extracellular Vesicle Fraction Capable of Accelerating Muscle Regeneration Through Enhancement of Angiogenesis. *Stem Cells Dev,* 26**,** 1316-1333.

MELO, T., MONTERO-BULLÓN, J. F., DOMINGUES, P. & DOMINGUES, M. R. 2019. Discovery of bioactive nitrated lipids and nitro-lipid-protein adducts using mass spectrometry-based approaches. *Redox Biol,* 23**,** 101106.

MINCIACCHI, V. R., FREEMAN, M. R. & DI VIZIO, D. 2015. Extracellular vesicles in cancer: exosomes, microvesicles and the emerging role of large oncosomes. *Semin Cell Dev Biol,* 40**,** 41-51.

MIRABELLI, P., COPPOLA, L. & SALVATORE, M. 2019. Cancer Cell Lines Are Useful Model Systems for Medical Research. *Cancers (Basel),* 11.

MITCHELL, K. E., WEISS, M. L., MITCHELL, B. M., MARTIN, P., DAVIS, D., MORALES, L., HELWIG, B., BEERENSTRAUCH, M., ABOU-EASA, K., HILDRETH, T., TROYER, D. & MEDICETTY, S. 2003. Matrix cells from Wharton's jelly form neurons and glia. *Stem Cells,* 21**,** 50-60.

MITCHELL, R. 2015. *Development of cell-free therapeutics to treat muscle wasting diseases.* PhD, University of Reading.

MITCHELL, R., MELLOWS, B., SHEARD, J., ANTONIOLI, M., KRETZ, O., CHAMBERS, D., ZEUNER, M. T., TOMKINS, J. E., DENECKE, B., MUSANTE, L., JOCH, B., DEBACQ-CHAINIAUX, F., HOLTHOFER, H., RAY, S., HUBER, T. B., DENGJEL, J., DE COPPI, P., WIDERA, D. & PATEL, K. 2019. Secretome of adipose-derived mesenchymal stem cells promotes skeletal muscle regeneration through synergistic action of extracellular vesicle cargo and soluble proteins. *Stem Cell Res Ther,* 10**,** 116.

MIZUKAMI, A., FERNANDES-PLATZGUMMER, A., CARMELO, J. G., SWIECH, K., COVAS, D. T., CABRAL, J. M. & DA SILVA, C. L. 2016. Stirred tank bioreactor culture combined with serum-/xenogeneic-free culture medium enables an efficient expansion of umbilical cord-derived mesenchymal stem/stromal cells. *Biotechnol J,* 11**,** 1048-59.

MÖBIUS, W., VAN DONSELAAR, E., OHNO-IWASHITA, Y., SHIMADA, Y., HEIJNEN, H. F., SLOT, J. W. & GEUZE, H. J. 2003. Recycling compartments and the internal vesicles of multivesicular bodies harbor most of the cholesterol found in the endocytic pathway. *Traffic,* 4**,** 222-31.

MOLINA, T., FABRE, P. & DUMONT, N. A. 2021. Fibro-adipogenic progenitors in skeletal muscle homeostasis, regeneration and diseases. *Open Biol,* 11**,** 210110.

MOLOFSKY, A. V., PARDAL, R. & MORRISON, S. J. 2004. Diverse mechanisms regulate stem cell self-renewal. *Curr Opin Cell Biol,* 16**,** 700-7.

MUÑOZ-CÁNOVES, P., SCHEELE, C., PEDERSEN, B. K. & SERRANO, A. L. 2013. Interleukin-6 myokine signaling in skeletal muscle: a double-edged sword? *Febs j,* 280**,** 4131-48.

MUTANEN, A., PIERRO, A. & ZANI, A. 2018. Perioperative Complications Following Surgery for Necrotizing Enterocolitis. *Eur J Pediatr Surg,* 28**,** 148-151.

NAGAMURA-INOUE, T. & HE, H. 2014. Umbilical cord-derived mesenchymal stem cells: Their advantages and potential clinical utility. *World J Stem Cells,* 6**,** 195-202.

NAPOLITANO, F., GIUDICE, V., D'ESPOSITO, V., PREVETE, N., SCALA, P., DE PAULIS, A., SELLERI, C., FORMISANO, P., ROSSI, F. W. & MONTUORI, N. 2025. Cell-free regenerative medicine: identifying the best source of mesenchymal stem cells for skin therapy in Systemic Sclerosis. *Front Cell Dev Biol,* 13**,** 1518412.

NAWAZ, A., BILAL, M., FUJISAKA, S., KADO, T., ASLAM, M. R., AHMED, S., OKABE, K., IGARASHI, Y., WATANABE, Y., KUWANO, T., TSUNEYAMA, K., NISHIMURA, A., NISHIDA, Y., YAMAMOTO, S., SASAHARA, M., IMURA, J., MORI, H., MATZUK, M. M., KUDO, F., MANABE, I., UEZUMI, A., NAKAGAWA, T., OISHI, Y. & TOBE, K. 2022. Depletion of CD206(+) M2-like macrophages induces fibro-adipogenic progenitors activation and muscle regeneration. *Nat Commun,* 13**,** 7058.

NGKELO, A., MEJA, K., YEADON, M., ADCOCK, I. & KIRKHAM, P. A. 2012. LPS induced inflammatory responses in human peripheral blood mononuclear cells is mediated through NOX4 and Giα dependent PI-3kinase signalling. *J Inflamm (Lond),* 9**,** 1.

NIE, Y., HAN, B.-M., LIU, X.-B., YANG, J.-J., WANG, F., CONG, X.-F. & CHEN, X. 2011. Identification of MicroRNAs Involved in Hypoxia- and Serum Deprivation-Induced Apoptosis in Mesenchymal Stem Cells. *International Journal of Biological Sciences,* 7**,** 762-768.

O'CONNELL, J. S., LI, B., ZITO, A., AHMED, A., CADETE, M., GANJI, N., LAU, E., ALGANABI, M., FARHAT, N., LEE, C., EATON, S., MITCHELL, R., RAY, S., DE COPPI, P., PATEL, K. & PIERRO, A. 2021. Treatment of necrotizing enterocolitis by conditioned medium derived from human amniotic fluid stem cells. *PLoS One,* 16**,** e0260522.

OLAOBA, O. T., KARINA DOS SANTOS, P., SELISTRE-DE-ARAUJO, H. S. & FERREIRA DE SOUZA, D. H. 2020. Snake Venom Metalloproteinases (SVMPs): A structure-function update. *Toxicon X,* 7**,** 100052.

OSTROWSKI, M., CARMO, N. B., KRUMEICH, S., FANGET, I., RAPOSO, G., SAVINA, A., MOITA, C. F., SCHAUER, K., HUME, A. N., FREITAS, R. P., GOUD, B., BENAROCH, P., HACOHEN, N., FUKUDA, M., DESNOS, C., SEABRA, M. C., DARCHEN, F., AMIGORENA, S., MOITA, L. F. & THERY, C. 2010. Rab27a and Rab27b control different steps of the exosome secretion pathway. *Nat Cell Biol,* 12**,** 19-30; sup pp 1-13.

PAKZAD, M., HASSANI, S. N., ABBASI, F., HAJIZADEH-SAFFAR, E., TAGHIYAR, L., FALLAH, N., HAGHPARAST, N., SAMADIAN, A., GANJIBAKHSH, M., DOMINICI, M. & BAHARVAND, H. 2022. A Roadmap for the Production of a GMP-Compatible Cell Bank of Allogeneic Bone Marrow-Derived Clonal Mesenchymal Stromal Cells for Cell Therapy Applications. *Stem Cell Rev Rep,* 18**,** 2279-2295.

PANCHALINGAM, K. M., JUNG, S., ROSENBERG, L. & BEHIE, L. A. 2015. Bioprocessing strategies for the large-scale production of human mesenchymal stem cells: a review. *Stem Cell Res Ther,* 6**,** 225.

PARK, B. S. & LEE, J. O. 2013. Recognition of lipopolysaccharide pattern by TLR4 complexes. *Exp Mol Med,* 45**,** e66.

PATEL, C. C. 1977. Hematologic abnormalities in acute necrotizing enterocolitis. *Pediatr Clin North Am,* 24**,** 579-84.

PAYÃO, T. S., PELLEGRINI, V., MORARI, J., GONÇALVES, G. M. S., DE GODOY, M. C. X., GAMBERO, A., REIS, L. O., VELLOSO, L. A., ARAÚJO, E. P. & PASCOAL, L. B. 2025. The Secretome of Human Deciduous Tooth-Derived Mesenchymal Stem Cells Enhances In Vitro Wound Healing and Modulates Inflammation. *Pharmaceutics,* 17.

PELLON-CARDENAS, O., CLANCY, J., UWIMPUHWE, H. & D'SOUZA-SCHOREY, C. 2013. ARF6-regulated endocytosis of growth factor receptors links cadherin-based adhesion to canonical Wnt signaling in epithelia. *Mol Cell Biol,* 33**,** 2963-75.

PEÑA, O. A. & MARTIN, P. 2024. Cellular and molecular mechanisms of skin wound healing. *Nat Rev Mol Cell Biol,* 25**,** 599-616.

PETRENKO, Y., SYKOVÁ, E. & KUBINOVÁ, Š. 2017. The therapeutic potential of three-dimensional multipotent mesenchymal stromal cell spheroids. *Stem Cell Res Ther,* 8**,** 94.

PHELPS, J., SANATI-NEZHAD, A., UNGRIN, M., DUNCAN, N. A. & SEN, A. 2018. Bioprocessing of Mesenchymal Stem Cells and Their Derivatives: Toward Cell-Free Therapeutics. *Stem Cells Int,* 2018**,** 9415367.

PICCIN, A., MURPHY, W. G. & SMITH, O. P. 2007. Circulating microparticles: pathophysiology and clinical implications. *Blood Rev,* 21**,** 157-71.

PICCININI, F., KISS, A. & HORVATH, P. 2015. CellTracker (not only) for dummies. *Bioinformatics,* 32**,** 955-957.

POLS, M. S. & KLUMPERMAN, J. 2009. Trafficking and function of the tetraspanin CD63. *Exp Cell Res,* 315**,** 1584-92.

PROBONINGRAT, A., FADHOLLY, A., ISKANDAR, R. P. D., ACHMAD, A. B., RANTAM, F. A. & SUDJARWO, S. A. 2019. The potency of chitosan-based Pinus merkusii bark extract nanoparticles as anti-cancer on HeLa cell lines. *Vet World,* 12**,** 1616-1623.

PULIDO-ESCRIBANO, V., TORRECILLAS-BAENA, B., CAMACHO-CARDENOSA, M., DORADO, G., GÁLVEZ-MORENO, M. & CASADO-DÍAZ, A. 2022. Role of hypoxia preconditioning in therapeutic potential of mesenchymal stem-cell-derived extracellular vesicles. *World J Stem Cells,* 14**,** 453-472.

PUNDLIK, S. S., BARIK, A., VENKATESHVARAN, A., SAHOO, S. S., JAYSINGH, M. A., MATH, R. G. H., LAL, H., HASHMI, M. A. & RAMANATHAN, A. 2024a. Senescent cells inhibit mouse myoblast differentiation via the SASP-lipid 15d-PGJ(2) mediated modification and control of HRas. *Elife,* 13.

PUNDLIK, S. S., BARIK, A., VENKATESHVARAN, A., SAHOO, S. S., JAYSINGH, M. A., MATH, R. G. H. & RAMANATHAN, A. 2024b. Senescent cells inhibit muscle differentiation via the SASP-lipid 15d-PGJ2 mediated modification and control of HRas. eLife Sciences Publications, Ltd.

RADUOLOVIC, K., MAK'ANYENGO, R., KAYA, B., STEINERT, A. & NIESS, J. H. 2018. Injections of Lipopolysaccharide into Mice to Mimic Entrance of Microbial-derived Products After Intestinal Barrier Breach. *J Vis Exp*.

RAFIQ, Q. A., COOPMAN, K., NIENOW, A. W. & HEWITT, C. J. 2016. Systematic microcarrier screening and agitated culture conditions improves human mesenchymal stem cell yield in bioreactors. *Biotechnol J,* 11**,** 473-86.

RAGNI, E., PERUCCA ORFEI, C., DE LUCA, P., MONDADORI, C., VIGANÒ, M., COLOMBINI, A. & DE GIROLAMO, L. 2020. Inflammatory priming enhances mesenchymal stromal cell secretome potential as a clinical product for regenerative medicine approaches through secreted factors and EV-miRNAs: the example of joint disease. *Stem Cell Res Ther,* 11**,** 165.

RAIBORG, C., BREMNES, B., MEHLUM, A., GILLOOLY, D. J., D'ARRIGO, A., STANG, E. & STENMARK, H. 2001. FYVE and coiled-coil domains determine the specific localisation of Hrs to early endosomes. *J Cell Sci,* 114**,** 2255-63.

RAMALHO-SANTOS, M. & WILLENBRING, H. 2007. On the origin of the term "stem cell". *Cell Stem Cell,* 1**,** 35-8.

RAO, S., REGHU, N., NAIR, B. G. & VANUOPADATH, M. 2024. The Role of Snake Venom Proteins in Inducing Inflammation Post-Envenomation: An Overview on Mechanistic Insights and Treatment Strategies. *Toxins (Basel),* 16.

RAY, F. A., PEABODY, D. S., COOPER, J. L., CRAM, L. S. & KRAEMER, P. M. 1990. SV40 T antigen alone drives karyotype instability that precedes neoplastic transformation of human diploid fibroblasts. *J Cell Biochem,* 42**,** 13-31.

RAZBAN, V., LOTFI, A. S., SOLEIMANI, M., AHMADI, H., MASSUMI, M., KHAJEH, S., GHAEDI, M., ARJMAND, S., NAJAVAND, S. & KHOSHDEL, A. 2012. HIF-1α Overexpression Induces Angiogenesis in Mesenchymal Stem Cells. *Biores Open Access,* 1**,** 174-83.

REGEV-RUDZKI, N., WILSON, D. W., CARVALHO, T. G., SISQUELLA, X., COLEMAN, B. M., RUG, M., BURSAC, D., ANGRISANO, F., GEE, M., HILL, A. F., BAUM, J. & COWMAN, A. F. 2013. Cell-cell communication between malaria-infected red blood cells via exosome-like vesicles. *Cell,* 153**,** 1120-33.

RIESCO, A., SANTOS-BUITRAGO, B., DE LAS RIVAS, J., KNAPP, M., SANTOS-GARCÍA, G. & TALCOTT, C. 2017. Epidermal Growth Factor Signaling towards Proliferation: Modeling and Logic Inference Using Forward and Backward Search. *BioMed Research International,* 2017**,** 1809513.

ROCHA, S., CARVALHO, J., OLIVEIRA, P., VOGLSTAETTER, M., SCHVARTZ, D., THOMSEN, A. R., WALTER, N., KHANDURI, R., SANCHEZ, J.-C., KELLER, A., OLIVEIRA, C. & NAZARENKO, I. 2019. 3D Cellular Architecture Affects MicroRNA and Protein Cargo of Extracellular Vesicles. *Advanced Science,* 6**,** 1800948.

ROEHLEN, N., CROUCHET, E. & BAUMERT, T. F. 2020. Liver Fibrosis: Mechanistic Concepts and Therapeutic Perspectives. *Cells,* 9.

RONG, Y., ZHANG, J., JIANG, D., JI, C., LIU, W., WANG, J., GE, X., TANG, P., YU, S., CUI, W. & CAI, W. 2021. Hypoxic pretreatment of small extracellular vesicles mediates cartilage repair in osteoarthritis by delivering miR-216a-5p. *Acta Biomaterialia,* 122**,** 325-342.

ROSENDAHL, A. H., SCHÖNBORN, K. & KRIEG, T. 2022. Pathophysiology of systemic sclerosis (scleroderma). *Kaohsiung J Med Sci,* 38**,** 187-195.

ROTA, C., MORIGI, M., CERULLO, D., INTRONA, M., COLPANI, O., CORNA, D., CAPELLI, C., RABELINK, T. J., LEUNING, D. G., ROTTOLI, D., BENIGNI, A., ZOJA, C. & REMUZZI, G. 2018. Therapeutic potential of stromal cells of non-renal or renal origin in experimental chronic kidney disease. *Stem Cell Res Ther,* 9**,** 220.

RUBIN, A. H., TERASAKI, M. & SANUI, H. 1979. Major intracellular cations and growth control: correspondence among magnesium content, protein synthesis, and the onset of DNA synthesis in BALB/c3T3 cells. *Proc Natl Acad Sci U S A,* 76**,** 3917-21.

SAGARADZE, G., GRIGORIEVA, O., NIMIRITSKY, P., BASALOVA, N., KALININA, N., AKOPYAN, Z. & EFIMENKO, A. 2019. Conditioned Medium from Human Mesenchymal Stromal Cells: Towards the Clinical Translation. *Int J Mol Sci,* 20.

SAKANE, H. & AKASAKI, K. 2018. The Major Lysosomal Membrane Proteins LAMP-1 and LAMP-2 Participate in Differentiation of C2C12 Myoblasts. *Biological and Pharmaceutical Bulletin,* 41**,** 1186-1193.

SALMIKANGAS, P., CARLSSON, B., KLUMB, C., REIMER, T. & THIRSTRUP, S. 2023. Potency testing of cell and gene therapy products. *Front Med (Lausanne),* 10**,** 1190016.

SARIN, D., KRISHNA, K., NEJADNIK, M. R., SURYANARAYANAN, R. & RATHORE, A. S. 2024. Impact of Excipient Extraction and Buffer Exchange on Recombinant Monoclonal Antibody Stability. *Mol Pharm,* 21**,** 1872-1883.

SATO, S., TERAMURA, Y., OGAWA, Y., SHIMIZU, E., OTAKE, M., HORI, K., KAMATA, T., SHU, Y., SETA, Y., KURAMOCHI, A., ASAI, K., SHIMIZU, S., NEGISHI, K. & HIRAYAMA, M. 2025. Conditioned media of stem cells from human exfoliated deciduous teeth contain factors related to extracellular matrix organization and promotes corneal epithelial wound healing. *Regen Ther,* 29**,** 148-161.

SCHLIENGER, S., CAMPBELL, S. & CLAING, A. 2014. ARF1 regulates the Rho/MLC pathway to control EGF-dependent breast cancer cell invasion. *Mol Biol Cell,* 25**,** 17-29.

SEGRE, E. & FULLERTON, J. N. 2016. Stimulated Whole Blood Cytokine Release as a Biomarker of Immunosuppression in the Critically Ill: The Need for a Standardized Methodology. *Shock,* 45**,** 490-4.

SENGUN, E., FRÖBERG, J., HE, X., ELEVELD, M., SMEETS, R. L., KOENEN, H., MÖLLER-HACKBARTH, K., WOLFS, T., OPHELDERS, D., HUYNEN, M. A., DE JONGE, M. I. & VAN DER MOLEN, R. G. 2025. Mesenchymal stem cells suppress NF-κB and ERK signalling while enhancing chemotaxis in CD4(+) T cells. *Sci Rep,* 15**,** 32000.

SHARMA, D. K., BROWN, J. C., CHOUDHURY, A., PETERSON, T. E., HOLICKY, E., MARKS, D. L., SIMARI, R., PARTON, R. G. & PAGANO, R. E. 2004. Selective stimulation of caveolar endocytosis by glycosphingolipids and cholesterol. *Mol Biol Cell,* 15**,** 3114-22.

SHAW, I. & GREGORY, K. 2022. Acid-base balance: a review of normal physiology. *BJA Educ,* 22**,** 396-401.

SHEN, C., LIE, P., MIAO, T., YU, M., LU, Q., FENG, T., LI, J., ZU, T., LIU, X. & LI, H. 2015. Conditioned medium from umbilical cord mesenchymal stem cells induces migration and angiogenesis. *Mol Med Rep,* 12**,** 20-30.

SHI, B., PHAN, T. K. & POON, I. K. H. 2025. Extracellular vesicles from the dead: the final message. *Trends Cell Biol,* 35**,** 439-452.

SHI, C. & PAMER, E. G. 2011. Monocyte recruitment during infection and inflammation. *Nat Rev Immunol,* 11**,** 762-74.

SHI, X., ZHANG, K., QI, Q., ZHOU, W., YU, F. & ZHANG, Y. 2024. Human umbilical cord-derived mesenchymal stem cells attenuate hepatic stellate cells activation and liver fibrosis. *Mol Biol Rep,* 51**,** 734.

SHIELDS, S. B., OESTREICH, A. J., WINISTORFER, S., NGUYEN, D., PAYNE, J. A., KATZMANN, D. J. & PIPER, R. 2009. ESCRT ubiquitin-binding domains function cooperatively during MVB cargo sorting. *J Cell Biol,* 185**,** 213-24.

SHIMIZU, Y., INOUE, Y., MATSUURA, N., ISHII, T., SOWA, Y., SUNAMI, H. & NTEGE, E. H. 2026. Mesenchymal stromal cell-derived extracellular vesicles in regenerative medicine: Standardisation, bioengineering and clinical translation. *Regen Ther,* 31**,** 101058.

SHRESTHA, C., ZHAO, L., CHEN, K., HE, H. & MO, Z. 2013. Enhanced healing of diabetic wounds by subcutaneous administration of human umbilical cord derived stem cells and their conditioned media. *Int J Endocrinol,* 2013**,** 592454.

SILACHEV, D. N., GORYUNOV, K. V., SHPILYUK, M. A., BEZNOSCHENKO, O. S., MOROZOVA, N. Y., KRAEVAYA, E. E., POPKOV, V. A., PEVZNER, I. B., ZOROVA, L. D., EVTUSHENKO, E. A., STARODUBTSEVA, N. L., KONONIKHIN, A. S., BUGROVA, A. E., EVTUSHENKO, E. G., PLOTNIKOV, E. Y., ZOROV, D. B. & SUKHIKH, G. T. 2019. Effect of MSCs and MSC-Derived Extracellular Vesicles on Human Blood Coagulation. *Cells,* 8.

SMIGIELSKA-CZEPIEL, K., VAN DEN BERG, A., JELLEMA, P., SLEZAK-PROCHAZKA, I., MAAT, H., VAN DEN BOS, H., VAN DER LEI, R. J., KLUIVER, J., BROUWER, E., BOOTS, A. M. & KROESEN, B. J. 2013. Dual role of miR-21 in CD4+ T-cells: activation-induced miR-21 supports survival of memory T-cells and regulates CCR7 expression in naive T-cells. *PLoS One,* 8**,** e76217.

SODER, R. P., DUDLEY, N. R. & DAWN, B. 2024. Microcarrier-based clinical-grade manufacturing of therapeutic Wharton's jelly mesenchymal stromal cells. *Cytotherapy,* 26**,** 1556-1565.

SODHI, C. P., AHMAD, R., JIA, H., FULTON, W. B., LOPEZ, C., GONZALEZ SALAZAR, A. J., ISHIYAMA, A., SAMPAH, M., STEINWAY, S., WANG, S., PRINDLE, T., JR., WANG, M., STEED, D. L., WESSEL, H., KIRSHNER, Z., BROWN, L. R., LU, P. & HACKAM, D. J. 2022. The administration of amnion-derived multipotent cell secretome ST266 protects against necrotizing enterocolitis in mice and piglets. *Am J Physiol Gastrointest Liver Physiol,* 323**,** G265-g282.

SONG, R., SUBBARAO, G. C. & MAHESHWARI, A. 2012. Haematological abnormalities in neonatal necrotizing enterocolitis. *J Matern Fetal Neonatal Med,* 25 Suppl 4**,** 22-5.

SONNTAG, J., WAGNER, M. H., WALDSCHMIDT, J., WIT, J. & OBLADEN, M. 1998. Multisystem organ failure and capillary leak syndrome in severe necrotizing enterocolitis of very low birth weight infants. *J Pediatr Surg,* 33**,** 481-4.

SOUZA-MOREIRA, L., SOARES, V. C., DIAS, S. D. S. G. & BOZZA, P. T. 2019. Adipose-derived Mesenchymal Stromal Cells Modulate Lipid Metabolism and Lipid Droplet Biogenesis via AKT/mTOR –PPARγ Signalling in Macrophages. *Scientific Reports,* 9**,** 20304.

SPICKETT, C. M. 2007. Chlorinated lipids and fatty acids: an emerging role in pathology. *Pharmacol Ther,* 115**,** 400-9.

SPURWAY, J., LOGAN, P. & PAK, S. 2012. The development, structure and blood flow within the umbilical cord with particular reference to the venous system. *Australas J Ultrasound Med,* 15**,** 97-102.

SRIRAMULU, S., BANERJEE, A., JOTHIMANI, G. & PATHAK, S. 2020. Conditioned medium from the human umbilical cord-mesenchymal stem cells stimulate the proliferation of human keratinocytes. *J Basic Clin Physiol Pharmacol,* 32**,** 51-56.

STEFAŃSKA, K., OŻEGOWSKA, K., HUTCHINGS, G., POPIS, M., MONCRIEFF, L., DOMPE, C., JANOWICZ, K., PIEŃKOWSKI, W., GUTAJ, P., SHIBLI, J. A., PRADO, W. M., PIOTROWSKA-KEMPISTY, H., MOZDZIAK, P., BRUSKA, M., ZABEL, M., KEMPISTY, B. & NOWICKI, M. 2020. Human Wharton's Jelly-Cellular Specificity, Stemness Potency, Animal Models, and Current Application in Human Clinical Trials. *J Clin Med,* 9.

STEYN, P. J., DZOBO, K., SMITH, R. I. & MYBURGH, K. H. 2019. Interleukin-6 Induces Myogenic Differentiation via JAK2-STAT3 Signaling in Mouse C2C12 Myoblast Cell Line and Primary Human Myoblasts. *Int J Mol Sci,* 20.

SU, G. L. 2002. Lipopolysaccharides in liver injury: molecular mechanisms of Kupffer cell activation. *Am J Physiol Gastrointest Liver Physiol,* 283**,** G256-65.

TABRIZI, S. N., ARABAMERI, A. & KLIDBARY, S. H. 2025. Modeling inflammation in allergic asthma: Exploring the role of mesenchymal stem cells in therapeutic strategies. *Comput Biol Med,* 197**,** 111015.

TAKAHASHI, K. & YAMANAKA, S. 2006. Induction of pluripotent stem cells from mouse embryonic and adult fibroblast cultures by defined factors. *Cell,* 126**,** 663-76.

TAKEICHI, M. & OKADA, T. S. 1972. Roles of magnesium and calcium ions in cell-to-substrate adhesion. *Experimental Cell Research,* 74**,** 51-60.

TALEPOOR, A. G., RASTEGARI, B., KALANI, M. & DOROUDCHI, M. 2021. Decrease in the inflammatory cytokines of LPS-stimulated PBMCs of patients with atherosclerosis by a TLR-4 antagonist in the co-culture with HUVECs. *International Immunopharmacology,* 101**,** 108295.

TANG, J., KANG, Y., ZHOU, Y., CHEN, Q., LAN, J., LIU, X. & PENG, Y. 2023. Umbilical cord mesenchymal stem cell-conditioned medium inhibits microglial activation to ameliorate neuroinflammation in amyotrophic lateral sclerosis mice and cell models. *Brain Research Bulletin,* 202**,** 110760.

TANG, X. D., SHI, L., MONSEL, A., LI, X. Y., ZHU, H. L., ZHU, Y. G. & QU, J. M. 2017. Mesenchymal Stem Cell Microvesicles Attenuate Acute Lung Injury in Mice Partly Mediated by Ang-1 mRNA. *Stem Cells,* 35**,** 1849-1859.

TEIXEIRA, F. G., PANCHALINGAM, K. M., ANJO, S. I., MANADAS, B., PEREIRA, R., SOUSA, N., SALGADO, A. J. & BEHIE, L. A. 2015. Do hypoxia/normoxia culturing conditions change the neuroregulatory profile of Wharton Jelly mesenchymal stem cell secretome? *Stem Cell Res Ther,* 6**,** 133.

TEO, H., PERISIC, O., GONZÁLEZ, B. & WILLIAMS, R. L. 2004. ESCRT-II, an endosome-associated complex required for protein sorting: crystal structure and interactions with ESCRT-III and membranes. *Dev Cell,* 7**,** 559-69.

THERET, M., ROSSI, F. M. V. & CONTRERAS, O. 2021. Evolving Roles of Muscle-Resident Fibro-Adipogenic Progenitors in Health, Regeneration, Neuromuscular Disorders, and Aging. *Frontiers in Physiology,* Volume 12 - 2021.

THÉRY, C., ZITVOGEL, L. & AMIGORENA, S. 2002. Exosomes: composition, biogenesis and function. *Nat Rev Immunol,* 2**,** 569-79.

THIPPABHOTLA, S., ZHONG, C. & HE, M. 2019. 3D cell culture stimulates the secretion of in vivo like extracellular vesicles. *Scientific Reports,* 9**,** 13012.

TIDBALL, J. G. 2017. Regulation of muscle growth and regeneration by the immune system. *Nature Reviews Immunology,* 17**,** 165-178.

TOKHANBIGLI, S., BAGHAEI, K., ASADIRAD, A., HASHEMI, S. M., ASADZADEH-AGHDAEI, H. & ZALI, M. R. 2019. Immunoregulatory impact of human mesenchymal-conditioned media and mesenchymal derived exosomes on monocytes. *Mol Biol Res Commun,* 8**,** 79-89.

TONG, W., ZHANG, X., ZHANG, Q., FANG, J., LIU, Y., SHAO, Z., YANG, S., WU, D., SHENG, X., ZHANG, Y. & TIAN, H. 2020. Multiple umbilical cord-derived MSCs administrations attenuate rat osteoarthritis progression via preserving articular cartilage superficial layer cells and inhibiting synovitis. *J Orthop Translat,* 23**,** 21-28.

TREMBLAY, É., THIBAULT, M. P., FERRETTI, E., BABAKISSA, C., BERTELLE, V., BETTOLLI, M., BURGHARDT, K. M., COLOMBANI, J. F., GRYNSPAN, D., LEVY, E., LU, P., MAYER, S., MÉNARD, D., MOUTERDE, O., RENES, I. B., SEIDMAN, E. G. & BEAULIEU, J. F. 2016. Gene expression profiling in necrotizing enterocolitis reveals pathways common to those reported in Crohn's disease. *BMC Med Genomics,* 9**,** 6.

TRENTESAUX, C., STRIEDINGER, K., POMERANTZ, J. H. & KLEIN, O. D. 2020. From gut to glutes: The critical role of niche signals in the maintenance and renewal of adult stem cells. *Curr Opin Cell Biol,* 63**,** 88-101.

TRICARICO, C., CLANCY, J. & D'SOUZA-SCHOREY, C. 2017. Biology and biogenesis of shed microvesicles. *Small GTPases,* 8**,** 220-232.

TSAI, C.-C., CHEN, Y.-J., YEW, T.-L., CHEN, L.-L., WANG, J.-Y., CHIU, C.-H. & HUNG, S.-C. 2011. Hypoxia inhibits senescence and maintains mesenchymal stem cell properties through down-regulation of E2A-p21 by HIF-TWIST. *Blood,* 117**,** 459-469.

TSAO, F. H. C., LI, Z., AMESSOUDJI, A. W., JAWDAT, D., SADAT, M., ARABI, Y. & MEYER, K. C. 2024. The Role of Serum Albumin and Secretory Phospholipase A2 in Sepsis. *Int J Mol Sci,* 25.

TSUJIMOTO, M., MOON, S. & ITO, Y. 2024. Effect of conditioned media on the angiogenic activity of mesenchymal stem cells. *Journal of Bioscience and Bioengineering,* 138**,** 163-170.

TU, H. & LI, Y.-L. 2023. Inflammation balance in skeletal muscle damage and repair. *Frontiers in Immunology,* Volume 14 - 2023.

VAIASICCA, S., MELONE, G., JAMES, D. W., QUINTELA, M., XIAO, J., YAO, S., FINNELL, R. H., CONLAN, R. S., FRANCIS, L. W. & CORRADETTI, B. 2024. Transcriptomic analysis reveals the anti-cancer effect of gestational mesenchymal stem cell secretome. *Stem Cells Transl Med,* 13**,** 693-710.

VALENTA, J., HLAVACKOVA, A., STACH, Z., STIKAROVA, J., HAVLICEK, M. & MICHALEK, P. 2022. Fibrinogenolysis in Venom-Induced Consumption Coagulopathy after Viperidae Snakebites: A Pilot Study. *Toxins (Basel),* 14.

VAN DEURSEN, J. M. 2014. The role of senescent cells in ageing. *Nature,* 509**,** 439-46.

VAN NIEL, G., D'ANGELO, G. & RAPOSO, G. 2018. Shedding light on the cell biology of extracellular vesicles. *Nat Rev Mol Cell Biol,* 19**,** 213-228.

VIETRI, M., RADULOVIC, M. & STENMARK, H. 2020. The many functions of ESCRTs. *Nat Rev Mol Cell Biol,* 21**,** 25-42.

VOLKMER, E., DROSSE, I., OTTO, S., STANGELMAYER, A., STENGELE, M., KALLUKALAM, B. C., MUTSCHLER, W. & SCHIEKER, M. 2008. Hypoxia in Static and Dynamic 3D Culture Systems for Tissue Engineering of Bone. *Tissue Engineering Part A,* 14**,** 1331-1340.

VU, D. M., NGUYEN, V. T., NGUYEN, T. H., DO, P. T. X., DAO, H. H., HAI, D. X., LE, N. T., NGUYEN, X. H. & THAN, U. T. T. 2022. Effects of Extracellular Vesicles Secreted by TGFβ-Stimulated Umbilical Cord Mesenchymal Stem Cells on Skin Fibroblasts by Promoting Fibroblast Migration and ECM Protein Production. *Biomedicines,* 10.

WALSH, M. C. & KLIEGMAN, R. M. 1986. Necrotizing enterocolitis: treatment based on staging criteria. *Pediatr Clin North Am,* 33**,** 179-201.

WANG, G. L., JIANG, B. H., RUE, E. A. & SEMENZA, G. L. 1995. Hypoxia-inducible factor 1 is a basic-helix-loop-helix-PAS heterodimer regulated by cellular O2 tension. *Proc Natl Acad Sci U S A,* 92**,** 5510-4.

WANG, H. S., HUNG, S. C., PENG, S. T., HUANG, C. C., WEI, H. M., GUO, Y. J., FU, Y. S., LAI, M. C. & CHEN, C. C. 2004. Mesenchymal stem cells in the Wharton's jelly of the human umbilical cord. *Stem Cells,* 22**,** 1330-7.

WANG, L., LV, W., MAO, H., CHEN, Q., MA, Y., ZHANG, L., RUAN, Y. & ZHANG, C. 2025. Phospholipase A2 group IIA activates Indoleamine 2,3-dioxygenase 1 to drive the progression of pulmonary fibrosis. *Free Radic Biol Med,* 237**,** 251-269.

WANG, T., GILKES, D. M., TAKANO, N., XIANG, L., LUO, W., BISHOP, C. J., CHATURVEDI, P., GREEN, J. J. & SEMENZA, G. L. 2014. Hypoxia-inducible factors and RAB22A mediate formation of microvesicles that stimulate breast cancer invasion and metastasis. *Proceedings of the National Academy of Sciences,* 111**,** E3234-E3242.

WEISSMAN, I. L., ANDERSON, D. J. & GAGE, F. 2001. Stem and progenitor cells: origins, phenotypes, lineage commitments, and transdifferentiations. *Annu Rev Cell Dev Biol,* 17**,** 387-403.

WIEST, E. F. & ZUBAIR, A. C. 2025. Generation of Current Good Manufacturing Practices-Grade Mesenchymal Stromal Cell-Derived Extracellular Vesicles Using Automated Bioreactors. *Biology (Basel),* 14.

WILLIAMS, H. F., MELLOWS, B. A., MITCHELL, R., SFYRI, P., LAYFIELD, H. J., SALAMAH, M., VAIYAPURI, R., COLLINS-HOOPER, H., BICKNELL, A. B., MATSAKAS, A., PATEL, K. & VAIYAPURI, S. 2019. Mechanisms underpinning the permanent muscle damage induced by snake venom metalloprotease. *PLoS Negl Trop Dis,* 13**,** e0007041.

XIAO, H., PAN, H., LIAO, K., YANG, M. & HUANG, C. 2017. Snake Venom PLA(2), a Promising Target for Broad-Spectrum Antivenom Drug Development. *Biomed Res Int,* 2017**,** 6592820.

XU, Z., LIN, L., FAN, Y., HUSELSTEIN, C., DE ISLA, N., HE, X., CHEN, Y. & LI, Y. 2022. Secretome of Mesenchymal Stem Cells from Consecutive Hypoxic Cultures Promotes Resolution of Lung Inflammation by Reprogramming Anti-Inflammatory Macrophages. *Int J Mol Sci,* 23.

YAN, L. & WU, X. 2020. Exosomes produced from 3D cultures of umbilical cord mesenchymal stem cells in a hollow-fiber bioreactor show improved osteochondral regeneration activity. *Cell Biol Toxicol,* 36**,** 165-178.

YANG, C., LEI, D., OUYANG, W., REN, J., LI, H., HU, J. & HUANG, S. 2014. Conditioned media from human adipose tissue-derived mesenchymal stem cells and umbilical cord-derived mesenchymal stem cells efficiently induced the apoptosis and differentiation in human glioma cell lines in vitro. *Biomed Res Int,* 2014**,** 109389.

YANG, W. & HU, P. 2018. Skeletal muscle regeneration is modulated by inflammation. *J Orthop Translat,* 13**,** 25-32.

YANG, Y., LEE, E. H. & YANG, Z. 2022. Hypoxia-Conditioned Mesenchymal Stem Cells in Tissue Regeneration Application. *Tissue Engineering Part B: Reviews,* 28**,** 966-977.

YANG, Y., RAO, R., VALLIERE-DOUGLASS, J. & TREMINTIN, G. 2024. Automated high-throughput buffer exchange platform enhances rapid flow analysis of antibody drug conjugates by high resolution mass spectrometry. *J Chromatogr B Analyt Technol Biomed Life Sci,* 1235**,** 124007.

YIN, G., HU, G., WAN, R., YU, G., CANG, X., XIONG, J., NI, J., HU, Y., XING, M., FAN, Y., XIAO, W., QIU, L., TANG, M., ZHAO, Y., WANG, S. & WANG, X. 2016. Role of Microvesicles From Bone Marrow Mesenchymal Stem Cells in Acute Pancreatitis. *Pancreas,* 45**,** 1282-1293.

YIN, H., PRICE, F. & RUDNICKI, M. A. 2013. Satellite cells and the muscle stem cell niche. *Physiol Rev,* 93**,** 23-67.

ZAKRZEWSKI, W., DOBRZYŃSKI, M., SZYMONOWICZ, M. & RYBAK, Z. 2019. Stem cells: past, present, and future. *Stem Cell Res Ther,* 10**,** 68.

ZANI, A., CANANZI, M., FASCETTI-LEON, F., LAURITI, G., SMITH, V. V., BOLLINI, S., GHIONZOLI, M., D'ARRIGO, A., POZZOBON, M., PICCOLI, M., HICKS, A., WELLS, J., SIOW, B., SEBIRE, N. J., BISHOP, C., LEON, A., ATALA, A., LYTHGOE, M. F., PIERRO, A., EATON, S. & DE COPPI, P. 2014. Amniotic fluid stem cells improve survival and enhance repair of damaged intestine in necrotising enterocolitis via a COX-2 dependent mechanism. *Gut,* 63**,** 300-9.

ZANI, A. & PIERRO, A. 2015. Necrotizing enterocolitis: controversies and challenges. *F1000Res,* 4.

ZHANG, C., LV, P., LIANG, Q., ZHOU, J., WU, B. & XU, W. 2024. Conditioned Medium Derived From Human Dental Follicle Mesenchymal Stem Cells Alleviates Macrophage Proinflammatory Responses Through MAPK-ERK-EGR1 Axis. *Stem Cells Int,* 2024**,** 5514771.

ZHANG, L., CHU, Q., LIU, X. & XU, T. 2020. microRNA-21 negatively regulates NF-κB signaling pathway via targeting IL1R1 in miiuy croaker. *Developmental & Comparative Immunology,* 105**,** 103578.

ZHANG, L., HU, J. & ATHANASIOU, K. A. 2009. The role of tissue engineering in articular cartilage repair and regeneration. *Crit Rev Biomed Eng,* 37**,** 1-57.

ZHANG, Y., NA, T., ZHANG, K., YANG, Y., XU, H., WEI, L., XU, L., YAN, X., LIU, W., LIU, G., WANG, B., MENG, S. & DU, Y. 2022. GMP-grade microcarrier and automated closed industrial scale cell production platform for culture of MSCs. *Journal of Tissue Engineering and Regenerative Medicine,* 16**,** 934-944.

ZHAO, L., LIU, X., ZHANG, Y., LIANG, X., DING, Y., XU, Y., FANG, Z. & ZHANG, F. 2016. Enhanced cell survival and paracrine effects of mesenchymal stem cells overexpressing hepatocyte growth factor promote cardioprotection in myocardial infarction. *Exp Cell Res,* 344**,** 30-39.

ZHOU, J., XU, Y., WANG, G., MEI, T., YANG, H. & LIU, Y. 2022. The TLR7/8 agonist R848 optimizes host and tumor immunity to improve therapeutic efficacy in murine lung cancer. *Int J Oncol,* 61.

ZHOU, Y., XU, H., XU, W., WANG, B., WU, H., TAO, Y., ZHANG, B., WANG, M., MAO, F., YAN, Y., GAO, S., GU, H., ZHU, W. & QIAN, H. 2013. Exosomes released by human umbilical cord mesenchymal stem cells protect against cisplatin-induced renal oxidative stress and apoptosis in vivo and in vitro. *Stem Cell Res Ther,* 4**,** 34.